LOW-RANK MATRIX RECOVERY: BLIND DECONVOLUTION AND EFFICIENT SAMPLING OF CORRELATED SIGNALS

A Thesis
Presented to
The Academic Faculty

by

Ali Ahmed

In Partial Fulfillment
of the Requirements for the Degree
Doctor of Philosophy in the
School of Electrical and Computer Engineering

Georgia Institute of Technology
December, 2013

LOW-RANK MATRIX RECOVERY: BLIND DECONVOLUTION AND EFFICIENT SAMPLING OF CORRELATED SIGNALS

Approved by:

Professor Justin K. Romberg, Advisor
School of Electrical and Computer Engineering
Georgia Institute of Technology

Professor Aaron Lanterman
School of Electrical and Computer Engineering
Georgia Institute of Technology

Professor Mark A. Davenport
School of Electrical and Computer Engineering
Georgia Institute of Technology

Professor Vladimir Koltchinskii
School of Mathematics
Georgia Institute of Technology

Professor Christopher Rozell
School of Electrical and Computer Engineering
Georgia Institute of Technology

Date Approved: July 29, 2013

To my father Saleem Ahmed and my mother Falak Naz

ACKNOWLEDGEMENTS

I want to express my deepest gratitude to my thesis advisor Dr. Justin Romberg for his encouragement, advice, and guidance at every step during my PhD. I thank him for introducing me to exciting research problems. His interest in my research and his insightful suggestions was invaluable for me to produce as a graduate student. I am extremely grateful to him for his efforts in improving my technical writing and his contributions to my publication drafts. His devotion and keenness for his work are an inspiration for me and set a benchmark for me to follow in my career.

I would also like to thank my thesis committee: Dr. Mark Davenport, Dr. Vladimir Koltchinskii, Dr. Aaron Lanterman, and Dr. Christopher Rozell for reviewing my thesis. I am grateful for their thoughtful suggestions.

I would like to convey my special thanks to Dr. Kleywegt (ISYE), Dr. Koltchinskii (MATH), and Dr. Justin Romberg (ECE) for the material they have taught me in their classes, for being wonderful teachers, and for presenting all the concepts in a neat and clean form that made their classes a great learning experience for me. I am deeply indebted to Dr. Karim Lounici for always being very kind and helpful, and making time to discuss questions related to my research, and directing me to appropriate references.

This thesis and my stay in the US was co-funded by Fulbright and higher education commission (HEC) of Pakistan. I am grateful to both for giving me an opportunity to study in the US and work with the pioneers in my area of research.

I would like to acknowledge my fellow student Han Lun Yap for many in depth discussions related to my research problems. Our two person journal reading group was instrumental for me to develop an understanding of the key technical concepts

in our area of research. Had it not been your support my friend, I would still be hesitant of reading long papers full of technical content. I really enjoyed your company. Best wishes for you. I also had a great pleasure of working with my knowledgeable lab mates Alireza Aghasi, Aditya, Aurele, Chris, Darryl, Ning, Salman, Steve, and William who provided a fertile environment to study and develop new ideas. I want to especially thank Darryl for listening to me whenever I was bored of computer screen, for sharing thoughts in strolls to and back from CSIP. I wish all of you success in your future endeavors.

I cannot leave Georgia Tech without mentioning a good friend, Hassan Kingravi, whom I met the very first semester, I arrived at Georgia Tech. Thanks buddy for always being there to listen to my loser talk when I was feeling down and out. Thanks for always encouraging me and keeping my morale high. I especially thank you for introducing me to the world of guitar playing.

Thanks to my dear comrades Haider Ali, Basit Memon, Usman Ali, and Usman Gul for being a surrogate family. Thanks also to the crew at "Pakistan House" and other places around for counter strike games and cricket matches on weekends and making the stay at Georgia Tech worthy of remembrance.

This thesis would not have been possible without the unwavering support of S&A for always being there for me during this long and tough journey. I would not have contemplated this road if not for my parents. I will always be grateful to my mother for her prayers and affection, and my father who taught me and instilled within me the love of knowledge. To my parents, and my siblings, Ujala, Sonia, Musab, Hasaan, and Usama, thank you all!

TABLE OF CONTENTS

LIST OF FIGURES

SUMMARY

Low-dimensional signal structures naturally arise in a large set of applications in various fields such as medical imaging, machine learning, signal, and array processing. A ubiquitous low-dimensional structure in signals and images is sparsity, and a new sampling theory; namely, compressive sensing, proves that the sparse signals and images can be reconstructed from incomplete measurements. The signal recovery is achieved using efficient algorithms such as ℓ_1-minimization. Recently, the research focus has spun-off to encompass other interesting low-dimensional signal structures such as group-sparsity and low-rank structure.

This thesis considers low-rank matrix recovery (LRMR) from various structured-random measurement ensembles. These results are then employed for the in depth investigation of the classical blind-deconvolution problem from a new perspective, and for the development of a framework for the efficient sampling of correlated signals (the signals lying in a subspace).

In the first part, we study the blind deconvolution; separation of two unknown signals by observing their convolution. We recast the deconvolution of discrete signals $\boldsymbol{w}$ and $\boldsymbol{x}$ as a rank-1 matrix $\boldsymbol{w}\boldsymbol{x}^*$ recovery problem from a structured random measurement ensemble. The convex relaxation of the problem leads to a tractable semidefinite program. We show, using some of the mathematical tools developed recently for LRMR, that if we assume the signals convolved with one another live in known subspaces, then this semidefinite relaxation is provably effective.

In the second part, we design various efficient sampling architectures for signals acquired using large arrays. The sampling architectures exploit the correlation in the

signals to acquire them at a sub-Nyquist rate. The sampling devices are designed using analog components with clear implementation potential. For each of the sampling scheme, we show that the signal reconstruction can be framed as an LRMR problem from a structured-random measurement ensemble. The signals can be reconstructed using the familiar nuclear-norm minimization. The sampling theorems derived for each of the sampling architecture show that the LRMR framework produces the Shannon-Nyquist performance for the sub-Nyquist acquisition of correlated signals.

In the final part, we study low-rank matrix factorizations using randomized linear algebra. This specific method allows us to use a least-squares program for the reconstruction of the unknown low-rank matrix from the samples of its row and column space. Based on the principles of this method, we then design sampling architectures that not only acquire correlated signals efficiently but also require a simple least-squares program for the signal reconstruction.

A theoretical analysis of all of the LRMR problems above is presented in this thesis, which provides the sufficient measurements required for the successful reconstruction of the unknown low-rank matrix, and the upper bound on the recovery error in both noiseless and noisy cases. For each of the LRMR problem, we also provide a discussion of a computationally feasible algorithm, which includes a least-squares-based algorithm, and some of the fastest algorithms for solving nuclear-norm minimization.

Statement of Contributions

A brief list of the main contributions of this work is given below.

- A new method for the deconvolution of two unknown signals living in known subspaces. (Chapter 3)
- A method for protecting coded messages against an unknown channel in wireless communications. (Chapter 3)
- An experimental evaluation illustrating the potential of the proposed blind-deconvolution method in image deblurring. (Chapter 3)
- A theoretical analysis of the proposed blind-deconvolution method based on LRMR using the concept of duality in convex programming, which proves the exact recovery of signals from their convolution under a precise set of conditions. (Chapter 3)
- Design of multiple architectures for compressive sampling for array processing. (Chapter 4)
- Design of a compressive multiplexer; a low-power, efficient sampling architecture for micro-sensor arrays. (Chapter 5)
- A derivation of a sampling theorem, based on LRMR, for each of the proposed sampling architecture. The sampling theorems prove that the sub-Nyquist rate is sufficient for the successful signal reconstruction. (Chapter 4 and 5)
- A theoretical analysis based on the concept of duality in convex programming that proves the exact recovery of a low-rank matrix from a random block-diagonal measurement ensemble by solving a nuclear norm minimization program. (Chapter 4)

- Experimental and theoretical results showing that the sampling architectures perform gracefully in the presence of noise. (Chapter 4 and 5)
- Design of a universal compressive multiplexer for the acquisition of ensembles of correlated signals. (Chapter 5)
- Proof of the sampling theorem for the universal compressive multiplexer. Analysis is based on showing the restricted isometry property (RIP) over low-rank matrices of a structured-random measurement ensemble. This is the first known RIP for structured random measurement ensembles. (Chapter 5)
- A study of the applications of the proposed sampling architectures in compressive array processing and micro-sensor arrays. (Chapter 4 and 5)
- Design of multiple sampling architectures for compressive array processing that also allow for the signal reconstruction by solving a simple least-squares program. (Chapter 6)
- A theoretical analysis proving the exact low-rank matrix recovery using structured-random samples of its row and column space and by solving a simple least-squares program. (Chapter 6)
- Identification of some open problems in this line of research

CHAPTER I

INTRODUCTION

In a broad set of applications, we are interested in recovering a low-rank matrix from a partial or an incomplete set of observations. Such applications arise across different fields in science and engineering; for example, in collaborative filtering to recommend based on a limited set of ratings in the database, e.g., Netflix [12]; in reconstructing the low-dimensional geometry of the locations of objects based on an incomplete information of the distance between the objects [87, 89]; in systems and controls to fit a discrete time LTI state space model to a sequence of inputs [65]; in facial alignment, and recognition using the principal component analysis [24, 74]; in recovering the phase of a signal from the intensity only measurements [21]; in quantum state tomography [45]; and in graph theory to represent cliques in graphs [5]. This list by no means spans the vast set of applications in which the rank minimization arises. Randomness plays a key role in matrix recovery from a fewer generalized measurements. The results in the literature show that the unknown low-rank matrix can be recovered from a limited number of random Gaussian projections, or from the observations of a few of its randomly chosen entries. The problems studied in this thesis, however, require low-rank matrix recovery results from *structured*-random projections.

This thesis mainly presents low-rank matrix recovery (LRMR) results from various structured-random measurement ensembles. These results are then employed; first, to study a fundamental problem in signal processing and communications; namely, the blind deconvolution; and second, to develop methods for the sub-Nyquist acquisition of multiple signals lying in a subspace—such signals will be referred to as correlated

signals. Briefly, the blind-deconvolution problem can be framed as a rank-1 matrix recovery problem from a multi-Toeplitz measurement ensemble, and the efficient sampling problem of signals lying in an a priori unknown subspace of dimension R, can be viewed as a rank-R matrix recovery problem from a structured random measurement ensemble. This chapter introduces the blind-deconvolution problem and then poses it as a rank-1 matrix recovery problem. Moreover, we demonstrate its connections to other interesting problems such as the phase retrieval of a signal from its magnitude measurements, and the solution of bilinear equations. Furthermore, we will layout a simple presentation of our sampling techniques for the sub-Nyquist acquisition of correlated signals using a simple sampling architecture. Our introductory discussion on this topic will mainly focus on how to recast the reconstruction of correlated signals from limited samples as an LRMR problem. Before beginning our discussion, we specify here the notation that will be employed throughout the thesis.

1.1 Notation

Unless specified otherwise, we use uppercase bold, lowercase bold, and not bold letters for matrices, a vectors, and scalars, respectively. For example, $\boldsymbol{X}$ denotes a matrix, $\boldsymbol{x}$ represents a vector, and x refers to a scalar. We use $X[i,j]$ to specify the (i,j)-th entry of a matrix $\boldsymbol{X}$, and $x[i]$ to signify the i-th entry of a vector $\boldsymbol{x}$. Calligraphic letters specify linear operators, e.g., $\mathcal{A} : \mathbb{C}^{M\times N} \to \mathbb{R}^L$ denotes a linear operator that maps an $M \times N$ complex matrix to a length L real vector. The symbols C or c (sometimes with subscripts) refer to constant numbers, which may not refer to the same number every time they are used. The matrix $\boldsymbol{X}^*$, and the row vector $\boldsymbol{x}^*$ are obtained by taking conjugate transpose of $\boldsymbol{X}$, and column vector $\boldsymbol{x}$, respectively. In addition, $\mathcal{A}^*$ denotes the adjoint of a linear operator $\mathcal{A}$. The notations $\|\cdot\|$, $\|\cdot\|_*$, and $\|\cdot\|_F$ specify the operator, nuclear, and the Frobenius norms of matrices, respectively. Furthermore, we will use $\|\cdot\|_2$, and $\|\cdot\|_1$ to represent the vector ℓ_2, and ℓ_1 norms. A

brief overview of norms and inner products is provided in Section 2.1.

1.2 Blind deconvolution: Introduction and Motivation

In this section, we introduce the classical blind-deconvolution problem in signal processing and communications. We view this problem from a new perspective and recast it as a rank-1 matrix recovery problem, and briefly describe the conditions, developed in Chapter 3, under which the deconvolution is successful. Consider the blind-deconvolution problem: we observe the circular convolution of two unknown discrete signals $\boldsymbol{w} \in \mathbb{R}^L$ and $\boldsymbol{x} \in \mathbb{R}^L$, and want to separate them. The circular convolution of $\boldsymbol{w}$ and $\boldsymbol{x}$ is defined as

$$\boldsymbol{y} = \boldsymbol{w} * \boldsymbol{x}, \quad \text{or} \quad y[\ell] = \sum_{\ell'=1}^{L} w[\ell']x[\ell - \ell' + 1], \tag{1.2.1}$$

where the index $\ell - \ell' + 1$ in the sum above is understood to be modulo $\{1, \ldots, L\}$, and $y[\ell]$ denotes the ℓ-th entry of vector $\boldsymbol{y}$. We will specify the Fourier transform of a vector $\boldsymbol{z}$ by $\hat{\boldsymbol{z}} = \boldsymbol{F}\boldsymbol{z}$, where $\boldsymbol{F}$ is the L-point normalized discrete Fourier transform (DFT) matrix:

$$F[\omega, \ell] = \frac{1}{\sqrt{L}} \mathrm{e}^{-\mathrm{j}2\pi(\omega-1)(\ell-1)/L}, \qquad 1 \le \omega, \ell \le L,$$

and let $\boldsymbol{f}_\ell^* \in \mathbb{C}^L$ be the rows of $\boldsymbol{F}$. For a complex vector $\boldsymbol{z}$, the notation $\boldsymbol{z}^*$ represents the vector obtained by taking conjugate transpose of $\boldsymbol{z}$, and the vector $\boldsymbol{z}^{\mathrm{T}}$ denotes the row vector obtained by taking only the transpose (without conjugation). Furthermore, for vectors $\boldsymbol{x}$ and $\boldsymbol{y}$, the notation $\langle \cdot, \cdot \rangle$ signifies the standard ℓ_2 inner product defined as

$$\langle \boldsymbol{x}, \boldsymbol{y} \rangle = \boldsymbol{x}^* \boldsymbol{y},$$

and for matrices $\boldsymbol{X}$, and $\boldsymbol{Y}$, the same notation represents the matrix trace inner product:

$$\langle \boldsymbol{X}, \boldsymbol{Y} \rangle = \mathrm{Tr}\left(\boldsymbol{X}^* \boldsymbol{Y}\right),$$

where $\mathrm{Tr}\,(\cdot)$ takes a matrix and returns the sum of its diagonal entries. Using these definitions, we can write the convolution in the Fourier domain as

$$\begin{aligned}\hat{y}[\ell] &= \sqrt{L}\cdot \hat{w}[\ell]\hat{x}[\ell], \quad \ell = 1,\ldots,L \\ &= \sqrt{L}\cdot \langle \boldsymbol{f}_\ell, \boldsymbol{w}\rangle\langle \boldsymbol{f}_\ell, \boldsymbol{x}\rangle = \sqrt{L}\cdot (\boldsymbol{f}_\ell^*\boldsymbol{w})(\boldsymbol{f}_\ell^*\boldsymbol{x}),\end{aligned} \tag{1.2.2}$$

where $\hat{y}[\ell],\ \ell = 1,\ldots,L$ denote the entries of the measurement vector $\hat{\boldsymbol{y}}$. The key observation here is that although the observations $\boldsymbol{y}$ are non linear in $\boldsymbol{w}$ and $\boldsymbol{x}$, but are linear in the matrix $\boldsymbol{w}\boldsymbol{x}^T$, i.e., measurements in (1.2.2) can be equivalently written as

$$\hat{y}[\ell] = \sqrt{L}\cdot \langle \boldsymbol{f}_\ell \boldsymbol{f}_\ell^{\mathrm{T}}, \boldsymbol{w}\boldsymbol{x}^{\mathrm{T}}\rangle, \tag{1.2.3}$$

where $\boldsymbol{f}_\ell^{\mathrm{T}}$ denotes the transpose (without taking the conjugate) of the complex Fourier vector $\boldsymbol{f}_\ell$. Thus, the blind-deconvolution problem reduces to finding a rank-1 matrix $\boldsymbol{w}\boldsymbol{x}^{\mathrm{T}}$ from the observations $\hat{\boldsymbol{y}}$. However, this insight does not make the problem any easier as we are still looking to solve for an $L\times L$ unknown matrix $\boldsymbol{w}\boldsymbol{x}^{\mathrm{T}}$ form L observations. We will make a structural assumption that the length L signals live in known subspaces of $\mathbb{R}^L$ whose dimensions are K and N. That is, we can write

$$\boldsymbol{w} = \boldsymbol{B}\boldsymbol{h}, \quad \boldsymbol{h}\in\mathbb{R}^K, \qquad \boldsymbol{x} = \boldsymbol{C}\boldsymbol{m}, \quad \boldsymbol{m}\in\mathbb{R}^N \tag{1.2.4}$$

for some $L\times K$ matrix $\boldsymbol{B}$ and an $L\times N$ matrix $\boldsymbol{C}$. The columns of these matrices span the subspaces in which $\boldsymbol{w}$ and $\boldsymbol{x}$ live; recovering $\boldsymbol{h}$ and $\boldsymbol{m}$, then, is equivalent to recovering $\boldsymbol{w}$ and $\boldsymbol{x}$. Let $\hat{\boldsymbol{b}}_\ell^* = \boldsymbol{f}_\ell^*\boldsymbol{B}$ be a row vector in $\mathbb{C}^K$, and $\hat{\boldsymbol{c}}_\ell = \sqrt{L}\boldsymbol{f}_\ell^*\boldsymbol{C}$ be the column vector in $\mathbb{C}^N$, then the observations in (1.2.3) can be framed as

$$\hat{y}[\ell] = \langle \boldsymbol{A}_\ell, \boldsymbol{h}\boldsymbol{m}^*\rangle = \mathrm{Tr}\,(\boldsymbol{A}_\ell^*\boldsymbol{X}_0), \quad \boldsymbol{A}_\ell = \hat{\boldsymbol{b}}_\ell\hat{\boldsymbol{c}}_\ell^*,$$

and the unknown matrix is now a smaller $K\times N$ matrix $\boldsymbol{X}_0 = \boldsymbol{h}\boldsymbol{m}^*$. Define a linear operator $\mathcal{A}:\mathbb{R}^{K\times N}\to\mathbb{R}^L$ as

$$\mathcal{A}(\boldsymbol{X}_0) = \{\mathrm{Tr}\,(\boldsymbol{A}_\ell^*\boldsymbol{X}_0) : \ell = 1,\ldots,L\},$$

that is, the measurements of $\boldsymbol{X}_0$ can be compactly expressed as $\hat{\boldsymbol{y}} = \mathcal{A}(\boldsymbol{X}_0)$. The equivalent formulation of the blind-deconvolution problem above is then

$$\begin{array}{ll} \text{find} & \boldsymbol{X} \\ \text{subject to} & \mathcal{A}(\boldsymbol{X}) = \hat{\boldsymbol{y}} \\ & \text{rank}\,(\boldsymbol{X}) = 1 \end{array} \quad \Longleftrightarrow \quad \begin{array}{ll} \min & \text{rank}\,(\boldsymbol{X}) \\ \text{subject to} & \mathcal{A}(\boldsymbol{X}) = \hat{\boldsymbol{y}}. \end{array} \tag{1.2.5}$$

The rank minimization is intractable; however, the problem can be convexified. In Chapter 2, we will examine rank minimization, its convex relaxation, and the conditions on $\mathcal{A}$ that guarantee exact and stable recovery of $\boldsymbol{X}_0$. Figure 1 shows an experiment that illustrates that deconvolution using rank minimization works in practice.

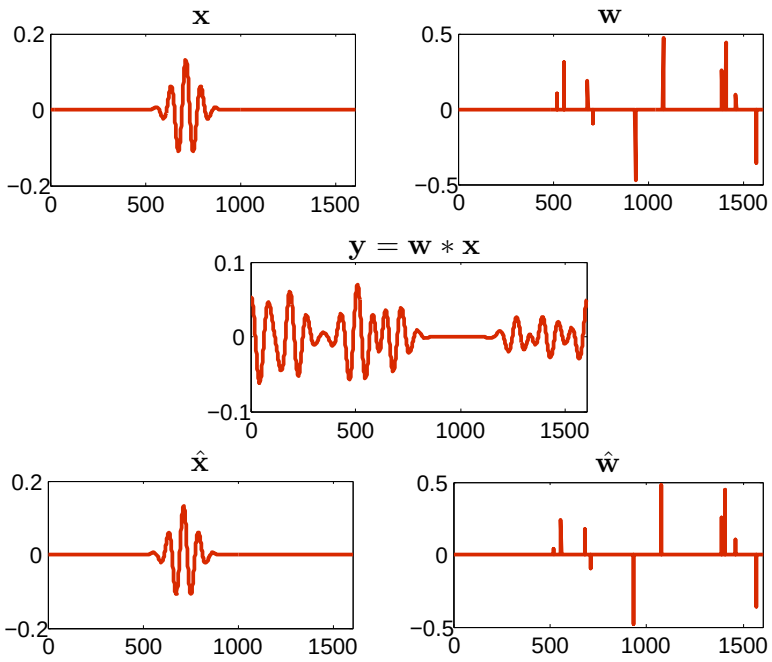

Figure 1: Rank minimization for deconvolution. Two signals $\boldsymbol{x}$ and $\boldsymbol{w}$ each of length $L = 1600$ are convolved. The support of the non-zero entries of both signals is known in advance. The number of non-zero entries of $\boldsymbol{x}$ and $\boldsymbol{w}$ are $N = 350$ and $K = 10$, respectively. The signals $\hat{\boldsymbol{x}}$ and $\hat{\boldsymbol{w}}$ are recovered exactly by observing only the convolution $\boldsymbol{w} * \boldsymbol{x}$ and solving a convex surrogate of the rank-minimization program.

The blind-deconvolution problem can be split into several cases depending upon whether the matrices $\boldsymbol{B}$ and $\boldsymbol{C}$ are deterministic or random. We will now discuss some of these cases in context of some applications.

1.2.1 Applications

In this section, we motivate the blind deconvolution with a few of its applications.

Chapter 3 considers an interesting case of the blind deconvolution; matrix $\boldsymbol{B}$ is deterministic and consists of a subset of the columns of the identity matrix, and the matrix $\boldsymbol{C}$ is random. For now, the precise distribution of the random matrix $\boldsymbol{C}$ is unimportant. Qualitatively, the results say that if both $\boldsymbol{w}$ and $\boldsymbol{x}$ have length L, $\boldsymbol{w}$ lives in a fixed subspace (spanned by the columns of $\boldsymbol{B}$) of dimension K and is spread out in the frequency domain, and $\boldsymbol{x}$ lives in a "generic" subspace chosen at random (spanned by the columns of $\boldsymbol{C}$), then $\boldsymbol{w}$ and $\boldsymbol{x}$ are separable with high probability.

This particular result has a direct application in the context of channel coding for transmitting a message over an unknown multipath channel. The problem is illustrated in Figure 2. A message vector $\boldsymbol{m} \in \mathbb{R}^N$ is encoded through an $L \times N$ encoding matrix $\boldsymbol{C}$. The protected message $\boldsymbol{x} = \boldsymbol{C}\boldsymbol{m}$ travels through a channel whose impulse response is $\boldsymbol{w}$. The receiver observes $\boldsymbol{y} = \boldsymbol{w} * \boldsymbol{x}$, and from this would like to jointly estimate the channel and determine the message that was sent. In this case, a reasonable model for the channel response $\boldsymbol{w}$ is that it is nonzero in relatively small number of known locations. Each of these entries corresponds to a different path over which the encoded message traveled; we are assuming that we know the timing delays for each of these paths, but not the fading coefficients. The matrix $\boldsymbol{B}$ in this case is a subset of columns from the identity, and the $\boldsymbol{b}_\ell$ are partial Fourier vectors. In this context, our main result on blind deconvolution in Theorem 3.1.1 tell us that a length N message can be protected against a channel with K *reflections* that is relatively flat in the frequency domain with a random code of length $L \gtrsim (K+N)\log^3(KN)$.

Essentially, we have a theoretical guarantee that we can estimate the channel without knowledge of the message from a single transmitted codeword.

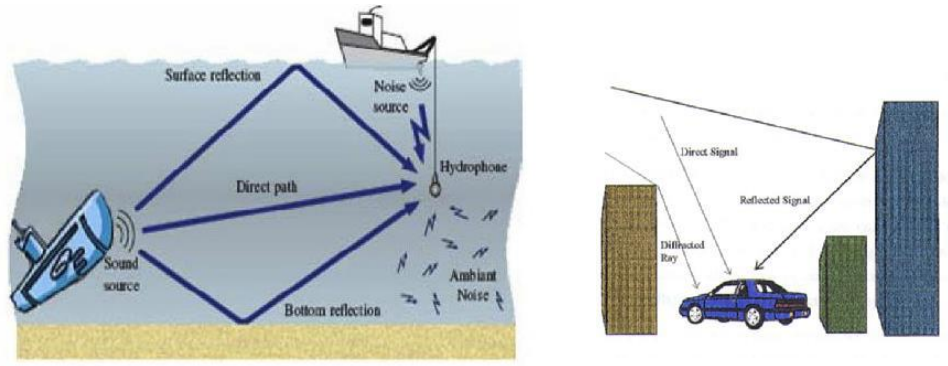

Figure 2: Example of multipath channels. (a) Underwater multipath channel (taken from http://www.doc.ic.ac.uk) (b) Multipath channel in urban environment (taken from http://en.wikipedia.org)

In another case, we can choose both $\boldsymbol{B}$ and $\boldsymbol{C}$ to be random matrices. An approach similar to the previous case confirms that if $\boldsymbol{w}$, and $\boldsymbol{x}$ live in the random subspaces spanned by the columns of $\boldsymbol{B}$, and $\boldsymbol{C}$, respectively, then $\boldsymbol{w}$, and $\boldsymbol{x}$ are separable. Suppose, the matrices $\boldsymbol{B}$ and $\boldsymbol{C}$ contain the columns of an $L \times L$ identity matrix chosen at random. Then the result in this case would mean that two sparse vectors $\boldsymbol{w}$, and $\boldsymbol{x}$ with "generic" support can be successfully deconvolved with high probability when $L \gtrsim (K+N)\log^3(KN)$.

The blind-deconvolution method introduced above is also useful for image deblurring. Figure 3 shows the result of rank minimization on image deblurring, when we have an estimate of the subspace in which the image and the blur kernel live; for details, see, Chapter 3.

The technique to convert the measurement constraints (1.2.2), quadratic in $\boldsymbol{w}$ and $\boldsymbol{x}$, into constraints that are linear in $\boldsymbol{w}\boldsymbol{x}^*$ is referred to as lifting. This technique can directly be applied to solve other interesting problems, such as solving bilinear equations and recovering phase from intensity-only measurements. These results are

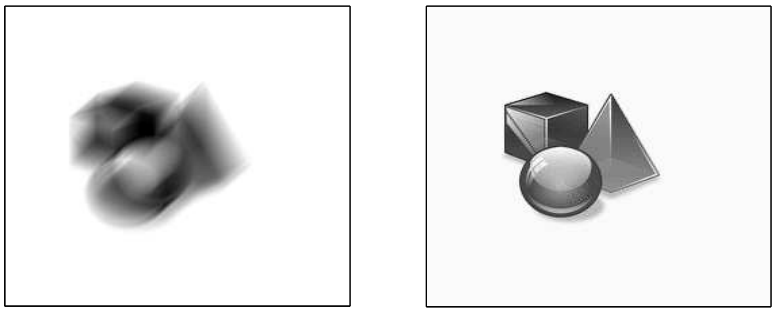

(a) (b)

Figure 3: Image deblurring. (a) Blurred Image: Convolution of *unknown* image with an *unknown* blur kernel. (b) Deblurred Image: Deconvolution using rank minimization.

briefly described below.

1.2.2 Solving systems of bilinear equations

Blind deconvolution of $\boldsymbol{w} * \boldsymbol{x}$, as is apparent from (1.2.1), is equivalent to solving a system of bilinear equations in the entries of $\boldsymbol{w}$ and $\boldsymbol{x}$. The discussion in Section 1.2 shows how this system of quadratic equations can be recast as a linear set of equations with a rank constraint. In fact, this same recasting can be used for any system of bilinear equations in $\boldsymbol{w}$ and $\boldsymbol{x}$. The reason is simple: taking the outer product of $\boldsymbol{w}$ and $\boldsymbol{x}$ produces a rank-1 matrix that contains all the different combinations of the entries of $\boldsymbol{w}$ multiplied with the entries in $\boldsymbol{x}$:

$$\boldsymbol{w}\boldsymbol{x}^* = \begin{bmatrix} w[1]x[1] & w[1]x[2] & \cdots & w[1]x[L] \\ w[2]x[1] & w[2]x[2] & \cdots & w[2]x[L] \\ \vdots & \vdots & & \vdots \\ w[L]x[1] & w[L]x[2] & \cdots & w[L]x[L] \end{bmatrix}. \tag{1.2.6}$$

Then any bilinear equation can be written as a linear combination of the entries in this matrix, and any system of equations can be written as a linear operator acting on this matrix. The subspace constraints in the blind-deconvolution problem can be interpreted as adding additional linear constraints on the matrix in (1.2.6).

The phase-retrieval problem, as will be described below, is a special case of the blind-deconvolution problem considered above. Suppose that instead of observing the element wise product of the Fourier transform of two vectors in (1.2.2), we are observing the element wise product of the Fourier transform of $\boldsymbol{x}$ and its conjugate, i.e., the measurements are

$$\begin{aligned}\hat{y}[\ell] &= \sqrt{L} \cdot \hat{x}[\ell]\hat{x}^*[\ell], \quad \ell = 1, \ldots, L \\ &= \sqrt{L} \cdot |\hat{x}[\ell]|^2 = \sqrt{L} \cdot |\langle \boldsymbol{f}_\ell, \boldsymbol{x} \rangle|^2 \\ &= \sqrt{L} \cdot (\boldsymbol{f}_\ell^* \boldsymbol{x})(\boldsymbol{f}_\ell^* \boldsymbol{x})^*.\end{aligned}$$

We are observing only the magnitude in the Fourier transform of $\boldsymbol{x}$ and our goal is to recover the lost phase component from the measurements $\hat{\boldsymbol{y}}$. This problem is referred to as the phase retrieval problem. Using the same lifting strategy as before, we can express the quadratic constraints in $\boldsymbol{x}$ as linear constraints in terms of rank-1 matrix $\boldsymbol{x}\boldsymbol{x}^*$ to obtain

$$\hat{y}[\ell] = \sqrt{L} \cdot \langle \boldsymbol{f}_\ell \boldsymbol{f}_\ell^*, \boldsymbol{x}\boldsymbol{x}^* \rangle, \quad \ell = 1, \ldots, L.$$

Recent work on *phase retrieval* [21] has used the same methodology of "lifting" a quadratic problem into a linear problem with a rank constraint to show that a vector $\boldsymbol{x} \in \mathbb{R}^N$ can be recovered from $O(N \log N)$ measurements when $\boldsymbol{x}$ is a member of a "generic" subspace, chosen at random. In particular, the results suggest that when $\boldsymbol{C}$ is random then the phase can be recovered, within a global phase factor, from phaseless measurements.

1.3 Efficient Sampling of Correlated Signals: Introduction and Motivation

An ensemble $\boldsymbol{X}_c(t) = \{x_1(t), \ldots, x_M(t)\}$ of M signals, each of which is bandlimited to $W/2$ radians per second, can be captured completely at MW samples per second. Suppose, the signals lie in a small subspace of dimension $R \ll M$, i.e., the ensemble

$\boldsymbol{X}_c(t)$ is

$$\boldsymbol{X}_c(t) = \{x_m(t) : x_m(t) \approx \sum_{r=1}^{R} A[m,r]s_r(t),\ 1 \le m \le M\},$$

where $A[m,r]$ are the entries of a matrix $\boldsymbol{A} \in \mathbb{R}^{M\times R}$. The signal structure is illustrated in Figure 4. We want to exploit the low-dimensional signal structure in the ensemble $\boldsymbol{X}_c(t)$, and come up with sampling strategies for the signal acquisition at a rate comparatively much smaller than the Nyquist rate MW. For this purpose, we will design sampling architectures using implementable components that can acquire such an ensemble at a sub-Nyquist rate [2, 3]. The problem is challenging as the matrix $\boldsymbol{A}$ is unknown, that is, we only know that the signals live in a low-dimensional subspace but the subspace itself is not known in advance. In this thesis, we pro-

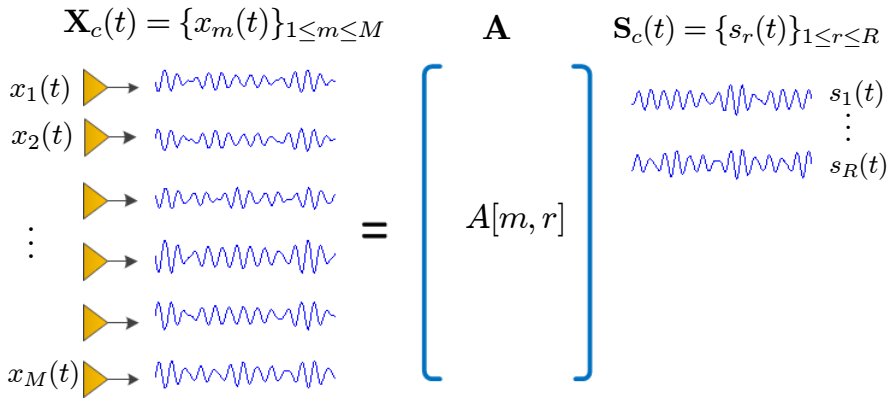

Figure 4: Acquire an ensemble of M signals, each bandlimited to $W/2$ radians per second. The signals lie in a subspace of dimension R, i.e., M signals $\{x_m(t)\}_m$ can be well approximated by the linear combination of R underlying signals $\{s_r(t)\}_r$. In other words, we can write M signals in ensemble $\boldsymbol{X}_c(t)$ (on the left) as a tall matrix $\boldsymbol{A}$ multiplied by an ensemble of R underlying independent signals.

pose several sampling architectures for the efficient sampling of correlated signals. For an introductory discussion, we will present here a particularly simple acquisition architecture; namely, the modulating multiplexer (M-Mux) shown in Figure 5. The M-Mux takes a two-step approach for signal acquisition. Briefly, in the first step, each

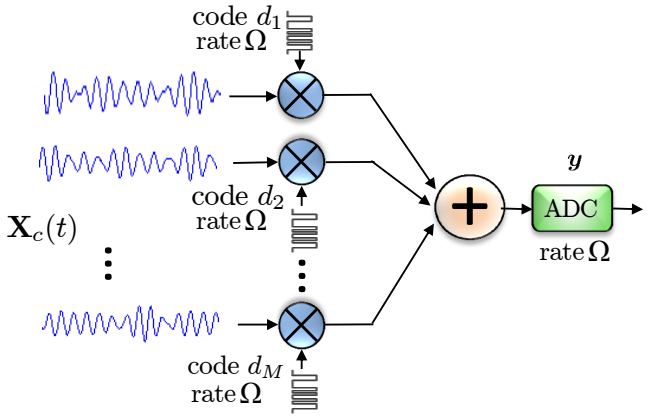

Figure 5: The M-Mux for efficient acquisition of correlated ensembles. Signals $\{x_m(t)\}_{1\leq m\leq M}$ in the ensemble $\boldsymbol{X}_c(t)$ are multiplied by independently generated random binary waveform $d_1(t), d_2(t), \cdots, d_M(t)$, respectively. The binary waveforms alternate at rate Ω. After the modulation the signals are added and sampled at rate Ω. The reconstruction algorithm uses the nuclear-norm minimization.

signal $x_m(t)$ in the ensemble is modulated with a ± 1-binary waveform $d_m(t)$ alternating at rate Ω; the modulation is performed by pointwise multiplication $x_m(t) \cdot d_m(t)$ of each signal $x_m(t)$ with the waveform $d_m(t)$. We will take $\Omega > W$, i.e., the binary waveforms are alternating at a rate greater than the Nyquist rate W. In the second step, the coded signals $x_m(t) \cdot d_m(t)$ are then added together and sampled using a single ADC at rate Ω. Define a matrix $\boldsymbol{X}_0$ with rows $\boldsymbol{x}_m \in \mathbb{R}^{\Omega}$ that contain the uniformly spaced Ω-rate samples in $t \in [0,1)$ of $x_m(t)$. The rows $\boldsymbol{x}_m$ are

$$\boldsymbol{x}_m := \{x_m(t_k) : t_k \in \{0, \frac{1}{\Omega}, \ldots, 1 - \frac{1}{\Omega}\}\}.$$

Since the signals $\boldsymbol{X}_m(t)$ live in an R-dimensional subspace, the matrix $\boldsymbol{X}_0$ is an $M \times \Omega$ matrix with rank $(\boldsymbol{X}) = R$. In addition, define

$$\boldsymbol{d}^{(m)} := \{d_m(t_k) : t_k \in \{0, \frac{1}{\Omega}, \ldots, 1 - \frac{1}{\Omega}\}\}.$$

The ω-th sample taken by the ADC in $t \in [0,1)$ is

$$y[\omega] = \sum_{m=1}^{M} d^{(m)}[\omega] x_m[\omega], \quad \omega = 1, \ldots, \Omega.$$

Let $\boldsymbol{d}_\omega = [d^{(1)}[\omega], \ldots, d^{(M)}[\omega]]^{\mathrm{T}} \in \mathbb{R}^M$. Then the sample $y[\omega]$ can be equivalently expressed as

$$y[\omega] = \langle \boldsymbol{d}_\omega \boldsymbol{e}_\omega^*, \boldsymbol{X}_0 \rangle, \quad \omega = 1, \ldots, \Omega,$$

where $\{\boldsymbol{e}_\omega\}_{1 \leq \omega \leq \Omega}$ are the standard basis vectors of dimension Ω. How many samples $y[\omega]$ are necessary for the reconstruction of the ensemble $\boldsymbol{X}_c(t)$ in the time window $t \in [0, 1)$? In other words, how many measurements $y[\omega]$ are required to recover $M \times \Omega$ matrix $\boldsymbol{X}_0$? Since $\boldsymbol{X}_0$ is of rank R, its degrees of freedom are $R(M + \Omega - R)$. As the number of measurements always obey $\Omega < R(M + \Omega - R)$, it is impossible to recover $\boldsymbol{X}_0$ from measurements $y[\omega]$. However, we can use the fact that the signals $x_m(t),\ 1 \leq m \leq M$ are bandlimited to $W/2$, that is, we can write

$$\boldsymbol{x}_m = \tilde{\boldsymbol{F}} \boldsymbol{c}_m,$$

where $\tilde{\boldsymbol{F}} : \mathbb{C}^{\Omega \times W}$ is the partial DFT matrix containing a subset of the columns of the $\Omega \times \Omega$ orthonormal DFT matrix. The selected subset of the columns corresponds to the W active frequency components in the bandlimited signals $x_m(t)$. Now define a matrix $\boldsymbol{C}_0$ with $\boldsymbol{c}_m^* \in \mathbb{C}^W$ as its rows; it follows that $\mathrm{rank}\,(\boldsymbol{C}_0) = R$. Using the fact that the signals are bandlimited, we can write the measurements $y[\omega]$ as

$$\begin{aligned} y[\omega] &= \langle \boldsymbol{d}_\omega \boldsymbol{e}_\omega^*, \boldsymbol{X}_0 \rangle = \langle \boldsymbol{d}_\omega \boldsymbol{e}_\omega^*, \boldsymbol{C}_0 \tilde{\boldsymbol{F}}^* \rangle \\ &= \langle \boldsymbol{d}_\omega \boldsymbol{e}_\omega^* \tilde{\boldsymbol{F}}, \boldsymbol{C}_0 \rangle = \langle \boldsymbol{d}_\omega \boldsymbol{f}_\omega^*, \boldsymbol{C}_0 \rangle \\ &= \mathrm{Tr}\,(\boldsymbol{A}_\omega^* \boldsymbol{C}_0)\,,\ \omega = 1, \ldots, \Omega, \end{aligned}$$

where $\boldsymbol{f}_\omega^* \in \mathbb{C}^W$ are the rows of $\tilde{\boldsymbol{F}}$. Thus, using the fact that the signals are bandlimited, we have reduced the dimension of the unknown rank R matrix to $M \times W$. Define a linear operator $\mathcal{A} : \mathbb{C}^{M \times W} \to \mathbb{R}^\Omega$ that maps $\boldsymbol{C}_0$ to measurement vector $\boldsymbol{y}$ as follows:

$$\mathcal{A}(\boldsymbol{C}_0) = \{\mathrm{Tr}\,(\boldsymbol{A}_\omega^* \boldsymbol{C}_0) : \omega = 1, \ldots, \Omega\}.$$

The measurements $\boldsymbol{y}$ are then equivalently expressed as $\boldsymbol{y} = \mathcal{A}(\boldsymbol{C}_0)$. The reconstruction of ensemble $\boldsymbol{X}_c(t)$ in $t \in [0, 1)$ follows from the recovery of $\boldsymbol{C}_0$. Recovery of

low-rank $\boldsymbol{C}_0$ from limited measurements $y[\omega]$ can be recast as the rank-minimization problem below:

$$\begin{aligned} &\text{find} \quad \boldsymbol{C} \\ &\text{subject to} \quad \mathcal{A}(\boldsymbol{C}) = \boldsymbol{y} \\ &\text{rank}\,(\boldsymbol{X}) = R \end{aligned} \qquad \Longleftrightarrow \qquad \begin{aligned} &\min \quad \text{rank}\,(\boldsymbol{C}) \\ &\text{subject to} \quad \mathcal{A}(\boldsymbol{C}) = \boldsymbol{y}. \end{aligned} \tag{1.3.1}$$

Our main results in Chapter 5 show that if we take the vectors $\boldsymbol{d}_\omega \in \mathbb{R}^M$ to be rademacher vectors with independent entries, which amounts to $d_m(t)$ being independent random binary waveforms switching their polarity after every interval of width $1/\Omega$, than the signal ensemble $\boldsymbol{X}_c(t)$ can be reconstructed exactly from the samples $\boldsymbol{y}$ with high probability when the sampling rate Ω obeys $\Omega \gtrsim R(W+M)\log^3(WM)$.

Correlated signals often arise in large sensor arrays in various signal processing applications, some of which are outlined in Chapter 4, and 5. In such applications, often the task is to estimate the signal parameters from their covariance matrix, e.g., the MUSIC algorithm in array processing uses the covariance matrix to estimate the signal parameters, such as the estimation of the angle of arrival. In several wideband signal processing applications, the sampling rate required to acquire the covariance matrix; which turns out to be a low-rank matrix, may be prohibitive. This is especially true in view of the increasing trend of using high frequency spectrum in some applications in array processing. Our proposed sampling architecture can be employed to estimate the covariance matrix of the input signal ensemble with a much fewer samples; hence, relieving the burden on the analog-to-digital converters (ADCs).

In comparison to the standard Gaussian linear operator $\mathcal{A}$ for which the corresponding $\boldsymbol{A}_i$'s are dense random matrices with iid Gaussian entries, the linear operators $\mathcal{A}$ considered in each of the context above the corresponding $\boldsymbol{A}_i$'s are formed by the outer product of two vectors, which are either random or deterministic vectors, i.e., the randomness appears in a structured form. These kind of measurement

ensembles are referred to as structured random measurement ensembles.

1.4 An Overview of the Results in the Thesis

In this thesis, we mainly study the effectiveness of convex optimization to recover low-rank matrices from structured random measurement ensembles. Our theoretical results for each of the measurement ensemble provide the number of measurements, and the incoherence conditions for the exact recovery of unknown low-rank matrix in the noiseless case. In the noisy case, we present stable recovery results, which bound the Frobenius error of the estimated matrix. The LRMR results using structured-random measurement ensembles are then applied to study the blind-deconvolution problem in signal processing and communications, and to develop efficient sampling architectures for large arrays.

The main contributions of this thesis can be broadly classified into three categories described in the following three subsections.

1.4.1 Blind deconvolution using convex programming

In Chapter 3, we consider the problem of recovering two unknown vectors, $\boldsymbol{w}$ and $\boldsymbol{x}$, of length L from their circular convolution. We make the structural assumption that the two vectors are members of known subspaces, one with dimension N and the other with dimension K. Although the observed convolution is nonlinear in both $\boldsymbol{w}$ and $\boldsymbol{x}$, it is linear in the rank-1 matrix formed by their outer product $\boldsymbol{w}\boldsymbol{x}^*$. This observation allows us to recast the deconvolution problem as low-rank matrix recovery problem from linear measurements, whose natural convex relaxation is a nuclear-norm-minimization program.

We prove the effectiveness of this relaxation by showing that for "generic" signals, the program can deconvolve $\boldsymbol{w}$ and $\boldsymbol{x}$ exactly when the maximum of N and K is almost on the order of L. That is, we show that if $\boldsymbol{x}$ is drawn from a random subspace of dimension N, and $\boldsymbol{w}$ is a vector in a subspace of dimension K whose basis vectors

are "spread out" in the frequency domain, then nuclear-norm minimization recovers $\boldsymbol{w}\boldsymbol{x}^*$ without error.

We discuss this result in the context of blind channel estimation in communications. If we have a message of length N which we code using a random $L \times N$ coding matrix, and the encoded message travels through an unknown linear time-invariant channel of maximum length K, then the receiver can recover both the channel response and the message when $L \gtrsim N + K$, to within constant and log factors.

1.4.2 Sampling architectures for compressive array processing

Chapters 4 is devoted to the design and analysis of sampling architectures for the efficient acquisition of multiple signals lying in a subspace (referred to as correlated signals). Although the signal subspace is unknown in advance, the proposed sampling architecture acquires the signals at a sub-Nyquist rate using the latent low-dimensional signal structure. Prior to sampling at a sub-Nyquist rate, the analog signals are diversified using analog preprocessing. The preprocessing step is carried out using implementable components that inject "structured" randomness into the signals. We frame the signal reconstruction from fewer samples as an LRMR problem from a limited generalized linear measurements. Our results also include a sampling theorem that provides the sufficient sampling rate for the exact reconstruction of the signals using the nuclear-norm minimization. We also discusses an application of the sampling architectures in the estimation of the covariance matrix, required for parameter estimation in several important array processing applications, from much fewer samples.

1.4.3 Compressive multiplexers for correlated signals

In Chapter 5, we propose two compressive multiplexers for the efficient sampling of ensembles of correlated signals. The proposed multiplexers acquire correlated ensembles, taking advantage of their (a priori-unknown) correlation structure, at a sub-Nyquist rate. The multiplexers are constructed using simple analog devices such as modulators and filters. We recast the reconstruction of the ensemble as an LRMR problem from generalized linear measurements. Our main theoretical results include sampling theorems that provide sufficient sampling rate for the successful reconstruction of the signal ensembles using the nuclear-norm minimization. We complete the discussion with the applications of the proposed architectures in micro-sensor arrays.

1.4.4 Sampling architectures with least-squares reconstruction

In Chapter 6, we study the randomized linear algebra for low-rank matrix factorizations. The advantage of the randomized linear algebra is that we can solve an easier least-squares program for LRMR. The least-squares program, however, requires a more restrictive class of sampling techniques compared to the nuclear-norm minimization. In particular, we need to observe the samples of the row and the column space of the unknown low-rank matrix in order to use least squares for matrix recovery; whereas, we can work with a more generalized set of samples composed of the linear combinations of the entries of the unknown low-rank matrix.

LRMR results using least squares and random samples of the row and the column space of the unknown low-rank matrix have been well-studied in the literatures. Our main contribution in Chapter 6 shows that the *structured*-random samples work just as well as the *completely*-random samples of the row and column space. Using this result, we design a new set of sampling architectures for the efficient acquisition of correlated signals. The advantage of these sampling architectures is that we can use a computationally less expensive least-squares program (compared to the nuclear-norm

minimization). Our results include the sampling theorems for each of the architecture. The sampling theorems prove the sub-Nyquist rate suffices for the successful signal reconstruction using least squares.

In particular, the results in Chapter 4, 6, and 5 indicate that we can recover an ensemble of correlated signals containing M signals composed of $R \ll M$ independent signals, each bandlimited to $W/2$ Hz, by taking $O(RW \log^q W)$ (assuming $W \geq M$) samples per second, where $q > 1$ is a small constant. All of the sampling theorems are matrix recovery results form various structured random measurement ensembles.

CHAPTER II

BACKGROUND

In Chapter 1, we introduced some of the main problems addressed in this thesis. Since the problems boil down to the recovery of a matrix with a minimum rank subject to measurement constraints, we dedicate this chapter on the development of mathematical preliminaries for the LRMR problem. We begin with an introduction to some useful vector and matrix norms that will be used in this thesis.

2.1 Vector and matrix norms

Mostly, we will be working with signals and images that are elements of a finite dimensional space, e.g., an N-dimensional Euclidean space $\mathbb{R}^N$, or $\mathbb{C}^N$. The vector norms of interest include the ℓ_1-norm of a vector $\boldsymbol{x}$: $\|\boldsymbol{x}\|_1 = |x_1| + \cdots + |x_N|$; the ℓ_2-norm of a vector $\boldsymbol{x}$: $\|\boldsymbol{x}\|_2 = \sqrt{|x_1|^2 + \cdots + |x_N|^2}$; and the ℓ_∞-norm of a vector $\boldsymbol{x}$: $\|\boldsymbol{x}\|_\infty = \max\{|x_1|, \cdots, |x_N|\}$. In general,

$$\|\boldsymbol{x}\|_p := \left(\sum_{i=1}^{N} |x_i|^p \right)^{1/p}$$

defines an ℓ_p-norm of an N-dimensional vector $\boldsymbol{x}$. Equivalence of the above mentioned norms is given by the following inequalities

$$\|\boldsymbol{x}\|_\infty \leq \|\boldsymbol{x}\|_2 \leq \|\boldsymbol{x}\|_1 \leq \sqrt{N}\|\boldsymbol{x}\|_2 \leq N\|\boldsymbol{x}\|_\infty.$$

The Euclidean space ℓ_2 is also equipped with an inner product between vectors $\boldsymbol{x}$, and $\boldsymbol{y}$, which is defined as

$$\langle \boldsymbol{x}, \boldsymbol{y} \rangle := \boldsymbol{y}^* \boldsymbol{x} = \sum_{i=1}^{N} x_i y_i^*.$$

We will be frequently using the Holder's, and the Cauchy-Schwartz inequalities, which are listed in the same order below.

$$\langle \boldsymbol{x}, \boldsymbol{y} \rangle \leq \|\boldsymbol{x}\|_1 \|\boldsymbol{y}\|_\infty \quad \langle \boldsymbol{x}, \boldsymbol{y} \rangle \leq \|\boldsymbol{x}\|_2 \|\boldsymbol{y}\|_2.$$

The vectors norms, defined above, have natural generalization to matrices. Let $\boldsymbol{X}$ be an $M \times N$ matrix, with σ_i being its i-th singular value. The rank of matrix $\boldsymbol{X}$ will be denoted by R, which is equal to the number of non zero singular values of $\boldsymbol{X}$. For matrices $\boldsymbol{X}$, and $\boldsymbol{Y}$ of same dimensions, we will often use the trace inner product

$$\langle \boldsymbol{X}, \boldsymbol{Y} \rangle := \mathrm{Tr}\left(\boldsymbol{X}^* \boldsymbol{Y}\right) = \sum_{i,j} X^*[i,j] Y[i,j].$$

The trace inner product induces the Frobenius norm $\|\cdot\|_F$, which is defined as

$$\|\boldsymbol{X}\|_F^2 := \mathrm{Tr}\left(\boldsymbol{X}^* \boldsymbol{X}\right) = \sum_{i,j} |X[i,j]|^2 = \sum_{i=1}^{R} \sigma_i^2.$$

The operator norm of $\boldsymbol{X}$ equals its largest singular value, i.e.,

$$\|\boldsymbol{X}\| := \sigma_1,$$

and finally, the nuclear norm is the sum of the singular values

$$\|\boldsymbol{X}\|_* = \sum_{i=1}^{R} \sigma_i.$$

Equivalence relation between some useful matrix norms is

$$\|\boldsymbol{X}\| \leq \|\boldsymbol{X}\|_F \leq \|\boldsymbol{X}\|_* \leq \sqrt{R} \|\boldsymbol{X}\|_F \leq R \|\boldsymbol{X}\|.$$

The Holder's and the Cauchy-Schwartz's inequalities for matrices are

$$\langle \boldsymbol{X}, \boldsymbol{Y} \rangle \leq \|\boldsymbol{X}\|_* \|\boldsymbol{Y}\|, \quad \langle \boldsymbol{X}, \boldsymbol{Y} \rangle \leq \|\boldsymbol{X}\|_F \|\boldsymbol{Y}\|_F,$$

respectively. In addition to the above mentioned matrix norms, some other useful matrix norms are $\|\boldsymbol{X}\|_\infty := \max_{i,j} |X[i,j]|$ and $\|\boldsymbol{X}\|_1 = \sum_{i,j} |X[i,j]|$.

2.2 Matrix-rank Minimization

As remarked earlier, the matrix-rank minimization often emerges in this work; therefore, we start with the rank-minimization problem subject to convex constraint set $\mathcal{C}$

$$\begin{aligned} &\min \quad \operatorname{rank}(\boldsymbol{X}) \\ &\text{subject to} \quad \boldsymbol{X} \in \mathcal{C}, \end{aligned} \tag{2.2.1}$$

where $\boldsymbol{X} : \mathbb{R}^{M \times N}$. Mainly, we will focus on the rank-minimization problem in which the feasible set is affine in $\boldsymbol{X}$, i.e., we observe limited measurements $\boldsymbol{y} = \mathcal{A}(\boldsymbol{X}_0)$ of an unknown matrix $\boldsymbol{X}_0$. Then to find a matrix with minimum rank that obeys the affine measurements constraints above, we solve

$$\begin{aligned} &\min \quad \operatorname{rank}(\boldsymbol{X}) \\ &\text{subject to} \quad \boldsymbol{y} = \mathcal{A}(\boldsymbol{X}), \end{aligned} \tag{2.2.2}$$

where linear map $\mathcal{A} : \mathbb{R}^{M \times N} \to \mathbb{R}^L$ and measurement vector $\boldsymbol{y}$ are known, and the optimization program seeks a matrix $\boldsymbol{X}$ with minimum rank in the affine space $\boldsymbol{y} = \mathcal{A}(\boldsymbol{X})$. The optimization problems in (2.2.1) and (2.2.2) are, in general, intractable, non-convex, and NP-hard problems and the complexity of the algorithms to solve these problems scales exponentially with the dimension of the matrix.

2.2.1 Convex relaxation of the rank function: Nuclear norm

To solve the minimization of rank efficiently, we can resort to the best convex relaxation of the rank function; the nuclear norm. We state here the result in [40, 42].

Theorem 2.2.1 (Theorem 1, [42])**.** *The convex envelop of the function* $\operatorname{rank}(X)$ *on the convex set*

$$\{\boldsymbol{X} \in \mathbb{R}^{M \times N} : \|\boldsymbol{X}\| \leq 1\}$$

is $\|\boldsymbol{X}\|_*$.

The proof of this statement follows from the facts that the nuclear norm is a biconjugate of the rank function on the above set, and that the biconjugate of the rank function is its convex envelop. As a result, the best convex surrogate for the minimization of the rank function subject to affine equality constraints (2.2.2) is

$$\begin{aligned} &\min \quad \|\boldsymbol{X}\|_* \\ &\text{subject to} \quad \boldsymbol{y} = \mathcal{A}(\boldsymbol{X}). \end{aligned} \tag{2.2.3}$$

In contrast to the rank-minimization problem, nuclear-norm minimization is a convex program that can be solved in polynomial time and recently many algorithms and software packages have been introduced to solve it efficiently; see, for example, [9, 11, 15–17, 66, 90]. The affine nuclear-norm minimization (2.2.3) reduces to the familiar ℓ_1 minimization subject to affine constraints when matrix $\boldsymbol{X}$ is constrained to be diagonal. The nuclear-norm minimization problem is studied extensively in last few years [19, 22, 75, 76] and the conditions under which it is guaranteed to yield the optimal solution, are characterized.

2.2.2 Formulation as an SDP

The nuclear-norm minimization can be formulated as a semi-definite program (SDP). To accomplish that, we first give here the definition of the dual norm $\|\cdot\|_d$ of a norm $\|\cdot\|$ in an inner-product space

$$\|\boldsymbol{X}\|_d := \max_{\boldsymbol{X}} \{\langle \boldsymbol{X}, \boldsymbol{Y} \rangle : \|\boldsymbol{Y}\| \leq 1\}.$$

It can be verified from the above definition that the dual norm of the nuclear norm is the operator norm, i.e.,

$$\|\boldsymbol{X}\|_* = \max_{\boldsymbol{X}} \{\mathrm{Tr}\,(\boldsymbol{X}^* \boldsymbol{Y}) : \|\boldsymbol{Y}\| \leq 1\}.$$

Using this fact, we can write the dual of the optimization program (2.2.3) as the SDP

$$\begin{aligned} \max_{\boldsymbol{X}} \quad & \mathrm{Tr}(\boldsymbol{X}^*\boldsymbol{Y}) \\ \text{s.t.} \quad & \begin{bmatrix} \boldsymbol{I}_M & \boldsymbol{Y} \\ \boldsymbol{Y}^* & \boldsymbol{I}_N \end{bmatrix} \succeq 0 \\ & \boldsymbol{y} = \mathcal{A}(\boldsymbol{X}). \end{aligned} \tag{2.2.4}$$

The dual of the above SDP [42] is

$$\begin{aligned} \min_{\boldsymbol{W}_1,\boldsymbol{W}_2,\boldsymbol{X}} \quad & \tfrac{1}{2}\mathrm{Tr}(\boldsymbol{W}_1) + \tfrac{1}{2}\mathrm{Tr}(\boldsymbol{W}_2) \\ \text{s.t.} \quad & \begin{bmatrix} \boldsymbol{W}_1 & \boldsymbol{X} \\ \boldsymbol{X}^* & \boldsymbol{W}_2 \end{bmatrix} \succeq 0 \\ & \boldsymbol{y} = \mathcal{A}(\boldsymbol{X}), \end{aligned} \tag{2.2.5}$$

which is completely equivalent to the nuclear-norm minimization program subject to the affine constraints. Standard solvers exist to solve the SDP.

2.3 Guarantees for the Success of the Nuclear-norm Minimization

In this section, we provide conditions on the linear map $\mathcal{A} : \mathbb{R}^{M\times N} \to \mathbb{R}^L$ to ensure that the solution $\tilde{\boldsymbol{X}}$ to the convex optimization program in (2.2.3) equals the unknown rank-R matrix $\boldsymbol{X}_0$ with high probability. First, we present the restricted isometry property of linear map $\mathcal{A}$ that guarantees the recovery of matrices $\boldsymbol{X}$ of rank $(X) \leq R$ using nuclear-norm minimization. Second, we will describe the dual-certificate approach to guarantee the exact recovery of $\boldsymbol{X}$ using the nuclear-norm minimization under some isometry conditions on linear map $\mathcal{A}$.

2.3.1 The restricted isometry property for low-rank matrices

We begin with the definition of the restricted isometry property (RIP) for low-rank matrices [76]. The RIP for low-rank matrices can be thought of as an extension of

the RIP for sparse vectors. In fact, it can be shown that the LRMR problem reduces to a sparse-vector recovery problem if the matrices to be recovered are restricted to be the diagonal matrices.

Definition 1. *A linear map $\mathcal{A} : \mathbb{R}^{M\times N} \to \mathbb{R}^L$ is said to satisfy the R-RIP if for every integer $1 \le R \le \min(M, N)$, we have a smallest constant δ_R such that*

$$(1 - \delta_R)\|\boldsymbol{X}\|_F \le \|\mathcal{A}(\boldsymbol{X})\|_2 \le (1 + \delta_R)\|\boldsymbol{X}\|_F$$

for all matrices of $\operatorname{rank}(X) \le R$.

The scalar δ_R is the smallest number that satisfies the above condition and it determines the behavior of $\mathcal{A}$ on the set of matrices of rank less than or equal to R. The RIP of $\mathcal{A}$ for low-rank matrices [18, 76] follows if $\mathcal{A}$ is nearly isometrically distributed.

Theorem 2.3.1 (Theorem 2.3, [18])**.** *Fix $0 \le \delta < 1$, and let $\mathcal{A}$ be a random measurement ensemble obeying the following condition: for any $\boldsymbol{X} : M \times N$, and any fixed $0 < t < 1$,*

$$\mathrm{P}\left\{|\|\mathcal{A}(\boldsymbol{X})\|_2^2 - \|\boldsymbol{X}\|_F^2| > t\|\boldsymbol{X}\|_F^2\right\} \le C\exp(-cL), \tag{2.3.1}$$

where $C, c > 0$ are constants that may depend on t. Suppose now that $L \ge D\max(M, N)R$, then $\mathcal{A}$ satisfies R-RIP for $\delta_R \le \delta$ with probability exceeding $1 - Ce^{-dL}$ for fixed constants $d, D > 0$.

This concentration statement can be extended to the matrix RIP by using a simple covering argument for the set of low-rank matrices; for details, see Theorem 2.3 in [18]. The standard Gaussian and Bernoulli measurement ensembles $\mathcal{A}$ are isometrically distributed, and hence obey the matrix RIP. We will show in Chapter 5, the matrix RIP of $\mathcal{A}$ obtained by multiplying the columns of a random multi-Toeplitz matrix with binary random variables.

Suppose, we obtain measurements $\boldsymbol{y}$

$$\boldsymbol{y} = \mathcal{A}(\boldsymbol{X}_0) \tag{2.3.2}$$

of a rank-R matrix $\boldsymbol{X}_0$, where $\mathcal{A}$ is an operator that obeys RIP. Following two theorems demonstrate the role of δ_R in establishing when the solution to the nuclear-norm minimization in (2.2.3) equals $\boldsymbol{X}_0$.

Theorem 2.3.2 (Theorem 3.2, [76]). *Suppose that $\delta_{2R} < 1$ for some integer $R \geq 1$. Then $\boldsymbol{X}_0$ is the only matrix of rank at most R satisfying $\mathcal{A}(\boldsymbol{X}) = \boldsymbol{y}$.*

The proof of this theorem follows directly from the matrix RIP.

Theorem 2.3.3 (Theorem 3.3, [76]). *Suppose that $R \geq 1$ such that $\delta_{5R} < 0.1$. Then $\tilde{\boldsymbol{X}} = \boldsymbol{X}_0$.*

The matrix RIP also guarantees stable matrix recovery in noise. Suppose, the measurement $\boldsymbol{y}$ are contaminated with noise, i.e.,

$$\boldsymbol{y} = \mathcal{A}(\boldsymbol{X}_0) + \boldsymbol{z}, \tag{2.3.3}$$

where $\boldsymbol{z}$ is the noise term such that $\|\boldsymbol{z}\|_2 \leq \delta$ holds. Then the solution $\tilde{\boldsymbol{X}}$ to the optimization program

$$\begin{aligned} &\min \quad \|\boldsymbol{X}\|_* \\ &\text{subject to} \quad \|\boldsymbol{y} - \mathcal{A}(\boldsymbol{X})\|_2 \leq \delta \end{aligned} \tag{2.3.4}$$

obeys the following theorem.

Theorem 2.3.4 (Theorem 4, [41]). *Assume that $\delta_{5R} < 0.1$, then*

$$\|\tilde{\boldsymbol{X}} - \boldsymbol{X}_0\|_F \leq C_0 . \frac{\|\boldsymbol{X}_0 - \boldsymbol{X}_{0,R}\|_*}{\sqrt{R}} + C_1 \delta,$$

where C_0 and C_1 are small constants that depend on isometry constant δ_{5R}.

The matrix $\boldsymbol{X}_{0,R}$ is the best rank-R approximation of $\boldsymbol{X}_0$. Again, the proof hinges mainly on the matrix RIP to guarantee the stable recovery. Note that the solution $\tilde{\boldsymbol{X}}$ gives the best rank-R approximation of $\boldsymbol{X}_0$ if the noise strength $\delta = 0$.

2.3.2 Duality

Suppose, matrix $\boldsymbol{X}_0 \in \mathbb{R}^{M\times N}$ is an unknown rank-R matrix and its reduced form SVD is

$$\boldsymbol{X}_0 = \boldsymbol{U}\boldsymbol{\Sigma}\boldsymbol{V}^*. \tag{2.3.5}$$

Let $T \oplus T^\perp = \mathbb{R}^{M\times N}$ be the orthogonal decomposition of the space $\mathbb{R}^{M\times N}$, where

$$T = \{\boldsymbol{Z}_1\boldsymbol{V}^* + \boldsymbol{U}\boldsymbol{Z}_2^* : \boldsymbol{Z}_1 \in \mathbb{R}^{M\times R}, \boldsymbol{Z}_2 \in \mathbb{R}^{W\times R}\}.$$

The orthogonal projections $\mathcal{P}_T$ and $\mathcal{P}_{T^\perp}$ can be defined as

$$\mathcal{P}_T(\boldsymbol{X}) = \boldsymbol{P}_U\boldsymbol{X} + \boldsymbol{X}\boldsymbol{P}_V - \boldsymbol{P}_U\boldsymbol{X}\boldsymbol{P}_V, \quad \mathcal{P}_{T^\perp}(\boldsymbol{X}) = (\boldsymbol{I}_M - \boldsymbol{P}_U)\boldsymbol{X}(\boldsymbol{I}_N - \boldsymbol{P}_V),$$

respectively.

Suppose, we measure unknown $\boldsymbol{X}_0$ using (2.3.2). Then a matrix $\boldsymbol{X}$ is optimal for (2.2.3) if there exists a dual vector $\boldsymbol{\lambda} \in \mathbb{R}^L$ such that

$$\mathcal{A}^*(\boldsymbol{\lambda}) \in \partial\|\boldsymbol{X}\|_* \quad \boldsymbol{y} = \mathcal{A}(\boldsymbol{X})$$

holds [13], where $\partial\|\boldsymbol{X}\|_*$ denotes the subdifferential of the nuclear norm at $\boldsymbol{X}$. The subgradient of the nuclear norm at $\boldsymbol{X}_0$ [62, 100] is given by

$$\partial\|\boldsymbol{X}_0\|_* = \{\boldsymbol{U}\boldsymbol{V}^* + \boldsymbol{W} : \boldsymbol{W}^*\boldsymbol{U} = 0, \boldsymbol{W}\boldsymbol{V} = 0, \quad \text{and} \quad \|\boldsymbol{W}\| \leq 1\},$$

where $\boldsymbol{U}$ and $\boldsymbol{V}$ denote the left and right singular vectors of $\boldsymbol{X}_0$, as in (2.3.5). The following lemma gives the conditions for exact recovery when solving (2.2.3); for details, see, for example [19, 44, 75].

Lemma 2.3.1. *Suppose we take the measurements of $\boldsymbol{X}_0$ as in* (2.3.2)*. The matrix $\boldsymbol{X}_0$ is the unique minimizer of* (2.2.3) *if there exists a $\boldsymbol{Y} \in$ Range$(\mathcal{A}^*)$ such that*

$$\langle \boldsymbol{U}\boldsymbol{V}^* - \mathcal{P}_T(\boldsymbol{Y}), \mathcal{P}_T(\boldsymbol{Z})\rangle - \langle \mathcal{P}_{T^\perp}(\boldsymbol{Y}), \mathcal{P}_{T^\perp}(\boldsymbol{Z})\rangle + \|\mathcal{P}_{T^\perp}(\boldsymbol{Z})\|_* > 0$$

for all $\boldsymbol{Z} \in$ Null$(\mathcal{A})$.

Proof. Let $\tilde{\boldsymbol{X}}$ denote the solution to (2.2.3). To exhibit exact recovery, it will be enough to show

$$\forall \boldsymbol{Z} \in \text{Null}(\mathcal{A}); \boldsymbol{Z} \neq \boldsymbol{0} \Rightarrow \|\boldsymbol{X}_0 + \boldsymbol{Z}\|_* > \|\boldsymbol{X}_0\|_* . \tag{2.3.6}$$

Using (2.3.6), we have

$$\boldsymbol{Z} = \tilde{\boldsymbol{X}} - \boldsymbol{X}_0 \in \text{Null}(\mathcal{A}), \tag{2.3.7}$$

and using the definition of $\tilde{\boldsymbol{X}}$

$$\|\tilde{\boldsymbol{X}}\|_* \leq \|\boldsymbol{X}_0\|_*. \tag{2.3.8}$$

Then (2.3.6), (2.3.7) and (2.3.8) imply that $\tilde{\boldsymbol{X}} = \boldsymbol{X}_0$. Now,

$$\|\boldsymbol{X}_0 + \boldsymbol{Z}\|_* - \|\boldsymbol{X}_0\|_* \geq \langle \boldsymbol{\Delta}, \boldsymbol{Z} \rangle, \quad \boldsymbol{\Delta} \in \partial \|\boldsymbol{X}_0\|_*.$$

The gradient of the nuclear norm at $\boldsymbol{X}_0$ is

$$\partial \|\boldsymbol{X}_0\|_* = \boldsymbol{U}\boldsymbol{V}^* + \mathcal{P}_{T^\perp}(\boldsymbol{W}), \quad \|\boldsymbol{W}\| \leq 1.$$

This gives us

$$\|\boldsymbol{X}_0 + \boldsymbol{Z}\|_* - \|\boldsymbol{X}_0\|_* \geq \langle \boldsymbol{U}\boldsymbol{V}^*, \boldsymbol{Z} \rangle + \langle \boldsymbol{W}, \mathcal{P}_{T^\perp}(\boldsymbol{Z}) \rangle.$$

If we maximize the second inner product w.r.t. $\|\boldsymbol{W}\| \leq 1$, then by the definition of the dual of the operator norm, we have

$$\|\boldsymbol{X}_0 + \boldsymbol{Z}\|_* - \|\boldsymbol{X}_0\|_* \geq \langle \boldsymbol{U}\boldsymbol{V}^*, \boldsymbol{Z} \rangle + \|\mathcal{P}_{T^\perp}(\boldsymbol{Z})\|_*.$$

For $\forall \boldsymbol{Y} \in \text{Range}(\mathcal{A}^*)$, we can write

$$\begin{aligned}\|\boldsymbol{X}_0 + \boldsymbol{Z}\|_* - \|\boldsymbol{X}_0\|_* &\geq \langle \boldsymbol{U}\boldsymbol{V}^* - \boldsymbol{Y}, \boldsymbol{Z} \rangle + \|\mathcal{P}_{T^\perp}(\boldsymbol{Z})\|_* \\ &= \langle \boldsymbol{U}\boldsymbol{V}^* - \mathcal{P}_T(\boldsymbol{Y}), \mathcal{P}_T(\boldsymbol{Z}) \rangle - \langle \mathcal{P}_{T^\perp}(\boldsymbol{Y}), \mathcal{P}_{T^\perp}(\boldsymbol{Z}) \rangle + \|\mathcal{P}_{T^\perp}(\boldsymbol{Z})\|_*.\end{aligned}$$

Thus, to guarantees that the solution to the nuclear norm minimization (2.2.3) is exact, it is enough to show that the R.H.S is greater than zero. This proves the lemma. □

In light of Lemma 2.3.1, it is enough to show that $\exists \boldsymbol{Y} \in \text{Range}(\mathcal{A}^*)$, which meets the condition given in the lemma. Such a $\boldsymbol{Y}$ is called the dual certificate; the geometry of the dual certificate is illustrated in Figure 6.

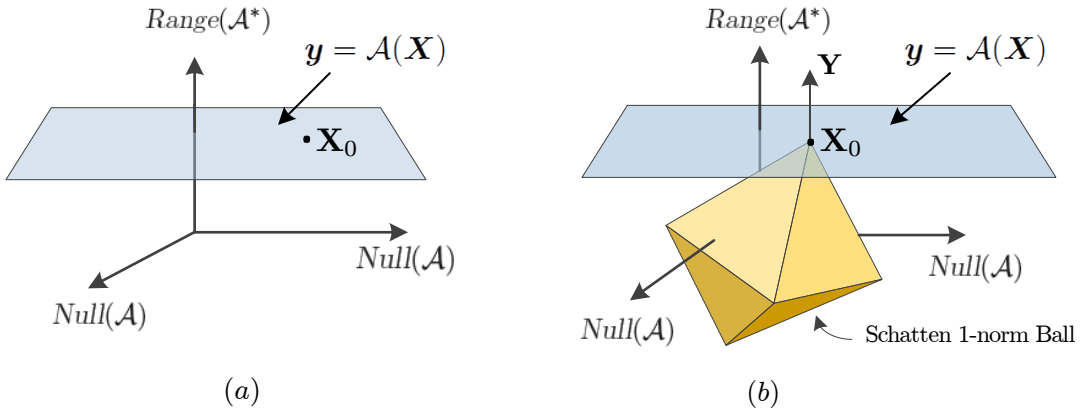

Figure 6: Geometry of the dual certificate [44]. (a) The unknown matrix $\boldsymbol{X}_0$ belongs to the linear space of dimensions $M \times N$. The axis labeled Range($\mathcal{A}^*$) signifies the range of the operator $\mathcal{A}$, and the axis labeled Null($\mathcal{A}$) specifies the orthogonal complement of Range($\mathcal{A}^*$). The set of feasible matrices forms an affine hyperplane labeled as $\boldsymbol{y} = \mathcal{A}(\boldsymbol{X})$. (b) The unknown matrix $\boldsymbol{X}_0$ is recovered by solving the nuclear norm minimization program in (2.2.3) when $\boldsymbol{X}_0$ is the unique minimizer of the nuclear norm restricted to the plane $\boldsymbol{y} = \mathcal{A}(\boldsymbol{X})$. Thus, a sufficient condition for the exact recovery is that the subgradient $\boldsymbol{Y}$ at $\boldsymbol{X}_0$ of the nuclear norm ball is perpendicular to the affine feasible set $\boldsymbol{y} = \mathcal{A}(\boldsymbol{X})$.

2.3.3 Matrix completion

In this section, we consider a specific example of LRMR; namely, the matrix-completion problem, where we *fill* in the missing entries in a matrix from the partial observation of a few randomly chosen entries. Before discussing the results of the matrix completion, we briefly investigate the incoherence requirements on the unknown matrix $\boldsymbol{X}_0$ for the matrix-completion problem to be effective. Let us write the SVD of matrix $\boldsymbol{X}_0$:

$$\boldsymbol{X}_0 = \boldsymbol{U}\boldsymbol{\Sigma}\boldsymbol{V}^*, \tag{2.3.9}$$

where $\boldsymbol{U} \in \mathbb{R}^{M\times R}$, $\boldsymbol{V} \in \mathbb{R}^{W\times R}$ are orthogonal matrices and $\boldsymbol{\Sigma} \in \mathbb{R}^{R\times R}$ is a diagonal matrix of singular values. To state the main results of matrix completion, we first need to define the coherence [19] of $\boldsymbol{X}_0$.

Definition 2 (**Coherence**, [19]). *Let $\boldsymbol{U}$, and $\boldsymbol{V}$ be as defined in* (2.3.9). *Then the coherence μ_0^2 is defined as*

$$\mu_0^2 = \max\{\frac{M}{R}\max_{1\le i\le M}\|\boldsymbol{U}^*\boldsymbol{e}_i\|_2^2, \frac{N}{R}\max_{1\le i\le N}\|\boldsymbol{V}^*\boldsymbol{e}_i\|_2^2, \frac{MN}{R}\|\boldsymbol{U}\boldsymbol{V}^*\|_\infty^2\}.$$

The coherence parameter μ_0^2 quantifies the correlation between the left, and right singular vectors of $\boldsymbol{X}_0$ with the standard basis vectors in the quantities

$$\mu^2(U) := \frac{M}{R}\max_{1\le i\le M}\|\boldsymbol{U}^*\boldsymbol{e}_i\|_2^2, \quad \mu^2(V) := \frac{N}{R}\max_{1\le i\le N}\|\boldsymbol{V}^*\boldsymbol{e}_i\|_2^2,$$

respectively. Thus, the parameters $\mu^2(U)$, and $\mu^2(V)$ are a measure of the sparsity of the singular vectors. The parameter $\mu^2(U)$ varies in the range $1 \le \mu^2(U) \le M/R$. For example, an orthonormal matrix $\boldsymbol{U}$ with each entry of magnitude $1/\sqrt{M}$ achieves $\mu^2(U) = 1$; the smallest value of the coherence parameter $\mu^2(U)$. On the other hand an orthonormal matrix that contains standard basis vectors in at least one of its columns achieves $\mu^2(U) = M/R$, the largest value of $\mu^2(U)$. Similarly, the range of parameter $\mu^2(V)$ is $1 \le \mu^2(V) \le W/R$. Also, the quantity

$$\mu^2(UV^*) := \frac{MN}{R}\|\boldsymbol{U}\boldsymbol{V}^*\|_\infty^2,$$

estimates the sparsity of the *sign* matrix $\boldsymbol{U}\boldsymbol{V}^*$ of $\boldsymbol{X}_0$. It can easily be verified that

$$1 \le \mu^2(UV^*) \le \frac{MN}{R}.$$

Also, it follows form the Cauchy-Schwartz inequality that

$$\frac{MN}{R}\|\boldsymbol{U}\boldsymbol{V}^*\|_\infty^2 \le R\mu^2(U)\mu^2(V).$$

Let $\boldsymbol{Z} \in \mathbb{R}^{M\times N}$ represent the noise perturbations and Γ be the set of cardinality $|\Gamma| = L$ selected uniformly at random from the index set $\{(i,j) \in \{1,\dots,M\}\times\{1,\dots,W\}\}$

of matrix $\boldsymbol{X}_0$. Each observation $Y[i,j]$ of matrix $\boldsymbol{X}_0$ contaminated with noise $Z[i,j]$ is

$$Y[i,j] = X_0[i,j] + Z[i,j], \quad (i,j) \in \Gamma. \tag{2.3.10}$$

Let us define an operator $\mathcal{R}_\Gamma : \mathbb{R}^{M\times N} \to \mathbb{R}^{M\times N}$ that maps a given matrix $\boldsymbol{X}$ to a new matrix with entries in the set Γ^c set to zero, i.e.,

$$\mathcal{R}_\Gamma(\boldsymbol{X}) = \begin{cases} X[i,j], & (i,j) \in \Gamma \\ 0, & (i,j) \in \Gamma^c. \end{cases} \tag{2.3.11}$$

That is, we can equivalently write (2.3.10) as

$$\boldsymbol{Y} = \mathcal{R}_\Gamma(\boldsymbol{X}_0) + \mathcal{R}_\Gamma(\boldsymbol{Z}).$$

We state here the recovery results of matrix $\boldsymbol{X}_0$ from observations $\boldsymbol{Y}$ in the noiseless and noisy case in the following Theorem.

Theorem 2.3.5 (Matrix completion, [22,27,75])**.** *Let $\boldsymbol{X}_0$ be as in* (2.3.9) *with coherence μ_0^2 defined in* (2)*. Suppose L entries of $\boldsymbol{X}_0$ are observed with locations sampled uniformly at random. Then if*

$$L \geq C\beta\mu_0^2 R \max(M,N) \log^2(\max(M,N)) \tag{2.3.12}$$

for some $\beta > 1$. Then

1. *In the noiseless case ($\mathcal{R}_\Gamma(\boldsymbol{Z}) = 0$) the minimizer $\tilde{\boldsymbol{X}}$ to the problem*

$$\begin{aligned} &\textit{minimize} \quad \|\boldsymbol{X}\|_* \\ &\textit{subject to} \quad \mathcal{R}_\Gamma(\boldsymbol{X}) = \mathcal{R}_\Gamma(\boldsymbol{X}_0) \end{aligned}$$

   is unique and equal to $\boldsymbol{X}$ with probability at least $1 - O(\max(M,N)^{-\beta})$

2. *In the noisy case with noise level $\|\mathcal{R}_\Gamma(\boldsymbol{Z})\|_F \leq \delta$, under some conditions [22] that are true provided L satisfies* (2.3.12) *with probability at least $1 - O(\max(M,N)^{-\beta})$,*

the solution $\tilde{\boldsymbol{X}}$ *to the following optimization program*

$$\begin{aligned} &\textit{minimize} && \|\boldsymbol{X}\|_* \\ &\textit{subject to} && \|\boldsymbol{Y} - \mathcal{R}_\Gamma(\boldsymbol{X})\|_F \leq \delta \end{aligned}$$

obeys

$$\|\tilde{\boldsymbol{X}} - \boldsymbol{X}_0\|_F \leq 4\sqrt{\frac{C_K \min(M,N)}{K}}\delta + 2\delta$$

with $C_K = 2 + K$*, where* K *is the fraction of the number of observed entries* L *to the total number of entries* MN *in* $\boldsymbol{X}_0$*.*

2.4 Randomized Linear Algebra for Low-rank Matrix Recovery

Nuclear-norm minimization is an effective way of LRMR from various measurement ensembles $\mathcal{A}$ such as the Gaussian measurement ensemble, the random sampling measurement ensemble in (2.3.11), the random multi-Toeplitz measurement ensemble in Chapter 3, and the random block-diagonal measurement ensemble in Chapter 4. The LRMR from limited measurements can also be achieved using randomized algorithms for partial matrix factorizations. These algorithms use random sampling to approximate the row and the column subspaces of unknown low-rank matrix $\boldsymbol{X}_0$. Given the knowledge of these subspaces, we use a matrix least-squares approach that determines the small linkage matrix to compute the estimate $\tilde{\boldsymbol{X}}$. In Chapter 6, we present matrix least-squares based sampling schemes, which will be useful for the compressive acquisition of correlated signals. In addition, we derive sampling theorems that will portray the desired sampling rate for the stable recovery of multiple signals lying in a subspace (referred to as correlated signals). In the following section, we illustrate the LRMR using least squares from limited measurements.

2.4.1 Estimation of the row and column spaces

We want to reconstruct an unknown low-rank matrix $\boldsymbol{X}_0$ of rank-R from limited measurements of its rows and column space. In particular, we observe

$$\text{Row measurements:} \quad \boldsymbol{Y}_1 = \boldsymbol{\Phi}_1 \boldsymbol{X}_0 \tag{2.4.1}$$

$$\text{Column measurements:} \quad \boldsymbol{Y}_2 = \boldsymbol{X}_0 \boldsymbol{\Phi}_2^*, \tag{2.4.2}$$

where $\boldsymbol{\Phi}_1 : \Delta \times M$, and $\boldsymbol{\Phi}_2 : \Omega \times W$ are the measurement matrices. We will study random matrices with various distributions that can be used as measurement matrices. The measurements $\boldsymbol{Y}_1$, and $\boldsymbol{Y}_2$ produce an orthonormal basis for the row and the column space of $\boldsymbol{X}_0$. As we will see later, the knowledge of the row and the column space of the unknown $\boldsymbol{X}_0$ allows us to use a convenient least-squares program for LRMR.

The randomness in the measurement matrices $\boldsymbol{\Phi}_1$, and $\boldsymbol{\Phi}_2$ plays a central role in the successful reconstruction. To see this, consider a simple example [47]: Suppose, we seek a basis for the column space of a matrix $\boldsymbol{X}_0$ of *exact* rank R. Form a vector

$$\boldsymbol{y}_i = \boldsymbol{X}_0 \boldsymbol{\phi}_i, \quad i = 1, \ldots, R,$$

where ϕ_i is a random vector. Intuitively, the vector $\boldsymbol{y}_i$ is a random sample of the column space of $\boldsymbol{X}_0$. Repeat this process R times, each time with a new choice of a random vector $\boldsymbol{\phi}_i$ to obtain a set of samples $\{\boldsymbol{y}_i : i = 1, \ldots, R\}$ of the column space of $\boldsymbol{X}_0$. Since the vectors $\{\boldsymbol{\phi}_i : i = 1, \ldots, R\}$ are independent, it is improbable that these vectors will fall into the null space of $\boldsymbol{X}_0$. This implies that the vectors $\{\boldsymbol{y}_i : i = 1, \ldots, R\}$ are also independent and span the column space of $\boldsymbol{X}_0$, and hence the basis of column space can be obtained from these samples. Exact same reasoning applies to the construction of the basis of the row space of $\boldsymbol{X}_0$.

In general, if the matrix $\boldsymbol{X}_0$ is not *exactly* rank R but is rather compressible, that is, the spectrum of the singular values of $\boldsymbol{X}_0$ decays rapidly after first R significant

singular values, then we can write such a matrix $\boldsymbol{X}_0 = \boldsymbol{Z} + \boldsymbol{\xi}$, where $\boldsymbol{Z}$ is a rank-R matrix under consideration and $\boldsymbol{\xi}$ accounts for the perturbation. Now we take the samples of the range space of $\boldsymbol{X}_0$, and we observe

$$\boldsymbol{y}_i = \boldsymbol{X}_0\boldsymbol{\phi}_i = \boldsymbol{Z}\boldsymbol{\phi}_i + \boldsymbol{\xi}\boldsymbol{\phi}_i, \quad i = 1, \ldots, R + \kappa,$$

where κ is the amount of oversampling. We are interested in the column space of $\boldsymbol{Z}$; instead, the samples $\{\boldsymbol{y}_i\}$ observed are deviated outside of the column space of $\boldsymbol{Z}$ because of the perturbation $\boldsymbol{\xi}$. Intuitively, we oversample to make sure that we cover as much of the column space of $\boldsymbol{X}_0$ as possible. As will be clear from theoretical results presented later that a small amount of oversampling, $\kappa = 5, 10$, suffices for many practical situations; for details, see [47].

2.4.2 Least squares for matrix recovery

We estimate the basis column and row spaces of $\boldsymbol{X}_0$ by computing SVDs, truncated to top R singular values, of $\boldsymbol{Y}_1$ and $\boldsymbol{Y}_2$. We factor

$$\begin{aligned} \boldsymbol{Y}_1 &\approx \boldsymbol{U}_1\boldsymbol{\Sigma}_1\boldsymbol{V}_1^* \\ \boldsymbol{Y}_2 &\approx \boldsymbol{U}_2\boldsymbol{\Sigma}_2\boldsymbol{V}_2^*, \end{aligned} \tag{2.4.3}$$

where $\boldsymbol{U}_1 : \Delta \times R$, $\boldsymbol{\Sigma}_1 : R \times R$, $\boldsymbol{V}_1 : W \times R$, $\boldsymbol{U}_2 : M \times R$, $\boldsymbol{\Sigma}_2 : R \times R$, and $\boldsymbol{V}_2 : \Omega \times R$. We will use $\boldsymbol{U}_2$ as an orthobasis for the column space of our estimate and $\boldsymbol{V}_1$ as an orthobasis for the row space of our estimate; we will take

$$\tilde{\boldsymbol{X}} = \boldsymbol{U}_2\boldsymbol{A}\boldsymbol{V}_1^*, \tag{2.4.4}$$

for some $R \times R$ matrix $\boldsymbol{A}$. We will choose $\boldsymbol{A}$ so that $\boldsymbol{\Phi}_1\tilde{\boldsymbol{X}}$ and $\tilde{\boldsymbol{X}}\boldsymbol{\Phi}_2^*$ are as close to $\boldsymbol{Y}_1$ and $\boldsymbol{Y}_2$, respectively, as possible. That is, we take

$$\begin{aligned} \tilde{\boldsymbol{A}} &= \operatorname{argmin}_{\boldsymbol{A}} \|\boldsymbol{U}_2\boldsymbol{A}\boldsymbol{V}_1^*\boldsymbol{\Phi}_2^* - \boldsymbol{Y}_2\|_F^2 + \|\boldsymbol{\Phi}_1\boldsymbol{U}_2\boldsymbol{A}\boldsymbol{V}_1^* - \boldsymbol{Y}_1\|_F^2 \\ &= \operatorname{argmin}_{\boldsymbol{A}} \|\boldsymbol{A}\boldsymbol{V}_1^*\boldsymbol{\Phi}_2^* - \boldsymbol{U}_2^*\boldsymbol{Y}_2\|_F^2 + \|\boldsymbol{\Phi}_1\boldsymbol{U}_2\boldsymbol{A} - \boldsymbol{Y}_1\boldsymbol{V}_1\|_F^2. \end{aligned} \tag{2.4.5}$$

Suppose the measurement matrices $\mathbf{\Phi}_1$, and $\mathbf{\Phi}_2$ are standard Gaussian. Then, the following theorem gives an error bound on the estimate computed using the least squares approach descried above.

Theorem 2.4.1 (Theorem 10.7, [47]). *Suppose that $\boldsymbol{X}_0$ is a real $M \times W$ matrix with singular values $\sigma_1 \geq \sigma_2 \geq \sigma_3 \geq \cdots$. Choose a target rank $R \geq 2$, and $\Delta, \Omega \geq R + \kappa$, where $\kappa \geq 4$, and $\Delta, \Omega \leq \min(M, W)$. Draw a $\Delta \times M$ standard Gaussian matrix $\mathbf{\Phi}_1$, and a $\Omega \times W$ standard Gaussian matrix $\mathbf{\Phi}_2$. Observe the measurements $\boldsymbol{Y}_1 = \mathbf{\Phi}_1 \boldsymbol{X}_0$, and $\boldsymbol{Y}_2 = \boldsymbol{X}_0 \mathbf{\Phi}_2^*$ with SVDs in* (2.4.3). *Then for all $t \geq 1$, the solution $\tilde{\boldsymbol{X}}$ to the least-squares program in* (2.4.5) *obeys*

$$\|\tilde{\boldsymbol{X}} - \boldsymbol{X}_0\|_F \leq \left(1 + t \cdot \sqrt{\frac{3R}{\kappa + 1}}\right) \left(\sum_{j>R} \sigma_j^2\right)^{1/2}$$

with failure probability at most $2t^{-\kappa}$.

The least-squares approach for LRMR is in some sense similar to the greedy algorithms for the recovery of S-sparse vector $\boldsymbol{x}$ of length N from limited measurements. In the sparse-recovery algorithms; see, for example, [72, 95], the support of non-zero entries of $\boldsymbol{x}$ is first determined and then by solving a least-squares problem on this support, one can decode $\boldsymbol{x}$. Likewise, in the LRMR, one needs to first detect the row and the column space of matrix $\boldsymbol{X}_0$. Since the dimension R of the row and the column space is much smaller than $\min(M, W)$, i.e., $R \ll \min(M, W)$, the idea is to determine the row and the column space and solve a *smaller* least-squares problem on this subspace from limited measurements [47, 101].

2.5 Concentration inequalities

This section provides an overview of concentration inequalities to bound sums of random scalar, vector, and matrix variables. Proving some of the key theoretical results in this thesis revolves around estimating the sizes of sums of these random variables using the concentration inequalities listed below. These random variables

are either the absolute value of a sum of independent random scalars, the euclidean norm of a sum of independent random vectors (or equivalently, the Frobenius norm of a sum of random matrices), or the operator norm (maximum singular value) of a sum of random linear operators. In this section, we very briefly overview the tools from probability theory that we will use to make these estimates. The essential tool is the recently developed matrix Bernstein inequality [93].

We start by recalling the classical scalar Bernstein inequality. A nice proof of the result in this form can be found in [37, Chapter 2].

Proposition 1 (Scalar Bernstein, subexponential version)**.** *Let $z_1, \dots, z_K$ be independent random variables with $\mathrm{E}[z_k] = 0$, $\sigma_k^2 := \mathrm{E}[z_k^2]$, and*

$$\mathrm{P}\left\{|z_k| > u\right\} \;\leq\; C\mathrm{e}^{-u/\sigma_k}, \tag{2.5.1}$$

for some constants C and σ_k, $k = 1, \dots, K$ with

$$\sigma^2 = \sum_{k=1}^{K} \sigma_k^2 \quad \textit{and} \quad B = \max_{1 \leq k \leq K} \sigma_k.$$

Then

$$\mathrm{P}\left\{|z_1 + \cdots + z_K| > u\right\} \;\leq\; 2\exp\left(\frac{-u^2}{2C\sigma^2 + 2Bu}\right),$$

and so

$$|z_1 + \cdots + z_K| \;\leq\; 2\max\left\{\sqrt{C}\sigma\sqrt{t + \log 2},\; 2B(t + \log 2)\right\}$$

with probability exceeding $1 - \mathrm{e}^{-t}$.

To make the statement (and usage) of the concentration inequalities more compact in the vector and matrix case, we will characterize the size of random scalars, vectors, and matrices using their Orlicz-α norms.

Definition 3. *Let $\boldsymbol{Z}$ be a random matrix. We will use $\|\cdot\|_{\psi_1}$ to denote the Orlicz-α norm:*

$$\|\boldsymbol{Z}\|_{\psi_\alpha} = \inf_{u \geq 0}\left\{\mathrm{E}[\exp(\|\boldsymbol{Z}\|^\alpha / u^\alpha)] \leq 2\right\},\; \alpha \geq 1, \tag{2.5.2}$$

where $\|\boldsymbol{Z}\|$ is the spectral norm of $\boldsymbol{Z}$.

Note that the definition above also applies when $\boldsymbol{Z}$ is a vector ($M \times 1$ matrix) as in this case the operator norm $\|\boldsymbol{Z}\|$ in (2.5.2) reduces to the ℓ_2 vector norm. Similarly, when $\boldsymbol{Z}$ specifies a scalar (1×1 matrix), the same definition applies as the operator norm is simply the absolute value of the scalar random variable.

The next basic result shows that the Orlicz-α norm of a random variable can be systematically related to the rate at which the distribution function approaches 1 (i.e. σ_k in (2.5.1)).

Lemma 2.5.1 (Lemma 2.2.1, [37]). *Let Z be a random variable which obeys $\mathrm{P}\{|X| > u\} \leq \beta \mathrm{e}^{-\gamma u^\alpha}$ for constants β and γ, and for $\alpha \geq 1$. Then $\|X\|_{\psi_\alpha} \leq ((1+\beta)/\gamma)^{1/\alpha}$.*

Following lemmas give some useful facts about the Orlicz norms.

Lemma 2.5.2 (Lemma 5.9 in [99]). *Consider a finite number Q of independent subgaussian random variable X_q. Then,*

$$\left\| \sum_{q=1}^{Q} X_q \right\|_{\psi_2}^2 \leq c \sum_{q=1}^{Q} \|X_q\|_{\psi_2}^2,$$

where c is an absolute constant.

Lemma 2.5.3 (Lemma 5.14 in [99]). *A random variable X is subgaussian iff X^2 is subexponential. Futhermore,*

$$\|X\|_{\psi_2}^2 \leq \|X^2\|_{\psi_1} \leq 2\|X\|_{\psi_2}^2.$$

Lemma 2.5.4. *Let X_1, and X_2 be two subgaussian random variables, i.e., $\|X_1\|_{\psi_2} < \infty$, and $\|X_2\|_{\psi_2} < \infty$. Then the product $X_1 X_2$ is a subexponential random variable with*

$$\|X_1 X_2\|_{\psi_1} \leq c \|X_1\|_{\psi_2} \|X_2\|_{\psi_2}.$$

Proof. For a subgaussian random variable, the tail behaviour is

$$\mathrm{P}\{|X| > t\} \leq \mathrm{e} \cdot \exp\left(\frac{-ct^2}{\|X\|_{\psi_2}^2}\right) \quad \forall t > 0;$$

see, for example, [99]. We are interested in

$$\begin{aligned}\mathrm{P}\left\{|X_1X_2|>\lambda\right\} &\leq \mathrm{P}\left\{|X_1|>t\right\}+\mathrm{P}\left\{|X_2|>\lambda/t\right\}\\ &\leq \mathrm{e}\cdot\exp\left(-ct^2/\|X_1\|_{\psi_2}^2\right)+\mathrm{e}\cdot\exp\left(-c\lambda^2/t^2\|X_2\|_{\psi_2}^2\right).\end{aligned}$$

Select $t^2=\lambda\|X_1\|_{\psi_2}/\|X_2\|_{\psi_2}$, which gives

$$\mathrm{P}\left\{|X_1X_2|>\lambda\right\}\leq 2\mathrm{e}\cdot\exp\left(-c\lambda/\|X_1\|_{\psi_2}\|X_2\|_{\psi_2}\right).$$

Now Lemma 2.2.1 in [37] imples that if a random variable Z obeys $\mathrm{P}\left\{|Z|>u\right\}\leq \alpha\mathrm{e}^{-\beta u}$, then $\|Z\|_{\psi_1}\leq(1+\alpha)/\beta$. Using this result, we obtain

$$\|X_1X_2\|_{\psi_1}\leq c\|X_1\|_{\psi_2}\|X_2\|_{\psi_2},$$

which proves the result. □

Using the Definition 3, we have a following powerful tool for bounding the size of a sum of independent random vectors or matrices. This result is mostly due to [93], but appears in the form below in [53].

Proposition 2 (Matrix Bernstein, Orlicz-norm version)**.** *Let $\boldsymbol{Z}_1,\ldots,\boldsymbol{Z}_Q$ be independent $M\times N$ random matrices with $\mathrm{E}[\boldsymbol{Z}_q]=\mathbf{0}$. Let B_α be an upper bound on the Orlicz-α norms:*

$$\max_{1\leq q\leq Q}\|\boldsymbol{Z}_q\|_{\psi_\alpha}\ \leq\ B_\alpha,$$

and define

$$\sigma^2=\max\left\{\left\|\sum_{q=1}^{Q}\mathrm{E}[\boldsymbol{Z}_q\boldsymbol{Z}_q^*]\right\|,\left\|\sum_{q=1}^{Q}\mathrm{E}[\boldsymbol{Z}_q^*\boldsymbol{Z}_q]\right\|\right\}. \tag{2.5.3}$$

Then there exists a constant C such that for all $t\geq 0$

$$\|\boldsymbol{Z}_1+\cdots+\boldsymbol{Z}_Q\|\ \leq\ C\max\left\{\ \sigma\sqrt{t+\log(M+N)},\ B_\alpha\log\left(\frac{\sqrt{Q}B_\alpha}{\sigma}\right)(t+\log(M+N))\ \right\}, \tag{2.5.4}$$

with probability at least $1-\mathrm{e}^{-t}$.

Essential to establishing some important results in this thesis is bounding both the upper and lower eigenvalues of the operator $\mathcal{A}\mathcal{A}^*$. We do this in e.g., Lemma 3.3.2 with a relatively straightforward application of the following Chernoff-like bound for sums of random positive symmetric matrices.

Proposition 3 (Matrix Chernoff [93])**.** *Let $\boldsymbol{Z}_1, \dots, \boldsymbol{Z}_Q$ be independent $M \times M$ random self-adjoint matrices whose eigenvalues obey*

$$0 \leq \lambda_{\min}(\boldsymbol{Z}_q) \leq \lambda_{\max}(\boldsymbol{Z}_q) \leq R \quad \textit{almost surely.}$$

Define

$$\rho_{\min} := \lambda_{\min}\left(\sum_{q=1}^{Q} \mathrm{E}[\boldsymbol{Z}_q]\right) \quad \textit{and} \quad \rho_{\max} := \lambda_{\max}\left(\sum_{q=1}^{Q} \mathrm{E}[\boldsymbol{Z}_q]\right).$$

Then

$$\mathrm{P}\left\{\lambda_{\min}\left(\sum_{q=1}^{Q} \boldsymbol{Z}_q\right) \leq t\rho_{\min}\right\} \;\leq\; M\,\mathrm{e}^{-(1-t)^2\rho_{\min}/2R} \quad \textit{for} \quad t \in [0,1], \tag{2.5.5}$$

and

$$\mathrm{P}\left\{\lambda_{\max}\left(\sum_{q=1}^{Q} \boldsymbol{Z}_q\right) \geq t\rho_{\max}\right\} \;\leq\; M\,\left[\frac{\mathrm{e}}{t}\right]^{t\rho_{\max}/R} \quad \textit{for} \quad t \geq \mathrm{e}. \tag{2.5.6}$$

This ends a whirlwind tour of the background material required to understand the main results in this thesis.

CHAPTER III

BLIND DECONVOLUTION USING CONVEX PROGRAMMING

3.1 Introduction

This chapter[1] considers a fundamental problem in signal processing and communications: we observe the convolution of two unknown signals, $\boldsymbol{w}$ and $\boldsymbol{x}$, and want to separate them. We will show that this problem can be naturally relaxed as a semidefinite program (SDP), in particular, a nuclear norm minimization program. We then use this fact in conjunction with recent results on recovering low-rank matrices from underdetermined linear observations to provide conditions under which $\boldsymbol{w}$ and $\boldsymbol{x}$ can be deconvolved exactly. Qualitatively, these results say that if both $\boldsymbol{w}$ and $\boldsymbol{x}$ have length L, $\boldsymbol{w}$ lives in a fixed subspace of dimension K and is spread out in the frequency domain, and $\boldsymbol{x}$ lives in a "generic" subspace chosen at random, then $\boldsymbol{w}$ and $\boldsymbol{x}$ are separable with high probability.

The general statement of the problem is as follows. We will assume that the length L signals live in known subspaces of $\mathbb{R}^L$ whose dimensions are K and N. That is, we can write

$$\boldsymbol{w} = \boldsymbol{B}\boldsymbol{h}, \quad \boldsymbol{h} \in \mathbb{R}^K$$

$$\boldsymbol{x} = \boldsymbol{C}\boldsymbol{m}, \quad \boldsymbol{m} \in \mathbb{R}^N$$

for some $L \times K$ matrix $\boldsymbol{B}$ and $L \times N$ matrix $\boldsymbol{C}$. The columns of these matrices provide bases for the subspaces in which $\boldsymbol{w}$ and $\boldsymbol{x}$ live; recovering $\boldsymbol{h}$ and $\boldsymbol{m}$, then, is equivalent to recovering $\boldsymbol{w}$ and $\boldsymbol{x}$.

[1]This chapter is taken from article "Blind Deconvolution using Convex Programming" by Ali Ahmed, Benjamin Recht, and Justin Romberg.

We observe the circular convolution of $\boldsymbol{w}$ and $\boldsymbol{x}$:

$$\boldsymbol{y} = \boldsymbol{w} * \boldsymbol{x}, \quad \text{or} \quad y[\ell] = \sum_{\ell'=1}^{L} w[\ell']x[\ell - \ell' + 1], \tag{3.1.1}$$

where the index $\ell - \ell' + 1$ in the sum above is understood to be modulo $\{1, \ldots, L\}$. It is clear that without structural assumptions on $\boldsymbol{w}$ and $\boldsymbol{x}$, there will not be a unique separation given the observations $\boldsymbol{y}$. But we will see that once we account for our knowledge that $\boldsymbol{w}$ and $\boldsymbol{x}$ lie in the span of the columns of $\boldsymbol{B}$ and $\boldsymbol{C}$, respectively, they can be uniquely separated in many situations. Detailing one such set of conditions under which this separation is unique and can be computed by solving a tractable convex program is the topic of this chapter.

3.1.1 Matrix observations

We can break apart the convolution in (3.1.1) by expanding $\boldsymbol{x}$ as a linear combination of the columns $\boldsymbol{C}_1, \ldots, \boldsymbol{C}_N$ of $\boldsymbol{C}$,

$$\begin{aligned}\boldsymbol{y} &= m(1)\boldsymbol{w} * \boldsymbol{C}_1 + m(2)\boldsymbol{w} * \boldsymbol{C}_2 + \cdots + m(N)\boldsymbol{w} * \boldsymbol{C}_N \\ &= \begin{bmatrix}\text{circ}(\boldsymbol{C}_1) & \text{circ}(\boldsymbol{C}_2) & \cdots & \text{circ}(\boldsymbol{C}_N)\end{bmatrix} \begin{bmatrix} m(1)\boldsymbol{w} \\ m(2)\boldsymbol{w} \\ \vdots \\ m(N)\boldsymbol{w} \end{bmatrix},\end{aligned}$$

where $\text{circ}(\boldsymbol{C}_n)$ corresponds to the $L \times L$ circulant matrix whose action corresponds to circular convolution with the vector $\boldsymbol{C}_n$. Expanding $\boldsymbol{w}$ as a linear combination of the columns of $\boldsymbol{B}$, this becomes

$$\boldsymbol{y} = \begin{bmatrix}\text{circ}(\boldsymbol{C}_1)\boldsymbol{B} & \text{circ}(\boldsymbol{C}_2)\boldsymbol{B} & \cdots & \text{circ}(\boldsymbol{C}_N)\boldsymbol{B}\end{bmatrix} \begin{bmatrix} m(1)\boldsymbol{h} \\ m(2)\boldsymbol{h} \\ \vdots \\ m(N)\boldsymbol{h} \end{bmatrix}. \tag{3.1.2}$$

We will find it convenient to write (3.1.2) in the Fourier domain. Let $\boldsymbol{F}$ be the L-point normalized discrete Fourier transform (DFT) matrix

$$\boldsymbol{F}(\omega,\ell) = \frac{1}{\sqrt{L}}\mathrm{e}^{-\mathrm{j}2\pi(\omega-1)(\ell-1)/L}, \qquad 1 \le \omega, \ell \le L.$$

We will use $\hat{\boldsymbol{C}} = \boldsymbol{F}\boldsymbol{C}$ for the $\boldsymbol{C}$-basis transformed into the Fourier domain, and also $\hat{\boldsymbol{B}} = \boldsymbol{F}\boldsymbol{B}$. Then $\mathrm{circ}(\boldsymbol{C}_n) = \boldsymbol{F}^*\Delta_n\boldsymbol{F}$, where Δ_n is a diagonal matrix constructed from the nth column of $\hat{\boldsymbol{C}}$, $\Delta_n = \mathrm{diag}(\sqrt{L}\hat{\boldsymbol{C}}_n)$, and (3.1.2) becomes

$$\hat{\boldsymbol{y}} = \boldsymbol{F}\boldsymbol{y} = \begin{bmatrix} \Delta_1\hat{\boldsymbol{B}} & \Delta_2\hat{\boldsymbol{B}} & \cdots & \Delta_N\hat{\boldsymbol{B}} \end{bmatrix} \begin{bmatrix} m(1)\boldsymbol{h} \\ m(2)\boldsymbol{h} \\ \vdots \\ m(N)\boldsymbol{h} \end{bmatrix}. \tag{3.1.3}$$

Clearly, recovering $\hat{\boldsymbol{y}}$ is the same as recovering $\boldsymbol{y}$.

The expansions (3.1.2) and (3.1.3) make it clear that while $\boldsymbol{y}$ is a nonlinear combination of the coefficients $\boldsymbol{h}$ and $\boldsymbol{m}$, it is a *linear* combination of the entries of their outer product $\boldsymbol{X}_0 = \boldsymbol{h}\boldsymbol{m}^*$. We can pose the blind deconvolution problem as a linear inverse problem where we want to recover a $K \times N$ matrix from observations

$$\hat{\boldsymbol{y}} = \mathcal{A}(\boldsymbol{X}_0), \tag{3.1.4}$$

through a linear operator $\mathcal{A}$ which maps $K \times N$ matrices to $\mathbb{R}^L$. For $\mathcal{A}$ to be invertible over all matrices, we need at least as many observations as unknowns, $L \ge NK$. But since we know $\boldsymbol{X}_0$ has special structure, namely that its rank is 1, we will be able to recover it from $L \ll NK$ under certain conditions on $\mathcal{A}$.

As each entry of $\hat{\boldsymbol{y}}$ is a linear combination of the entries in $\boldsymbol{h}\boldsymbol{m}^*$, we can write them as trace inner products of different $K \times N$ matrices against $\boldsymbol{h}\boldsymbol{m}^*$. Using $\hat{\boldsymbol{b}}_\ell \in \mathbb{C}^K$ for the ℓth column of $\hat{\boldsymbol{B}}^*$ and $\hat{\boldsymbol{c}}_\ell \in \mathbb{C}^N$ as the ℓth row of $\sqrt{L}\hat{\boldsymbol{C}}$, we can translate one

entry in (3.1.3) as[2]

$$\begin{aligned}\hat{y}(\ell) &= \hat{c}_\ell(1)m(1)\langle \boldsymbol{h}, \hat{\boldsymbol{b}}_\ell\rangle + \hat{c}_\ell(2)m(2)\langle \boldsymbol{h}, \hat{\boldsymbol{b}}_\ell\rangle + \cdots + \hat{c}_\ell(N)m(N)\langle \boldsymbol{h}, \hat{\boldsymbol{b}}_\ell\rangle \\ &= \langle \hat{\boldsymbol{c}}_\ell, \boldsymbol{m}\rangle\langle \boldsymbol{h}, \hat{\boldsymbol{b}}_\ell\rangle \\ &= \mathrm{Tr}\left(\boldsymbol{A}_\ell^*(\boldsymbol{h}\boldsymbol{m}^*)\right), \quad \text{where} \quad \boldsymbol{A}_\ell = \hat{\boldsymbol{b}}_\ell\hat{\boldsymbol{c}}_\ell^*. \end{aligned} \tag{3.1.5}$$

Now that we have seen that separating two signals given their convolution can be recast as a matrix recovery problem, we turn our attention to a method for solving it. In the next section, we argue that a natural way to recover the expansion coefficients $\boldsymbol{m}$ and $\boldsymbol{h}$ from measurements of the form (3.1.3) is using nuclear norm minimization.

3.1.2 Convex relaxation

The previous section demonstrated how the blind deconvolution problem can be recast as a linear inverse problem over the (nonconvex) set of rank-1 matrices. A common heuristic to convexify the problem is to use the *nuclear norm*, the sum of the singular values of a matrix, as a proxy for rank [40]. In this section, we show how this heuristic provides a natural convex relaxation.

Given $\hat{\boldsymbol{y}} \in \mathbb{C}^L$, our goal is to find $\boldsymbol{h} \in \mathbb{R}^K$ and $\boldsymbol{m} \in \mathbb{R}^N$ that are consistent with the observations in (3.1.3). Making no assumptions about either of these vectors other than the dimension, the natural way to choose between multiple feasible points is using least-squares. We want to solve

$$\min_{\boldsymbol{u},\boldsymbol{v}} \ \|\boldsymbol{u}\|_2^2 + \|\boldsymbol{v}\|_2^2 \quad \text{subject to} \quad \hat{\boldsymbol{y}}(\ell) = \langle \hat{\boldsymbol{c}}_\ell, \boldsymbol{u}\rangle\langle \boldsymbol{v}, \hat{\boldsymbol{b}}_\ell\rangle, \quad \ell = 1, \ldots, L. \tag{3.1.6}$$

This is a non-convex quadratic optimization problem. The cost function is convex, but the quadratic equality constraints mean that the feasible set is non-convex. A standard approach to solving such quadratically constrained quadratic programs is

[2]As we are now manipulating complex numbers in the frequency domain, we will need to take a little bit of care with definitions. Here and below, we use $\langle \boldsymbol{u}, \boldsymbol{v}\rangle = \boldsymbol{v}^*\boldsymbol{u} = \mathrm{Tr}\left(\boldsymbol{u}\boldsymbol{v}^*\right)$ for complex vectors $\boldsymbol{u}$ and $\boldsymbol{v}$.

to use duality (see for example [73]). A standard calculation shows that the dual of (3.1.6) is the semi-definite program (SDP)

$$\begin{aligned} \max_{\boldsymbol{\lambda}} \quad & \mathrm{Re}\langle \hat{\boldsymbol{y}}, \boldsymbol{\lambda} \rangle \\ \text{subject to} \quad & \begin{bmatrix} \boldsymbol{I} & \sum_{\ell=1}^{L} \lambda(\ell) \boldsymbol{A}_\ell \\ \sum_{\ell=1}^{L} \lambda(\ell)^* \boldsymbol{A}_\ell^* & \boldsymbol{I} \end{bmatrix} \succeq 0, \end{aligned} \tag{3.1.7}$$

with the $\boldsymbol{A}_\ell = \hat{\boldsymbol{b}}_\ell \hat{\boldsymbol{c}}_\ell^*$ defined as in the previous section. Taking the dual again will give us a convex program which is in some sense as close to (3.1.6) as possible. The dual SDP of (3.1.7) is [76]

$$\begin{aligned} \min_{\boldsymbol{W}_1, \boldsymbol{W}_2, \boldsymbol{X}} \quad & \tfrac{1}{2} \mathrm{Tr}\,(\boldsymbol{W}_1) + \tfrac{1}{2} \mathrm{Tr}\,(\boldsymbol{W}_2) \\ \text{subject to} \quad & \begin{bmatrix} \boldsymbol{W}_1 & \boldsymbol{X} \\ \boldsymbol{X}^* & \boldsymbol{W}_2 \end{bmatrix} \succeq 0 \\ & \hat{\boldsymbol{y}} = \mathcal{A}(\boldsymbol{X}), \end{aligned} \tag{3.1.8}$$

which is equivalent to

$$\begin{aligned} \min \quad & \|\boldsymbol{X}\|_* \\ \text{subject to} \quad & \hat{\boldsymbol{y}} = \mathcal{A}(\boldsymbol{X}) \end{aligned} . \tag{3.1.9}$$

That is, the nuclear norm heuristic is the "dual-dual" relaxation of the intuitive but non-convex least-squares estimation problem (3.1.6).

Our technique for untangling $\boldsymbol{w}$ and $\boldsymbol{x}$ from their convolution, then, is to take the Fourier transform of the observation $\boldsymbol{y} = \boldsymbol{w} * \boldsymbol{x}$ and use it as constraints in the program (3.1.9). That (3.1.9) is the natural relaxation is fortunate, as an entire body of literature in the field of *low-rank recovery* has arisen in the past five years that is devoted to analyzing problems of the form (3.1.9). We will build on some of the techniques from this area in establishing the theoretical guarantees for when (3.1.9) is provably effective presented in the next section.

There have also been tremendous advances in algorithms for computing the solution to optimization problems of both types (3.1.6) and (3.1.9). In Section 3.2.1,

we will briefly detail one such technique we used to solve (3.1.6) on a relatively large scale for a series of numerical experiments in Sections 3.2.2–3.2.4.

3.1.3 Main results

We can guarantee the effectiveness of (3.1.9) for relatively large subspace dimensions K and N when $\boldsymbol{B}$ is incoherent in the Fourier domain, and when $\boldsymbol{C}$ is generic. Before presenting our main analytical result, Theorem 3.1.1 below, we will carefully specify our models for $\boldsymbol{B}$ and $\boldsymbol{C}$, giving a concrete definition to the terms 'incoherent' and 'generic' in the process.

We will assume, without loss of generality, that the matrix $\boldsymbol{B}$ is an arbitrary $L \times K$ matrix with orthonormal columns:

$$\boldsymbol{B}^* \boldsymbol{B} = \hat{\boldsymbol{B}}^* \hat{\boldsymbol{B}} = \sum_{\ell=1}^{L} \hat{\boldsymbol{b}}_\ell \hat{\boldsymbol{b}}_\ell^* = \boldsymbol{I}, \tag{3.1.10}$$

where the $\hat{\boldsymbol{b}}_\ell$ are the columns of $\hat{\boldsymbol{B}}^*$, as in (3.1.5). Our results will be most powerful when $\boldsymbol{B}$ is diffuse in the Fourier domain, meaning that the $\hat{\boldsymbol{b}}_\ell$ all have similar norms. We will use the (in)coherence parameter $\mu_{\max}$ to quantify the degree to which the columns of $\boldsymbol{B}$ are jointly concentrated in the Fourier domain:

$$\mu_{\max}^2 = \frac{L}{K} \max_{1 \leq \ell \leq L} \|\hat{\boldsymbol{b}}_\ell\|_2^2. \tag{3.1.11}$$

From (3.1.10), we know that the total energy in the rows of $\hat{\boldsymbol{B}}$ is $\sum_{\ell=1}^{L} \|\hat{\boldsymbol{b}}_\ell\|_2^2 = K$, and that $\|\hat{\boldsymbol{b}}_\ell\|_2^2 \leq 1$. Thus $1 \leq \mu_{\max}^2 \leq L/K$, with the coherence taking its minimum value when the energy in $\hat{\boldsymbol{B}}$ is evenly distributed throughout its rows, and its maximum value when the energy is completely concentrated on K of the L rows. Our results will also depend on the minimum of these norms

$$\mu_{\min}^2 = \frac{L}{K} \min_{1 \leq \ell \leq L} \|\hat{\boldsymbol{b}}_\ell\|_2^2. \tag{3.1.12}$$

We will always have $0 \leq \mu_{\min}^2 \leq 1$ and $\mu_{\min}^2 \leq \mu_{\max}^2$. An example of a maximally

incoherent $\boldsymbol{B}$, where $\mu_{\max}^2 = \mu_{\min}^2 = 1$, is

$$\boldsymbol{B} = \begin{bmatrix} \boldsymbol{I}_K \\ \boldsymbol{0} \end{bmatrix}, \tag{3.1.13}$$

where $\boldsymbol{I}_K$ is the $K \times K$ identity matrix. In this case, the range of $\boldsymbol{B}$ consists of "short" signals whose first K terms may be non-zero. The matrix $\hat{\boldsymbol{B}}$ is simply the first K columns of the discrete Fourier matrix, and so every entry has the same magnitude.

Our analytic results also depend on how diffuse the particular signal we are trying to recover $\boldsymbol{w} = \boldsymbol{B}\boldsymbol{h}$ is in the Fourier domain. With $\hat{\boldsymbol{w}} = \boldsymbol{F}\boldsymbol{w} = \hat{\boldsymbol{B}}\boldsymbol{h}$, we define

$$\mu_h^2 = L \max_{1 \le \ell \le L} |\hat{w}(\ell)|^2 = L \cdot \max_{1 \le \ell \le L} |\langle \boldsymbol{h}, \hat{\boldsymbol{b}}_\ell \rangle|^2. \tag{3.1.14}$$

Note that it is always the case that $1 \le \mu_h^2 \le \mu_{\max}^2 K$. The lower bound follows from the Cauchy-Schwartz's inequality, i.e.,

$$\mu_h^2 \le L \cdot \max_{1 \le \ell \le L} \|\hat{\boldsymbol{b}}_\ell\|_2^2 \|\boldsymbol{h}\|_2^2 \le K \mu_{\max}^2,$$

where the last inequality is the result of (3.1.11), and $\|\boldsymbol{h}\|_2 = 1$. To show the lower bound of μ_h^2, take a summation over ℓ on both sides

$$\sum_{\ell=1}^{L} \mu_h^2 = L \sum_{\ell=1}^{L} \max_{1 \le \ell \le L} |\langle \boldsymbol{h}, \hat{\boldsymbol{b}}_\ell \rangle|^2,$$

which means

$$\mu_h^2 \ge \sum_{\ell=1}^{L} |\langle \boldsymbol{h}, \hat{\boldsymbol{b}}_\ell \rangle|^2 = \|\boldsymbol{h}\|_2^2 = 1,$$

where the equality is true because $\hat{\boldsymbol{B}}$ is a matrix with orthonormal columns. As an illustration, if $\boldsymbol{B}$ is as in (3.1.13) (i.e., $\hat{\boldsymbol{B}}$ is the partial Fourier matrix), then μ_h^2 quantifies the dispersion of $\boldsymbol{w}$ in the frequency domain. In particular, if the signal $\boldsymbol{w}$ is more or less "flat" in the frequency domain, then μ_h^2 will be a small constant.

With the subspace in which $\boldsymbol{w}$ resides fixed, we will show that separating $\boldsymbol{w}$ and $\boldsymbol{x} = \boldsymbol{C}\boldsymbol{m}$ will be possible for "most" choices of the subspace $\boldsymbol{C}$ of a certain dimension

N — we do this by choosing the subspace at random from an isotropic distribution, and show that (3.1.9) is successful with high probability. For the remainder of the chapter, we will take the entries of $\boldsymbol{C}$ to be independent and identically distributed random variables,

$$C[\ell, n] \ \sim \ \text{Normal}(0, L^{-1}).$$

In the Fourier domain, the entries of $\hat{\boldsymbol{C}}$ will be complex Gaussian, and its columns will have conjugate symmetry (since the columns of $\boldsymbol{C}$ are real). Specifically, the rows of $\hat{\boldsymbol{C}}$ will be distributed as[3]

$$\hat{\boldsymbol{c}}_\ell \sim \begin{cases} \text{Normal}(0, \boldsymbol{I}) & \ell = 1 \\ \text{Normal}(0, 2^{-1/2}\boldsymbol{I}) + \text{jNormal}(0, 2^{-1/2}\boldsymbol{I}) & \ell = 2, \ldots, L/2+1 \end{cases}, \qquad (3.1.15)$$

$$\hat{\boldsymbol{c}}_\ell = \hat{\boldsymbol{c}}_{L-\ell+2}, \quad \text{for} \ \ \ell = L/2+2, \ldots, L.$$

Similar results to those we present here most likely hold for other models for $\boldsymbol{C}$. The key property that our analysis hinges critically on is the rows $\hat{\boldsymbol{c}}_\ell$ of $\hat{\boldsymbol{C}}$ are *independent* — this allows us to apply recently developed tools for estimating the spectral norm of a sum of independent random linear operators.

We now state our main result:

Theorem 3.1.1. *Suppose the bases $\boldsymbol{B}, \boldsymbol{C}$ and expansion coefficients $\boldsymbol{h}, \boldsymbol{m}$ satisfy the conditions* (3.1.10)*,* (3.1.11)*,* (3.1.14)*, and* (3.1.15) *above. Fix $\alpha \geq 1$. Then there exists a constant*[4] *$C_\alpha = O(\alpha)$ depending only on α, such that if*

$$\max\left(\mu_{\max}^2 K, \ \mu_h^2 N\right) \ \leq \ \frac{L}{C_\alpha \log^3 L}, \qquad (3.1.16)$$

then $\boldsymbol{X}_0 = \boldsymbol{h}\boldsymbol{m}^*$ is the unique solution to (3.1.9) *with probability $1 - O(L^{-\alpha+1})$.*

When the coherences are low, meaning that $\mu_{\max}$ and μ_h are on the order of a

[3] We are assuming here that L is even; the argument is straightforward to adapt to odd L.

[4] *Throughout the manuscript we will use the notation C_α to denote a constant which depends only on the probability exponent α. Its value may be different from instantiation to instantiation.*

constant, then (3.1.16) is tight to within a logarithmic factor, as we always have $\max(K, N) \leq L$.

While Theorem 3.1.1 establishes theoretical guarantees for specific types of subspaces specified by $\boldsymbol{B}$ and $\boldsymbol{C}$, we have found that treating blind deconvolution as a linear inverse problem with a rank constraint leads to surprisingly good results in many situations; see, for example, the image deblurring experiments in Section 3.2.4.

The recovery can also be made stable in the presence of noise, as described by our second theorem:

Theorem 3.1.2. *Let $\boldsymbol{X}_0 = \boldsymbol{h}\boldsymbol{m}^*$ and $\mathcal{A}$ as in* (3.1.4) *with N, K, L obeying* (3.1.16)*. We observe*

$$\hat{\boldsymbol{y}} = \mathcal{A}(\boldsymbol{X}_0) + \boldsymbol{z},$$

where $\boldsymbol{z} \in \mathbb{R}^L$ is an unknown noise vector with $\|\boldsymbol{z}\|_2 \leq \delta$, and estimate $\boldsymbol{X}_0$ by solving

$$\begin{array}{ll} \text{min} & \|\boldsymbol{X}\|_* \\ \text{subject to} & \|\hat{\boldsymbol{y}} - \mathcal{A}(\boldsymbol{X})\|_2 \leq \delta \end{array}. \tag{3.1.17}$$

Let $\lambda_{\min}$ be the smallest non-zero eigenvalue of $\mathcal{A}\mathcal{A}^*$, and $\lambda_{\max}$ be the largest. Then with the same probability $1 - L^{-\alpha+1}$ as in Theorem 3.1.1 the solution $\tilde{\boldsymbol{X}}$ to (3.1.17) *will obey*

$$\|\tilde{\boldsymbol{X}} - \boldsymbol{X}_0\|_F \;\leq\; C\,\frac{\lambda_{\max}}{\lambda_{\min}}\sqrt{\min(K, N)}\,\delta, \tag{3.1.18}$$

for a fixed constant C.

The program in (3.1.17) is also convex, and is solved with numerical techniques similar to the equality constrained program in (3.1.9). The performance bound relies on the conditioning of $\mathcal{A}\mathcal{A}^*$. Lemma 3.3.2 below tells us that when $\mathcal{A}$ is sufficiently underdetermined,

$$NK \;\geq\; \frac{C_\alpha}{\mu_{\min}^2}\, L \log^2 L, \tag{3.1.19}$$

then with high probability we can replace the ratio of eigenvalues in (3.1.18) with the ratio of coherence parameters for $\hat{\boldsymbol{B}}$, as

$$\frac{\lambda_{\max}}{\lambda_{\min}} \sim \frac{\mu_{\max}}{\mu_{\min}}.$$

For L large enough, there will be many N and K which satisfy (3.1.19) and (3.1.16) simultaneously.

In the end, we are interested in how well we recover $\boldsymbol{x}$ and $\boldsymbol{w}$. The stability result for $\boldsymbol{X}_0$ can easily be extended to a guarantee for the two unknown vectors.

Corollary 1. *Let $\tilde{\sigma}_1\tilde{\boldsymbol{u}}_1\tilde{\boldsymbol{v}}_1$ be the best rank-1 approximation to $\tilde{\boldsymbol{X}}$, and set $\tilde{\boldsymbol{h}} = \sqrt{\tilde{\sigma}_1}\tilde{\boldsymbol{u}}_1$ and $\tilde{\boldsymbol{m}} = \sqrt{\tilde{\sigma}_1}\tilde{\boldsymbol{v}}_1$. Set $\tilde{\delta} = \|\tilde{\boldsymbol{X}} - \boldsymbol{X}_0\|_F$. Then there exists a constant C such that*

$$\|\boldsymbol{h} - \alpha\tilde{\boldsymbol{h}}\|_2 \leq C \min\left(\tilde{\delta}/\|\boldsymbol{h}\|_2, \|\boldsymbol{h}\|_2\right), \qquad \|\boldsymbol{m} - \alpha^{-1}\tilde{\boldsymbol{m}}\|_2 \leq C \min\left(\tilde{\delta}/\|\boldsymbol{m}\|_2, \|\boldsymbol{m}\|_2\right).$$

for some scalar multiple α.

Proof of this corollary follows the exact same line of reasoning as the later part of Theorem 1.2 in [21].

3.1.4 Relationship to phase retrieval and other quadratic problems

Blind deconvolution of $\boldsymbol{w} * \boldsymbol{x}$, as is apparent from (3.1.1), is equivalent to solving a system of quadratic equations in the entries of $\boldsymbol{w}$ and $\boldsymbol{x}$. The discussion in Section 3.1.1 shows how this system of quadratic equations can be recast as a linear set of equations with a rank constraint. In fact, this same recasting can be used for any system of quadratic equations in $\boldsymbol{w}$ and $\boldsymbol{x}$. The reason is simple: taking the outer product of the concatenation of $\boldsymbol{w}$ and $\boldsymbol{x}$ produces a rank-1 matrix that contains all the different combinations of entries of $\boldsymbol{w}$ multiplied with each other and multiplied

by entries in $\boldsymbol{x}$:

$$\begin{bmatrix} \boldsymbol{w} \\ \boldsymbol{x} \end{bmatrix} \begin{bmatrix} \boldsymbol{w}^* & \boldsymbol{x}^* \end{bmatrix} = \left[\begin{array}{cccc|cccc} w[1]^2 & w[1]w[2] & \cdots & w[1]w[L] & w[1]x[1] & w[1]x[2] & \cdots & w[1]x[L] \\ w[2]w[1] & w[2]^2 & \cdots & w[2]w[L] & w[2]x[1] & w[2]x[2] & \cdots & w[2]x[L] \\ \vdots & & & & \vdots & & \vdots & \\ w[L]w[1] & w[L]w[2] & \cdots & w[L]^2 & w[L]x[1] & w[L]x[2] & \cdots & w[L]x[L] \\ \hline x[1]w[1] & x[1]w[2] & \cdots & x[1]w[L] & x[1]^2 & x[1]x[2] & \cdots & x[1]x[L] \\ x[2]w[1] & x[2]w[2] & \cdots & x[2]w[L] & x[2]x[1] & x[2]^2 & \cdots & x[2]x[L] \\ \vdots & & & & \vdots & & \vdots & \\ x[L]w[1] & x[L]w[2] & \cdots & x[L]w[L] & x[L]x[1] & x[L]x[2] & \cdots & x[L]^2 \end{array}\right]. \tag{3.1.20}$$

Then any quadratic equation can be written as a linear combination of the entries in this matrix, and any system of equations can be written as a linear operator acting on this matrix. For the particular problem of blind deconvolution, we are observing sums along the skew-diagonals of the matrix in the upper right-hand (or lower left-hand) quadrant. Incorporating the subspace constraints allows us to work with the smaller $K \times N$ matrix $\boldsymbol{h}\boldsymbol{m}^*$, but this could also be interpreted as adding additional linear constraints on the matrix in (3.1.20).

Recent work on *phase retrieval* [21] has used this same methodology of "lifting" a quadratic problem into a linear problem with a rank constraint to show that a vector $\boldsymbol{w} \in \mathbb{R}^N$ can be recovered from $O(N \log N)$ measurements of the form $|\langle \boldsymbol{w}, \boldsymbol{a}_n \rangle|^2$ for $\boldsymbol{a}_n$ selected uniformly at random from the unit sphere. In this case, the measurements are being made entirely in the upper left-hand (or lower-right hand) quadrant in (3.1.20), and the measurements in (3.1.5) have the form $\boldsymbol{A}_n = \boldsymbol{a}_n \boldsymbol{a}_n^*$. In fact, another way to interpret the results in [21] is that if a signal of length L is known to live in a generic subspace of dimension $\sim L/\log L$, then it can be recovered from an observation of a convolution with itself. Phase retrieval using convex programming was also explored in [32, 70]

In the current work, we are considering a non-symmetric rank-1 matrix being measured by matrices $\hat{\boldsymbol{b}}_\ell \hat{\boldsymbol{c}}_\ell^*$ formed by the outer product of two different vectors, one of which is random, and one of which is fixed. Another way to cast the problem, which perhaps brings these differences into sharper relief, is that we are measuring the symmetric matrix in (3.1.20) by taking inner products against rank-two matrices $\frac{1}{2}\left(\begin{bmatrix}\hat{\boldsymbol{b}}_\ell \\ \mathbf{0}\end{bmatrix}\begin{bmatrix}\mathbf{0} & \hat{\boldsymbol{c}}_\ell^*\end{bmatrix} + \begin{bmatrix}\mathbf{0} \\ \hat{\boldsymbol{c}}_\ell\end{bmatrix}\begin{bmatrix}\hat{\boldsymbol{b}}_\ell^* & \mathbf{0}\end{bmatrix}\right)$. These seemingly subtle differences lead to a much different mathematical treatment.

3.1.5 Application: Multipath channel protection using random codes

The results in Section 3.1.3 have a direct application in the context of channel coding for transmitting a message over an unknown multipath channel. The problem is illustrated in Figure 7. A message vector $\boldsymbol{m} \in \mathbb{R}^N$ is encoded through an $L \times N$ encoding matrix $\boldsymbol{C}$. The protected message $\boldsymbol{x} = \boldsymbol{C}\boldsymbol{m}$ travels through a channel whose impulse response is $\boldsymbol{w}$. The receiver observes $\boldsymbol{y} = \boldsymbol{w} * \boldsymbol{x}$, and from this would like to jointly estimate the channel and determine the message that was sent.

In this case, a reasonable model for the channel response $\boldsymbol{w}$ is that it is nonzero in relatively small number of known locations. Each of these entries corresponds to a different path over which the encoded message traveled; we are assuming that we know the timing delays for each of these paths, but not the fading coefficients. The matrix $\boldsymbol{B}$ in this case is a subset of columns from the identity, and the $\hat{\boldsymbol{b}}_\ell$ are partial Fourier vectors. This means that the coherence $\mu_{\max}$ in (3.1.11) takes its minimal value of $\mu_{\max}^2 = 1$, and the coherence μ_h^2 in (3.1.14) has a direct interpretation as the peak-value of the (normalized) frequency response of the unknown channel. The resulting linear operator $\mathcal{A}$ corresponds to a matrix comprised of N $L \times K$ random Toeplitz matrices, as shown in Figure 8. The first column of each of these matrices corresponds to a columns of $\boldsymbol{C}$. The formulation of this problem as a low-rank matrix recovery program was proposed in [7], which presented some first numerical

experiments.

In this context, Theorem 3.1.1 tell us that a length N message can be protected against a channel with K *reflections* that is relatively flat in the frequency domain with a random code whose length L obeys $L/\log^3 L \gtrsim (K+N)$. Essentially, we have a theoretical guarantee that we can estimate the channel without knowledge of the message from a single transmitted codeword.

It is instructive to draw a comparison in to previous work which connected error correction to structured solutions to underdetermined systems of equations. In [23, 82], it was shown that a message of length N could be protected against corruption in K unknown locations with a code of length $L \gtrsim N + K\log(N/K)$ using a random codebook. This result was established by showing how the decoding problem can be recast as a sparse estimation problem to which results from the field of compressed sensing can be applied.

For multipath protection, we have a very different type of corruption: rather than individual entries of the transmitted vector being tampered with, instead we observe overlapping copies of the transmission. We show that with the same type of codebook (i.e. entries chosen independently at random) can protect against K reflections during transmission, where the timing of these bounces is known (or can be reasonably estimated) but the fading coefficients (amplitude and phase change associated with each reflection) are not.

3.1.6 Other related work

As it is a ubiquitous problem, many different approaches for blind deconvolution have been proposed in the past, each using different statistical or deterministic models tailored to particular applications. A general overview for blind deconvolution techniques in imaging (including methods based on parametric modeling of the inputs and incorporating spatial constraints) can be found in [55]. An example of a

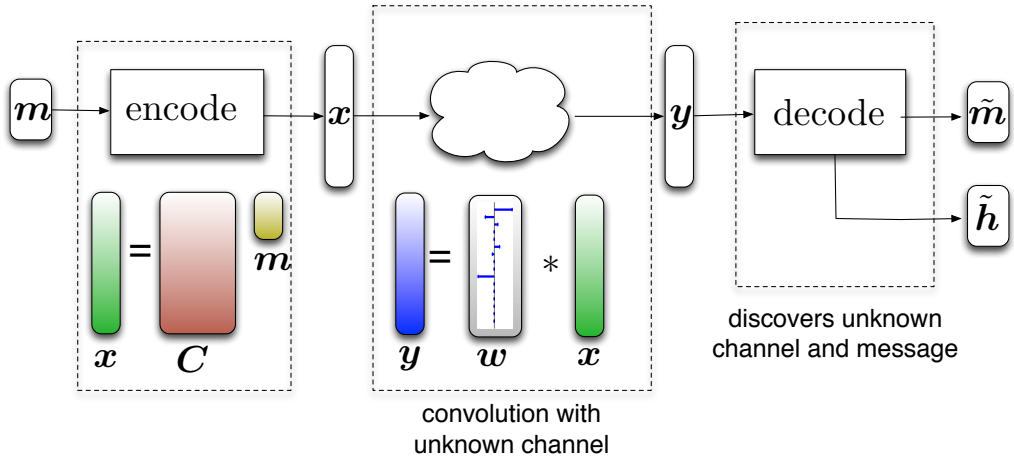

Figure 7: Overview of the channel protection problem. A message $\boldsymbol{m}$ is encoded by applying a tall matrix $\boldsymbol{C}$; the receiver observes the encoded message convolved with an unknown channel response $\boldsymbol{w} = \boldsymbol{B}\boldsymbol{h}$, where $\boldsymbol{B}$ is a subset of columns from the identity matrix. The decoder is faced with the task of separating the message and channel response from this convolution, which is a nonlinear combination of $\boldsymbol{h}$ and $\boldsymbol{m}$.

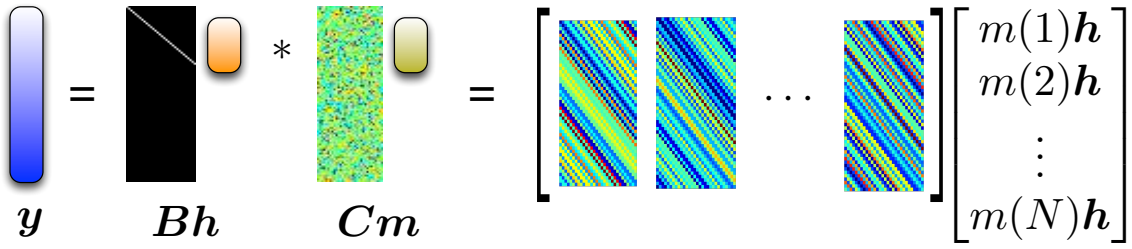

Figure 8: The multi-toeplitz matrix corresponding to the multipath channel protection problem in Section 3.1.5. In this case, the columns of $\boldsymbol{B}$ are sampled from the identity, the entries of $\boldsymbol{C}$ are chosen to be iid Gaussian random variables, and the corresponding linear operator $\mathcal{A}$ is formed by concatenating N $L \times K$ random Toeplitz matrices, each of which is generated by a column of $\boldsymbol{C}$.

more modern method can be found in [31], where it is demonstrated how an image, which is expected to have small total-variation with respect to its energy, can be effectively deconvolved from an unknown kernel with known compact support. In [61], a maximum-a-posteriori (MAP) based scheme is analyzed for image deblurring; the article illustrates the shortcomings of imposing sparsity enforcing priors on the gradients of natural images, and presents an alternative MAP estimator to recover only the blur kernel and then uses it to deblur the image. In wireless communications, knowledge of the modulation scheme [83] or an estimate of the statistics of the source signal [92] have been used for blind channel identification; these methods are overviewed in the review papers [43, 51, 64, 91]. An effective scheme based on a deterministic model was put forth in [102], where fundamental conditions for being able to identify multichannel responses from cross-correlations are presented. The work in this chapter differs from this previous work in that it relies only on a single observation of two convolved signals, the model for these signals is that they lie in known (but arbitrary) subspaces rather than have a prescribed length, and we give a concrete relationship between the dimensions of these subspaces and the length of the observation sufficient for perfect recovery.

Recasting the quadratic problem in (3.1.1) as the linear problem with a rank constraint in (3.1.5) is appealing since it puts the problem in a form for which we have recently acquired a tremendous amount of understanding. Recovering a $N \times K$ rank-R matrix from a set of linear observations has primarily been considered in two scenarios. In the case where the observations come through a random projection, where either the $\boldsymbol{A}_\ell$ are filled with independent Gaussian random variables or $\mathcal{A}$ is an orthoprojection onto a randomly chosen subspace, the nuclear norm minimization program in (3.1.9) is successful with high probability when [18, 76]

$$L \;\geq\; \text{Const} \cdot R \max(K, N).$$

When the observations are randomly chosen entries in the matrix, then subject to

incoherence conditions on the singular vectors of the matrix being measured, the number of samples sufficient for recovery, again with high probability, is [19, 22, 44, 75]

$$L \;\geq\; \text{Const} \cdot R \max(K, N) \log^2(\max(K, N)).$$

Our main result in Theorem 3.1.1 uses a completely different kind measurement system which exhibits a type of *structured randomness*; for example, when $\boldsymbol{B}$ has the form (3.1.13), $\mathcal{A}$ has the concatenated Toeplitz structure shown in Figure 8. In this chapter, we will only be concerned with how well this type of operator can recover rank-1 matrices, ongoing work has shown that it also effectively recover general low-rank matrices [2].

While this chapter is only concerned with recovery by nuclear norm minimization, other types of recovery techniques have proven effective both in theory and in practice; see for example [52, 53, 60]. It is possible that the guarantees given in this chapter could be extended to these other algorithms.

As we will see below, our mathematical analysis has mostly to do how matrices of the form in (3.1.2) act on rank-2 matrices in a certain subspace. Matrices of this type have been considered in the context of sparse recovery in the compressed sensing literature for applications including multiple-input multiple-output channel estimation [78], multi-user detection [6], and multiplexing of spectrally sparse signals [88].

3.2 Numerical Simulations

In this section, we illustrate the effectiveness of the reconstruction algorithm for the blind deconvolution of vectors $\boldsymbol{x}$ and $\boldsymbol{w}$ with numerical experiments[5]. In particular, we study phase diagrams, which demonstrate the empirical probability of success over a range of dimensions N and K for a fixed L; an image deblurring experiment,

[5]MATLAB code that reproduces all of the experiments in this section is available at `http://www.aliahmed.org/code.html`.

where the task is to recover an image blurred by an unknown blur kernel; a channel protection experiment, where we show the robustness of our algorithm in the presence of additive noise.

Some of the numerical experiments presented below are "large scale", with thousands (and even 10s of thousands) of unknown variables. Recent advances in SDP solvers, which we discuss in the following subsection, make the solution of such problems computationally feasible.

3.2.1 Large-scale solvers

To solve the semidefinite program (3.1.8) on instances where K and M are of practical size, we rely on the heuristic solver developed by Burer and Monteiro [15]. To implement this solver, we perform the variable substitution

$$\begin{bmatrix} \boldsymbol{H} \\ \boldsymbol{M} \end{bmatrix} \begin{bmatrix} \boldsymbol{H} \\ \boldsymbol{M} \end{bmatrix}^* = \begin{bmatrix} \boldsymbol{W}_1 & \boldsymbol{X} \\ \boldsymbol{X}^* & \boldsymbol{W}_2 \end{bmatrix}$$

where $\boldsymbol{H}$ is $K \times r$ and $\boldsymbol{M}$ is $N \times r$ for $r > 1$. Under this substitution, the semidefinite constraint is always satisfied and we are left with the nonlinear program:

$$\min_{\boldsymbol{M},\boldsymbol{H}} \ \|\boldsymbol{M}\|_F^2 + \|\boldsymbol{H}\|_F^2 \quad \text{subject to} \quad \hat{\boldsymbol{y}} = \mathcal{A}(\boldsymbol{H}\boldsymbol{M}^*), \quad \ell = 1, \ldots, L. \tag{3.2.1}$$

When $r = 1$, this reformulated problem is equivalent to (3.1.6). Burer and Monteiro showed that provided r is bigger than the rank of the optimal solution of (3.1.8), all of the local minima of (3.2.1) are global minima of (3.1.8) [16]. Since we expect a rank one solution, we can work with $r = 2$, declaring recovery when a rank deficient $\boldsymbol{M}$ or $\boldsymbol{H}$ is obtained. Thus, by doubling the size of the decision variable, we can avoid the non-global local solutions of (3.1.6). Burer and Monteiro's algorithm has had notable success in matrix completion problems, enabling some of the fastest solvers for nuclear-norm-based matrix completion [59, 77].

To solve (3.2.1), we implement the method of multipliers strategy initially suggested by Burer and Monteiro. Indeed, this algorithm is explained in detail by Recht

et al in the context of solving problem (3.1.9) [76]. The inner operation of minimizing the augmented Lagrangian term is performed using LBFGS as implemented by the Matlab solver minfunc [85]. This solver requires only being able to apply $\mathcal{A}$ and $\mathcal{A}^*$ quickly, both of which can be done in time $O(r \min\{N \log N, K \log K\})$. The parameters of the augmented Lagrangian are updated according to the schedule proposed by Burer and Monteiro [15]. This code allows us to solve problems where N and K are in the tens of thousands in seconds on a laptop.

3.2.2 Phase transitions

Our first set of numerical experiments delineates the boundary, in terms of values for K, N and L, for when (3.1.9) is effective on generic instances of four different types of problems. For a fixed value of L, we vary the subspace dimensions N and K and run 100 experiments, with different random instances of $\boldsymbol{w}$ and $\boldsymbol{x}$ for each experiment. The vectors $\boldsymbol{h}$ and $\boldsymbol{m}$ are selected to be standard Gaussian vectors with independent entries. Figures 9 and 10 show the collected frequencies of success for four different probabilistic models. We classify a recovery a success if its relative error is less than 2%[6], meaning that if $\hat{\boldsymbol{X}}$ is the solution to (3.1.9), then

$$\frac{\|\hat{\boldsymbol{X}} - \boldsymbol{w}\boldsymbol{x}^*\|_F}{\|\boldsymbol{w}\boldsymbol{x}^*\|_F} < 0.02. \tag{3.2.2}$$

Our first set of experiments mimics the channel protection problem from Section 3.1.5 and Figure 7. Figure 9 shows the empirical rate of success when $\boldsymbol{C}$ is taken as a dense $L \times N$ Gaussian random matrix. We fix $L = 2048$ and vary N and K from 25 to 1000. In Figure 9(a), we take $\boldsymbol{w}$ to be sparse with known support; we form $\boldsymbol{B}$ by randomly selecting K columns from the $L \times L$ identity matrix. For Figure 9(b), we take $\boldsymbol{w}$ to be "short", forming $\boldsymbol{B}$ from the first K columns of the identity. In both cases, the basis expansion coefficient were drawn to be iid Gaussian random vectors.

[6]The diagrams in Figures 9 and 10 do not change significantly if a smaller threshold, say on the order of 10^{-6}, is chosen.

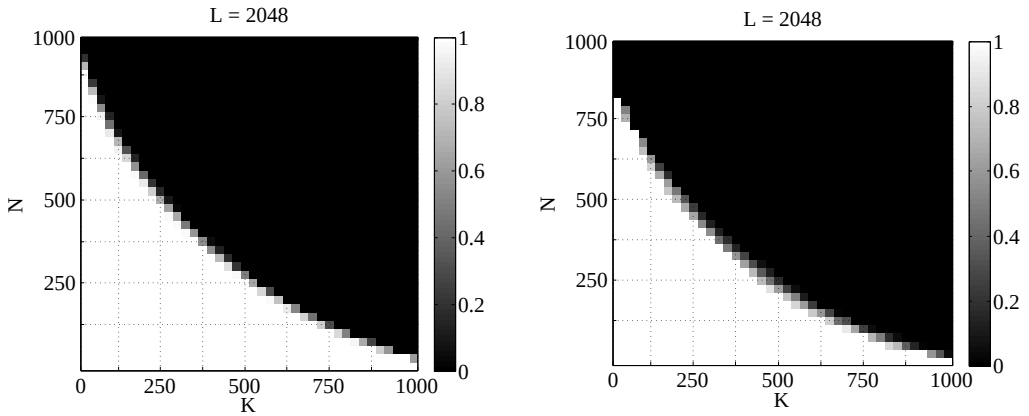

Figure 9: Empirical success rate for the deconvolution of two vectors $\boldsymbol{x}$ and $\boldsymbol{w}$. In these experiments, $\boldsymbol{x}$ is a random vector in the subspace spanned by the columns of an $L \times N$ matrix whose entries are independent and identically distributed Gaussian random variables. In part (a), $\boldsymbol{w}$ is a generic sparse vector, with support and nonzero entries chosen randomly. In part (b) $\boldsymbol{w}$ is a generic short vector whose first K terms are nonzero and chosen randomly.

In both cases, we are able to deconvolve this signals with a high rate of success when $L \gtrsim 2.7(K + N)$.

Figure 10 shows the results of a similar experiment, only here both $\boldsymbol{w}$ and $\boldsymbol{x}$ are randomly generated sparse vectors. We take L to be much larger than the previous experiment, $L = 32,768$, and vary N and K from 1000 to $16,000$. In Figure 10(a), we generate both $\boldsymbol{B}$ and $\boldsymbol{C}$ by randomly selecting columns of the identity — despite the difference in the model for $\boldsymbol{x}$ (sparse instead of randomly oriented) the resulting performance curve in this case is very similar to that in Figure 9(a). In Figure 10(b), we use the same model for $\boldsymbol{C}$ and $\boldsymbol{x}$, but use a "short" $\boldsymbol{w}$ (first K terms are nonzero). Again, despite the difference in the model for $\boldsymbol{x}$, the recovery curve looks almost identical to that in Figure 9(b).

3.2.3 Recovery in the presence of noise

Figure 11 demonstrates the robustness of the deconvolution algorithm in the presence of noise. We use the same basic experimental setup as in Figure 9(a), with $L = 2048$, $N = 500$ and $K = 250$, but instead of making a clean observation of $\boldsymbol{w} * \boldsymbol{x}$, we add

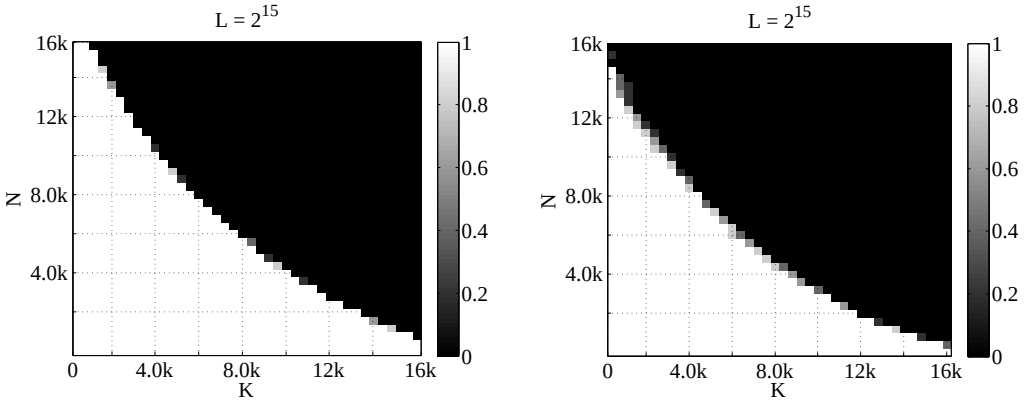

Figure 10: Empirical success rate for the deconvolution of two vectors $\boldsymbol{x}$ and $\boldsymbol{w}$. In these experiments, $\boldsymbol{x}$ is a random sparse vector whose support and N non-zero values on that support are chosen at random. In part (a), $\boldsymbol{w}$ is a generic sparse vector, with support and K nonzero entries chosen randomly. In part (b) $\boldsymbol{w}$ is a generic short vector whose first K terms are nonzero and chosen randomly.

a noise vector $\boldsymbol{z}$ whose entires are iid Gaussian with zero mean and variance σ^2. We solve the program (3.1.17) with $\delta = (L + \sqrt{4L})^{1/2}\sigma$, a value chosen since it will be an upper bound for $\|\boldsymbol{z}\|_2$ with high probability.

Figure 11(a) shows how the relative error of the recovery changes with the noise level σ. On a log-log scale, the recovery error (show as $10\log_{10}$ (relative error squared)) is linear in the signal-to-noise ratio (defined as SNR$= 10\log_{10}(\|\boldsymbol{w}\boldsymbol{x}^*\|_F^2/\|\boldsymbol{z}\|_2^2)$. For each SNR level, we calculate the average relative error squared over 100 iterations, each time using independent set of signals, coding matrix, and noise. Figure 11(b) shows how the recovery error is affected by the "oversampling ratio"; as L is made larger relative to $N + K$, the recovery error decreases. As before, each point is averaged over 100 independent iterations.

3.2.4 Image deblurring

The discrete signals $\boldsymbol{w}$ and $\boldsymbol{x}$ in the deconvolution problem (3.1.1) may also represent higher-dimensional objects such as images. For example, the unknown $\boldsymbol{x} \in \mathbb{R}^L$ may represent an image of the form $\boldsymbol{x}[\ell_1, \ell_2]$, and the unknown $\boldsymbol{w} \in \mathbb{R}^L$ may signify a

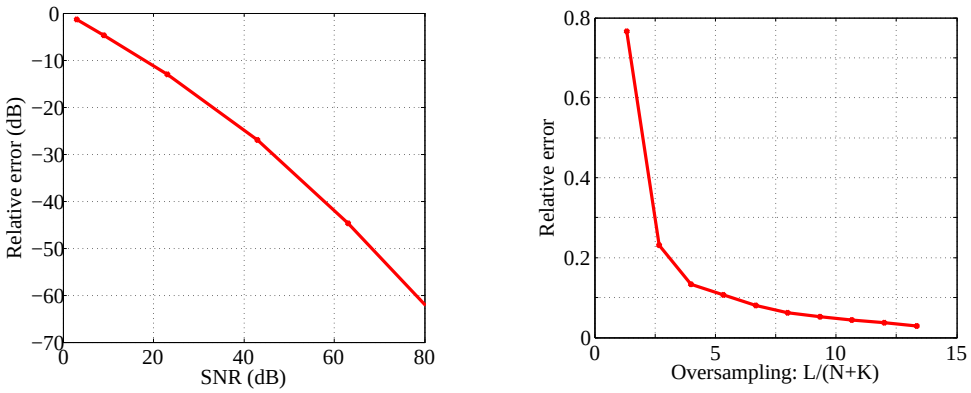

Figure 11: Performance of the blind deconvolution program in the presence of noise. In all of the experiments, $L = 2048$, $N = 500$, $K = 250$, $\boldsymbol{B}$ is a random selection of columns from the identity, and $\boldsymbol{C}$ is an iid Gaussian matrix. (a) Relative error vs. SNR on a log-log scale. (b) Oversampling rate vs. relative error for a fixed SNR of $20dB$

2D blur kernel $\boldsymbol{w}[\ell_1, \ell_2]$, where $1 \leq \ell_1 \leq L_1$, $1 \leq \ell_2 \leq L_2$, and $L = L_1 L_2$. The 2D convolution $\boldsymbol{y} = \boldsymbol{w} * \boldsymbol{x}$ produces blurred image $\boldsymbol{y}[\ell_1, \ell_2]$. Most natural images are sparse in some basis such as wavelets, DCT, or curvelets. If we have an estimate of the active coefficeints of the image $\boldsymbol{x}$, then the image can be expressed as the multiplication of a small set of basis functions arranged as the columns of matrix $\boldsymbol{C}$ and the corresponding short vector of active coefficients $\boldsymbol{m}$, i.e., $\boldsymbol{x} = \boldsymbol{C}\boldsymbol{m}$. In addition, if the non-zero components in the blur kernel $\boldsymbol{w}$ are much smaller than the total number of pixels L, and we have an estimate of the support of the active components in $\boldsymbol{w}$, then we can write $\boldsymbol{w} = \boldsymbol{B}\boldsymbol{h}$, where $\boldsymbol{B}$ is the matrix formed by a subset of the columns of the identity matrix, and $\boldsymbol{h}$ is an unknown short vector.

Figure 12, 13, and 14 illustrate an application of our blind deconvolution technique to two image deblurring problems. In the first problem, we assume that we have oracle knowledge of a low-dimensional subspace in which the image to be recovered lies. We observe a convolution of the $L = 65,536$ pixel Shapes image shown in Figure 12(a) with the motion blurring kernel shown in Figure 12(b); the observation is shown in Figure 12(c). The Shapes image can be very closely approximated using only

$N = 5000$ terms in a Haar wavelet expansion, which capture 99.9% of the energy in the image. We start by assuming (perhaps unrealistically) that we know the indices for these most significant wavelet coefficients; the corresponding wavelet basis functions are taken as columns of $\boldsymbol{B}$. We will also assume that we know the support of the blurring kernel, which consists of $K = 65$ connected pixels; the corresponding columns of the identity constitute $\boldsymbol{C}$. The image and blur kernel recovered by solving (3.1.9) are shown in Figure 13.

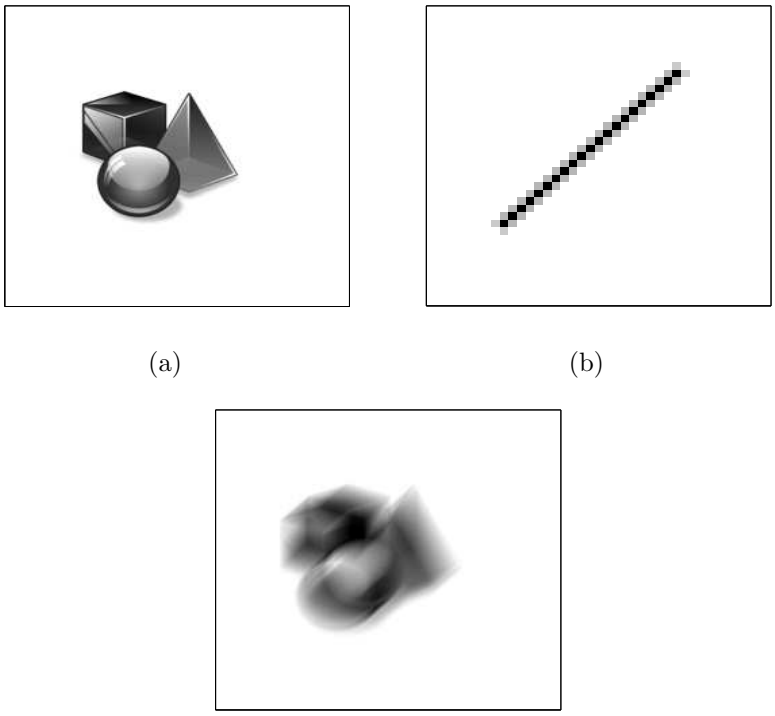

(a) (b)

(c)

Figure 12: Shapes image for deblurring experiment. (a) Original 256×256 Shapes image $\boldsymbol{x}$. (b) Blurring kernel $\boldsymbol{w}$ with a support size of 65 pixels, the locations of which are assumed to be known. (c) Convolution of (a) and (b).

Figure 14 shows a more realistic example where the support of the image in the wavelet domain is unknown. We take the blurred image shown in Figure 12(c) and, as before, we assume we know the support of the blurring kernel shown in Figure 12(b), with $K = 65$ non-zero elements, but here we use the blurred image to estimate the

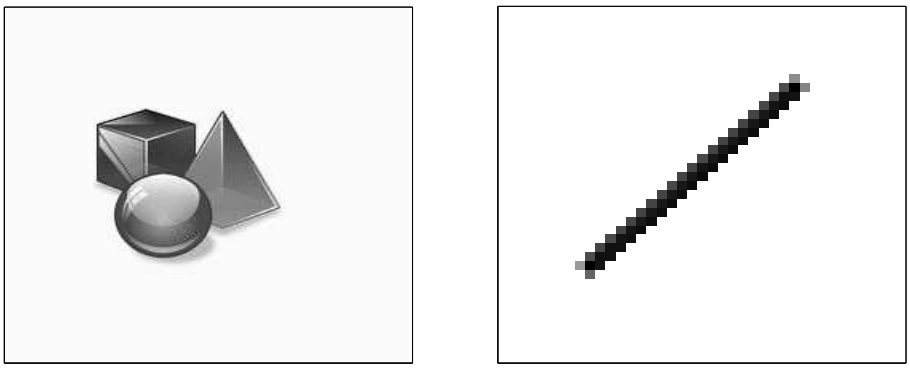

(a) (b)

Figure 13: An oracle assisted image deblurring experiment; we assume that we know the support of the 5000 most significant wavelet coefficients of the original image. These wavelet coefficients capture 99.9% of the energy in the original image. We obtain from the solution of (3.1.9): (a) Deconvolved image $\hat{\boldsymbol{x}}$ obtained from the solution of (3.1.9), with relative error of $\|\hat{\boldsymbol{x}} - \boldsymbol{x}\|_2 / \|\boldsymbol{x}\|_2 = 1.6 \times 10^{-2}$. (b) Estimated blur kernel $\hat{\boldsymbol{w}}$ with relative error of $\|\hat{\boldsymbol{w}} - \boldsymbol{w}\|_2 / \|\boldsymbol{w}\|_2 = 5.4 \times 10^{-1}$.

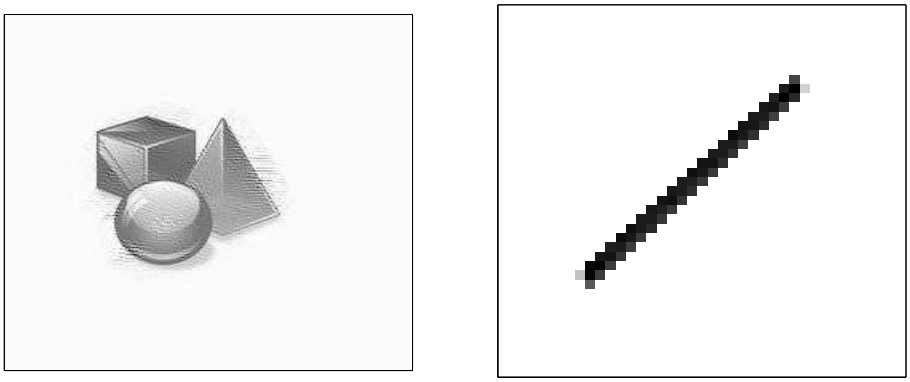

(a) (b)

Figure 14: Image recovery without oracle information. Take the support of the 9000 most-significant coefficients of Haar wavelet transform of the blurred image as our estimate of the subspace in which original image lives. (a) Deconvolved image obtained from the solution of (3.1.9), with relative error of 4.9×10^{-2}. (b) Estimated blur kernel; relative error $= 5.6 \times 10^{-1}$.

support in the wavelet domain — we take the Haar wavelet transform of the image in Figure 12(c), and select the indices of the $N = 9000$ largest wavelet coefficients as a proxy for the support of the significant coefficients of the original image. The wavelet coefficients of the original image at this estimated support capture 98.5% of

the energy in the blurred image. The recovery using (3.1.9) run with these linear models is shown in Figure 14(a) and Figure 14(b). Despite not knowing the linear model explicitly, we are able to estimate it well enough from the observed data to get a reasonable reconstruction.

3.3 Proof of main theorems

In this section, we will prove Theorems 3.1.1 and 3.1.2 by establishing a set of standard sufficient conditions for $\boldsymbol{X}_0$ to be the unique minimizer of (3.1.9). At a high level, the argument follows previous literature [19, 45] on low-rank matrix recovery by constructing a valid *dual certificate* for the rank-1 matrix $\boldsymbol{X}_0 = \boldsymbol{h}\boldsymbol{m}^*$. The main mathematical innovation in proving these results comes in Lemmas 3.3.2, 3.3.3, 3.3.4 and 3.3.5, which control the behavior of the random operator $\mathcal{A}$.

We will work through the main argument in this section, leaving the technical details (including the proofs of the main lemmas) until Sections 3.4 and 3.5.

Key to our argument is the subspace (of $\mathbb{R}^{K\times N}$) T associated with $\boldsymbol{X}_0 = \boldsymbol{h}\boldsymbol{m}^*$:

$$T = \left\{\boldsymbol{X} : \boldsymbol{X} = \alpha\boldsymbol{h}\boldsymbol{v}^* + \beta\boldsymbol{u}\boldsymbol{m}^*,\ \boldsymbol{v} \in \mathbb{R}^N,\ \boldsymbol{u} \in \mathbb{R}^K,\ \alpha, \beta \in \mathbb{R}\right\}$$

with the (matrix) projection operators

$$\mathcal{P}_T(\boldsymbol{X}) = \boldsymbol{P_H}\boldsymbol{X} + \boldsymbol{X}\boldsymbol{P_M} - \boldsymbol{P_H}\boldsymbol{X}\boldsymbol{P_M}$$
$$\mathcal{P}_{T^\perp}(\boldsymbol{X}) = (\boldsymbol{I} - \boldsymbol{P_H})\boldsymbol{X}(\boldsymbol{I} - \boldsymbol{P_M}),$$

where $\boldsymbol{P_H}$ and $\boldsymbol{P_M}$ are the (vector) projection matrices $\boldsymbol{P_H} = \boldsymbol{h}\boldsymbol{h}^*$ and $\boldsymbol{P_M} = \boldsymbol{m}\boldsymbol{m}^*$.

3.3.1 Theorem 3.1.1: Sufficient condition for a nuclear norm minimizer

The following proposition is a specialization of the more general sufficient conditions for verifying the solutions to the nuclear norm minimization problem (3.1.9) that have appeared multiple times in the literature in one form or another (see [75], for example).

Proposition 4. *The matrix* $\boldsymbol{X}_0 = \boldsymbol{h}\boldsymbol{m}^*$ *is the unique minimizer to* (3.1.9) *if there exists a* $\boldsymbol{Y} \in \text{Range}(\mathcal{A}^*)$ *such that*

$$\langle \boldsymbol{h}\boldsymbol{m}^* - \mathcal{P}_T(\boldsymbol{Y}), \mathcal{P}_T(\boldsymbol{Z})\rangle_F - \langle \mathcal{P}_{T^\perp}(\boldsymbol{Y}), \mathcal{P}_{T^\perp}(\boldsymbol{Z})\rangle_F + \|\mathcal{P}_{T^\perp}(\boldsymbol{Z})\|_* > 0$$

for all $\boldsymbol{Z} \in \text{Null}(\mathcal{A})$.

For any two matrices $\boldsymbol{A}$, $\boldsymbol{B}$ with same dimesensions, we will use the Holder's inequality:

$$\langle \boldsymbol{A}, \boldsymbol{B}\rangle_F \le \|\boldsymbol{A}\|\|\boldsymbol{B}\|_*,$$

and the Cauchy-Schwartz's inequality:

$$\langle \boldsymbol{A}, \boldsymbol{B}\rangle_F \le \|\boldsymbol{A}\|_F\|\boldsymbol{B}\|_F.$$

In view of the above ineqaulities, we have

$$\begin{aligned}\langle \boldsymbol{h}\boldsymbol{m}^* - \mathcal{P}_T(\boldsymbol{Y}),&\mathcal{P}_T(\boldsymbol{Z})\rangle_F - \langle \mathcal{P}_{T^\perp}(\boldsymbol{Y}), \mathcal{P}_{T^\perp}(\boldsymbol{Z})\rangle_F + \|\mathcal{P}_{T^\perp}(\boldsymbol{Z})\|_* \\ &\ge -\|\boldsymbol{h}\boldsymbol{m}^* - \mathcal{P}_T(\boldsymbol{Y})\|_F\|\mathcal{P}_T(\boldsymbol{Z})\|_F - \|\mathcal{P}_{T^\perp}(\boldsymbol{Y})\|\,\|\mathcal{P}_{T^\perp}(\boldsymbol{Z})\|_* + \|\mathcal{P}_{T^\perp}(\boldsymbol{Z})\|_*;\end{aligned}$$

therefore, it is enough to find a $\boldsymbol{Y} \in \text{Range}(\mathcal{A}^*)$ such that

$$-\|\boldsymbol{h}\boldsymbol{m}^* - \mathcal{P}_T(\boldsymbol{Y})\|_F\|\mathcal{P}_T(\boldsymbol{Z})\|_F + (1 - \|\mathcal{P}_{T^\perp}(\boldsymbol{Y})\|)\,\|\mathcal{P}_{T^\perp}(\boldsymbol{Z})\|_* \;>\; 0, \qquad (3.3.1)$$

for all $\boldsymbol{Z} \in \text{Null}(\mathcal{A})$.

In Lemma 3.3.1 in Section 3.3.4 below we show that $\|\mathcal{A}\| \le \sqrt{(\alpha+1)N\log L} =: \gamma$ with probability at least $1 - L^{-\alpha+1}$. Corollary 2 below also shows that (3.1.16) implies

$$\|\mathcal{A}(\mathcal{P}_T(\boldsymbol{Z}))\|_F \ge 2^{-1/2}\|\mathcal{P}_T(\boldsymbol{Z})\|_F \quad \text{for all} \quad \boldsymbol{Z} \in \text{Null}(\mathcal{A}),$$

with high probability. Then, since

$$\begin{aligned}0 &= \|\mathcal{A}(\boldsymbol{Z})\|_F \\ &\ge \|\mathcal{A}(\mathcal{P}_T(\boldsymbol{Z}))\|_F - \|\mathcal{A}(\mathcal{P}_{T^\perp}(\boldsymbol{Z}))\|_F \\ &\ge \frac{1}{\sqrt{2}}\|\mathcal{P}_T(\boldsymbol{Z})\|_F - \gamma\|\mathcal{P}_{T^\perp}(\boldsymbol{Z})\|_F,\end{aligned}$$

we will have that

$$\|\mathcal{P}_T(\boldsymbol{Z})\|_F \;\leq\; \sqrt{2}\gamma\|\mathcal{P}_{T^\perp}(\boldsymbol{Z})\|_F \;\leq\; \sqrt{2}\gamma\|\mathcal{P}_{T^\perp}(\boldsymbol{Z})\|_*. \tag{3.3.2}$$

Applying this fact to (3.3.1), we see that it is sufficient to find a $\boldsymbol{Y} \in \text{Range}(\mathcal{A}^*)$ such that

$$\left(1 - \sqrt{2}\gamma\|\boldsymbol{h}\boldsymbol{m}^* - \mathcal{P}_T(\boldsymbol{Y})\|_F - \|\mathcal{P}_{T^\perp}(\boldsymbol{Y})\|\right)\|\mathcal{P}_{T^\perp}(\boldsymbol{Z})\|_* \;>\; 0.$$

Since Lemma 3.3.3 also implies that $\mathcal{P}_{T^\perp}(\boldsymbol{Z}) \neq \boldsymbol{0}$ for $\boldsymbol{Z} \in \text{Null}(\mathcal{A})$, our approach will be to construct a $\boldsymbol{Y} \in \text{Range}(\mathcal{A}^*)$ such that

$$\|\boldsymbol{h}\boldsymbol{m}^* - \mathcal{P}_T(\boldsymbol{Y})\|_F \leq \frac{1}{4\sqrt{2}\gamma} \quad \text{and} \quad \|\mathcal{P}_{T^\perp}(\boldsymbol{Y})\| < \frac{3}{4}. \tag{3.3.3}$$

In the next section, we will show how such a $\boldsymbol{Y}$ can be found using Gross's *golfing scheme* [44, 45].

3.3.2 Construction of the dual certificate via golfing

The golfing scheme works by dividing the L linear observations of $\boldsymbol{X}_0$ into P disjoint subsets of size Q, and then using these subsets of observations to iteratively construct the dual certificate $\boldsymbol{Y}$. We index these subsets by $\Gamma_1, \Gamma_2, \ldots, \Gamma_P$; by construction $|\Gamma_p| = Q$, $\bigcup_p \Gamma_p = \{1, \ldots, L\}$, and $\Gamma_p \cap \Gamma_{p'} = \emptyset$. We define $\mathcal{A}_p$ be the operator that returns the measurements indexed by the set Γ_p:

$$\mathcal{A}_p(\boldsymbol{W}) = \{\text{Tr}\,(\boldsymbol{c}_k\boldsymbol{b}_k^*\boldsymbol{W})\}_{k\in\Gamma_p}, \qquad \mathcal{A}_p^*\mathcal{A}_p\boldsymbol{W} = \sum_{k\in\Gamma_p} \boldsymbol{b}_k\boldsymbol{b}_k^*\boldsymbol{W}\boldsymbol{c}_k\boldsymbol{c}_k^*.$$

The $\mathcal{A}_p^*\mathcal{A}_p$ are random linear operators; the expectation of their action on a fixed matrix $\boldsymbol{W}$ is

$$\text{E}[\mathcal{A}_p^*\mathcal{A}_p\boldsymbol{W}] = \sum_{k\in\Gamma_p} \boldsymbol{b}_k\boldsymbol{b}_k^*\boldsymbol{W}.$$

For reasons that will become clear as we proceed through the argument below, we would like this expectation to be as close to a scalar multiple of $\boldsymbol{W}$ as possible for all p. In other words, we would like to partition the L rows of the matrix $\hat{\boldsymbol{B}}$ into P

different $Q \times K$ submatrices, each of which is well-conditioned (i.e. the columns are almost orthogonal to one another).

Results from the literature on compressive sensing have shown that such a partition exists for $L \times K$ matrices with orthonormal columns whose rows all have about the same energy. In particular, the proof of Theorem 1.2 in [20] shows that if $\hat{\boldsymbol{B}}$ is a $L \times K$ matrix with $\hat{\boldsymbol{B}}^* \hat{\boldsymbol{B}} = \boldsymbol{I}$, Γ is a randomly selected subset of $\{1, \ldots, L\}$ of size Q, and the rows $\boldsymbol{b}_k^*$ of $\hat{\boldsymbol{B}}$ have coherence $\mu_{\max}^2$ as in (3.1.11), then there exists a constant C such that for any $0 < \epsilon < 1$ and $0 < \delta < 1$,

$$Q \;\geq\; C \frac{\mu_{\max}^2 K}{\epsilon^2} \max\left\{\log K, \log(1/\delta)\right\},$$

implies

$$\left\| \sum_{k \in \Gamma} \boldsymbol{b}_k \boldsymbol{b}_k^* - \frac{Q}{L} \boldsymbol{I} \right\| \;\leq\; \frac{\epsilon Q}{L}.$$

with probability exceeding $1 - \delta$. If our partition $\Gamma_1, \Gamma_2, \ldots, \Gamma_P$ is random, then, applying the above result with $\delta = L^{-1}$ and $\epsilon = 1/4$ tells us that if

$$Q \;\geq\; C\, \mu_{\max}^2 K \log L, \tag{3.3.4}$$

then

$$\max_{1 \leq p \leq P} \left\| \sum_{k \in \Gamma_p} \boldsymbol{b}_k \boldsymbol{b}_k^* - \frac{Q}{L} \boldsymbol{I} \right\| \;\leq\; \frac{Q}{4L} \quad \Rightarrow \quad \max_{1 \leq p \leq P} \left\| \sum_{k \in \Gamma_p} \boldsymbol{b}_k \boldsymbol{b}_k^* \right\| \;\leq\; \frac{5Q}{4L}, \tag{3.3.5}$$

with positive probability. This means that with Q chosen to obey (3.3.4), at least one such partition must exist and we move forward assuming that (3.3.5) holds.

Along with the expectation of each of the $\mathcal{A}_p^* \mathcal{A}_p$ being close to a multiple of the identity, we will also need tail bounds stating that $\mathcal{A}_p^* \mathcal{A}_p$ is close to its expectation with high probability. These probabilities can be made smaller by making the subset size Q larger. As detailed below (in Lemmas 3.3.3,3.3.4, and 3.3.5), taking

$$Q \;=\; C_\alpha\, M \log(L) \log(M), \quad \text{where} \quad M = \max\left(\mu_{\max}^2 K, \mu_h^2 N\right), \tag{3.3.6}$$

will make these probability bounds meaningful. For C_α chosen appropriately, this means (3.3.4) will hold.

The construction of $\boldsymbol{Y}$ that obeys the conditions (3.3.3) relies on three technical lemmas which are stated below in Section 3.3.4. Their proofs rely heavily on re-writing different quantities of interest (linear operators, vectors, and scalars) as a sum of independent subexponential random variables and then using a specialized version of the "Matrix Bernstein Inequality" to estimate their sizes. Section 2.5 below contains a brief overview of these types of probabilistic bounds. The proofs of the key lemmas (3.3.3, 3.3.4, and 3.3.5) are in Section 3.4. These proofs rely on several miscellaneous lemmas which compute simple expectations and tail bounds for various random variables; these are presented separately in Section 3.5.

With the Γ_p chosen and the key lemmas established, we construct $\boldsymbol{Y}$ as follows. Let $\boldsymbol{Y}_0 = \boldsymbol{0}$, and then iteratively define

$$\boldsymbol{Y}_p = \boldsymbol{Y}_{p-1} + \frac{L}{Q}\,\mathcal{A}_p^*\mathcal{A}_p\left(\boldsymbol{h}\boldsymbol{m}^* - \mathcal{P}_T(\boldsymbol{Y}_{p-1})\right).$$

We will show that under appropriate conditions on L, taking $\boldsymbol{Y} := \boldsymbol{Y}_P$ will satisfy both parts of (3.3.3) with high probability.

Let $\boldsymbol{W}_p$ be the residual between $\boldsymbol{Y}_p$ projected onto T and the target $\boldsymbol{h}\boldsymbol{m}^*$:

$$\boldsymbol{W}_p = \mathcal{P}_T(\boldsymbol{Y}_p) - \boldsymbol{h}\boldsymbol{m}^*.$$

Notice that $\boldsymbol{W}_p \in T$ and

$$\boldsymbol{W}_0 = -\boldsymbol{h}\boldsymbol{m}^*, \qquad \boldsymbol{W}_p = \frac{L}{Q}\left(\frac{Q}{L}\mathcal{P}_T - \mathcal{P}_T\mathcal{A}_p^*\mathcal{A}_p\mathcal{P}_T\right)\boldsymbol{W}_{p-1}. \tag{3.3.7}$$

Applying Lemma 3.3.3 iteratively to the $\boldsymbol{W}_p$ tells us that

$$\|\boldsymbol{W}_p\|_F \;\le\; \frac{1}{2}\|\boldsymbol{W}_{p-1}\|_F \;\le\; 2^{-p}\|\boldsymbol{h}\boldsymbol{m}^*\|_F = 2^{-p}, \qquad p = 1, \ldots, P, \tag{3.3.8}$$

with probability exceeding $1 - 3L^{-\alpha+1}$. Thus we will have the first condition in (3.3.3),

$$\|\boldsymbol{h}\boldsymbol{m}^* - \mathcal{P}_T(\boldsymbol{Y}_P)\|_F \le \frac{1}{4\sqrt{2}\gamma},$$

for

$$P \;=\; \frac{L}{Q} \;\geq\; \frac{\log(4\sqrt{2}\gamma)}{\log 2},$$

which can be achieved with Q as in (3.3.6) and $M = \max(\mu_{\max^2} K, \mu_h^2 N)$ as in (3.1.16).

To bound $\|\mathcal{P}_{T^\perp}(\boldsymbol{Y}_p)\|$, we use the expansion

$$\begin{aligned}\boldsymbol{Y}_p = \boldsymbol{Y}_{p-1} - \frac{L}{Q}\mathcal{A}_p^*\mathcal{A}_p\boldsymbol{W}_{p-1} \;&=\; \boldsymbol{Y}_{p-2} - \frac{L}{Q}\mathcal{A}_{p-1}^*\mathcal{A}_{p-1}\boldsymbol{W}_{p-2} - \frac{L}{Q}\mathcal{A}_p^*\mathcal{A}_p\boldsymbol{W}_{p-1} \;=\; \cdots \\ &= -\sum_{p=1}^{P}\frac{L}{Q}\mathcal{A}_p^*\mathcal{A}_p\boldsymbol{W}_{p-1},\end{aligned}$$

and so

$$\begin{aligned}\|\mathcal{P}_{T^\perp}(\boldsymbol{Y}_P)\| &= \left\|\mathcal{P}_{T^\perp}\left(\sum_{p=1}^{P}\frac{L}{Q}\mathcal{A}_p^*\mathcal{A}_p\boldsymbol{W}_{p-1}\right)\right\| \\ &= \frac{L}{Q}\left\|\mathcal{P}_{T^\perp}\left(\sum_{p=1}^{P}\mathcal{A}_p^*\mathcal{A}_p\boldsymbol{W}_{p-1} - \frac{Q}{L}\boldsymbol{W}_{p-1}\right)\right\|, \qquad (\text{since } \boldsymbol{W}_{p-1}\in T) \\ &\leq \frac{L}{Q}\left\|\sum_{p=1}^{P}\mathcal{A}_p^*\mathcal{A}_p\boldsymbol{W}_{p-1} - \frac{Q}{L}\boldsymbol{W}_{p-1}\right\| \\ &\leq \sum_{p=1}^{P}\frac{L}{Q}\left\|\mathcal{A}_p^*\mathcal{A}_p\boldsymbol{W}_{p-1} - \frac{Q}{L}\boldsymbol{W}_{p-1}\right\|.\end{aligned}$$

Lemma 3.3.5 shows that with probability exceeding $1 - L^{-\alpha+1}$,

$$\left\|\mathcal{A}_p^*\mathcal{A}_p\boldsymbol{W}_{p-1} - \frac{Q}{L}\boldsymbol{W}_{p-1}\right\| \;\leq\; 2^{-p}\frac{3Q}{4L}, \quad \text{for all} \quad p = 1,\ldots,P.$$

and so

$$\|\mathcal{P}_{T^\perp}(\boldsymbol{Y}_P)\| \;\leq\; \sum_{p=1}^{P} 3\cdot 2^{-p-2} \;<\; \frac{3}{4}.$$

Collecting the results above, we see that both conditions in (3.3.3) will hold with probability exceeding $1 - O(L^{-\alpha+1})$ when M is chosen as in (3.1.16).

3.3.3 Theorem 3.1.2: Stability

With the condition (3.1.16), we know though the arguments in the previous section that with the required probability there will exist a dual certificate $\boldsymbol{Y}$ that obeys the conditions (3.3.3) and that $\mathcal{A}^*\mathcal{A}$ is well conditioned on T: $\|\mathcal{P}_T\mathcal{A}^*\mathcal{A}\mathcal{P}_T - \mathcal{P}_T\| \leq 1/2$.

With these facts in place, the stability proof follows the template set in [27, 45]. We start with two observations; first, the feasibility of $\boldsymbol{X}_0$ implies

$$\|\tilde{\boldsymbol{X}}\|_* \leq \|\boldsymbol{X}_0\|_*, \tag{3.3.9}$$

and

$$\|\mathcal{A}(\tilde{\boldsymbol{X}} - \boldsymbol{X}_0)\|_2 \leq \|\hat{\boldsymbol{y}} - \mathcal{A}(\boldsymbol{X}_0)\|_2 + \|\mathcal{A}(\tilde{\boldsymbol{X}}) - \hat{\boldsymbol{y}}\|_2 \leq 2\delta. \tag{3.3.10}$$

Set $\tilde{\boldsymbol{X}} = \boldsymbol{X}_0 + \boldsymbol{\xi}$. With $\mathcal{P}_{\mathcal{A}}$ as the projection operator onto the row space of $\mathcal{A}$, we break apart the recovery error as

$$\begin{aligned} \|\boldsymbol{\xi}\|_F^2 &= \|\mathcal{P}_{\mathcal{A}}(\boldsymbol{\xi})\|_F^2 + \|\mathcal{P}_{\mathcal{A}^\perp}(\boldsymbol{\xi})\|_F^2 \\ &= \|\mathcal{P}_{\mathcal{A}}(\boldsymbol{\xi})\|_F^2 + \|\mathcal{P}_T\mathcal{P}_{\mathcal{A}^\perp}(\boldsymbol{\xi})\|_F^2 + \|\mathcal{P}_{T^\perp}\mathcal{P}_{\mathcal{A}^\perp}(\boldsymbol{\xi})\|_F^2. \end{aligned} \tag{3.3.11}$$

A direct result of of Proposition 4 is that there exists a constant $C > 0$ such that for all $\boldsymbol{Z} \in \text{Null}(\mathcal{A})$, $\|\boldsymbol{X}_0 + \boldsymbol{Z}\|_* - \|\boldsymbol{X}_0\|_* \geq C\|\mathcal{P}_{T^\perp}(\boldsymbol{Z})\|_*$ (this is developed cleanly in [75]). Since $\mathcal{P}_{\mathcal{A}^\perp}(\boldsymbol{\xi}) \in \text{Null}(\mathcal{A})$, we have

$$\|\boldsymbol{X}_0 + \mathcal{P}_{\mathcal{A}^\perp}(\boldsymbol{\xi})\|_* - \|\boldsymbol{X}_0\|_* \ \geq C\|\mathcal{P}_{T^\perp}\mathcal{P}_{\mathcal{A}^\perp}(\boldsymbol{\xi})\|_*.$$

Combining this with (3.3.9) and the triangle inequality yields

$$\|\boldsymbol{X}_0\|_* \geq \|\boldsymbol{X}_0\|_* + C\|\mathcal{P}_{T^\perp}\mathcal{P}_{\mathcal{A}^\perp}(\boldsymbol{\xi})\|_* - \|\mathcal{P}_{\mathcal{A}}(\boldsymbol{\xi})\|_*,$$

which implies

$$\begin{aligned} \|\mathcal{P}_{T^\perp}\mathcal{P}_{\mathcal{A}^\perp}(\boldsymbol{\xi})\|_* &\leq C\|\mathcal{P}_{\mathcal{A}}(\boldsymbol{\xi})\|_* \\ &\leq C\sqrt{\min(K, N)}\|\mathcal{P}_{\mathcal{A}}(\boldsymbol{\xi})\|_F. \end{aligned}$$

In addition, in (3.3.2) we established that for all $\boldsymbol{Z} \in \text{Null}(\mathcal{A})$, we have

$$\|\mathcal{P}_T\mathcal{P}_{\mathcal{A}^\perp}(\boldsymbol{\xi})\|_F^2 \ \leq \ 2\lambda_{\max}^2\|\mathcal{P}_{T^\perp}\mathcal{P}_{\mathcal{A}^\perp}(\boldsymbol{\xi})\|_F^2,$$

and as a result

$$\|\mathcal{P}_{\mathcal{A}^\perp}(\boldsymbol{\xi})\|_F^2 \ \leq \ (2\lambda_{\max}^2 + 1)\|\mathcal{P}_{T^\perp}\mathcal{P}_{\mathcal{A}^\perp}(\boldsymbol{\xi})\|_F^2.$$

Revisiting (3.3.11), we have

$$\begin{aligned}\|\tilde{\boldsymbol{X}} - \boldsymbol{X}_0\|_F^2 &\leq (2\lambda_{\max}^2 + 1)\|\mathcal{P}_{T^\perp}\mathcal{P}_{\mathcal{A}^\perp}(\boldsymbol{\xi})\|_F^2 + \|\mathcal{P}_{\mathcal{A}}(\boldsymbol{\xi})\|_F^2 \\ &\leq C(2\lambda_{\max}^2 + 1)\min(K,N)\|\mathcal{P}_{\mathcal{A}}(\boldsymbol{\xi})\|_F^2 + \|\mathcal{P}_{\mathcal{A}}(\boldsymbol{\xi})\|_F^2,\end{aligned}$$

and then absorbing all the constants into C,

$$\begin{aligned}\|\tilde{\boldsymbol{X}} - \boldsymbol{X}_0\|_F &\leq C\lambda_{\max}\sqrt{\min(K,N)}\|\mathcal{P}_{\mathcal{A}}(\boldsymbol{\xi})\|_F \\ &\leq C\sqrt{\min(K,N)}\,\lambda_{\max}\|\mathcal{A}^\dagger\|\,\|\mathcal{A}(\boldsymbol{\xi})\|_2,\end{aligned}$$

where $\mathcal{A}^\dagger$ is the pseudo-inverse of $\mathcal{A}$. Using (3.3.10) and the fact that $\|\mathcal{A}^\dagger\| = \lambda_{\min}^{-1}$, we obtain the final result

$$\|\tilde{\boldsymbol{X}} - \boldsymbol{X}_0\|_F \leq C\frac{\lambda_{\max}}{\lambda_{\min}}\sqrt{\min(K,N)}\delta. \tag{3.3.12}$$

3.3.4 Key lemmas

We start with two lemmas which characterize the singular values of the random linear operator $\mathcal{A}$. The first, which gives a loose upper bound on the maximum singular value, holds for all N, K, L. The second gives a tighter bound on the maximum singular value and a comparable lower bound on the minimum singular value, but requires $\mathcal{A}$ to be sufficiently underdetermined.

Lemma 3.3.1 (Operator norm of $\mathcal{A}$)**.** *Let $\mathcal{A}$ be defined with $\boldsymbol{A}_k = \boldsymbol{b}_k\boldsymbol{c}_k^*$ as in Section 3.1.3. Fix $\alpha \geq 1$. Then*

$$\|\mathcal{A}\| \;\leq\; \sqrt{N(\log(NL/2) + \alpha\log L)},$$

with probability exceeding $1 - L^{-\alpha}$.

Proof. Writing $\mathcal{A}$ in matrix form we have

$$\begin{aligned}
\|\mathcal{A}\|^2 \;=\; \left\| \begin{bmatrix} \Delta_1 \hat{\boldsymbol{B}} & \Delta_2 \hat{\boldsymbol{B}} & \cdots & \Delta_N \hat{\boldsymbol{B}} \end{bmatrix} \right\|^2 &= \left\| \begin{bmatrix} \hat{\boldsymbol{B}}^* \Delta_1^* \\ \hat{\boldsymbol{B}}^* \Delta_2^* \\ \vdots \\ \hat{\boldsymbol{B}}^* \Delta_N^* \end{bmatrix} \right\|^2 \\
&\leq \left\| \begin{bmatrix} \Delta_1^* \\ \Delta_2^* \\ \vdots \\ \Delta_N^* \end{bmatrix} \right\| \\
&\leq \|\Delta_1\|^2 + \|\Delta_2\|^2 + \cdots + \|\Delta_N\|^2 \\
&\leq N \max_{1 \leq n \leq N} \|\Delta_n\|^2 \\
&= N \max_{1 \leq n \leq N} \max_{1 \leq \ell \leq L/2} |\hat{c}_\ell[n]|^2.
\end{aligned}$$

Since the $|\hat{c}_\ell[n]|^2$ are independent chi-squared random variables,

$$\mathrm{P}\left\{ \max_{n,\ell} |\hat{c}_\ell[n]|^2 > \lambda \right\} \;\leq\; \frac{NL}{2}\, \mathrm{e}^{-\lambda},$$

and the lemma follows by taking $\lambda = \log(NL/2) + \alpha \log L$. □

Lemma 3.3.2 ($\mathcal{A}\mathcal{A}^*$ is well conditioned.)**.** *Let $\mathcal{A}$ be as defined in* (3.1.4)*, with coherences $\mu^2_{\max}$ and $\mu^2_{\min}$ as defined in* (3.1.11) *and* (3.1.12)*. Suppose that $\mathcal{A}$ is sufficiently underdetermined in that*

$$NK \;\geq\; \frac{C_\alpha}{\mu^2_{\min}} L \log^2 L \tag{3.3.13}$$

for some constant $C_\alpha > 1$. Then with probability exceeding $1 - O(L^{-\alpha+1})$, the eigenvalues of $\mathcal{A}\mathcal{A}^*$ obey

$$0.48 \mu^2_{\min} \frac{NK}{L} \leq \lambda_{\min}(\mathcal{A}\mathcal{A}^*) \leq \lambda_{\max}(\mathcal{A}\mathcal{A}^*) \leq 4.5 \mu^2_{\max} \frac{NK}{L}.$$

The proof of Lemma 3.3.2 in Section 3.4 decomposes $\mathcal{A}\mathcal{A}^*$ as a sum of independent random matrices, and then applies a Chernoff-like bound discussed in Section 2.5.

Our third key lemma tells us that, with high probability, $\mathcal{A}$ is well conditioned when restricted to the subspace T.

Lemma 3.3.3 (Conditioning on T)**.** *With the coherences $\mu^2_{\max}$ and μ^2_h defined in Section 3.1.3, let*

$$M = \max(\mu^2_{\max} K, \mu^2_h N). \tag{3.3.14}$$

Fix $\alpha \geq 1$. Choose the subsets $\Gamma_1, \ldots, \Gamma_P$ described in Section 3.3.2 so that they have size

$$|\Gamma_p| = Q \;=\; C'_\alpha \cdot M \log(L) \log(M), \tag{3.3.15}$$

where $C'_\alpha = O(\alpha)$ is a constant chosen below, and such that (3.3.5) holds. Then the linear operators $\mathcal{A}_1, \ldots, \mathcal{A}_P$ defined in Section 3.3.2 will obey

$$\max_{1 \leq p \leq P} \left\| \mathcal{P}_T \mathcal{A}_p^* \mathcal{A}_p \mathcal{P}_T - \frac{Q}{L} \mathcal{P}_T \right\| \;\leq\; \frac{Q}{2L},$$

with probability exceeding $1 - 3PL^{-\alpha} \geq 1 - 3L^{-\alpha+1}$.

Corollary 2. *Let $\mathcal{A}$ be the operator defined in (3.1.4), and M be defined as in (3.3.14). Then there exists a constant $C_\alpha = O(\alpha)$ such that*

$$M \;\leq\; \frac{L}{C_\alpha \log^2 L}, \tag{3.3.16}$$

implies

$$\|\mathcal{P}_T \mathcal{A}^* \mathcal{A} \mathcal{P}_T - \mathcal{P}_T\| \;\leq\; \frac{1}{2},$$

with probability exceeding $1 - 3L^{-\alpha}$.

Lemma 3.3.4. *Let M, Q, the Γ_p, and the $\mathcal{A}_p$ be the same as in Lemma 3.3.3. Let $\boldsymbol{W}_p$ be as in (3.3.7), and define*

$$\mu_p^2 = L \max_{\ell \in \Gamma_{p+1}} \|\boldsymbol{W}_p^* \hat{\boldsymbol{b}}_\ell\|_2^2. \tag{3.3.17}$$

Then there exists a constant $C_\alpha = O(\alpha)$ such that if

$$M \;\leq\; \frac{L}{C_\alpha \log^{3/2} L}, \tag{3.3.18}$$

then

$$\mu_p \;\leq\; \frac{\mu_{p-1}}{2}, \quad \textit{for} \;\; p = 1, \ldots, P, \tag{3.3.19}$$

with probability exceeding $1 - 2L^{-\alpha+1}$.

Lemma 3.3.5. *Let* α, M, Q, *the* Γ_p, *and the* $\mathcal{A}_p$ *be the same as in Lemma 3.3.3, and* μ_p *and* $\boldsymbol{W}_p$ *be the same as in Lemma 3.3.4. Assume that* (3.3.8) *and* (3.3.19) *hold:*

$$\|\boldsymbol{W}_{p-1}\|_F \leq 2^{-p+1} \quad \textit{and} \quad \mu_{p-1} \leq 2^{-p+1}\mu_h.$$

Then with probability exceeding $1 - PL^{-\alpha} \geq 1 - L^{-\alpha+1}$,

$$\max_{1\leq p\leq P} \left\| \mathcal{A}_p^* \mathcal{A}_p \boldsymbol{W}_{p-1} - \frac{Q}{L}\boldsymbol{W}_{p-1} \right\| \;\leq\; 2^{-p}\frac{3Q}{4L}.$$

3.4 Proof of key lemmas

3.4.1 Proof of Lemma 3.3.2

The proof of Lemma 3.3.2 is essentially an application of the matrix Chernoff bound in Proposition 3.

Using the matrix form of $\mathcal{A}$,

$$\mathcal{A} = \left[\Delta_1 \hat{\boldsymbol{B}} \quad \Delta_2 \hat{\boldsymbol{B}} \quad \cdots \quad \Delta_N \hat{\boldsymbol{B}} \right],$$

we can write $\mathcal{A}\mathcal{A}^*$ as sum of random matrices

$$\mathcal{A}\mathcal{A}^* = \sum_{n=1}^{N} \Delta_n \hat{\boldsymbol{B}} \hat{\boldsymbol{B}}^* \Delta_n^*,$$

where $\Delta_n = \mathrm{diag}(\{\hat{c}_\ell[n]\}_\ell)$ as in (3.1.3). To apply Proposition 3, we will need to condition on the maximum of the magnitudes of the $\hat{c}_\ell[n]$ not exceeding a certain size. To this end, given an α (which we choose later), we define the event

$$\Gamma_\alpha = \left\{ \max_{\substack{1\leq n\leq N \\ 1\leq \ell\leq L/2}} |\hat{c}_\ell[n]| \leq \alpha \right\},$$

and since the $|\hat{c}_\ell|^2$ are Rayleigh random variables,

$$\mathrm{P}\left\{\Gamma_\alpha^c\right\} \;\leq\; \frac{NL}{2} e^{-\alpha^2}.$$

We can now breakdown the calculation as

$$\mathrm{P}\left\{\lambda_{\max}(\mathcal{A}\mathcal{A}^*) > v\right\} \leq \mathrm{P}\left\{\lambda_{\max}(\mathcal{A}\mathcal{A}^*) > v \mid \Gamma_\alpha\right\} \mathrm{P}\left\{\Gamma_\alpha\right\} + \mathrm{P}\left\{\Gamma_\alpha^c\right\} \tag{3.4.1}$$

$$\leq \mathrm{P}\left\{\lambda_{\max}(\mathcal{A}\mathcal{A}^*) > v \mid \Gamma_\alpha\right\} + \mathrm{P}\left\{\Gamma_\alpha^c\right\}, \tag{3.4.2}$$

and similarly for $\mathrm{P}\left\{\lambda_{\min}(\mathcal{A}\mathcal{A}^*) > v\right\}$. Conditioned on Γ_α, the complex Gaussian random variables $\hat{c}_\ell[n]$ are still zero mean and independent; we denote these conditional random variables as $\hat{c}'_\ell[n]$, and set $\Delta'_n = \mathrm{diag}(\{\hat{c}'_\ell[n]\}_\ell)$, noting that

$$\mathrm{E}[|\hat{c}'_\ell[n]|^2] = \mathrm{E}[|\hat{c}_\ell[n]|^2 \mid \Gamma_\alpha] = \frac{1-(\alpha^2+1)\mathrm{e}^{-\alpha^2}}{1-\mathrm{e}^{-\alpha^2}} =: \sigma_\alpha^2 \leq 1.$$

We now apply Proposition 3 with

$$R = \max_n \left\{\lambda_{\max}(\Delta'_n \hat{\boldsymbol{B}}\hat{\boldsymbol{B}}^* \Delta'^*_n)\right\} \leq \max_n \left\{\lambda_{\max}(\Delta'_n)\lambda_{\max}(\hat{\boldsymbol{B}}\hat{\boldsymbol{B}}^*)\lambda_{\max}(\Delta'^*_n)\right\} \leq \alpha^2,$$

and

$$\begin{aligned}\rho_{\max} &= \lambda_{\max}\left(\sum_{n=1}^N \mathrm{E}[\Delta'_n \hat{\boldsymbol{B}}\hat{\boldsymbol{B}}^* \Delta'^*_n]\right) = N\lambda_{\max}\left(\mathrm{E}[\Delta'_n \hat{\boldsymbol{B}}\hat{\boldsymbol{B}}^* \Delta'^*_n]\right) \\ &\leq\; N\sigma_\alpha^2 \max_\ell \|\hat{\boldsymbol{b}}_\ell\|_2^2 \;=\; \mu_{\max}^2 N\frac{K}{L},\end{aligned}$$

and

$$\rho_{\min} = \lambda_{\min}\left(\sum_{n=1}^N \mathrm{E}\left[\Delta'_n \hat{\boldsymbol{B}}\hat{\boldsymbol{B}}^* \Delta'^*_n\right]\right) \;=\; N\sigma_\alpha^2 \min_\ell \|\hat{\boldsymbol{b}}_\ell\|_2^2 \;=\; \sigma_\alpha^2 \mu_{\min}^2 N\frac{K}{L},$$

which yields

$$\mathrm{P}\left\{\lambda_{\min}(\mathcal{A}\mathcal{A}^*) < \frac{\sigma_\alpha^2 \mu_{\min}^2 NK}{2L} \;\middle|\; \Gamma_\alpha\right\} \;\leq\; L\exp\left(-\frac{\sigma_\alpha^2 \mu_{\min}^2 NK}{8\alpha^2 L}\right),$$

where we have take $t = 1/2$ in (2.5.5), and

$$\mathrm{P}\left\{\lambda_{\max}(\mathcal{A}\mathcal{A}^*) > \frac{\mathrm{e}^{3/2}\mu_{\max}^2 NK}{L} \;\middle|\; \Gamma_\alpha\right\} \;\leq\; L\exp\left(-\frac{2\mu_{\max}^2 NK}{\alpha^2 L}\right),$$

where we have taken $t = \mathrm{e}^{3/2}$ in (2.5.6). Then taking $\alpha = \sqrt{2\log L}$ establishes the lemma.

3.4.2 Proof of Lemma 3.3.3

The proof of the Lemma and its corollary follow the exact same line of argumentation. We will start with the conditioning of the partial operators $\mathcal{A}_p$ on T; after this, the argument for the conditioning of the full operator $\mathcal{A}$ will be clear.

We start by fixing p, and set $\Gamma = \Gamma_p$. With

$$\boldsymbol{A}_k = \boldsymbol{b}_k \boldsymbol{c}_k^*,$$

where the $\boldsymbol{b}_k \in \mathbb{C}^K$ obey (3.1.10),(3.1.11),(3.1.14) and the $\boldsymbol{c}_k \in \mathbb{C}^N$ are random vectors distributed as in (3.1.15), we are interested in how the random operator

$$\mathcal{P}_T \mathcal{A}_p^* \mathcal{A}_p \mathcal{P}_T = \sum_{k \in \Gamma} \mathcal{P}_T(\boldsymbol{A}_k) \otimes \mathcal{P}_T(\boldsymbol{A}_k)$$

concentrates around its mean in the operator norm. This operator is a sum of independent random rank-1 operators on $N \times K$ matrices, and so we can use the matrix Bernstein inequality in Proposition 2 to estimate its deviation.

Since $\boldsymbol{A}_k = \boldsymbol{b}_k \boldsymbol{c}_k^*$, $\mathcal{P}_T(\boldsymbol{A}_k)$ is the rank-2 matrix given by

$$\begin{aligned} \mathcal{P}_T(\boldsymbol{A}_k) &= \langle \boldsymbol{b}_k, \boldsymbol{h} \rangle \boldsymbol{h} \boldsymbol{c}_k^* + \langle \boldsymbol{m}, \boldsymbol{c}_k \rangle \boldsymbol{b}_k \boldsymbol{m}^* - \langle \boldsymbol{b}_k, \boldsymbol{h} \rangle \langle \boldsymbol{m}, \boldsymbol{c}_k \rangle \boldsymbol{h} \boldsymbol{m}^* \\ &= \boldsymbol{h} \boldsymbol{v}_k^* + \boldsymbol{u}_k \boldsymbol{m}^*, \end{aligned}$$

where $\boldsymbol{v}_k = \langle \boldsymbol{h}, \boldsymbol{b}_k \rangle \boldsymbol{c}_k$ and $\boldsymbol{u}_k = \langle \boldsymbol{m}, \boldsymbol{c}_k \rangle (\boldsymbol{b}_k - \langle \boldsymbol{b}_k, \boldsymbol{h} \rangle \boldsymbol{h}) = \langle \boldsymbol{m}, \boldsymbol{c}_k \rangle (\boldsymbol{I} - \boldsymbol{h}\boldsymbol{h}^*) \boldsymbol{b}_k$.

The linear operator $\mathcal{P}_T(\cdot)$, since it maps $K \times N$ matrices to $K \times N$ matrix, can itself be represented as a $KN \times KN$ matrix that operates on a matrix that has been rasterized (in column order here) into a vector of length KN. We will find it convenient to denote these matrices in block form: $\{M(i,j)\}_{i,j}$, where $M(i,j)$ is a $K \times K$ matrix that occupies rows $(i-1)K+1, \ldots, iK$ and columns $(j-1)K+1, \ldots, jK$. Using this notation, we can write $\mathcal{P}_T$ as the matrix

$$\mathcal{P}_T = \{\boldsymbol{h}\boldsymbol{h}^* \delta(i,j)\}_{i,j} + \{m[i]m[j]\boldsymbol{I}\}_{i,j} - \{m[i]m[j]\boldsymbol{h}\boldsymbol{h}^*\}_{i,j}, \tag{3.4.3}$$

where $\delta(i,j) = 1$ if $i = j$ and is zero otherwise.

We will make repeated use the following three facts about block matrices below:

1. Let $\mathcal{M}$ be an operator that we can write in matrix form as

$$\mathcal{M} = \{\boldsymbol{M}\delta(i,j)\}_{i,j}$$

for some $K \times K$ matrix $\boldsymbol{M}$. Then the action of $\mathcal{M}$ on a matrix $\boldsymbol{X}$ is

$$\mathcal{M}(\boldsymbol{X}) = \boldsymbol{M}\boldsymbol{X},$$

and so $\|\mathcal{M}\| = \|\boldsymbol{M}\|$. Also, $\mathcal{M}^*(\boldsymbol{X}) = \boldsymbol{M}^*\boldsymbol{X}$.

2. Now suppose we can write $\mathcal{M}$ in matrix form as

$$\mathcal{M} = \{p[i]^* q[j]\boldsymbol{I}\}_{i,j},$$

for some $\boldsymbol{p}, \boldsymbol{q} \in \mathbb{C}^N$. Then the action of $\mathcal{M}$ on a matrix $\boldsymbol{X}$ is

$$\mathcal{M}(\boldsymbol{X}) = \boldsymbol{X}\boldsymbol{q}\boldsymbol{p}^*,$$

and so $\|\mathcal{M}\| = \|\boldsymbol{q}\boldsymbol{p}^*\| = \|\boldsymbol{q}\|_2\|\boldsymbol{p}\|_2$. Also, $\mathcal{M}^*(\boldsymbol{X}) = \boldsymbol{X}\boldsymbol{p}\boldsymbol{q}^*$.

3. Now let

$$\mathcal{M} = \{p[i]^* q[j]\boldsymbol{M}\}_{i,j}.$$

Then the action of $\mathcal{M}$ on a matrix $\boldsymbol{X}$ is

$$\mathcal{M}(\boldsymbol{X}) = \boldsymbol{M}\boldsymbol{X}\boldsymbol{q}\boldsymbol{p}^*,$$

and so $\|\mathcal{M}\| = \|\boldsymbol{M}\|\,\|\boldsymbol{q}\boldsymbol{p}^*\| = \|\boldsymbol{M}\|\,\|\boldsymbol{q}\|_2\|\boldsymbol{p}\|_2$. Also $\mathcal{M}^*(\boldsymbol{X}) = \boldsymbol{M}^*\boldsymbol{X}\boldsymbol{p}\boldsymbol{q}^*$.

We will break $\mathcal{P}_T(\boldsymbol{A}_k) \otimes \mathcal{P}_T(\boldsymbol{A}_k)$ into four different tensor products of rank-1 matrices, and treat each one in turn:

$$\mathcal{P}_T(\boldsymbol{A}_k)\otimes\mathcal{P}_T(\boldsymbol{A}_k) = \boldsymbol{h}\boldsymbol{v}_k^*\otimes\boldsymbol{h}\boldsymbol{v}_k^* + \boldsymbol{h}\boldsymbol{v}_k^*\otimes\boldsymbol{u}_k\boldsymbol{m}^* + \boldsymbol{u}_k\boldsymbol{m}^*\otimes\boldsymbol{h}\boldsymbol{v}_k^* + \boldsymbol{u}_k\boldsymbol{m}^*\otimes\boldsymbol{u}_k\boldsymbol{m}^*. \quad (3.4.4)$$

To handle these terms in matrix form, note that if $\boldsymbol{u}_1\boldsymbol{v}_1^*$ and $\boldsymbol{u}_2\boldsymbol{v}_2^*$ are rank-1 matrices, with $\boldsymbol{u}_i \in \mathbb{C}^K$ and $\boldsymbol{v}_i \in \mathbb{C}^N$, then the operator given by their tensor product can be written as

$$\boldsymbol{u}_1\boldsymbol{v}_1^* \otimes \boldsymbol{u}_2\boldsymbol{v}_2^* = \begin{bmatrix} v_1[1]^* v_2[1]\boldsymbol{u}_1\boldsymbol{u}_2^* & v_1[1]^* v_2[2]\boldsymbol{u}_1\boldsymbol{u}_2^* & \cdots & v_1[1]^* v_2[N]\boldsymbol{u}_1\boldsymbol{u}_2^* \\ v_1[2]^* v_2[1]\boldsymbol{u}_1\boldsymbol{u}_2^* & v_1[2]^* v_2[2]\boldsymbol{u}_1\boldsymbol{u}_2^* & \cdots & v_1[2]^* v_2[N]\boldsymbol{u}_1\boldsymbol{u}_2^* \\ \vdots & & \ddots & \\ v_1[N]^* v_2[1]\boldsymbol{u}_1\boldsymbol{u}_2^* & \cdots & \cdots & v_1[N]^* v_2[N]\boldsymbol{u}_1\boldsymbol{u}_2^* \end{bmatrix} = \{v_1[i]^* v_2[j]\boldsymbol{u}_1\boldsymbol{u}_2^*\}_{i,j}.$$

For the expectation of the sum, we compute the following:

$$\begin{aligned} \mathrm{E}[\boldsymbol{h}\boldsymbol{v}_k^* \otimes \boldsymbol{h}\boldsymbol{v}_k^*] &= |\langle \boldsymbol{h}, \boldsymbol{b}_k \rangle|^2 \, \mathrm{E}[\{\hat{c}_k[i]^* \hat{c}_k[j]\boldsymbol{h}\boldsymbol{h}^*\}_{i,j}] \\ &= |\langle \boldsymbol{h}, \boldsymbol{b}_k \rangle|^2 \, \{\delta(i,j)\boldsymbol{h}\boldsymbol{h}^*\}_{i,j}, \end{aligned}$$

and

$$\begin{aligned} \mathrm{E}[\boldsymbol{u}_k\boldsymbol{m}^* \otimes \boldsymbol{u}_k\boldsymbol{m}^*] &= \mathrm{E}[|\langle \boldsymbol{m}, \boldsymbol{c}_k \rangle|^2] \, \{m[i]m[j](\boldsymbol{I} - \boldsymbol{h}\boldsymbol{h}^*)\boldsymbol{b}_k\boldsymbol{b}_k^*(\boldsymbol{I} - \boldsymbol{h}\boldsymbol{h}^*)\}_{i,j} \\ &= \{m[i]m[j](\boldsymbol{I} - \boldsymbol{h}\boldsymbol{h}^*)\boldsymbol{b}_k\boldsymbol{b}_k^*(\boldsymbol{I} - \boldsymbol{h}\boldsymbol{h}^*)\}_{i,j}, \end{aligned}$$

since $\mathrm{E}[|\langle \boldsymbol{m}, \boldsymbol{c}_k \rangle|^2] = \|\boldsymbol{m}\|_2^2 = 1$, and

$$\begin{aligned} \mathrm{E}[\boldsymbol{h}\boldsymbol{v}_k^* \otimes \boldsymbol{u}_k\boldsymbol{m}^*] &= \mathrm{E}\{v_k[i]^* m[j]\boldsymbol{h}\boldsymbol{u}_k^*\}_{i,j} \\ &= \langle \boldsymbol{b}_k, \boldsymbol{h} \rangle \, \{\mathrm{E}[\hat{c}_k[i]^* \langle \boldsymbol{c}_k, \boldsymbol{m} \rangle] m[j]\boldsymbol{h}\boldsymbol{b}_k^*(\boldsymbol{I} - \boldsymbol{h}\boldsymbol{h}^*)\}_{i,j} \\ &= \langle \boldsymbol{b}_k, \boldsymbol{h} \rangle \, \{m[i]m[j]\boldsymbol{h}\boldsymbol{b}_k^*(\boldsymbol{I} - \boldsymbol{h}\boldsymbol{h}^*)\}_{i,j}, \end{aligned}$$

and

$$\begin{aligned} \mathrm{E}[\boldsymbol{u}_k\boldsymbol{m}^* \otimes \boldsymbol{h}\boldsymbol{v}_k^*] &= \langle \boldsymbol{h}, \boldsymbol{b}_k \rangle \, \{\mathrm{E}[\hat{c}_k[j] \langle \boldsymbol{m}, \boldsymbol{c}_k \rangle] m[i](\boldsymbol{I} - \boldsymbol{h}\boldsymbol{h}^*)\boldsymbol{b}_k\boldsymbol{h}^*\}_{i,j} \\ &= \langle \boldsymbol{h}, \boldsymbol{b}_k \rangle \, \{m[i]m[j](\boldsymbol{I} - \boldsymbol{h}\boldsymbol{h}^*)\boldsymbol{b}_k\boldsymbol{h}^*\}_{i,j}. \end{aligned}$$

A straightforward calculation combines these four results with (3.4.3) to verify that

$$\mathrm{E}[\mathcal{P}_T(\boldsymbol{A}_k) \otimes \mathcal{P}_T(\boldsymbol{A}_k)] = \mathcal{P}_T(\{\boldsymbol{b}_k\boldsymbol{b}_k^*\delta(i,j)\}_{i,j}\mathcal{P}_T).$$

In light of (3.3.5), this means

$$\mathrm{E}\left[\sum_{k\in\Gamma}\mathcal{P}_T(\boldsymbol{A}_k)\otimes\mathcal{P}_T(\boldsymbol{A}_k)\right]=\frac{Q}{L}\mathcal{P}_T+\mathcal{G}, \tag{3.4.5}$$

where $\|\mathcal{G}\|\le Q/4L$.

We now derive tail bounds for how far the sum over Γ for each of the terms in (3.4.4) deviates from their respective means. Starting with first term, we use the compact notation

$$\mathcal{Z}_k=\boldsymbol{h}\boldsymbol{v}_k^*\otimes\boldsymbol{h}\boldsymbol{v}_k^*-\mathrm{E}[\boldsymbol{h}\boldsymbol{v}_k^*\otimes\boldsymbol{h}\boldsymbol{v}_k^*],$$

for each addend. To apply Proposition 2, we need to uniformly bound the size (Orlicz ψ_1 norm) of each individual $\mathcal{Z}_k$ as well as the variance σ^2 in (2.5.3). For the uniform size bound,

$$\begin{aligned}\|\mathcal{Z}_k\|&=|\langle\boldsymbol{h},\boldsymbol{b}_k\rangle|^2\,\|\{(\hat{c}_k[i]^*\hat{c}_k[j]-\delta(i,j))\boldsymbol{h}\boldsymbol{h}^*\}_{i,j}\|\\&=|\langle\boldsymbol{h},\boldsymbol{b}_k\rangle|^2\,\|\{(\hat{c}_k[i]^*\hat{c}_k[j]-\delta(i,j))\boldsymbol{I}\}\{\boldsymbol{h}\boldsymbol{h}^*\delta(i,j)\}_{i,j}\|\\&\le|\langle\boldsymbol{h},\boldsymbol{b}_k\rangle|^2\,\|\boldsymbol{h}\boldsymbol{h}^*\|\,\|\boldsymbol{c}_k\boldsymbol{c}_k^*-\boldsymbol{I}\|\\&\le\frac{\mu_h^2}{L}\max(\|\boldsymbol{c}_k\|_2^2,1).\end{aligned}$$

Applying Lemma 3.5.2,

$$\mathrm{P}\left\{\max(\|\boldsymbol{c}_k\|_2^2,1)>u\right\}\;\le\;1.2\,\mathrm{e}^{-u/8N},$$

and combined with Lemma 2.5.1 this means

$$\|\mathcal{Z}_k\|_{\psi_1}\;\le\;\frac{\mu_h^2}{L}\|\max(\|\boldsymbol{c}_k\|_2^2,1)\|_{\psi_1}\;\le\;C\,\frac{\mu_h^2N}{L}.$$

For the variance, we need to compute $\mathrm{E}[\mathcal{Z}_k^*\mathcal{Z}_k]$. This will be easiest if we rewrite the action of $\mathcal{Z}_k$ on a matrix $\boldsymbol{X}$ as

$$\mathcal{Z}_k(\boldsymbol{X})=|\langle\boldsymbol{h},\boldsymbol{b}_k\rangle|^4\boldsymbol{h}\boldsymbol{h}^*\boldsymbol{X}(\boldsymbol{c}_k\boldsymbol{c}_k^*-\boldsymbol{I}),$$

and so

$$\mathcal{Z}_k^*\mathcal{Z}_k(\boldsymbol{X})=|\langle\boldsymbol{h},\boldsymbol{b}_k\rangle|^4\|\boldsymbol{h}\|_2^2\boldsymbol{h}\boldsymbol{h}^*\boldsymbol{X}(\boldsymbol{c}_k\boldsymbol{c}_k^*-\boldsymbol{I})^2,$$

and

$$\begin{aligned}\mathrm{E}[\mathcal{Z}_k^*\mathcal{Z}_k(\boldsymbol{X})] &= |\langle \boldsymbol{h}, \boldsymbol{b}_k\rangle|^4 \|\boldsymbol{h}\|_2^2 \boldsymbol{h}\boldsymbol{h}^*\boldsymbol{X}\,\mathrm{E}[(\boldsymbol{c}_k\boldsymbol{c}_k^* - \boldsymbol{I})^2] \\ &= N|\langle \boldsymbol{h}, \boldsymbol{b}_k\rangle|^4 \boldsymbol{h}\boldsymbol{h}^*\boldsymbol{X},\end{aligned}$$

and finally

$$\begin{aligned}\left\|\sum_{k\in\Gamma}\mathrm{E}[\mathcal{Z}_k^*\mathcal{Z}_k]\right\| &= N\sum_{k\in\Gamma}|\langle \boldsymbol{h}, \boldsymbol{b}_k\rangle|^4 \\ &\le \frac{\mu_h^2 N}{L}\sum_{k\in\Gamma}|\langle \boldsymbol{h}, \boldsymbol{b}_k\rangle|^2 \\ &\le \frac{5\mu_h^2 NQ}{4L^2},\end{aligned}$$

where we have used (3.3.5) in the last step. Collecting these results and applying Proposition 2 with $t = \alpha \log L$ yields

$$\begin{aligned}&\left\|\sum_{k\in\Gamma}\boldsymbol{h}\boldsymbol{v}_k^*\otimes\boldsymbol{h}\boldsymbol{v}_k^* - \mathrm{E}[\boldsymbol{h}\boldsymbol{v}_k^*\otimes\boldsymbol{h}\boldsymbol{v}_k^*]\right\| \le \\ &C_\alpha\,\frac{\mu_h\sqrt{N\log L}}{L}\max\left\{\sqrt{Q}, \mu_h\sqrt{N\log L}\log(\mu_h^2 N)\right\},\end{aligned} \tag{3.4.6}$$

with probability exceeding $1 - L^{-\alpha}$.

For the sum over the second term in (3.4.4), set

$$\begin{aligned}\mathcal{Z}_k &= \boldsymbol{u}_k\boldsymbol{m}^*\otimes\boldsymbol{u}_k\boldsymbol{m}^* - \mathrm{E}[\boldsymbol{u}_k\boldsymbol{m}^*\otimes\boldsymbol{u}_k\boldsymbol{m}^*] \\ &= \left(|\langle \boldsymbol{m}, \boldsymbol{c}_k\rangle|^2 - 1\right)\{m[i]m[j](\boldsymbol{I} - \boldsymbol{h}\boldsymbol{h}^*)\boldsymbol{b}_k\boldsymbol{b}_k^*(\boldsymbol{I} - \boldsymbol{h}\boldsymbol{h}^*)\}_{i,j},\end{aligned}$$

then using the fact that $\|\boldsymbol{I} - \boldsymbol{h}\boldsymbol{h}^*\| \le 1$ (since $\|\boldsymbol{h}\|_2 = 1$), we have

$$\begin{aligned}\|\mathcal{Z}_k\| &= \left|\,|\langle \boldsymbol{m}, \boldsymbol{c}_k\rangle|^2 - 1\right|\,\|(\boldsymbol{I} - \boldsymbol{h}\boldsymbol{h}^*)\boldsymbol{b}_k\|_2^2\,\|\boldsymbol{m}\|_2^2 \\ &\le \left|\,|\langle \boldsymbol{m}, \boldsymbol{c}_k\rangle|^2 - 1\right|\,\|\boldsymbol{b}_k\|_2^2 \\ &\le \left|\,|\langle \boldsymbol{m}, \boldsymbol{c}_k\rangle|^2 - 1\right|\,\frac{\mu_{\max}^2 K}{L}.\end{aligned}$$

This is again a subexponential random variable whose size we can characterize using Lemma 3.5.4:

$$\||\langle \boldsymbol{m}, \boldsymbol{c}_k\rangle|^2 - 1\|_{\psi_1} \le C \quad \text{and so} \quad \|\mathcal{Z}_k\|_{\psi_1} \;\le\; C\,\frac{\mu_{\max}^2 K}{L}.$$

To bound the variance in (2.5.4), we again write out the action of $\mathcal{Z}_k$ on an arbitrary $K \times N$ matrix $\boldsymbol{X}$:

$$\mathcal{Z}_k(\boldsymbol{X}) = (|\langle \boldsymbol{m}, \boldsymbol{c}_k \rangle|^2 - 1)(\boldsymbol{I} - \boldsymbol{h}\boldsymbol{h}^*)\boldsymbol{b}_k \boldsymbol{b}_k^* (\boldsymbol{I} - \boldsymbol{h}\boldsymbol{h}^*)\boldsymbol{X}\boldsymbol{m}\boldsymbol{m}^*,$$

and so

$$\begin{aligned}
\mathrm{E}[\mathcal{Z}_k^* \mathcal{Z}_k(\boldsymbol{X})] &= \mathrm{E}[(|\langle \boldsymbol{m}, \boldsymbol{c}_k \rangle|^2 - 1)^2] \|(\boldsymbol{I} - \boldsymbol{h}\boldsymbol{h}^*)\boldsymbol{b}_k\|_2^2 (\boldsymbol{I} - \boldsymbol{h}\boldsymbol{h}^*)\boldsymbol{b}_k \boldsymbol{b}_k^* (\boldsymbol{I} - \boldsymbol{h}\boldsymbol{h}^*)\boldsymbol{X}\boldsymbol{m}\boldsymbol{m}^* \\
&= \|(\boldsymbol{I} - \boldsymbol{h}\boldsymbol{h}^*)\boldsymbol{b}_k\|_2^2 (\boldsymbol{I} - \boldsymbol{h}\boldsymbol{h}^*)\boldsymbol{b}_k \boldsymbol{b}_k^* (\boldsymbol{I} - \boldsymbol{h}\boldsymbol{h}^*)\boldsymbol{X}\boldsymbol{m}\boldsymbol{m}^*,
\end{aligned}$$

where in the last step we have used the fact that $|\langle \boldsymbol{m}, \boldsymbol{c}_k \rangle|^2$ is a chi-square random variable with two degrees of freedom with variance $\mathrm{E}[(|\langle \boldsymbol{m}, \boldsymbol{c}_k \rangle|^2 - 1)^2] = 1$. This gives us

$$\begin{aligned}
\left\| \sum_{k \in \Gamma} \mathrm{E}[\mathcal{Z}_k^* \mathcal{Z}_k] \right\| &= \left\| \sum_{k \in \Gamma} \|(\boldsymbol{I} - \boldsymbol{h}\boldsymbol{h}^*)\boldsymbol{b}_k\|_2^2 (\boldsymbol{I} - \boldsymbol{h}\boldsymbol{h}^*)\boldsymbol{b}_k \boldsymbol{b}_k^* (\boldsymbol{I} - \boldsymbol{h}\boldsymbol{h}^*) \right\| \\
&\leq \max_{k \in \Gamma} \left(\|(\boldsymbol{I} - \boldsymbol{h}\boldsymbol{h}^*)\boldsymbol{b}_k\|_2^2 \right) \left\| \sum_{k \in \Gamma} (\boldsymbol{I} - \boldsymbol{h}\boldsymbol{h}^*)\boldsymbol{b}_k \boldsymbol{b}_k^* (\boldsymbol{I} - \boldsymbol{h}\boldsymbol{h}^*) \right\| \\
&\leq \frac{\mu_{\max}^2 K}{L} \left\| \sum_{k \in \Gamma} \boldsymbol{b}_k \boldsymbol{b}_k^* \right\| \\
&\leq \frac{5\mu_{\max}^2 K Q}{4L^2}.
\end{aligned}$$

Collecting these results and applying Proposition 2 with $t = \alpha \log L$ yields

$$\begin{aligned}
&\left\| \sum_{k \in \Gamma} \boldsymbol{u}_k \boldsymbol{m}^* \otimes \boldsymbol{u}_k \boldsymbol{m}^* - \mathrm{E}[\boldsymbol{u}_k \boldsymbol{m}^* \otimes \boldsymbol{u}_k \boldsymbol{m}^*] \right\| \leq \\
&C_\alpha \frac{\mu_{\max} \sqrt{K \log L}}{L} \max \left\{ \sqrt{Q}, \mu_{\max} \sqrt{K \log L} \log(\mu_{\max}^2 K) \right\}, \qquad (3.4.7)
\end{aligned}$$

with probability exceeding $1 - L^{-\alpha}$.

The last two terms in (3.4.4) are adjoints of one another, so they will have the same operator norm. We now set

$$\begin{aligned}
\mathcal{Z}_k &= \boldsymbol{h}\boldsymbol{v}_k^* \otimes \boldsymbol{u}_k \boldsymbol{m}^* - \mathrm{E}[\boldsymbol{h}\boldsymbol{v}_k^* \otimes \boldsymbol{u}_k \boldsymbol{m}^*] \\
&= \langle \boldsymbol{h}, \boldsymbol{b}_k \rangle \{ m[i](\hat{c}_k[j] \langle \boldsymbol{m}, \boldsymbol{c}_k \rangle - m[j])(\boldsymbol{I} - \boldsymbol{h}\boldsymbol{h}^*)\boldsymbol{b}_k \boldsymbol{h}^* \}_{i,j},
\end{aligned}$$

and so the action of $\mathcal{Z}_k$ on an arbitrary matrix $\boldsymbol{X}$ is given by

$$\mathcal{Z}_k(\boldsymbol{X}) = \langle \boldsymbol{h}, \boldsymbol{b}_k \rangle (\boldsymbol{I} - \boldsymbol{h}\boldsymbol{h}^*)\boldsymbol{b}_k \boldsymbol{h}^* \boldsymbol{X} (\boldsymbol{c}_k \boldsymbol{c}_k^* - \boldsymbol{I}) \boldsymbol{m}\boldsymbol{m}^*,$$

from which we can see

$$\begin{aligned} \|\mathcal{Z}_k\| &\leq |\langle \boldsymbol{h}, \boldsymbol{b}_k \rangle| \, \|\boldsymbol{b}_k\|_2 \|(\boldsymbol{c}_k \boldsymbol{c}_k^* - \boldsymbol{I})\boldsymbol{m}\|_2 \\ &\leq \frac{\mu_h \mu_{\max} \sqrt{K}}{L} \, \|(\boldsymbol{c}_k \boldsymbol{c}_k^* - \boldsymbol{I})\boldsymbol{m}\|_2. \end{aligned}$$

From Lemmas 3.5.5 and 2.5.1, we that the random variable $\|(\boldsymbol{c}_k \boldsymbol{c}_k^* - \boldsymbol{I})\boldsymbol{m}\|_2$ is subexponential with $\|(\boldsymbol{c}_k \boldsymbol{c}_k^* - \boldsymbol{I})\boldsymbol{m}\|_{\psi_1} \leq C\sqrt{N}$, and so

$$\|\mathcal{Z}_k\|_{\psi_1} \;\leq\; C \frac{\mu_h \mu_{\max} \sqrt{KN}}{L}.$$

For the variance σ^2 in (2.5.3), we need to bound the sizes of both $\mathcal{Z}_k^* \mathcal{Z}_k$ and $\mathcal{Z}_k \mathcal{Z}_k^*$. Starting with the former, we have

$$\mathrm{E}[\mathcal{Z}_k^* \mathcal{Z}_k(\boldsymbol{X})] = |\langle \boldsymbol{h}, \boldsymbol{b}_k \rangle|^2 \|(\boldsymbol{I} - \boldsymbol{h}\boldsymbol{h}^*)\|_2^2 \boldsymbol{h}\boldsymbol{h}^* \boldsymbol{X} \, \mathrm{E}[(\boldsymbol{c}_k \boldsymbol{c}_k^* - \boldsymbol{I})\boldsymbol{m}\boldsymbol{m}^*(\boldsymbol{c}_k \boldsymbol{c}_k^* - \boldsymbol{I})],$$

and then applying Lemma 3.5.6 yields

$$\begin{aligned} \left\| \sum_{k \in \Gamma} \mathrm{E}[\mathcal{Z}_k^* \mathcal{Z}_k] \right\| &= \sum_{k \in \Gamma} |\langle \boldsymbol{h}, \boldsymbol{b}_k \rangle|^2 \, \|(\boldsymbol{I} - \boldsymbol{h}\boldsymbol{h}^*)\boldsymbol{b}_k\|_2^2 \\ &\leq \sum_{k \in \Gamma} |\langle \boldsymbol{h}, \boldsymbol{b}_k \rangle|^2 \, \|\boldsymbol{b}_k\|_2^2 \\ &\leq \frac{\mu_{\max}^2 K}{L} \sum_{k \in \Gamma} |\langle \boldsymbol{h}, \boldsymbol{b}_k \rangle|^2 \\ &\leq \frac{5\mu_{\max}^2 KQ}{4L^2}. \end{aligned}$$

For $\mathcal{Z}_k \mathcal{Z}_k^*$,

$$\mathrm{E}[\mathcal{Z}_k \mathcal{Z}_k^*(\boldsymbol{X})] = |\langle \boldsymbol{h}, \boldsymbol{b}_k \rangle|^2 (\boldsymbol{I} - \boldsymbol{h}\boldsymbol{h}^*)\boldsymbol{b}_k \boldsymbol{b}_k^* (\boldsymbol{I} - \boldsymbol{h}\boldsymbol{h}^*) \boldsymbol{X}\boldsymbol{m}\boldsymbol{m}^* \, \mathrm{E}[(\boldsymbol{c}_k \boldsymbol{c}_k^* - \boldsymbol{I})^2]\boldsymbol{m}\boldsymbol{m}^*,$$

and then applying Lemma 3.5.3 yields

$$\begin{aligned}\left\|\sum_{k\in\Gamma}\mathrm{E}[\mathcal{Z}_k\mathcal{Z}_k^*]\right\| &= N\left\|(\boldsymbol{I}-\boldsymbol{h}\boldsymbol{h}^*)\left(\sum_{k\in\Gamma}|\langle\boldsymbol{h},\boldsymbol{b}_k\rangle|^2\boldsymbol{b}_k\boldsymbol{b}_k^*\right)(\boldsymbol{I}-\boldsymbol{h}\boldsymbol{h}^*)\right\| \\ &\leq N\left\|\sum_{k\in\Gamma}|\langle\boldsymbol{h},\boldsymbol{b}_k\rangle|^2\boldsymbol{b}_k\boldsymbol{b}_k^*\right\| \\ &\leq \frac{\mu_h^2 N}{L}\left\|\sum_{k\in\Gamma}\boldsymbol{b}_k\boldsymbol{b}_k^*\right\| \\ &\leq \frac{5\mu_h^2 NQ}{4L^2}.\end{aligned}$$

Collecting these results and applying Proposition 2 with $t = \alpha\log L$ and $M = \max\{\mu_{\max}^2 K, \mu_h^2 N\}$ yields

$$\left\|\sum_{k\in\Gamma}\boldsymbol{h}\boldsymbol{v}_k^*\otimes\boldsymbol{u}_k\boldsymbol{m}^* - \mathrm{E}[\boldsymbol{h}\boldsymbol{v}_k^*\otimes\boldsymbol{u}_k\boldsymbol{m}^*]\right\| \leq C_\alpha\frac{\sqrt{M\log L}}{L}\max\left\{\sqrt{Q},\sqrt{M\log L}\log(M)\right\}, \tag{3.4.8}$$

with probability exceeding $1-L^{-\alpha}$.

Using the triangle inequality

$$\left\|\mathcal{P}_T\mathcal{A}_p^*\mathcal{A}_p\mathcal{P}_T - \frac{Q}{L}\mathcal{P}_T\right\| \leq \left\|\mathcal{P}_T\mathcal{A}_p^*\mathcal{A}_p\mathcal{P}_T - \mathrm{E}[\mathcal{P}_T\mathcal{A}_p^*\mathcal{A}_p\mathcal{P}_T]\right\| + \left\|\mathrm{E}[\mathcal{P}_T\mathcal{A}_p^*\mathcal{A}_p\mathcal{P}_T] - \frac{Q}{L}\mathcal{P}_T\right\|,$$

we can combine (3.4.5) with (3.4.6), (3.4.7), and (3.4.8) to establish that

$$\left\|\mathcal{P}_T\mathcal{A}_p^*\mathcal{A}_p\mathcal{P}_T - \frac{Q}{L}\mathcal{P}_T\right\| \leq C_\alpha\frac{\sqrt{M\log L}}{L}\max\left\{\sqrt{Q},\sqrt{M\log L}\log(M)\right\} + \frac{Q}{4L},$$

with probability exceeding $1-3L^{-\alpha}$. With Q chosen as in (3.3.15), this becomes

$$\begin{aligned}\left\|\mathcal{P}_T\mathcal{A}_p^*\mathcal{A}_p\mathcal{P}_T - \frac{Q}{L}\mathcal{P}_T\right\| &\leq C_\alpha\frac{Q}{L}\max\left\{\frac{1}{\sqrt{C'_\alpha\log M}},\frac{1}{C'_\alpha}\right\} + \frac{Q}{4L} \\ &\leq \frac{Q}{2L},\end{aligned}$$

for C'_α chosen appropriately. Applying the union bound establishes the lemma.

To prove the corollary, we take $\Gamma = \{1,\ldots,L\}$ and $Q = L$ above. In this case, we will have $\sum_{k\in\Gamma}\boldsymbol{b}_k\boldsymbol{b}_k^* = \boldsymbol{I}$, and so $\mathcal{G} = 0$ in (3.4.5). We have

$$\|\mathcal{P}_T\mathcal{A}^*\mathcal{A}\mathcal{P}_T - \mathcal{P}_T\| \leq C_\alpha\max\left\{\sqrt{\frac{M\log L}{L}},\frac{M\log(L)\log(M)}{L}\right\},$$

with probability exceeding $1 - 3L^{-\alpha}$. Then taking L as in (3.3.16) will guarantee the desired conditioning.

3.4.3 Proof of Lemma 3.3.4

We start by fixing $\ell \in \Gamma_{p+1}$ and estimating $\|\boldsymbol{W}_p^* \hat{\boldsymbol{b}}_\ell\|_2$. We can re-write $\boldsymbol{W}_p$ as a sum of independent random matrices: since $\boldsymbol{W}_{p-1} \in T$, $\mathcal{P}_T(\boldsymbol{W}_{p-1}) = \boldsymbol{W}_{p-1}$ and

$$\begin{aligned}
\boldsymbol{W}_p &= \mathcal{P}_T\left(\mathcal{A}_p^*\mathcal{A}_p\boldsymbol{W}_{p-1} - \frac{Q}{L}\boldsymbol{W}_{p-1}\right) \\
&= \mathcal{P}_T\left(\sum_{k\in\Gamma_p} \boldsymbol{b}_k\boldsymbol{b}_k^*\boldsymbol{W}_{p-1}\boldsymbol{c}_k\boldsymbol{c}_k^* - \sum_{k\in\Gamma_p} \boldsymbol{b}_k\boldsymbol{b}_k^*\boldsymbol{W}_{p-1}\right) + \mathcal{P}_T\left(\sum_{k\in\Gamma_p} \boldsymbol{b}_k\boldsymbol{b}_k^*\boldsymbol{W}_{p-1} - \frac{Q}{L}\boldsymbol{W}_{p-1}\right) \\
&= \sum_{k\in\Gamma_p} \mathcal{P}_T(\boldsymbol{Z}_k) + \mathcal{P}_T\left(\sum_{k\in\Gamma_p} \boldsymbol{b}_k\boldsymbol{b}_k^*\boldsymbol{W}_{p-1} - \frac{Q}{L}\boldsymbol{W}_{p-1}\right),
\end{aligned}$$

where $\boldsymbol{Z}_k = \boldsymbol{b}_k\boldsymbol{b}_k^*\boldsymbol{W}_{p-1}(\boldsymbol{c}_k\boldsymbol{c}_k^* - \boldsymbol{I})$. Then

$$\|\boldsymbol{W}_p^*\hat{\boldsymbol{b}}_\ell\|_2 \le \left\|\sum_{k\in\Gamma_p} \hat{\boldsymbol{b}}_\ell^*\mathcal{P}_T(\boldsymbol{Z}_k)\right\|_2 + \left\|\hat{\boldsymbol{b}}_\ell^*\mathcal{P}_T\left(\sum_{k\in\Gamma_p} \boldsymbol{b}_k\boldsymbol{b}_k^*\boldsymbol{W}_{p-1} - \frac{Q}{L}\boldsymbol{W}_{p-1}\right)\right\|_2. \tag{3.4.9}$$

For the second term above

$$\begin{aligned}
\left\|\hat{\boldsymbol{b}}_\ell^*\mathcal{P}_T\left(\sum_{k\in\Gamma_p} \boldsymbol{b}_k\boldsymbol{b}_k^*\boldsymbol{W}_{p-1} - \frac{Q}{L}\boldsymbol{W}_{p-1}\right)\right\|_2 &\le \left\|\mathcal{P}_T\left(\sum_{k\in\Gamma_p} \boldsymbol{b}_k\boldsymbol{b}_k^*\boldsymbol{W}_{p-1} - \frac{Q}{L}\boldsymbol{W}_{p-1}\right)\right\| \|\hat{\boldsymbol{b}}_\ell\|_2 \\
&\le \sqrt{\frac{\mu_{\max}^2 K}{L}}\left\|\sum_{k\in\Gamma_p} \boldsymbol{b}_k\boldsymbol{b}_k^*\boldsymbol{W}_{p-1} - \frac{Q}{L}\boldsymbol{W}_{p-1}\right\| \\
&\le \sqrt{\frac{\mu_{\max}^2 K}{L}}\left\|\sum_{k\in\Gamma_p} \boldsymbol{b}_k\boldsymbol{b}_k^* - \frac{Q}{L}\boldsymbol{I}\right\| \|\boldsymbol{W}_{p-1}\|_F \\
&\le \frac{2^{-p+1}\mu_{\max}\sqrt{K}Q}{4L^{3/2}},
\end{aligned}$$

where we have used (3.3.5) and the fact that the Frobenius norms of the $\boldsymbol{W}_p$ decrease geometrically with p; see (3.3.8).

The first term in (3.4.9) is the norm of a sum of independent zero-mean random vectors, which we will bound using Propositions 1 and 2. We set $\boldsymbol{w}_k = \boldsymbol{W}_{p-1}^*\boldsymbol{b}_k$ and

expand $\hat{\boldsymbol{b}}_\ell^* \mathcal{P}_T(\boldsymbol{Z}_k)$ as

$$\hat{\boldsymbol{b}}_\ell^* \mathcal{P}_T(\boldsymbol{Z}_k) = \langle \boldsymbol{h}, \hat{\boldsymbol{b}}_\ell \rangle \langle \boldsymbol{b}_k, \boldsymbol{h} \rangle \boldsymbol{w}_k^* (\boldsymbol{c}_k \boldsymbol{c}_k^* - \boldsymbol{I}) + \\ + \langle \boldsymbol{b}_k, \hat{\boldsymbol{b}}_\ell \rangle \boldsymbol{w}_k^* (\boldsymbol{c}_k \boldsymbol{c}_k^* - \boldsymbol{I}) \boldsymbol{m}\boldsymbol{m}^* - \langle \boldsymbol{h}, \hat{\boldsymbol{b}}_\ell \rangle \langle \boldsymbol{b}_k, \boldsymbol{h} \rangle \boldsymbol{w}_k^* (\boldsymbol{c}_k \boldsymbol{c}_k^* - \boldsymbol{I}) \boldsymbol{m}\boldsymbol{m}^*,$$

and so

$$\left\| \sum_{k \in \Gamma_p} \hat{\boldsymbol{b}}_\ell^* \mathcal{P}_T(\boldsymbol{Z}_k) \right\|_2 \leq \left\| \sum_{k \in \Gamma_p} \boldsymbol{z}_k \right\|_2 + \left| \sum_{k \in \Gamma_p} z_k \right|, \tag{3.4.10}$$

where the $\boldsymbol{z}_k$ are independent random vectors, and the z_k are independent random scalars:

$$\boldsymbol{z}_k = \langle \hat{\boldsymbol{b}}_\ell, \boldsymbol{h} \rangle \langle \boldsymbol{h}, \boldsymbol{b}_k \rangle (\boldsymbol{c}_k \boldsymbol{c}_k^* - \boldsymbol{I}) \boldsymbol{w}_k, \qquad z_k = \langle \boldsymbol{b}_k, (\boldsymbol{I} - \boldsymbol{h}\boldsymbol{h}^*) \hat{\boldsymbol{b}}_\ell \rangle \, \langle (\boldsymbol{c}_k \boldsymbol{c}_k^* - \boldsymbol{I}) \boldsymbol{m}, \boldsymbol{w}_k \rangle.$$

Using Lemma 3.5.7, we have a tail bound for each term in the scalar sum:

$$\mathrm{P}\left\{ |z_k| > \lambda \right\} \leq 2\mathrm{e} \cdot \exp\left(- \frac{\lambda}{\|\boldsymbol{w}_k\|_2 |\langle \boldsymbol{b}_k, (\boldsymbol{I} - \boldsymbol{h}\boldsymbol{h}^*) \hat{\boldsymbol{b}}_\ell \rangle|} \right).$$

Applying the scalar Bernstein inequality (Proposition 1) with

$$B = \max_k \|\boldsymbol{w}_k\|_2 |\langle \boldsymbol{b}_k, (\boldsymbol{I} - \boldsymbol{h}\boldsymbol{h}^*) \hat{\boldsymbol{b}}_\ell \rangle| \;\leq\; \frac{\mu_{p-1} \mu_{\max}^2 K}{L^{3/2}},$$

and

$$\begin{aligned} \sigma^2 &= \sum_{k \in \Gamma_p} \|\boldsymbol{w}_k\|_2^2 |\langle \boldsymbol{b}_k, (\boldsymbol{I} - \boldsymbol{h}\boldsymbol{h}^*) \hat{\boldsymbol{b}}_\ell \rangle|^2 \\ &\leq \frac{\mu_{p-1}^2}{L} \sum_{k \in \Gamma_p} |\langle \boldsymbol{b}_k, (\boldsymbol{I} - \boldsymbol{h}\boldsymbol{h}^*) \hat{\boldsymbol{b}}_\ell \rangle|^2 \\ &\leq \frac{5 \mu_{p-1}^2 Q}{4L^2} \|(\boldsymbol{I} - \boldsymbol{h}\boldsymbol{h}^*) \hat{\boldsymbol{b}}_\ell\|_2^2 \\ &\leq \frac{5 \mu_{p-1}^2 \mu_{\max}^2 K Q}{4L^3}, \end{aligned}$$

and $t = \alpha \log L$ tells us that

$$\left| \sum_{k \in \Gamma_p} z_k \right| \leq C_\alpha \, \frac{\mu_{p-1} \mu_{\max} \sqrt{K \log L}}{L^{3/2}} \max\left\{ \sqrt{Q}, \mu_{\max} \sqrt{K \log L} \right\}, \tag{3.4.11}$$

with probability at least $1 - L^{-\alpha}$.

For the vector term in (3.4.10), we apply Lemmas 3.5.5 and 2.5.1 to see that

$$\begin{aligned}\|\boldsymbol{z}_k\|_{\psi_1} &\leq C\sqrt{N}\|\boldsymbol{w}_k\|_2|\langle\hat{\boldsymbol{b}}_\ell, \boldsymbol{h}\rangle\langle\boldsymbol{h}, \boldsymbol{b}_k\rangle| \\ &\leq C\frac{\mu_{p-1}\mu_h^2\sqrt{N}}{L^{3/2}}.\end{aligned}$$

For the variance terms, we calculate

$$\begin{aligned}\sum_{k\in\Gamma_p}\mathrm{E}[\boldsymbol{z}_k^*\boldsymbol{z}_k] &= \sum_{k\in\Gamma_p}|\langle\boldsymbol{h}, \hat{\boldsymbol{b}}_\ell\rangle|^2|\langle\boldsymbol{b}_k, \boldsymbol{h}\rangle|^2\boldsymbol{w}_k^*\,\mathrm{E}[(\boldsymbol{c}_k\boldsymbol{c}_k^* - \boldsymbol{I})^2]\boldsymbol{w}_k \\ &= N\sum_{k\in\Gamma_p}|\langle\boldsymbol{h}, \hat{\boldsymbol{b}}_\ell\rangle|^2|\langle\boldsymbol{b}_k, \boldsymbol{h}\rangle|^2\|\boldsymbol{w}_k\|_2^2 \qquad \text{(by Lemma 3.5.3)} \\ &\leq \frac{\mu_{p-1}^2\mu_h^2 N}{L^2}\sum_{k\in\Gamma_p}|\langle\boldsymbol{b}_k, \boldsymbol{h}\rangle|^2 \\ &\leq \frac{5\mu_{p-1}^2\mu_h^2 NQ}{4L^3},\end{aligned}$$

and

$$\begin{aligned}\left\|\sum_{k\in\Gamma_p}\mathrm{E}[\boldsymbol{z}_k\boldsymbol{z}_k^*]\right\| &= \left\|\sum_{k\in\Gamma_p}|\langle\boldsymbol{h}, \hat{\boldsymbol{b}}_\ell\rangle|^2|\langle\boldsymbol{b}_k, \boldsymbol{h}\rangle|^2\,\mathrm{E}[(\boldsymbol{c}_k\boldsymbol{c}_k^* - \boldsymbol{I})\boldsymbol{w}_k\boldsymbol{w}_k^*(\boldsymbol{c}_k\boldsymbol{c}_k^* - \boldsymbol{I})]\right\| \\ &= \left\|\sum_{k\in\Gamma_p}|\langle\boldsymbol{h}, \hat{\boldsymbol{b}}_\ell\rangle|^2|\langle\boldsymbol{b}_k, \boldsymbol{h}\rangle|^2\|\boldsymbol{w}_k\|_2^2\boldsymbol{I}\right\| \qquad \text{(by Lemma 3.5.6)} \\ &\leq \frac{\mu_{p-1}^2\mu_h^2}{L^2}\sum_{k\in\Gamma_p}|\langle\boldsymbol{b}_k, \boldsymbol{h}\rangle|^2 \\ &\leq \frac{5\mu_{p-1}^2\mu_h^2 Q}{4L^3}.\end{aligned}$$

Thus

$$\left\|\sum_{k\in\Gamma_p}\boldsymbol{z}_k\right\|_2 \leq C_\alpha\,\frac{\mu_{p-1}\mu_h\sqrt{N\log L}}{L^{3/2}}\max\left\{\sqrt{Q}, \mu_h\log(\mu_h)\sqrt{\log L}\right\} \tag{3.4.12}$$

with probability at least $1 - L^{-\alpha}$.

Combining (3.4.11) and (3.4.12) and taking the union bound over all $\ell \in \Gamma_{p+1}$ yields

$$\mu_p \leq \mu_{p-1}\,\frac{C_\alpha\sqrt{MQ\log L}}{L},$$

with probability exceeding $1 - 2QL^{-\alpha}$. Then taking Q as in (3.3.15) and the union bound over $1 \le p \le P$ establishes the lemma.

3.4.4 Proof of Lemma 3.3.5

We start by fixing p and writing

$$\left\| \mathcal{A}_p^* \mathcal{A}_p \boldsymbol{W}_{p-1} - \frac{Q}{L} \boldsymbol{W}_{p-1} \right\| \;\le\; \left\| \mathcal{A}_p^* \mathcal{A}_p \boldsymbol{W}_{p-1} - \mathrm{E}[\mathcal{A}_p^* \mathcal{A}_p \boldsymbol{W}_{p-1}] \right\| + \left\| \mathrm{E}[\mathcal{A}_p^* \mathcal{A}_p \boldsymbol{W}_{p-1}] - \frac{Q}{L} \boldsymbol{W}_{p-1} \right\|.$$

We will derive a concentration inequality to bound the first term, and use (3.3.5) for the second. We can write the first term above as the spectral norm of a sum of random rank-1 matrices:

$$\mathcal{A}_p^* \mathcal{A}_p \boldsymbol{W}_{p-1} - \mathrm{E}[\mathcal{A}_p^* \mathcal{A}_p \boldsymbol{W}_{p-1}] = \sum_{k \in \Gamma_p} \boldsymbol{Z}_k, \qquad \boldsymbol{Z}_k := \boldsymbol{b}_k \boldsymbol{b}_k^* \boldsymbol{W}_{p-1} (\boldsymbol{c}_k \boldsymbol{c}_k^* - \boldsymbol{I}). \quad (3.4.13)$$

We will use Proposition 2 to estimate the size of this random sum; we proceed by calculating the key quantities involved. With $\boldsymbol{w}_k = \boldsymbol{W}_{p-1}^* \boldsymbol{b}_k$, we can bound the size of each term in the sum as

$$\begin{aligned} \|\boldsymbol{Z}_k\| &= \|\boldsymbol{b}_k \boldsymbol{b}_k^* \boldsymbol{W}_p (\boldsymbol{c}_k \boldsymbol{c}_k^* - \boldsymbol{I})\| \\ &= \|\boldsymbol{b}_k\|_2 \, \|(\boldsymbol{c}_k \boldsymbol{c}_k^* - \boldsymbol{I}) \boldsymbol{w}_k\|_2 \\ &\le \mu_{\max} \sqrt{\frac{K}{L}} \, \|(\boldsymbol{c}_k \boldsymbol{c}_k^* - \boldsymbol{I}) \boldsymbol{w}_k\|_2 \end{aligned}$$

and then applying Lemmas 3.5.5 and 2.5.1 yields

$$\|\boldsymbol{Z}_k\|_{\psi_1} \le C \, \mu_{\max} \sqrt{\frac{KN}{L}} \, \|\boldsymbol{w}_k\|_2 \;\le\; C \, \mu_{\max} \mu_p \sqrt{\frac{KN}{L}}.$$

For the variance terms, we calculate

$$\begin{aligned} \left\| \sum_{k \in \Gamma_p} \mathrm{E}[\boldsymbol{Z}_k^* \boldsymbol{Z}_k] \right\| &= \left\| \sum_{k \in \Gamma_p} \|\boldsymbol{b}_k\|_2^2 \, \mathrm{E}[(\boldsymbol{c}_k \boldsymbol{c}_k^* - \boldsymbol{I}) \boldsymbol{w}_k \boldsymbol{w}_k^* (\boldsymbol{c}_k \boldsymbol{c}_k^* - \boldsymbol{I})] \right\| \\ &= \sum_{k \in \Gamma_p} \|\boldsymbol{b}_k\|_2^2 \|\boldsymbol{w}_k\|_2^2 \qquad \text{(by Lemma 3.5.6)} \\ &\le \frac{\mu_{\max}^2 K}{L} \sum_{k \in \Gamma_p} \|\boldsymbol{W}_p^* \boldsymbol{b}_k\|_2^2 \\ &\le \frac{5 \mu_{\max}^2 K Q}{4L^2} \|\boldsymbol{W}_p\|_F^2 \qquad \text{(using (3.3.5))}, \end{aligned}$$

and

$$\begin{aligned}\left\|\sum_{k\in\Gamma_p}\mathrm{E}[\boldsymbol{Z}_k\boldsymbol{Z}_k^*]\right\| &= \left\|\sum_{k\in\Gamma_p}\boldsymbol{b}_k\boldsymbol{w}_k^*\,\mathrm{E}[(\boldsymbol{c}_k\boldsymbol{c}_k^*-\boldsymbol{I})^2]\boldsymbol{w}_k\boldsymbol{b}_k^*\right\| \\ &= N\left\|\sum_{k\in\Gamma_p}\|\boldsymbol{w}_k\|_2^2\boldsymbol{b}_k\boldsymbol{b}_k^*\right\| \qquad \text{(by Lemma 3.5.3)} \\ &\le \frac{\mu_p^2 N}{L}\left\|\sum_{k\in\Gamma_p}\boldsymbol{b}_k\boldsymbol{b}_k^*\right\| \\ &\le \frac{5\mu_p^2 NQ}{4L^2}.\end{aligned}$$

Then with $M = \max\{\mu_{\max}^2 K, \mu_h^2 N\}$, we apply Proposition 2 with $t = \alpha\log L$ to get

$$\|\mathcal{A}_p^*\mathcal{A}_p\boldsymbol{W}_{p-1} - \mathrm{E}[\mathcal{A}_p^*\mathcal{A}_p\boldsymbol{W}_{p-1}]\| \le C_\alpha\, 2^{-p}\,\frac{\sqrt{M\log L}}{L}\max\left\{\sqrt{Q}, \sqrt{M\log L}\log(M)\right\},$$

with probability exceeding $1 - L^{-\alpha}$. With Q as in (3.3.15), this becomes

$$\begin{aligned}\|\mathcal{A}_p^*\mathcal{A}_p\boldsymbol{W}_{p-1} - \mathrm{E}[\mathcal{A}_p^*\mathcal{A}_p\boldsymbol{W}_{p-1}]\| &\le C_\alpha\, 2^{-p}\,\frac{Q}{L}\max\left\{\frac{1}{\sqrt{C'_\alpha\log M}}, \frac{1}{C'_\alpha}\right\} \\ &\le 2^{-p}\frac{Q}{4L},\end{aligned}$$

for an appropriate choice of C'_α. Thus

$$\begin{aligned}\left\|\mathcal{A}_p^*\mathcal{A}_p\boldsymbol{W}_{p-1} - \frac{Q}{L}\boldsymbol{W}_{p-1}\right\| &\le \left\|\mathcal{A}_p^*\mathcal{A}_p\boldsymbol{W}_{p-1} - \mathrm{E}[\mathcal{A}_p^*\mathcal{A}_p\boldsymbol{W}_{p-1}]\right\| + \left\|\mathrm{E}[\mathcal{A}_p^*\mathcal{A}_p\boldsymbol{W}_{p-1}] - \frac{Q}{L}\boldsymbol{W}_{p-1}\right\| \\ &\le 2^{-p}\frac{Q}{4L} + \left\|\sum_{k\in\Gamma_p}\boldsymbol{b}_k\boldsymbol{b}_k^* - \frac{Q}{L}\right\|\,\|\boldsymbol{W}_{p-1}\|_F \\ &\le 2^{-p}\frac{Q}{4L} + 2^{-p+1}\frac{Q}{4L}.\end{aligned}$$

Applying the union bound over all $p = 1, \ldots, P$ establishes the lemma.

3.5 Supporting Lemmas

Lemma 3.5.1. *Let $\boldsymbol{c}_k \in \mathbb{C}^N$ be normally distributed as in* (3.1.15)*, and let $\boldsymbol{u} \in \mathbb{C}^N$ be an arbitrary vector. Then $|\langle \boldsymbol{c}_k, \boldsymbol{u}\rangle|^2$ is a chi-square random variable with two degrees*

of freedom and

$$\mathrm{P}\left\{|\langle \boldsymbol{c}_k, \boldsymbol{u}\rangle|^2 > \lambda\right\} \;\leq\; \mathrm{e}^{-\lambda/\|\boldsymbol{u}\|_2^2}.$$

Lemma 3.5.2. *Let $\boldsymbol{c}_k \in \mathbb{C}^N$ be normally distributed as in* (3.1.15)*. Then*

$$\mathrm{P}\left\{\|\boldsymbol{c}_k\|_2^2 > Nu\right\} \;\leq\; 1.2\,\mathrm{e}^{-u/8}, \qquad \textit{for all } u \geq 0, \tag{3.5.1}$$

and since $1.2\mathrm{e}^{-1/8N} \geq 1$ for all $N \geq 1$,

$$\mathrm{P}\left\{\max(\|\boldsymbol{c}_k\|_2^2, 1) > Nu\right\} \;\leq\; 1.2\,\mathrm{e}^{-u/8}.$$

Proof. It is well-known (see, for example, [35]) that

$$\mathrm{P}\left\{\|\boldsymbol{c}_k\|_2^2 > N(1+\lambda)\right\} \;\leq\; \begin{cases} \mathrm{e}^{-\lambda^2/8} & 0 \leq \lambda \leq 1 \\ \mathrm{e}^{-\lambda/8} & \lambda \geq 1 \end{cases} \;\leq\; 1.05\,\mathrm{e}^{-\lambda/8}, \quad \lambda \geq 0. \tag{3.5.2}$$

Plugging in $\lambda = u - 1$ above yields

$$\mathrm{P}\left\{\|\boldsymbol{c}_k\|_2^2 > Nu\right\} \;\leq\; 1.2\,\mathrm{e}^{-u/8}, \quad u \geq 1.$$

Since $1.2\,\mathrm{e}^{-1/8} > 1$, the bound above can be extended for all $u \geq 0$. □

Lemma 3.5.3. *Let $\boldsymbol{c}_k \in \mathbb{C}^N$ be normally distributed as in* (3.1.15)*. Then*

$$\mathrm{E}[(\boldsymbol{c}_k\boldsymbol{c}_k^* - \boldsymbol{I})^2] = N\boldsymbol{I}.$$

Proof. Using the expansion

$$(\boldsymbol{c}_k\boldsymbol{c}_k^* - \boldsymbol{I})^2 = \|\boldsymbol{c}_k\|_2^2\boldsymbol{c}_k\boldsymbol{c}_k^* - 2\boldsymbol{c}_k\boldsymbol{c}_k^* + \boldsymbol{I},$$

we see that the only non-trivial term is $\boldsymbol{R} = \|\boldsymbol{c}_k\|_2^2\boldsymbol{c}_k\boldsymbol{c}_k^*$. We compute the expectation of an entry in this matrix as

$$\mathrm{E}[R(i,j)] = \sum_{n=1}^{N} \mathrm{E}[|\hat{c}_k[n]|^2\hat{c}_k[i]\hat{c}_k[j]^*] = \begin{cases} \sum_n \mathrm{E}[|\hat{c}_k[n]|^2|\hat{c}_k[i]|^2] & i = j \\ 0 & i \neq j \end{cases}.$$

For the addends in the diagonal term

$$\mathrm{E}[|\hat{c}_k[n]|^2|\hat{c}_k[i]|^2] = \begin{cases} \mathrm{E}[|\hat{c}_k[n]|^4] = 2 & n = i \\ 1 & n \neq i \end{cases},$$

where the calculation for $n = i$ relies on the fact that $\mathrm{E}[|\hat{c}_k[n]|^4]$ is the second moment of a chi-square random variable with two degrees of freedom. Thus $\mathrm{E}[\boldsymbol{R}] = (N+1)\boldsymbol{I}$, and

$$\mathrm{E}[(\boldsymbol{c}_k\boldsymbol{c}_k^* - \boldsymbol{I})^2] = (N+1)\boldsymbol{I} - 2\boldsymbol{I} + \boldsymbol{I} = N\boldsymbol{I}.$$

□

Lemma 3.5.4. *Let $\boldsymbol{c}_k \in \mathbb{C}^N$ be normally distributed as in* (3.1.15)*, and let $\boldsymbol{v}$ be an arbitrary vector. Then* $\mathrm{E}[|\langle \boldsymbol{c}_k, \boldsymbol{v}\rangle|^2] = \|\boldsymbol{v}\|_2^2$ *and*

$$\mathrm{P}\left\{\left||\langle \boldsymbol{c}_k, \boldsymbol{v}\rangle|^2 - \|\boldsymbol{v}\|_2^2\right| > \lambda\right\} \;\leq\; 2.1\,\exp\left(-\frac{\lambda}{8\|\boldsymbol{v}\|_2^2}\right).$$

Proof. A slight variation of (3.5.2) gives us that

$$\mathrm{P}\left\{\left||\langle \boldsymbol{c}_k, \boldsymbol{v}\rangle|^2 - \|\boldsymbol{v}\|_2^2\right| > \lambda\right\} \;\leq\; \begin{cases} 2\mathrm{e}^{-\lambda^2/8\|\boldsymbol{v}\|_2^2} & 0 \leq \lambda \leq 1 \\ \mathrm{e}^{-\lambda/8\|\boldsymbol{v}\|_2^2} & \lambda > 1 \end{cases}.$$

The lemma follows from combining these two cases into one subexponential bound.

□

Lemma 3.5.5. *Let $\boldsymbol{c}_k \in \mathbb{C}^N$ be normally distributed as in* (3.1.15)*, and let $\boldsymbol{v} \in \mathbb{C}^N$ be an arbitrary vector. Then*

$$\mathrm{P}\left\{\|(\boldsymbol{c}_k\boldsymbol{c}_k^* - \boldsymbol{I})\boldsymbol{v}\|_2 > \lambda\right\} \;\leq\; 3\exp\left(-\frac{\lambda}{\sqrt{8N}\|v\|_2}\right).$$

Proof. We have

$$\|(\boldsymbol{c}_k\boldsymbol{c}_k^* - \boldsymbol{I})\boldsymbol{v}\|_2 = \|\langle \boldsymbol{v}, \boldsymbol{c}_k\rangle\boldsymbol{c}_k - \boldsymbol{v}\|_2 \leq |\langle \boldsymbol{v}, \boldsymbol{c}_k\rangle|\|\boldsymbol{c}_k\|_2 + \|\boldsymbol{v}\|_2.$$

For the first term above, we have for any $\tau > 0$,

$$\begin{aligned}\mathrm{P}\left\{|\langle \boldsymbol{v}, \boldsymbol{c}_k\rangle|\,\|\boldsymbol{c}_k\|_2 > \lambda\sqrt{N}\|\boldsymbol{v}\|_2\right\} &\leq \mathrm{P}\left\{|\langle \boldsymbol{v}, \boldsymbol{c}_k\rangle| > \sqrt{\lambda}\|\boldsymbol{v}\|_2/\tau\right\} + \mathrm{P}\left\{\|\boldsymbol{c}_k\|_2 > \tau\sqrt{\lambda N}\right\} \\ &= \mathrm{P}\left\{|\langle \boldsymbol{v}, \boldsymbol{c}_k\rangle|^2 > \lambda\|\boldsymbol{v}\|_2^2/\tau^2\right\} + \mathrm{P}\left\{\|\boldsymbol{c}_k\|_2^2 > \tau^2\lambda N\right\}\end{aligned}$$

We can then use the fact that $|\langle \boldsymbol{v}, \boldsymbol{c}_k\rangle|^2$ is a chi-squared random variable along with (3.5.1) above to derive the following tail bound:

$$\begin{aligned}\mathrm{P}\left\{|\langle \boldsymbol{v}, \boldsymbol{c}_k\rangle|\,\|\boldsymbol{c}_k\|_2 > \lambda\sqrt{N}\|\boldsymbol{v}\|_2\right\} &\leq \mathrm{e}^{-\lambda/\tau^2} + 1.05\,\mathrm{e}^{-\tau^2\lambda/8} \\ &= 2.05\,\mathrm{e}^{-\lambda/\sqrt{8}},\end{aligned}$$

where we have chosen $\tau^2 = \sqrt{8}$. Thus

$$\mathrm{P}\left\{|\langle \boldsymbol{v}, \boldsymbol{c}_k\rangle|\,\|\boldsymbol{c}_k\|_2 + \|\boldsymbol{v}\|_2 > \lambda\right\} \leq 2.05\,\mathrm{e}^{1/\sqrt{8}} \cdot \mathrm{e}^{-\lambda/\sqrt{8N}}.$$

□

Lemma 3.5.6. *Let $\boldsymbol{c}_k \in \mathbb{C}^N$ be normally distributed as in* (3.1.15)*, and let $\boldsymbol{v} \in \mathbb{C}^N$ be an arbitrary vector. Then*

$$\mathrm{E}[(\boldsymbol{c}_k\boldsymbol{c}_k^* - \boldsymbol{I})\boldsymbol{v}\boldsymbol{v}^*(\boldsymbol{c}_k\boldsymbol{c}_k^* - \boldsymbol{I})] = \|\boldsymbol{v}\|_2^2\boldsymbol{I}.$$

Proof. We have

$$\begin{aligned}\mathrm{E}[(\boldsymbol{c}_k\boldsymbol{c}_k^* - \boldsymbol{I})\boldsymbol{v}\boldsymbol{v}^*(\boldsymbol{c}_k\boldsymbol{c}_k^* - \boldsymbol{I})] &= \mathrm{E}[|\langle \boldsymbol{v}, \boldsymbol{c}_k\rangle|^2\boldsymbol{c}_k\boldsymbol{c}_k^* - \boldsymbol{c}_k\boldsymbol{c}_k^*\boldsymbol{v}\boldsymbol{v}^* - \boldsymbol{v}\boldsymbol{v}^*\boldsymbol{c}_k\boldsymbol{c}_k^* - \boldsymbol{v}\boldsymbol{v}^*] \\ &= \mathrm{E}[|\langle \boldsymbol{v}, \boldsymbol{c}_k\rangle|^2\boldsymbol{c}_k\boldsymbol{c}_k^*] - \boldsymbol{v}\boldsymbol{v}^*.\end{aligned}$$

Let $R(i,j)$ be the entries of the first matrix above:

$$\begin{aligned}R(i,j) &= \mathrm{E}[|\langle \boldsymbol{v}, \boldsymbol{c}_k\rangle|^2\hat{c}_k[i]\hat{c}_k[j]^*] \\ &= \sum_{n_1,n_2} v[n_1]v[n_2]\,\mathrm{E}[\hat{c}_k[n_1]\hat{c}_k[n_2]^*\hat{c}_k[i]\hat{c}_k[j]^*].\end{aligned}$$

On the diagonal, where $i = j$, all of the terms in the sum above are zero except when $n_1 = n_2$, and so

$$R(i,i) = \sum_{n=1}^{N} |v[n]|^2\,\mathrm{E}\left[|\hat{c}_k[n]|^2|\hat{c}_k[i]|^2\right].$$

Using the fact that

$$\mathrm{E}\left[|\hat{c}_k[n]|^2|\hat{c}_k[i]|^2\right] = \begin{cases} 2 & n = i \\ & \\ 1 & n \neq i \end{cases},$$

we see that $R(i,i) = |v[i]|^2 + \|\boldsymbol{v}\|_2^2$. Off the diagonal, where $i \neq j$, we see immediately that $\mathrm{E}[\hat{c}_k[n_1]\hat{c}_k[n_2]^*\hat{c}_k[i]\hat{c}_k[j]^*]$ will be zero unless one of two (non-overlapping) conditions hold: $(n_1 = i, n_2 = j)$ or $(n_1 = j, n_2 = i)$. Thus

$$R(i,j) = v[i]v[j]\,\mathrm{E}[\hat{c}_k[i]^2]\,\mathrm{E}[\hat{c}_k[j]^2] + v[j]v[i]\,\mathrm{E}[|\hat{c}_k[j]|^2]\,\mathrm{E}[|\hat{c}_k[i]|^2].$$

Note the lack of absolute values in the first term on the right above; in fact, since the $\hat{c}_k[i]$ have uniformly distributed phase, $\mathrm{E}[\hat{c}_k[i]^2] = \mathrm{E}[\hat{c}_k[j]^2] = 0$, and so $R(i,j) = v[i]v[j]$. As such

$$\mathrm{E}[(\boldsymbol{c}_k\boldsymbol{c}_k^* - \boldsymbol{I})\boldsymbol{v}\boldsymbol{v}^*(\boldsymbol{c}_k\boldsymbol{c}_k^* - \boldsymbol{I})] = \mathrm{E}[|\langle \boldsymbol{v}, \boldsymbol{c}_k\rangle|^2\boldsymbol{c}_k\boldsymbol{c}_k^*] - \boldsymbol{v}\boldsymbol{v}^* = \boldsymbol{v}\boldsymbol{v}^* + \|\boldsymbol{v}\|_2^2\boldsymbol{I} - \boldsymbol{v}\boldsymbol{v}^* = \boldsymbol{I}.$$

□

Lemma 3.5.7. *Let $\boldsymbol{c}_k \in \mathbb{C}^N$ be normally distributed as in* (3.1.15)*, and let $\boldsymbol{u}, \boldsymbol{v} \in \mathbb{C}^N$ be arbitrary vectors. Then*

$$\mathrm{P}\left\{|\langle \boldsymbol{c}_k, \boldsymbol{v}\rangle\langle \boldsymbol{u}, \boldsymbol{c}_k\rangle - \langle \boldsymbol{u}, \boldsymbol{v}\rangle| > \lambda\right\} \leq 2\mathrm{e} \cdot \exp\left(-\frac{\lambda}{\|\boldsymbol{u}\|_2\|\boldsymbol{v}\|_2}\right).$$

Proof. For any $t > 0$,

$$\begin{aligned}
\mathrm{P}\left\{|\langle \boldsymbol{c}_k, \boldsymbol{v}\rangle\langle \boldsymbol{u}, \boldsymbol{c}_k\rangle| > \lambda\right\} &\leq \mathrm{P}\left\{|\langle \boldsymbol{c}_k, \boldsymbol{v}\rangle| > t\right\} + \mathrm{P}\left\{|\langle \boldsymbol{u}, \boldsymbol{c}_k\rangle| > \lambda/t\right\} \\
&= \mathrm{P}\left\{|\langle \boldsymbol{c}_k, \boldsymbol{v}\rangle|^2 > t^2\right\} + \mathrm{P}\left\{|\langle \boldsymbol{u}, \boldsymbol{c}_k\rangle|^2 > \lambda^2/t^2\right\} \\
&\leq \exp\left(-\frac{t^2}{\|\boldsymbol{v}\|_2^2}\right) + \exp\left(-\frac{\lambda^2}{t^2\|\boldsymbol{u}\|_2^2}\right).
\end{aligned}$$

Choosing $t^2 = \lambda\|\boldsymbol{v}\|_2/\|\boldsymbol{u}\|_2$ yields

$$\mathrm{P}\left\{|\langle \boldsymbol{c}_k, \boldsymbol{v}\rangle\langle \boldsymbol{u}, \boldsymbol{c}_k\rangle| > \lambda\right\} \leq 2\exp\left(-\frac{\lambda}{\|\boldsymbol{u}\|_2\|\boldsymbol{v}\|_2}\right),$$

and so

$$\begin{aligned}
\mathrm{P}\left\{|\langle \boldsymbol{c}_k, \boldsymbol{v}\rangle\langle \boldsymbol{u}, \boldsymbol{c}_k\rangle - \langle \boldsymbol{u}, \boldsymbol{v}\rangle| > \lambda\right\} &\leq \mathrm{P}\left\{|\langle \boldsymbol{c}_k, \boldsymbol{v}\rangle\langle \boldsymbol{u}, \boldsymbol{c}_k\rangle| > \lambda - \|\boldsymbol{u}\|_2\|\boldsymbol{v}\|_2\right\} \\
&\leq 2\exp\left(-\frac{\lambda}{\|\boldsymbol{u}\|_2\|\boldsymbol{v}\|_2} + 1\right) \\
&= 2\mathrm{e}\cdot\exp\left(-\frac{\lambda}{\|\boldsymbol{u}\|_2\|\boldsymbol{v}\|_2}\right).
\end{aligned}$$

□

CHAPTER IV

SAMPLING ARCHITECTURES FOR COMPRESSIVE ARRAY PROCESSING

4.1 Introduction

In this chapter, we present sampling architectures for the efficient acquisition of multiple signals lying in a subspace. The problem is illustrated in Figure 15 and 16: M signals, each of which is bandlimited to $W/2$ radians/sec, are outputs from a sensor array. Since the signals are bandlimited, they can be captured completely at MW samples per second. This can be achieved using an ADC operating at the Nyquist rate for each signal. We show that if the signals lie in a small subspace of dimension $R \ll M$, meaning that all the signals in the ensemble can be written as (or closely approximated by) distinct linear combinations of $R \ll M$ underlying signals, then the net sampling rate can be reduced considerably by using *analog diversification* [2, 3]. The signals are diversified using implementable analog devices and then sampled at a smaller rate. In Section 4.2.4, we will show that these samples can be expressed as linear measurements of a low-rank matrix. Over the course of one second, we want to acquire an $M \times W$ matrix comprised of the Nyquist rate samples of the ensemble. The proposed sampling architecture produces a series of linear combinations of entries of this matrix. The conditions (on the signals and the acquisition system) under which this type of recovery is effective have undergone an intensive study in the recent literature [19, 40, 44, 76].

Multiple signals lying in a subspace often arise from the outputs of a sensor array in various signal processing applications, some of which are outlined in Section 4.2.6. In such application, often the task is to estimate the signal parameters from their

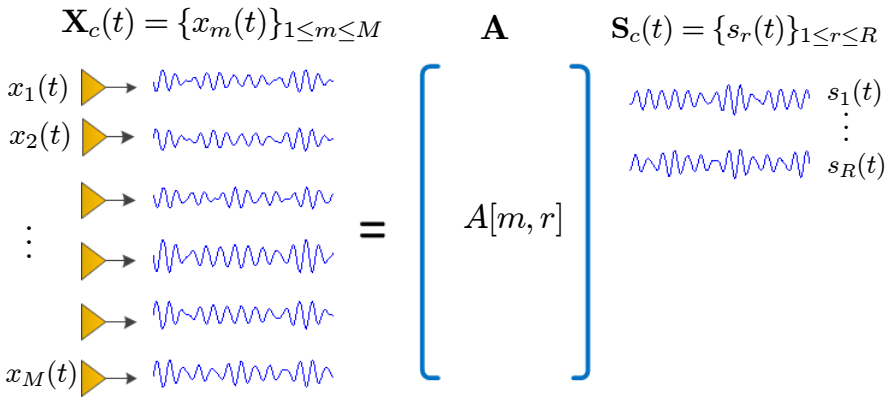

Figure 15: Acquire an ensemble of M signals, each bandlimited to B radians per second. The signals are *correlated*, i.e., M signals can be well approximated by the linear combination of R underlying signals. Therefore, we can write M signals in ensemble $\boldsymbol{X}_c(t)$ (on the left) as a tall matrix (a correlation structure) multiplied by an ensemble of R underlying independent signals.

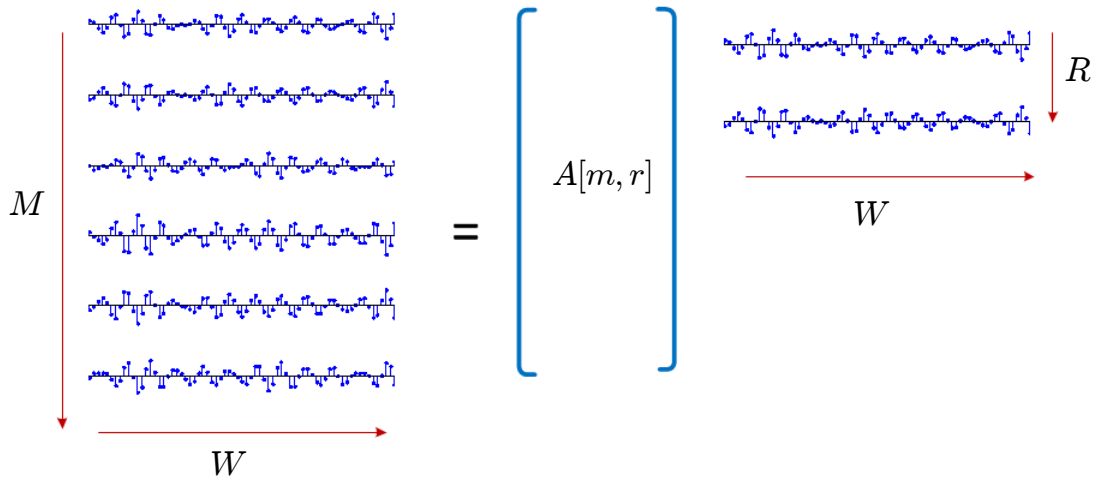

Figure 16: Samples $\boldsymbol{X}$ of ensemble $\boldsymbol{X}_c(t)$ inherit the low-rank property. Therefore, the problem of recovering $\boldsymbol{X_c(t)}$ from samples at a sub-Nyquist rate can be recast as a low-rank matrix recovery problem from partial-generalized measurements.

covariance matrix, e.g., the MUSIC algorithm in array processing uses the covariance matrix to estimate the signal parametrs, such as the estmation of angle of arrival, and frequency offsets. In several wideband signal processing applications, the sampling rate required to acquire the covariance matrix may be prohibitive; especially, in view of the increasing trend of using high frequency spectrum in some applications in array processing. Our proposed sampling architecture can be employed to estimate the covariance matrix of the input signal ensemble at a lower sampling rate; hence, relieving the sampling burden on the analog-to-digital converters (ADCs).

The main contributions of this chapter are the design of implementable sampling architectures, and a sampling theorem, which dictates the sampling rate required for the reconstruction of the signal ensemble, for each of the sampling architecture. In addition, we show that the proposed sampling schemes can be employed in several compressive array processing tasks. Specifically, we demonstrate that the sampling architectures can be used to compressively estimate the angle of arrival in several array processing applications.

The chapter is organized as follows. In Section 4.1.1, we describe the signal model followed by Section 4.1.2 that introduces architectural components. In Section 4.2, we present the sampling architectures, model the samples taken by the ADCs as the generalized measurements of a low-rank matrix, and state the releveant sampling theorems. In Section 4.2.6, we layout the applications in multiple signal parameter estimation problem. Numerical simulations, illustrating our theoretical results, are presented in Section 4.3. Finally, Sections 4.5, and 4.8 provide the derivation of the theoretical results.

4.1.1 Signal model

We will use notation $\boldsymbol{X_c}(t)$ to denote a signal ensemble of interest and $x_1(t), \ldots, x_M(t)$ to denote the individual signals within that ensemble. Conceptually, we may think

of $\boldsymbol{X_c}(t)$ as a "matrix" with finite M number of rows, but each row contains a bandlimited signal. Our underlying assumption is that the signals in the ensemble lie in a subspace $\mathcal{S}$ of dimension R; that is, we can write

$$\boldsymbol{X}_c(t) \approx \boldsymbol{A}\boldsymbol{S}_c(t), \tag{4.1.1}$$

where $\boldsymbol{S}_c(t)$ is a smaller signal ensemble with R signals that lie in subspace $\mathcal{S}$ and $\boldsymbol{A}$ is a $M \times R$ matrix with entries $A[m, r]$. We will use the convention that fixed matrices operating to the left of the signal ensembles simply "mix" the signals point-by-point, and so (4.1.1) is equivalent to

$$x_m(t) \approx \sum_{r=1}^{R} A[m, r] s_r(t).$$

The only structure we will impose on individual signals is that they are real-valued, bandlimited, and periodic. We will extend the results to a more general class of non-periodic signals in Section 5.2.6. Thus, signals live in a finite-dimensional linear subspace and provide a natural way of discretizing the problem; that is, what exists in $\boldsymbol{X_c}(t)$ for $t \in [0, 1]$ is all there is to know, and each signal can be captured exactly with W equally-spaced samples, which, for the most part, reduces the clutter in mathematics. In a detailed manuscript under preparation, we discuss how to adapt our results to more realistic signal models in which the (non-periodic) signal is windowed in time and overlapping sections are reconstructed jointly. Each bandlimited, periodic signal in the ensemble can be written as

$$x_m(t) = \sum_{f=-B}^{B} \alpha_m[f]\, e^{j2\pi f t},$$

where $\alpha_m[f]$ are complex but have symmetry $\alpha_m[-f] = \alpha_m[f]^*$ to ensure that $x_m(t)$ is real. We can capture $x_m(t)$ perfectly by taking $W = 2B + 1$ equally spaced samples per row. We will call this the $M \times W$ matrix of samples $\boldsymbol{X}$; of course, knowing every entry in this matrix is the same as knowing the entire signal ensemble. We can write

$$\boldsymbol{X} = \boldsymbol{C}\boldsymbol{F}, \tag{4.1.2}$$

where $\boldsymbol{F}$ is a $W \times W$ normalized discrete Fourier matrix and $\boldsymbol{C}$ is a $M \times W$ matrix whose rows contain Fourier series coefficients for the signals in $\boldsymbol{X}_c(t)$. Matrix $\boldsymbol{F}$ is orthonormal, while $\boldsymbol{C}$ inherits the correlation structure of the original ensemble. The estimate of the covariance matrix of the ensemble from W samples is then defined as

$$\boldsymbol{R}_{XX} = \lim_{W \to \infty} \frac{1}{W} \boldsymbol{X}\boldsymbol{X}^*.$$

We will be concerned with estimating $\boldsymbol{R}_{XX}$ from much fewer samples than dictated by Shannon-Nyquist framework.

4.1.2 Architectural components

In addition to analog-to-digital converters, our proposed architectures will use three standard components: analog vector-matrix multipliers, modulators, and linear time-invariant filters. The analog vector-matrix multiplier (AVMM) produces an output

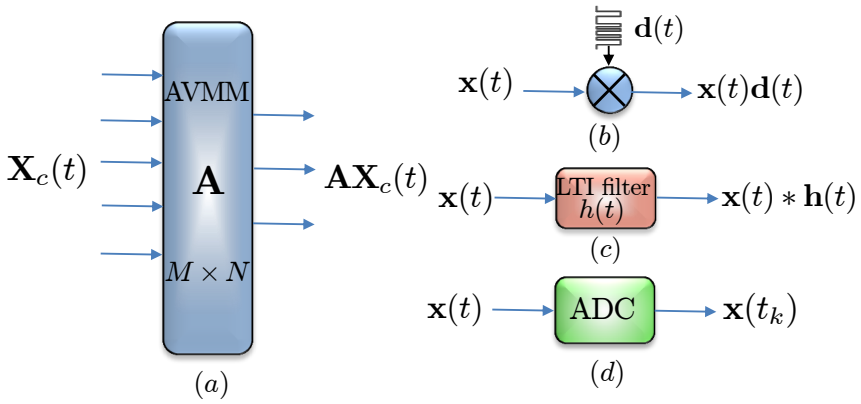

Figure 17: (a)The analog vector matrix multiplier (AVMM) takes random linear combinations of M input signals to produce N output signals. The action of AVMM can be thought of as the left multiplication of random matrix $\boldsymbol{A}$ to ensemble $\boldsymbol{X}_c(t)$. Intuitively, this operation amounts to distributing energy in the ensemble equally across channels. (b) Modulators multiply a signal in analog with a random binary waveform that disperses energy in the Fourier transform of the signal. (c) Random LTI filters randomize the phase information in the Fourier transform of a given signal by convolving it with $h_c(t)$ in analog, which distributes energy in time. (d) Finally, ADCs convert an analog stream of information in discrete form. We use both uniform and non-uniform sampling devices in our architectures.

signal ensemble $\boldsymbol{A}\boldsymbol{X}_c(t)$ when we input it with signal ensemble $\boldsymbol{X}_c(t)$, where $\boldsymbol{A}$ is an $N \times M$ matrix whose elements are fixed. Since the matrix operates pointwise on the ensemble of signals, sampling output $\boldsymbol{A}\boldsymbol{X}_c(t)$ is the same as applying $\boldsymbol{A}$ to matrix $\boldsymbol{X}$ of the samples (i.e., sampling commutes with the application of $\boldsymbol{A}$). Currently, analog VMM blocks can be built with hundreds of inputs and outputs and with bandwidths in the tens-to-hundreds of megahertz [33, 84]. We will use the VMM block to ensure that energy disperses more or less evenly throughout the channels. If $\boldsymbol{A}$ is a random orthogonal transform, it is highly probable that each signal in $\boldsymbol{A}\boldsymbol{X}_{\boldsymbol{c}}(t)$ will contain about the same amount of energy regardless of how the energy is distributed among the signals in $\boldsymbol{X}_{\boldsymbol{c}}(t)$ (formalized in Lemma 4.2.1 below), allowing us to deploy equal sampling resources in each channel while ensuring that resources on channels that are "quiet" are not being wasted.

The second component of the proposed architecture is the modulators, which simply take a single signal $x(t)$ and multiply it by fixed and known signal $d_c(t)$. We will take $d_c(t)$ to be a binary ± 1 waveform that is constant over time intervals of a certain length $1/W$. That is, the waveform alternates at the Nyquist sampling rate. If we take W samples of $d_c(t)x(t)$ on $[0, 1]$, then we can write the vector of samples $\boldsymbol{y}$ as

$$\boldsymbol{y} = \boldsymbol{D}\boldsymbol{x}, \tag{4.1.3}$$

where $\boldsymbol{x}$ is the W-vector containing the Fourier coefficients of $x(t)$, and $\boldsymbol{D}$ is an $\Omega \times \Omega$ diagonal matrix whose entries are samples $\boldsymbol{d} \in \mathbb{R}^{\Omega}$ of $d_c(t)$. We will choose a binary sequence that randomly generates $d_c(t)$, which amounts to $\boldsymbol{D}$ being a random matrix of the following form:

$$\boldsymbol{D} = \begin{bmatrix} d[0] & & & \\ & d[1] & & \\ & & \ddots & \\ & & & d[W-1] \end{bmatrix} \quad \text{where } d[n] = \pm 1 \text{ with probability } 1/2, \tag{4.1.4}$$

and the $d[n]$ are independent. Conceptually, the modulator disperses the information in the entire band of $x(t)$ — this allows us to acquire the information at a smaller rate by filtering a sub-band as will be shown in Section 4.2.

Compressive sampling architectures based on the random modulator have been analyzed previously in the literature [67,96]. The principal finding is that if the input signal is spectrally sparse (meaning the total size of the support of its Fourier transform is a small percentage of the entire band), then the modulator can be followed by a low-pass filter and an ADC that takes samples at a rate comparable to the size of the active band. This architecture has been implemented in hardware in multiple applications [49, 50, 56, 68, 71].

The third type of component we will use to preprocess the signal ensemble is a linear time-invariant (LTI) filter that takes an input $x(t)$ and convolves it with a fixed and known impulse response $h_c(t)$. We will assume that we have complete control over $h_c(t)$, even though this brushes aside admittedly important implementation questions. Because $x(t)$ is periodic and bandlimited, we can write the action of the LTI filter as a $W \times W$ circular matrix $\boldsymbol{H}$ operating on samples $\boldsymbol{x}$ (the first row of $\boldsymbol{H}$ consists of samples $\boldsymbol{h}$ of $h_c(t)$). We will make repeated use of the fact that $\boldsymbol{H}$ is diagonalized by the discrete Fourier transform:

$$\boldsymbol{H} = \boldsymbol{F}^{\mathrm{H}} \hat{\boldsymbol{H}} \boldsymbol{F}, \tag{4.1.5}$$

where $\boldsymbol{F}$ is the $W \times W$ normalized discrete Fourier matrix with entries, and $\hat{\boldsymbol{H}}$ is a diagonal matrix whose entries are $\hat{\boldsymbol{h}} = \sqrt{W}\boldsymbol{F}\boldsymbol{h}$. The vector $\hat{\boldsymbol{h}}$ is a scaled version of the non-zero Fourier series coefficients of $h(t)$.

To generate the impulse response, we will use a random unit-magnitude sequence

in the Fourier domain . In particular, we will take

$$\hat{\boldsymbol{H}} = \begin{bmatrix} \hat{h}(0) & & & \\ & \hat{h}(1) & & \\ & & \ddots & \\ & & & \hat{h}(W-1) \end{bmatrix} \tag{4.1.6}$$

where

$$\hat{h}(\omega) = \begin{cases} \pm 1, \text{with prob. } 1/2, & \omega = 0 \\ e^{\jmath\theta_\omega}, \text{ with } \theta_\omega \sim \text{Uniform}([0, 2\pi]), & 1 \leq \omega \leq (W-1)/2 \\ \hat{h}(W-\omega+1)^*, & (W+1)/2 \leq \omega \leq W-1 \end{cases} . \tag{4.1.7}$$

These symmetry constraints are imposed so that $\boldsymbol{h}$ (and hence, $h_c(t)$) is real-valued. Conceptually, convolution with $h_c(t)$ disperses a signal over time while maintaining fixed energy (note that $\boldsymbol{H}$ is an orthonormal matrix).

Convolution with a random pulse followed by sub-sampling has also been analyzed in the compressed sensing literature [46, 48, 79, 97]. If the random filter is created in the Fourier domain as above, then following the filter with an ADC that samples at random locations produces a universally efficient compressive sampling architecture — the number of samples that we need to recover a signal with only S active terms at unknown locations in any fixed basis scales linearly in S and logarithmically in ambient-dimension W.

4.2 Main Results: Sampling Architectures

This section presents the main results and their implications on the problem of efficient sampling of the ensemble of correlated signals. We will present a simplistic case of a known correlation structure first to motivate the problem followed by a discussion on each sampling architecture and a presentation of the main results.

4.2.1 Known correlation structure

If the mixing matrix $\boldsymbol{A}$ for ensemble $\boldsymbol{X}_c(t)$ is known at the receiver, then a straightforward way exists to sample the ensemble efficiently. Let $\boldsymbol{A} = \boldsymbol{U}\boldsymbol{\Sigma}\boldsymbol{V}^T$ be the singular value decomposition of $\boldsymbol{A}$, where $\boldsymbol{U}$ is $M \times R$ matrix with orthogonal columns, $\boldsymbol{\Sigma}$ is $R \times R$ diagonal matrix, and $\boldsymbol{V}$ is $W \times R$ with orthogonal rows. Then an efficient way is to *whiten* ensemble $\boldsymbol{A}$ with $\boldsymbol{U}^T$ and sample the resulting R signals (each at rate W). This scheme is shown in Figure 18. $\boldsymbol{X}$ can be written as a multiplication of matrix $\boldsymbol{U}$ and $R \times W$ matrix $\boldsymbol{Y}$, which contains the Nyquist samples of signals $\boldsymbol{x}_1(t), \cdots, \boldsymbol{x}_R(t)$ respectively in its R rows. The signal ensemble can the be obtained using the multiplicaion

$$\boldsymbol{X} = \boldsymbol{U}\boldsymbol{Y}.$$

Therefore, if we know the correlation structure $\boldsymbol{U}$, then $\boldsymbol{X}$ and hence $\boldsymbol{X}_c(t)$ (using sinc interpolation of samples in $\boldsymbol{X}$) can be recovered from the optimal total sampling rate of RW samples per second. In practice, the correlation structure of ensemble $\boldsymbol{X}_c(t)$ is

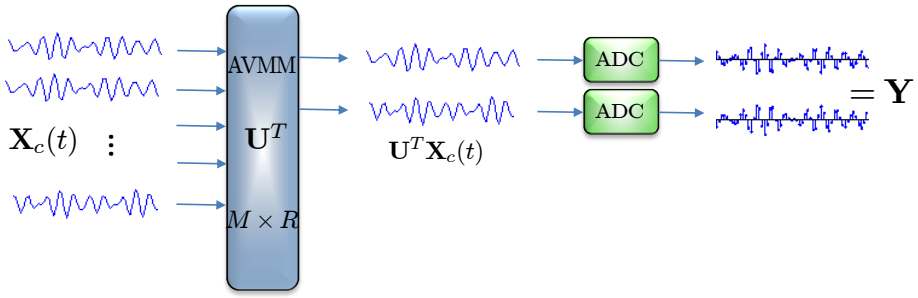

Figure 18: If, we know the correlation structure then efficient sampling structure is to *whiten* with $\boldsymbol{U}^T$ and then sample, which requires R ADCs, each operating at a rate W samples per second. Hence, ADCs take a total of RW samples per second, RW being the degrees of freedom in the R signals bandlimited to $W/2$.

not known and in this paper, we focus on designing sampling strategies that enable the blind acquisition (unknown correlation structure) of the signal ensemble at a sampling rate within log factors of the optimal sampling rate of RW samples per second. The

sampling schemes take generalized samples of signals by performing some analog preprocessing of the signals using VMMs, filters, and modulators. The randomness introduced by these components disperses energy over time and across channels so that the ADCs are always sensing information; that is, injection of randomness allows the wise use of sampling resources.

4.2.2 Matrix recovery

The generalized samples of the signals obtained by the sampling architectures can be used for the recovery of ensemble $\boldsymbol{X}_c(t)$ using convex optimization. Given L linear samples in $\boldsymbol{y}$ of matrix $\boldsymbol{X}_0$ through linear operator $\mathcal{A}$, i.e.,

$$\boldsymbol{y} = \mathcal{A}(\boldsymbol{X}_0), \quad \boldsymbol{y} \in \mathbb{R}^L, \quad \boldsymbol{X}_0 \in \mathbb{R}^{M \times W},$$

we solve

$$\begin{aligned} \min_{\boldsymbol{X}} \quad & \|\boldsymbol{X}\|_* \\ \text{subject to} \quad & \boldsymbol{y} = \mathcal{A}(\boldsymbol{X}) \end{aligned} \tag{4.2.1}$$

where $\|\boldsymbol{X}\|_*$ is the nuclear norm; the sum of the singular values of $\boldsymbol{X}$. But when noise $\boldsymbol{\xi}$, such that $\|\boldsymbol{\xi}\|_2 \leq \delta$, contaminates the measurements

$$\boldsymbol{y} = \mathcal{A}(\boldsymbol{X}_0) + \boldsymbol{\xi}, \tag{4.2.2}$$

we instead solve the following quadratically constrained convex optimization program

$$\begin{aligned} \min_{\boldsymbol{X}} \quad & \|\boldsymbol{X}\|_* \\ \text{subject to} \quad & \|\boldsymbol{y} - \mathcal{A}(\boldsymbol{X})\|_2 \leq \delta. \end{aligned} \tag{4.2.3}$$

An *optimal* sampler would recover $\boldsymbol{X}_0$ from $\boldsymbol{y}$ when we sample at a rate of RW, which is roughly the information content in the correlated signal ensemble $\boldsymbol{X}_c(t)$.

4.2.3 Architecture 1: Random sampling of time-dispersed correlated signals

The architecture presented in this section simply consists of a non-uniform sampling (nus) ADC per channel. The ADC in each channel operates randomly and independently of the ADCs in the rest of the channels. In the time window $t \in [0, 1)$, an nus ADC takes input signal $x_m(t)$ and returns the samples $\{x_m(t_k) : t_k \in T_m \subset \{0, 1/W, \cdots, 1 - 1/W\}$. The average sampling rate is $|T_m| = \Omega$ for each of the ADC. Thus, the bank of M nus ADCs sample input signal ensemble randomly on a uniform grid at rate $M\Omega$. The sampling architecture is shown in Figure 19. The sampling

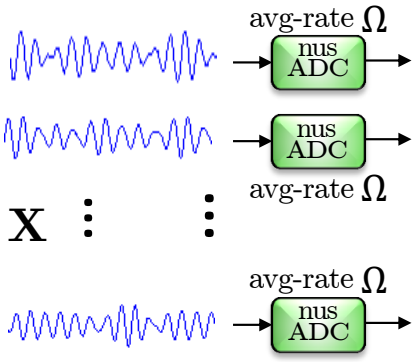

Figure 19: M signals recorded by the sensors are sampled separately by the independent random sampling ADCs, each of which samples on a uniform grid at an average rate of Ω samples per second. This sampling scheme takes on the average a total of $M\Omega$ samples per second and is equivalent to observing $M\Omega$ entries of the matrix $\boldsymbol{X}$ at random

model is equivalent to observing $L = M\Omega$ randomly chosen entries of the matrix of samples $\boldsymbol{X}$, defined in (4.1.2). This problem is exactly the same as the matrix-completion problem [19, 27], which states that given a small number of entries of a low-rank matrix, we can *fill in* missing entries under some incoherence assumptions on the matrix $\boldsymbol{X}$. Since $\boldsymbol{X}$ is rank-R, its svd is

$$\boldsymbol{X} = \boldsymbol{U}\boldsymbol{\Sigma}\boldsymbol{V}^*, \tag{4.2.4}$$

where $\boldsymbol{U} \in \mathbb{R}^{M\times R}$, $\boldsymbol{\Sigma} \in \mathbb{R}^{R\times R}$, and $\boldsymbol{V} \in \mathbb{R}^{W\times R}$. The coherence is then defined as

$$\mu_0^2 = \max\left\{ \frac{M}{R} \max_{1\le i\le M} \|\boldsymbol{U}^*\mathbf{e}_i\|_2^2 , \frac{W}{R} \max_{1\le i\le W} \|\boldsymbol{V}^*\mathbf{e}_i\|_2^2 , \frac{MW}{R} \|\boldsymbol{U}\boldsymbol{V}^*\|_\infty^2 \right\}. \qquad (4.2.5)$$

Now the matrix-completion results [19, 27] in the noiseless case assert that if $M\Omega \gtrsim C\mu_0^2 R(W+M)\log^2(W)$, the solution of the nuclear norm minimization program (4.2.1) (with $\mathcal{A} : \mathbb{R}^{M\times W} \to \mathbb{R}^{M\varphi}$ such that $\mathcal{A}$ maps $\boldsymbol{X}$ to randomly chosen entries of $\boldsymbol{X}$) exactly equals $\boldsymbol{X}$ with high probability. The result indicates that the sampling rate scales (within some log factors) with the number R of independent signals rather than with the total number M of signals in the ensemble. When the measurements $\boldsymbol{y}$ are contaiminated with noise as in (4.2.2) then the the result in [27] suggest that the solution $\tilde{\boldsymbol{X}}$ to the optimization problem (4.2.3) satisfies

$$\|\tilde{\boldsymbol{X}} - \boldsymbol{X}\|_F \le C_{\mu_0}\sqrt{\min(M,W)}\delta,$$

where C_{μ_0} is a contant that depends on the coherence μ_0, defined in (4.2.5).

As discussed before, the number of samples for the matrix completion incearse with increasing μ_0^2. The coherence parameter is small for matrices with even distribution of energy among their entries; see, [19] for details. Furthermore, signals are also known to be bandlimited, which implies that Architecture 1 is more effective for the efficient sampling of signals dispersed across channels and time. We will show in Section 4.2.5 that using AVMM and filters at the front end of the sampling scheme forces the signal energy to be distributed evenly. This will allow us to build sampling architectures that are effective uniformly for all SlS.

4.2.4 Architecture 2: The random modulator for correlated signals

To efficiently acquire the signal ensemble lying in a subspace, the architecture 2, shown in Figure 20, follows a two-step approach. In the first step, each of the M signals undergo analog preprocessing, which involves modulation, and low-pass filtering. The modulator takes an input signal $x_m(t)$ and multiplies it by a fixed and known $d_m(t)$.

We will take $d_m(t)$ to be a binary ± 1 waveform that is constant over an interval of length $1/W$. Intuitively, the modulation results in the diversification of the signal *information* over the frequency band of width W. The diversified analog signals are then processed by an analog-low-pass filter; implemented using an integrator, see [96] for details. The low-pass filter only selects a frequency sub-band (or a subspace) of width roughly equal to Ω, and as will be shown in Theorem 4.2.1, this partial information is enough for the signal reconstruction. The partial information suffices as the signals are scrambled using modulators before low-pass filtering. Note that the low-pass filter in each channel in Fig. 20 can be replaced; in general, by a band-pass filter, i.e., the location of the band does not matter only its width does. This also explains why we don't need to know the subspace in which signals live in advance.

In the second step, the filtered signal is sampled by an ADC in each channel at a lower rate Ω. The result in Theorem 4.2.1 asserts that Ω is roughly of a factor of R/M smaller than the Nyquist rate W.

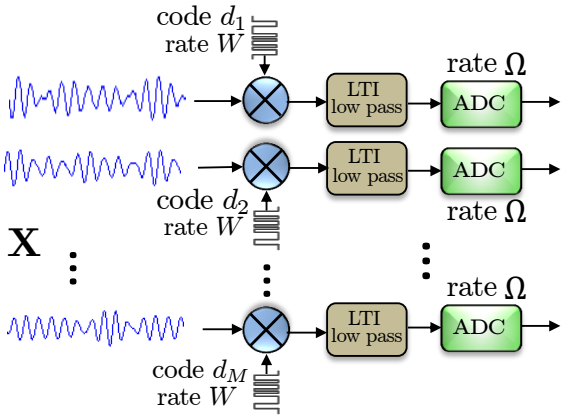

Figure 20: The random demodulator for multiple signals lying in a subspace: M signals lying in a subspace are preprocessed in analog using a bank of independent modulators, and low-pass filters. The resultant signal is then sampled uniformly by an ADC in each channel operating at rate Ω samples per second. The net sampling rate is $L = \Omega M$ samples per second.

System in matrix form

Each of the M input signals $x_m(t), 1 \leq m \leq M$ is multiplied by an independently

generated random binary waveform $d_m(t), 1 \leq m \leq M$ alternating at rate W. That is, the output after the modulation in the mth channel is

$$y_m(t) = x_m(t) \cdot d_m(t), \quad m = 1, \cdots, M, \text{ and } t \in [0, 1).$$

The $y_m(t)$ are then low-pass filtered using an integrator, which integrates $y_m(t)$ over an interval of width $1/\Omega$ and the result is then sampled at rate Ω using an ADC. The samples taken by the ADC in the mth channel are

$$y_m[n] = \int_{(n-1)/\Omega}^{n/\Omega} y_m(t)dt, \quad n = 1, \cdots, \Omega.$$

The integration operation commutes with the modulation process; hence, we can equivalently integrate the signals $x_m(t), 1 \leq m \leq M$ over the interval of width $1/W$, and treat them as samples $\boldsymbol{X}_0 \in \mathbb{R}^{M \times W}$ of the ensemble $\boldsymbol{X}_c(t)$. The entries $X_0[m, n]$ of the matrix $\boldsymbol{X}_0$ are

$$\begin{aligned} X_0[m, n] &= \int_{(n-1)/W}^{n/W} x_m(t)dt, \\ &= \sum_{|\omega| \leq W/2} C[m, \omega] \left[\frac{e^{\iota 2\pi\omega/W} - 1}{\iota 2\pi\omega} \right] e^{-\iota 2\pi\omega n/W}, \end{aligned}$$

where the bracketed term representing the low-pass filter

$$\tilde{L}[\omega] = \left[\frac{e^{\iota 2\pi\omega/W} - 1}{\iota 2\pi\omega} \right]$$

is evaluated in the window $\omega = 0, \pm 1, \cdots, \pm(W/2-1), W/2$. We will use an equivalent evaluation $L[\omega]$ of $\tilde{L}[\omega]$ in the window $\omega = 1, \cdots, W$. The Fourier coefficients of $C[m, \omega]$ of $\boldsymbol{X}$ defined in (4.1.2) are related to the Fourier coefficients $C_0[m, \omega]$ of $\boldsymbol{X}_0$

$$C_0[m, \omega] = C[m, \omega]L[\omega] \quad \omega = 1, \cdots, W, \tag{4.2.6}$$

and in time domain

$$\boldsymbol{X}_0 = \boldsymbol{C}_0 \boldsymbol{L} \boldsymbol{F}, \tag{4.2.7}$$

where $\boldsymbol{L}$ is a $W \times W$ diagonal matrix containing $L[\omega]$ as its diagonal entries, $\boldsymbol{F}$ is the $W \times W$ DFT matrix, and $\boldsymbol{C}_0$ is the coefficients matrix with entries defined in (4.2.6).

Since $\boldsymbol{C}_0$ inherits its low-rank structure from $\boldsymbol{C}$; therefore, $\boldsymbol{X}_0$ is also a low-rank matrix of rank R. In the rest of this write up, we will consider recovering the rank R matrix $\boldsymbol{X}_0$. Since $\boldsymbol{L}$ is well-conditioned, the recovery of $\boldsymbol{X}_0$ implies the recovery of $\boldsymbol{X}$ in (4.1.2).

In light of (4.1.3), the W equally-spaced samples of $d_m(t)x_m(t)$ are $\boldsymbol{D}_m\boldsymbol{x}_m$, where $\boldsymbol{x}_m$ is contains the W uniformly-spaced samples of $x_m(t)$, and $\boldsymbol{D}_m$, as in (4.1.4), is a random diagonal matrix containing random binary signs $d_m[n]$ along the diagonal. The binary waveform for the modulators in each channel is independently generated, which amounts to $\{\boldsymbol{D}_m\}$ being independent.

The samples $\boldsymbol{y}_m \in \mathbb{R}^{\Omega}$ in $t \in [0, 1)$ taken by the ADC in the mth branch are

$$\boldsymbol{y}_m = \boldsymbol{P}\boldsymbol{D}_m\boldsymbol{x}_m, \quad 1 \leq m \leq M,$$

where $\boldsymbol{x}_m \in \mathbb{R}^W$ are the rows of $\boldsymbol{X}_0$ defined in (4.2.7); $\boldsymbol{D}_m$ is the independent instantiation of $W \times W$ random diagonal matrix defined in (4.1.4), and corresponds to the modulator in the mth branch; and $\boldsymbol{P} : \Omega \times W$ is the matrix for the integrator (used as low-pass filter; for more details, see [96]) that contains ones in locations $(\alpha, \beta) \in (j, \mathcal{B}_j)$, for $j = 1, \cdots, \Omega$, where

$$\mathcal{B}_j = \{(j-1)W/\Omega + 1 : jW/\Omega\} \quad 1 \leq j \leq \Omega,$$

where we are assuming for simplicity that Ω is a factor of W. Since the action of the integrator commutes with the action of the modulator, the operation of the integrator can be simply represented as a block-diagonal matrix $\boldsymbol{P}$ operating on the modulated entries of the rows of $\boldsymbol{X}_0$, which contains the samples of the integrated signals. Putting it all together, the samples acquired by the ADCs can be written as a random block-diagonal matrix times the vector $\mathrm{vec}(\boldsymbol{X}_0)$, formed by stacking the

rows of low-rank $\boldsymbol{X}_0$ as

$$\boldsymbol{y} = \begin{bmatrix} \boldsymbol{y}_1 \\ \vdots \\ \boldsymbol{y}_M \end{bmatrix} = \begin{bmatrix} \boldsymbol{P}\boldsymbol{D}_1 & & \\ & \ddots & \\ & & \boldsymbol{P}\boldsymbol{D}_M \end{bmatrix} \cdot \mathrm{vec}(\boldsymbol{X}_0), \tag{4.2.8}$$

where $\boldsymbol{y} \in \mathbb{R}^{\Omega M}$ is the vector containing the samples acquired by all the ADCs. We will denote by L, the total number of samples per second $M\Omega$ taken by all the ADCs.

Sampling theorem: Exact and stable recovery

Clearly, the samples $\boldsymbol{y}$ at the ADCs are a linear transformation $\mathcal{A}$ of the rank-R matrix $\boldsymbol{X}_0$

$$\boldsymbol{y} = \mathcal{A}(\boldsymbol{X}_0).$$

Let $\boldsymbol{X}_0 = \boldsymbol{U}\boldsymbol{\Sigma}\boldsymbol{V}^T$ be the reduced form svd of $\boldsymbol{X}_0$ with $\boldsymbol{U} : M \times R$, $\boldsymbol{V} : W \times R$ being the matrices of left and right singular vectors, respectively, and $\boldsymbol{\Sigma} : R \times R$ being a diagonal matrix containing singular values of $\boldsymbol{X}_0$. Let $\{\boldsymbol{e}_i\}_{1 \le i \le M}$, and $\{\bar{\boldsymbol{e}}_k\}_{1 \le k \le W}$ be the standard basis vectors of dimensions M, and W, respectively. The coherences of $\boldsymbol{X}_0$ is defined as

$$\mu_1^2 = \frac{M}{R} \max_{1 \le i \le M} \|\boldsymbol{U}^* \boldsymbol{e}_i\|_2^2, \tag{4.2.9}$$

$$\mu_2^2 = \frac{W}{R} \max_{1 \le j \le W} \|\boldsymbol{V}^* \bar{\boldsymbol{e}}_j\|_2^2, \tag{4.2.10}$$

and

$$\mu_3^2 = \frac{M\Omega}{R} \max_{\substack{1 \le i \le M \\ 1 \le j \le \Omega}} \sum_{k \sim \mathcal{B}_j} \langle \boldsymbol{U}\boldsymbol{V}^*, \boldsymbol{e}_i \bar{\boldsymbol{e}}_k^* \rangle^2. \tag{4.2.11}$$

A simple calculation shows that $1 \le \mu_1^2 \le M/R$, and $1 \le \mu_2^2 \le W/R$; see, [19] for details. We will only show here that $1 \le \mu_3^2 \le MW/R$. Begin with

$$\begin{aligned} \sum_{k \sim \mathcal{B}_j} \langle \boldsymbol{U}\boldsymbol{V}^*, \boldsymbol{e}_i \bar{\boldsymbol{e}}_k^* \rangle^2 &\le \sum_{k \sim \mathcal{B}_j} \max_i \|\boldsymbol{U}^* \boldsymbol{e}_i\|_2^2 \cdot \max_k \|\boldsymbol{V}^* \bar{\boldsymbol{e}}_k\|_2^2 \\ &= |\mathcal{B}_j| \mu_1^2 \mu_2^2 \frac{R^2}{MW}, \end{aligned}$$

where the first inequality follows from the Cauchy-Schwartz's inequality, and the last equality follows from the definitions in (4.2.9), and (4.2.10). The fact that

$\mu_3^2 \leq MW/R$ follows by using the upper bounds on μ_1^2, and μ_2^2, and plugging in the definition. Similarly, the lower bound is obtained by summing over j on both sides of the definition as follows

$$\sum_j \mu_3^2 \geq \frac{M\Omega}{R} \sum_j \sum_{k \sim \mathcal{B}_j} \langle \boldsymbol{U}\boldsymbol{V}^*, \boldsymbol{e}_i \bar{\boldsymbol{e}}_k^* \rangle^2,$$

which implies that

$$\Omega \cdot \mu_3^2 \geq \frac{M\Omega}{R} \|\boldsymbol{U}\boldsymbol{e}_i^*\|_2^2,$$

and it follows that $\mu_3^2 \geq 1$ by using the fact that $\mu_1^2 \geq 1$. All three coherence quantities take smallest values for equally dispersed singular vectors and largest values for sparse singular vectors [19]. In our context, this implies that the coherence parameters quantify the dispersion of the signal-ensemble energy across time and channels.

Theorem 4.2.1. *Suppose $L = M\Omega$ measurements of the ensemble $\boldsymbol{X}_0$ are taken using* (4.2.8)*. If*

$$\Omega \geq C\beta R \max((W/M) \max(\mu_1^2 \mu_3^2), \max(\mu_2^2, \mu_3^2)) \log^3(WM) \tag{4.2.12}$$

for some $\beta > 2$, then the minimizer $\tilde{\boldsymbol{X}}$ to the problem (4.2.1) *is unique and equal to $\boldsymbol{X}_0$ with probability at least $1 - O((WM)^{1-\beta})$.*

The result indicates that each ADC operates at a rate Ω that is smaller than the Nyquist rate W by a factor of R/M. The net sampling rate L scales with the number R of independent signals rather than with the total number M of signals in the ensemble. Thus, the random demodulator provably acquires multiple signals lying in a subspace at a rate that is within log factors of the optimal sampling rate without knowing the subspace in advance. The coherence terms suggest that the sampling architecture is more effective for sampling signals with energy dispersed evenly across channels and time.

Stable recovery

In a realistic scenario, the measurements are almost always contaminated with noise, as in (4.2.2). In the case, when the noise is bounded, i.e., $\|\boldsymbol{\xi}\|_2 \leq \delta$, then following the template of the proof in [27], it can be shown that under the conditions of Theorem 4.2.1, the solution $\tilde{\boldsymbol{X}}$ of (4.2.3) obeys

$$\|\tilde{\boldsymbol{X}} - \boldsymbol{X}_0\|_F \leq C\sqrt{\min(W, M)}\delta, \tag{4.2.13}$$

with high probability; for more details on this, see a similar stability result in Theorem 2 in [4]. The above stability result is weak due to the multiplication factor $\sqrt{\min(W, M)}$. In contrast to the optimization program in (4.2.3), the solution $\tilde{\boldsymbol{X}}$ to a slightly different optimization program:

$$\tilde{\boldsymbol{X}} = \text{argmin}_{\boldsymbol{X}}\{\|\boldsymbol{X}\|_F^2 - 2\langle \boldsymbol{y}, \mathcal{A}(\boldsymbol{X})\rangle + \lambda \|\boldsymbol{X}\|_*\}, \tag{4.2.14}$$

proposed in [53] can be theoretically shown to obey essentially optimal stable recovery results. By completing the square, it is easy to see that the above esimator is equivalent to

$$\tilde{\boldsymbol{X}} = \text{argmin}_{\boldsymbol{X}}\{\|\boldsymbol{X} - \mathcal{A}^*(\boldsymbol{y})\|_F^2 + \lambda\|\boldsymbol{X}\|_*\}.$$

Taking the sub-differential $\partial C(\boldsymbol{X})$ of the cost function $C(\boldsymbol{X}) = \{\|\boldsymbol{X} - \mathcal{A}^*(\boldsymbol{y})\|_F^2 + \lambda\|\boldsymbol{X}\|_*\}$ and using the fact $\tilde{\boldsymbol{X}}$ is the minimizer iff $\boldsymbol{0} \in \partial C(\boldsymbol{X})$, it can be shown [53] that the estimate $\tilde{\boldsymbol{X}}$ is a soft thresholding of the singular values of the matrix $\boldsymbol{X}_{\mathcal{A}} = \mathcal{A}^*(\boldsymbol{y}) \in \mathbb{R}^{M\times W}$

$$\tilde{\boldsymbol{X}} = \sum_i \{\sigma_i(\boldsymbol{X}_{\mathcal{A}}) - \frac{\lambda}{2}\}_+ \boldsymbol{u}_i(\boldsymbol{X}_{\mathcal{A}})\boldsymbol{v}_i^*(\boldsymbol{X}_{\mathcal{A}}),$$

where $x_+ = \max\{x, 0\}$; in addition, $\boldsymbol{u}_i(\boldsymbol{X}_{\mathcal{A}})$, and $\boldsymbol{v}_i(\boldsymbol{X}_{\mathcal{A}})$ are the left and right singular vectors of the matrix $\boldsymbol{X}_{\mathcal{A}}$, respectively; and $\sigma_i(\boldsymbol{X}_{\mathcal{A}})$ is the corresponding singular value.

In comparison to the estimator (4.2.14), the matrix Lasso in (4.2.3) does not use the knowledge of the known distribution of $\mathcal{A}$ and instead minimizes the empirical

risk $\|\boldsymbol{y} - \mathcal{A}(\boldsymbol{X})\|_2 = \|\boldsymbol{y}\|_2^2 - 2\langle \boldsymbol{y}, \mathcal{A}(\boldsymbol{X})\rangle + \|\mathcal{A}(\boldsymbol{X})\|_2^2$. Knowing the distribution, and the fact that $\mathrm{E}\,\mathcal{A}^*\mathcal{A} = \mathcal{I}$ holds in our case, we replace $\|\mathcal{A}(\boldsymbol{X})\|_2^2$, by its expected value $\mathrm{E}\,\|\mathcal{A}(\boldsymbol{X})\|_2^2 = \|\boldsymbol{X}\|_F^2$ in the empirical risk to obtain the estimator in (4.2.14). Although the KLT estimator is easier to analyze, and gives optimal stable recovery results in theory but it does not empirically perform as well as matrix Lasso.

Before stating the stable recovery results, we introduce the statistical assumptions on the additive measurement noise $\boldsymbol{\xi}$, which are given as

$$\max_{ij} \mathrm{E} \exp\left(\frac{|\xi_{ij}|^2}{\sigma^2}\right) < \tilde{c} \tag{4.2.15}$$

$$\|\boldsymbol{\xi}\|_{\psi_2}^2 = c\sum_{i,j} \mathrm{E}\,\xi_{ij}^2 = cL\sigma^2, \tag{4.2.16}$$

where ψ_2 denotes the Orlicz-2 norm of vector $\boldsymbol{\xi} \in \mathbb{R}^L$ that contains ξ_{ij} as its entries. The choice of the indexing with double-index i, j will be clear in Section 4.5. With this the following result is in order.

Theorem 4.2.2. *Let $\boldsymbol{X}_0 \in \mathbb{R}^{M\times W}$ be a rank R matrix, and suppose that we observe y_{ij} as in (4.2.2) contaminated with noise ξ_{ij} such that (4.2.15) holds. Then with probability at least $1 - O((WM)^{-\beta})$ for some $\beta > 1$, the solution $\tilde{\boldsymbol{X}}$ to (4.2.14) will obey*

$$\|\hat{\boldsymbol{X}} - \boldsymbol{X}_0\|_F \leq C\|\boldsymbol{\xi}\|_{\psi_2}, \tag{4.2.17}$$

for a fixed constant C, when $\Omega \geq C\beta\mu_3^2 \max(W/M, 1)\log^2(WM)$

Roughly speaking, the stable recovery theorem states that the nuclear norm penalized estimators are stable in the presence of additive measurement noise. The results in Theorem 4.2.2 are derived assuming that ξ_{ij} are random with statisitcs in (4.2.15). In contrast, the stable recovery results in the compressed sensing literature only assume that the noise is bounded, i.e., $\|\boldsymbol{\xi}\|_2 \leq \delta$, where $\boldsymbol{\xi}$ is the noise vector introduced earlier. Here, we give a brief comparison of the results in Theorem (4.2.2) with the stable recovery results in [27, 41].

Compare the result in (4.2.13) with (4.2.17), it follows that our results improve upon the results in [27] by a factor of $1/(W \wedge M)$. We will also compare our stable recovery results against the stable recovery results derived in [41]. The result roughly states if the linear operator $\mathcal{A}$ satisfies the matrix RIP [76], and $\|\boldsymbol{\xi}\|_2 \leq \delta$, then the solution $\tilde{\boldsymbol{X}}$ to (4.2.3) obeys

$$\|\tilde{\boldsymbol{X}} - \boldsymbol{X}_0\|_F \leq C\delta. \tag{4.2.18}$$

The above result is essentially optimal stable recovery result. In comparison to (4.2.18), the result in (4.2.17) is also optimal, however, we prove it for a different estimator and under a statistical bound on the noise term $\|\boldsymbol{\xi}\|_{\psi_2} \leq \delta$. In addition, we also donot require the matrix RIP for $\mathcal{A}$.

The result in Theorem 4.2.1 is more effective for incoherent $\boldsymbol{X}$. Roughly speaking, the incoherence conditions are satisfied by a matrix with even distribution of energy among its entries. The incoherence conditions on the matrix of samples $\boldsymbol{X}_0$ when combined with the fact that the signals are also known to be bandlimited implies that Architectures 2 is also feasible for the efficient sampling of *spread out* correlated signal ensembles. In contrast, a *universal* sampling scheme will work for any ensemble of correlated signals. We can design such a sampling scheme by preprocessing signals in analog by components that transform (with high probability) matrix $\boldsymbol{X}$ to an incoherent matrix. We present such an architecture in the following section.

4.2.5 Architecture 3: Uniform sampling architectures

The performance of Architecture 1 and 2 depends on the coherences in defined (4.2.5); and (4.2.9), (4.2.10), (4.2.11) of ensemble $\boldsymbol{X}_c(t)$. That is, the net sampling rate depends on the energy distribution of the signal ensemble. In this section, we present uniform sampling architectures that sample any given ensemble of correlated signals with no prior requirements on the energy distribution. We will present *uniform* versions of Architecture 1 and 2 shown in Figure 21, and 22. In both uniform-sampling

schemes, we force the coherences to be small by adding a little analog preprocessing using AVMM and filters at the front end of the Architecture 1 and 2.

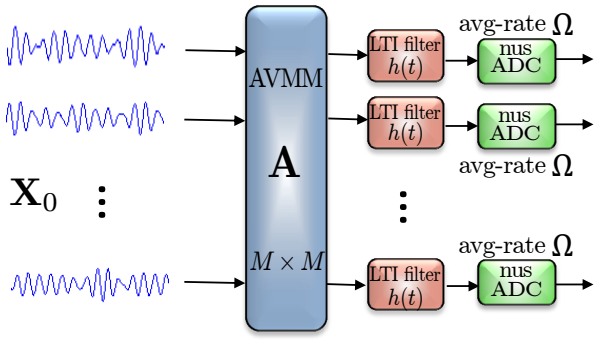

Figure 21: Analog vector-matrix multiplier (AVMM) takes random linear combinations of M input signals to produce M output signals. This equalizes energy across channels. The random LTI filters convolve the signals with a diverse waveform that results in dispersion of signals across time. The resultant signals are then sampled, at locations selected randomly on a uniform grid, at an average rate Ω, using a non-uniform sampling (nus) ADC in each channel.

The sampling architectures shown in Figure 21, and 22 preprocess the signals in analog with an analog-vector-matrix multiplier that spreads energy across channels. The analog ensemble is then processed by a bank of random filters that spread the energy over time. The combined action of the AVMM with a random matrix $\boldsymbol{A}$ and the analog LTI filters with a random matrix $\boldsymbol{H}$ forces the processed output $\boldsymbol{X}_{\mathtt{p}}$ to be incoherent w.h.p. The incoherent signals are then either sampled randomly with an nus ADC in each channel, as in Architecture 1, or sampled unifromly using a modulator, an integrator, and a uniform ADC in each channel, as in Architecture2.

The AVMM takes the random linear combination of M input signals to produce M output signals. The action of the AVMM can be modeled by left multiplication of random matrix $\boldsymbol{A} \in \mathbb{R}^{M \times M}$ with ensemble $\boldsymbol{X}$, which then equalizes w.h.p., the energy in each of the channels regardless of the initial energy distribution. Furthermore, the all pass LTI filters convolve the signals with a diverse impulse response $h_c(t)$, which disperses signal energy over time w.h.p. (see Lemma 4.2.1). We will use the same

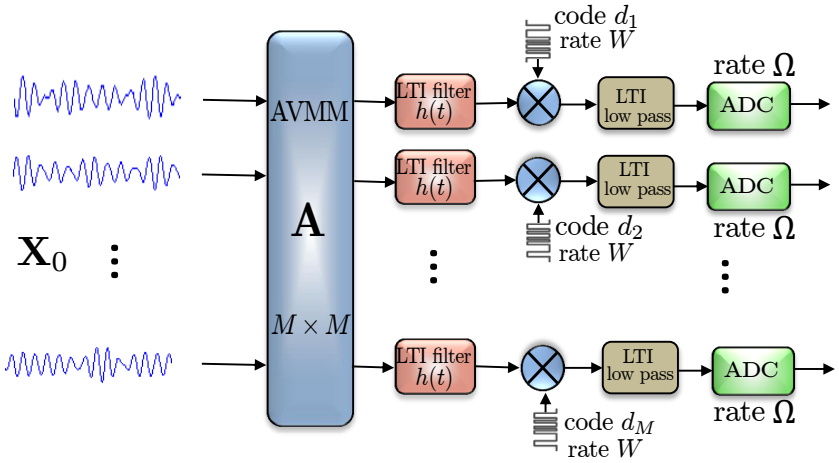

Figure 22: Analog vector-matrix multiplier (AVMM) takes random linear combinations of M input signals to produce M output signals. This equalizes energy across channels. The random LTI filters convolve the signals with a diverse waveform that results in dispersion of signals across time. The resultant signals are then sampled uniformly at rate Ω using the random demodulator in each channel.

random LTI filter $h_c(t)$ in each channel. The action of the random convolution [79] of $h_c(t)$ with each signal in the ensemble can be modeled by the right multiplication of a circulant random orthogonal matrix $\boldsymbol{H} \in \mathbb{R}^{W \times W}$ with $\boldsymbol{X}$, assuming W is even; it will be clear how to extend the argument to W odd. We can write $\boldsymbol{H} = \boldsymbol{W}\boldsymbol{Q}^*$, where

$$\boldsymbol{Q}[n,\omega] = \begin{cases} \frac{1}{\sqrt{W}} & \omega = 0 \\ \frac{2}{\sqrt{W}} \cos\left(\frac{2\pi\omega n}{W}\right) & \omega = [1, \frac{W}{2} - 1] \\ \frac{1}{\sqrt{W}}(-1)^{k-1} & \omega = \frac{W}{2} \\ \frac{2}{\sqrt{W}} \sin\left(\frac{2\pi\omega n}{W}\right) & \omega = [\frac{W}{2} + 1, W - 1] \end{cases} \tag{4.2.19}$$

$$\boldsymbol{W}[n,\omega] = \begin{cases} \frac{z_0}{\sqrt{W}}, & \omega = 0 \\ \frac{2}{\sqrt{W}} \cos\left(\frac{2\pi\omega n}{W} + \theta_\omega\right) & \omega = [1, \frac{W}{2} - 1] \\ \frac{z_{W/2}}{\sqrt{W}}(-1)^{k-1}, & \omega = \frac{W}{2} \\ \frac{2}{\sqrt{W}} \sin\left(\frac{2\pi\omega n}{W} + \theta_\omega\right), & \omega = [\frac{W}{2} + 1, W - 1] \end{cases} . \tag{4.2.20}$$

and $z_0, z_{W/2} = \pm 1$ with equal probability and θ_ω for $\omega = 1, \cdots, W/2 - 1$ are uniform on $[0, 2\pi]$ and all $W/2 + 1$ of these random variables are independent.

Application of the AVMM with random orthogonal $\boldsymbol{A}$ and the LTI random filters with random orthogonal $\boldsymbol{H}$ on input ensemble $\boldsymbol{X}$ spreads signals out across channels and over time w.h.p. As a result, we obtain $\boldsymbol{X}_\mathfrak{p} \in \mathbb{R}^{M \times W}$:

$$\boldsymbol{X}_\mathfrak{p} = \boldsymbol{A}\boldsymbol{X}\boldsymbol{H}^T = \boldsymbol{A}\boldsymbol{U}\boldsymbol{\Sigma}\boldsymbol{V}^T\boldsymbol{H}^T. \tag{4.2.21}$$

Let $\boldsymbol{U}_\mathfrak{p} = \boldsymbol{A}\boldsymbol{U}$ and $\boldsymbol{V}_\mathfrak{p} = \boldsymbol{H}\boldsymbol{V}$, where $\boldsymbol{U}_\mathfrak{p} \in \mathbb{R}^{M \times R}, \boldsymbol{V}_\mathfrak{p} \in \mathbb{C}^{W \times R}$ be the left and right singular vectors of matrix $\boldsymbol{X}_\mathfrak{p}$, respectively. Note that matrix $\boldsymbol{X}_\mathfrak{p}$ is an isometry with $\boldsymbol{X}$ and has the same rank as $\boldsymbol{X}$. The left and right singular vectors $\boldsymbol{U}_\mathfrak{p}$ and $\boldsymbol{V}_\mathfrak{p}$ of $\boldsymbol{X}_\mathfrak{p}$ are in some sense random orthogonal matrices and hence, incoherent w.h.p. The following Lemma shows the incoherence of matrix $\boldsymbol{X}_\mathfrak{p}$.

Lemma 4.2.1. *Fix matrices $\boldsymbol{U} \in \mathbb{R}^{M \times R}$ and $\boldsymbol{V} \in \mathbb{C}^{W \times R}$ of the left and right singular vectors, respectively, each of which consists of R orthogonal unit norm columns. Create random orthonormal matrices $\boldsymbol{A} \in \mathbb{R}^{M \times M}$ and $\boldsymbol{H} \in \mathbb{R}^{W \times W}$. Then*

- $\max_{1 \le i \le M} \|\boldsymbol{U}_\mathfrak{p}^* \mathbf{e}_i\|_2^2 \le C_\beta \max(R, \log M)/M$ *with a probability exceeding* $1 - M^{-\beta}$.
- $\max_{1 \le j \le W} \|\boldsymbol{V}_\mathfrak{p}^* \mathbf{e}_j\|_2^2 \le C_\beta \max(R, \log W)/W$ *with a probability exceeding* $1 - W^{-\beta}$.
- $\max_{\substack{1 \le i \le M \\ 1 \le j \le W}} \langle \boldsymbol{U}_\mathfrak{p}\boldsymbol{V}_\mathfrak{p}^*, \boldsymbol{e}_i \bar{\boldsymbol{e}}_j^* \rangle^2 \le C_\beta \log W \max(R, \log M)/MW$ *with a probability exceeding* $1 - O(W^{-\beta} + M^{-\beta})$.

- $\max_{\substack{1\le i\le M\\ 1\le j\le \Omega}} \sum_{k\sim\mathcal{B}_j} \langle \boldsymbol{U}_{\mathfrak{p}}\boldsymbol{V}_{\mathfrak{p}}^*, \boldsymbol{e}_i\bar{\boldsymbol{e}}_k\rangle^2 \le C_\beta \log W \max(R, \log M)/M\Omega$ *with a probability exceeding* $1 - O(W^{-\beta} + M^{-\beta})$.

Proof of Lemma 4.2.1 is presented in Section 4.4.

Sufficient sampling rate for the first uniform sampling architecture

Lemma 4.2.1 combined with the definition (4.2.5) shows tha the coherence parameter $\mu_0^2 \le C_\beta \log(W)$ holds for for $R > \log M$ with high probability. Using this bound in the matrix-completion results [19, 27] in the noiseless case asserts that if $M\Omega \gtrsim CR(W+M)\log^3(W)$, the solution of the nuclear norm minimization program (4.2.1) exactly equals $\boldsymbol{X}$ with high probability. We are paying an extra log factor in the measurements but now there is no dependence on the energy distribution of the ensemble.

Sufficient sampling rate for the second uniform sampling architecture

Combining Lemma 4.2.1 with Theorem 4.2.1 immediately provides with the following corollary.

Corollary 3. *Suppose* Ω *measurements of the ensemble* $\boldsymbol{X}_0$ *are taken through the uniform random demodulator setup. If*

$$\Omega \ge C\beta R \max(W/M, 1)\log^4(WM) \tag{4.2.22}$$

for some $\beta > 1$*, and* $R > \log M$*, the minimizer* $\tilde{\boldsymbol{X}}$ *to the problem* (4.2.1) *is unique and equal to* $\boldsymbol{X}_0$ *with probability at least* $1 - O(WM)^{-\beta}$.

Hence, we can recover $\tilde{\boldsymbol{X}}$ and hence, $\boldsymbol{X}$ in both uniform sampling architectures in Figure 21, and 22 using the nuclear-norm minimization.

4.2.6 Application: Compressive parameter estimation in array processing

In many array processing applications, the goal is to estimate the parameters of multiple signals from the samples acquired. The parameters of interest include: the angle

of arrival of wavefronts impinging on antenna arrays, this arises in several applications, such as surveillance radars, sonars, and seismic exploration; the estimation of frequency content of signals in several spectral estimation tasks; and the estimation of carrier frequency offsets in OFDMA-based wireless communications.

As an illustration, we will discuss here the angle-of-arrival estimation in wide-band radars. Suppose, an application at hand is concerned with the detection of the location of R point sources radiating energy. A reasonable assumption is that the energy arrives at the sensors as a sum of plane waves and the signals are narrow-band centered around frequency ω_c. The signal radiated by the rth point source is

$$s_r(t) = g(t)e^{-j\omega_c t},$$

where the narrow-band assumption implies that the envelop $g(t)$ is slowly varying, i.e., for small time delays τ, we have $g(t-\tau) \approx g(t)$. For this reason, the time delay only induces a phase shift on $s_r(t)$. This is to say,

$$s_r(t-\tau) \approx s_r(t)e^{-j\omega_c \tau}.$$

As a result, the signal $x_m(t)$ at the mth antenna element is

$$x_m(t) = \sum_{r=1}^{R} a_m(\theta_r) s_r(t - \tau_m(\theta_r)),$$

where $\tau_m(\theta_r)$ is the propagation delay at the mth antenna with respect to a reference point, and $a_m(\theta_r)$ is the mth array-element response to the plane wave incident at an angle θ_r. By arranging the signals $x_m(t), 1 \leq m \leq M$ as the rows of $\boldsymbol{X}_c(t)$, we can write the signal ensemble received at the antenna array as

$$\boldsymbol{X}_c(t) = \boldsymbol{A}(\theta)\boldsymbol{S}_c(t), \tag{4.2.23}$$

where $\boldsymbol{A}(\theta)$ is an $M \times R$ matrix containing as its rth column, the array gain vector at angle θ_r

$$\boldsymbol{a}(\theta_r) = [a_1(\theta_r)e^{-j\omega_c \tau_1(\theta_r)}, \cdots, a_M(\theta_r)e^{-j\omega_c \tau_M(\theta_r)}],$$

and $\boldsymbol{S}_c(t)$ can be thought of as a matrix containing R independent analog signals $s_r(t), 1 \leq r \leq R$ as its rows. The model in (4.2.23) is more general and is applicable to a wide variety of problems involving estimation of other parameters like frequency, or the estimation of location in an azimuth/elevation/range system, where the location of sources is specified by three angles θ, ϕ, and γ. In general, the number R of point

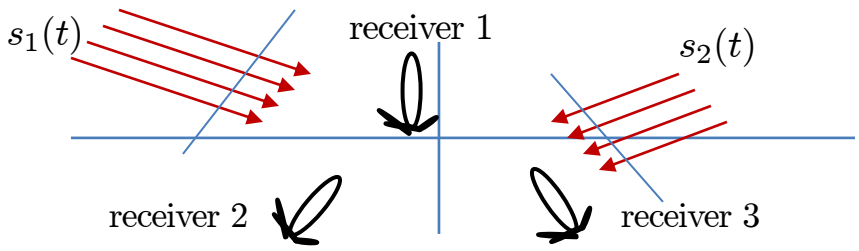

Figure 23: Problem Setup: Estimation of Location Parameters of Point Sources

sources is much smaller than the number M of antenna arrays; that is, the signal lives in a smaller subspace. Multiple signal classification algorithm such as MUSIC [86] estimate the signal subspace based on the estimate of the signal covariance matrix, and then find the intersection of this subspace with the array manifold, which is a set composed of all steering vectors $\boldsymbol{a}(\theta_r)$ for the entire range of the parameter θ_r [81]. This procedure reveals the estimates of the unknown parameter, which in this case is the direction of arrival. The central role in this computation is the estimation of the covariance matrix $\boldsymbol{R}_{XX}$, which requires sampling the signal ensemble $\boldsymbol{X}_c(t)$ to obtain the corresponding matrix of samples $\boldsymbol{X}$ given as

$$\boldsymbol{X} = \boldsymbol{A}(\theta)\boldsymbol{S}, \tag{4.2.24}$$

where $\boldsymbol{X} : M \times W$, and $\boldsymbol{S} : R \times W$ are the matrix of samples. The transformation from (4.2.23) to (4.2.24) involves sampling analog signals $x_m(t)$ using ADCs. With an ever increasing trend of radars operating at high frequencies in the range of 35-40 GHz, the sampling burden on the ADCs keeps escalating. The advances in the sampling rate

of the ADCs are not up to pace with the advances in signal processing. Therefore, it is important to design the systems in a way that reduces the sampling burden on the ADCs. Since $\boldsymbol{X}_c(t)$ is by construction an ensemble consisting of multiple signals lying in a subspace with $R \ll M$, the sampling architectures presented can be used to acquire the ensemble $\boldsymbol{X}_c(t)$ efficiently at a lower sampling rate. The benefits are two-fold: first, the covariance matrix $\boldsymbol{R}_{XX} := \lim_{W\to\infty} 1/W \boldsymbol{X}\boldsymbol{X}^*$ of input signal ensemble $\boldsymbol{X}_c(t)$ can be estimated accurately from fewer samples; second, in some cases the effective frequency range at which radar can operate can increase as the ADCs are sampling at sub-Nyquist rate.

In summary, the sampling architectures can be employed to efficiently acquire multiple signals lying in a subspace that can be useful in compressively estimating several parameters of interest in varoious signal processing applications.

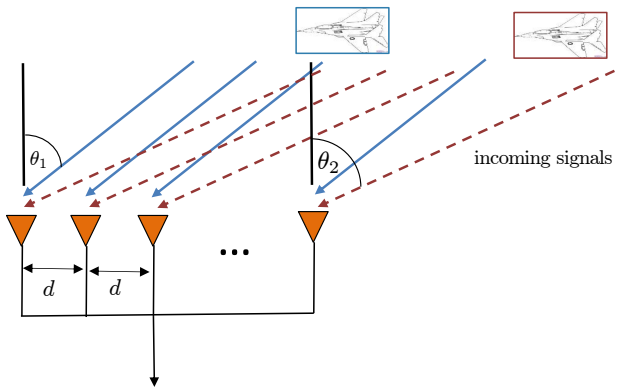

Figure 24: Angle of arrival detection in radar

4.3 Numerical Experiments

In this section, we study the performance of the proposed sampling architectures with some numerical experiments. Since the first sampling architecture reduces to

an already well-studied matrix completion problem, we have chosen here to present only the sampling performance of Architecture 2, which reduces to a matrix recovery problem from a block-diagonal measuremnt matrix that has not been studied before.

4.3.1 Sampling performance

In all of the experiments in this section, we generate the unknown rank-R matrix $\boldsymbol{X}_0$ by the multiplication of a tall $M \times R$, and a fat $R \times W$ Gaussian matrices. Our objective is to recover a batch of $M = 100$ signals, with $W = 1024$ samples taken in a given window of time using Architecture 2. We will use the following parameters to evaluate the performance of the sampling architecture:

$$\text{Oversampling factor} : \eta = \frac{M\Omega}{R(W + M - R)},$$

where the oversampling factor is the ratio between the combined sampling rate of all the ADCs in Figure 20, and the degrees of freedom in rank-R matrix of samples $\boldsymbol{X}_0$. The successful reconstruction is declared when the relative error obeys

$$\text{Relative error} := \frac{\|\tilde{\boldsymbol{X}} - \boldsymbol{X}_0\|_F}{\|\boldsymbol{X}_0\|_F} \leq 10^{-2}.$$

The first experiment shows a graph, in Figure 25(a), between the oversampling factor η, and R. Each point, marked with a black dot, represents the minimum sampling rate required for the successful reconstruction of a given value of rank R. The empirical probability of success for each point is 0.99. The empirical probability is computed over 100 iterations with a new instance of randomly generated $\boldsymbol{X}_0$ in each iteration. The red line shows the least-squares fit of the black points. It is clear from the plot that the for reasonably large values of R, the sampling rate is within a small constant of the optimal rate $R(W + M - R)$. In context of the application, and under the narrow-band assumption described in Section 4.2.6, the graph in Figure 25(b) shows that for a fixed number of sources $R = 10$, the sufficient sampling rate Ω required for the successful reconstruction of the ensemble decreases inversely with

increasing number M of the receiving antennas. Each black point gives the minimum sampling rate required for the successful reconstruction with probability 0.99. The red line is the least-squares fit of these marked points. In other words, Figure 25(b) illustrates the relationship between the number of ADCs, or receiving antennas M, and the sampling rate Ω of each of the ADC for a fixed number of sources $R = 10$. The important point is that as we increase the number of antennas the the sampling burden on each of the ADCs decreases.

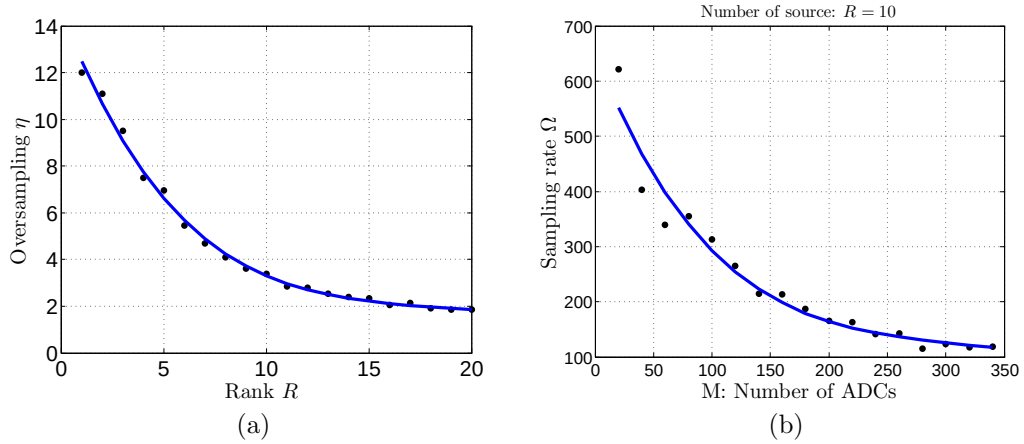

Figure 25: Performance of the random demodulator for multiple signals lying in a subspace. In these experiments, we take an ensemble of 100 signals, each bandlimited to 512Hz. The probability of success is computed over 100 iterations. (a) Oversampling factor η as a function of the number R of underlying independent signals. The blue line is the least-squares fit of the data points. (b) Sampling rate Ω versus the number M of recieving antennas. The blue line is the least-sqaures fit of the data points.

4.3.2 Stable recovery

In the second set of experiments, we study the performance of the the recovery algorithm when the measurements are contaminated with noise as in (4.2.2). The noise vector is standard Gaussian, i.e., $\boldsymbol{\xi} \sim \mathcal{N}(0, \sigma^2 \boldsymbol{I})$. We select $\delta \leq \sigma(L + \sqrt{L})^{1/2}$; a natural choice as the condition $\|\boldsymbol{xi}\|_2 \leq \delta$ holds with high probability. In the first set of experiments shown in Figure 26, we solve the optimization program in (4.2.3). The

plot in Figure 26(a) shows the relationship between the signal-to-noise ratio (SNR):

$$\text{SNR(dB)} = 10 \log \left(\frac{\|\boldsymbol{X}_0\|_F^2}{\|\boldsymbol{\xi}\|_2^2} \right),$$

and the realtive error(dB):

$$\text{Relative error (dB)} = 10 \log \left(\frac{\|\tilde{\boldsymbol{X}} - \boldsymbol{X}_0\|_F^2}{\|\boldsymbol{X}_0\|_F^2} \right)$$

for a fixed oversampling factor $\eta = 3.5$. The result shows that the relative error degrades gracefully with decreasing SNR. In the Figure 26(b), the plot depicts relative error as a function of the oversampling factor for a fixed SNR = 40dB. The relative error decrease with increasing sampling rate.

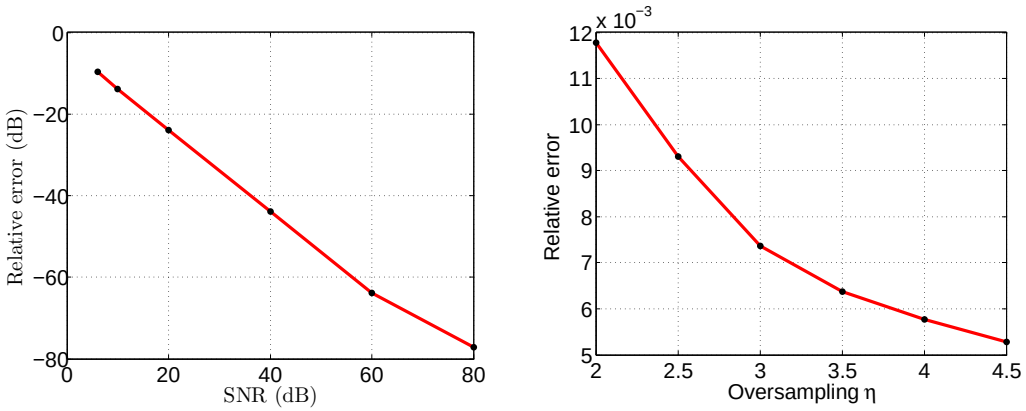

(a) (b)

Figure 26: Recovery using matix Lasso in the presence of noise. The input ensemble to the simulated random demodulator consists of 100 signals, each bandlimited to 512Hz with number $R = 15$ of latent independent signals.(a) The SNR in dB versus the relative error in dB. The oversampling factor $\eta = 3.5$. (b) Relative error as a function of the sampling rate. The SNR is fixed at 40dB.

4.4 Proof of Lemma 4.2.1

We start with the proof of Theorem 4.2.1

Proof. The point (1) is the standard result [57]. We give proof of (2) now. It is a fact that in (4.2.19) and (4.2.20) for fixed a and $\theta \sim \text{Uniform}([0, 2\pi])$, the random variables $\text{sign}(\cos(a + \theta))$ and $\text{sign}(\sin(a + \theta))$ are independent of one another. Thus

$\boldsymbol{H}$ has the same probability distribution as $\boldsymbol{WZQ}^*$, where $\boldsymbol{Z} = \text{diag}(\boldsymbol{z})$ and the entries of $\mathbf{z}$ are i.i.d ± 1 random variables. In light of this, we will replace $\boldsymbol{H}$ with $\boldsymbol{WZQ}^*$. For a fixed k, we can write

$$\begin{aligned}\tilde{\boldsymbol{V}}^* \boldsymbol{e}_k &= \boldsymbol{V}^* \boldsymbol{H}^* \boldsymbol{e}_k = \hat{\boldsymbol{V}}^* \boldsymbol{Z} \boldsymbol{w}_k \\ &= \sum_{\omega=1}^{W} \boldsymbol{z}(\omega) \boldsymbol{w}_k(\omega) \hat{\boldsymbol{v}}_\omega\end{aligned}$$

where $\hat{\boldsymbol{V}} = \boldsymbol{Q}^* \boldsymbol{V}$ and $\boldsymbol{w}_k = \boldsymbol{W}^* \boldsymbol{e}_k$ and $\hat{\boldsymbol{v}}_\omega = \hat{\boldsymbol{V}}^* \boldsymbol{e}_\omega$ is the ωth row of $\hat{\boldsymbol{V}}$. We will apply the following concentration inequality,

Theorem 4.4.1. *[58] Let $\eta \in \mathbb{R}^n$ be a vector whose entries are independent random variables with $|\boldsymbol{\eta}(i)| < 1$, and let $\boldsymbol{S}$ be a fixed $m \times n$ matrix. Then for every $t \geq 0$*

$$\text{P}\left\{\|\boldsymbol{S\eta}\|_2 \geq \text{E}\,\|\boldsymbol{S\eta}\|_2 + t\right\} \leq 2e^{-t^2/16\|\boldsymbol{S}\|^2},$$

where

$$\text{E}\,\|\boldsymbol{S\eta}\|_2 \leq \|\boldsymbol{S}\|_F\,.$$

We can apply the above theorem with $\boldsymbol{S} = \hat{\boldsymbol{V}}^* \boldsymbol{W}_k$, where $\boldsymbol{W}_k = \text{diag}(\boldsymbol{w}_k)$, and $\boldsymbol{\eta} = \boldsymbol{z}$. In this case, we have

$$\begin{aligned}\left\|\hat{\boldsymbol{V}}^* \boldsymbol{W}_k\right\|_F^2 &= \sum_{\omega=1}^{W} |\boldsymbol{w}_k(\omega)|^2 \, \|\hat{\boldsymbol{v}}_\omega\|_2^2 \\ &\leq \frac{2}{W} \sum_{\omega=1}^{W} \|\hat{\boldsymbol{v}}_\omega\|_2^2 \\ &\leq \frac{2R}{W},\end{aligned}$$

and

$$\|\hat{\boldsymbol{V}}^* \boldsymbol{W}_k\| \leq \sqrt{\frac{2}{W}} \|\hat{\boldsymbol{V}}^*\| = \sqrt{\frac{2}{W}}.$$

Thus,

$$\text{P}\left\{\|\tilde{\boldsymbol{V}}^* \boldsymbol{e}_k\|_2 > \sqrt{\frac{2R}{W}} + t\sqrt{\frac{2}{W}}\right\} \leq 2e^{-t^2/16},$$

and

$$\mathrm{P}\left\{\max_{1\le k\le W}\|\tilde{\boldsymbol{V}}^*\boldsymbol{e}_k\|_2 > \sqrt{\frac{2R}{W}}+t\sqrt{\frac{2}{W}}\right\}\le 2We^{-t^2/16}.$$

We can make this probability less than $W^{-\beta}$ by taking $t\ge C\sqrt{\log W}$, and (2) follows.

Now for (3), we can write $\boldsymbol{H}=\boldsymbol{W}\boldsymbol{Z}\boldsymbol{Q}^*$. Let $\boldsymbol{w}_\ell$ be the ℓth column of $\boldsymbol{W}^*$ and let $\tilde{\boldsymbol{u}}_k^*$ be the kth row of $\tilde{\boldsymbol{U}}$. For a fixed row index k and column index ℓ, we can write an entry of $\tilde{\boldsymbol{U}}\tilde{\boldsymbol{V}}^*$ as

$$\begin{aligned}\left(\tilde{\boldsymbol{U}}\tilde{\boldsymbol{V}}^*\right)(k,\ell) &= \tilde{\boldsymbol{U}}(\boldsymbol{W}\boldsymbol{Z}\boldsymbol{Q}^*\boldsymbol{V})^*\\ &= \tilde{\boldsymbol{U}}\tilde{\boldsymbol{Q}}^*\boldsymbol{Z}\boldsymbol{W}^*\\ &= (\tilde{\boldsymbol{Q}}\tilde{\boldsymbol{U}}_k)^*\boldsymbol{Z}\boldsymbol{w}_\ell\\ &= \sum_{\omega=1}^{W}(\tilde{\boldsymbol{Q}}\tilde{\boldsymbol{u}}_k(\omega))^*\boldsymbol{z}(\omega)\boldsymbol{w}_\ell(\omega),\end{aligned}$$

where $\tilde{\boldsymbol{Q}}=\boldsymbol{Q}^*\boldsymbol{V}$ is a tall orthonormal matrix. Since the $\boldsymbol{z}(\omega)$ are i.i.d. random variables, a standard applications of the Hoeffding inequality tells us that

$$\mathrm{P}\left\{\left|\left(\tilde{\boldsymbol{U}}\tilde{\boldsymbol{V}}^*\right)(k,\ell)\right|>\lambda\right\}\le 2e^{-\lambda^2/2\sigma^2},$$

where

$$\begin{aligned}\sigma^2 &= \sum_{\omega=1}^{W}\left|\left(\tilde{\boldsymbol{Q}}\tilde{\boldsymbol{u}}_k(\omega)\right)\right|^2|\boldsymbol{w}_\ell(\omega)|^2\\ &\le \frac{2\left\|\tilde{\boldsymbol{Q}}\tilde{\boldsymbol{u}}_k\right\|_2^2}{W}\\ &= \frac{2\|\tilde{\boldsymbol{u}}_k\|_2^2}{W}.\end{aligned}$$

Thus, with probability exceeding $1-2W^{-\beta}$

$$\max_{\substack{1\le k\le M\\ 1\le \ell\le W}}\left|\left(\tilde{\boldsymbol{U}}\tilde{\boldsymbol{V}}^*\right)(k,\ell)\right|^2\le\frac{4(\beta+2)\log W}{W}\max_{1\le\ell\le M}\|\tilde{\boldsymbol{u}}_k\|_2^2.$$

The point (1) tells us that

$$\max_{1\le k\le M}\|\tilde{\boldsymbol{u}}_k\|_2^2\le C_\beta\frac{\max(R,\log M)}{M}$$

with probability exceeding $1 - M^{-\beta}$. Thus (3) holds with probability exceeding $1 - O(W^{-\beta} + M^{-\beta})$. □

4.5 Proof of Theorem 4.2.1

Define a subspace $T \subset \mathbb{R}^{M \times W}$ associated with $\boldsymbol{X}_0$ with svd $\sum_{k=1}^{R} \sigma_k \boldsymbol{u}_k \boldsymbol{v}_k^*$:

$$T = \{\boldsymbol{X} : \boldsymbol{X} = \boldsymbol{U}\boldsymbol{Z}_1^* + \boldsymbol{Z}_2\boldsymbol{V}^*, \boldsymbol{Z}_1 \in \mathbb{R}^{W \times R}, \boldsymbol{Z}_2 \in \mathbb{R}^{M \times R}\}.$$

The orthogonal projection of $\mathcal{P}_T$ onto T is

$$\mathcal{P}_T(\boldsymbol{Z}) = \boldsymbol{U}\boldsymbol{U}^*\boldsymbol{Z} + \boldsymbol{Z}\boldsymbol{V}\boldsymbol{V}^* - \boldsymbol{U}\boldsymbol{U}^*\boldsymbol{Z}\boldsymbol{V}\boldsymbol{V}^*,$$

and its orthogonal complement

$$\mathcal{P}_{T^\perp}(\boldsymbol{Z}) = (\mathcal{I} - \mathcal{P}_T)(\boldsymbol{X}) = (\boldsymbol{I}_M - \boldsymbol{U}\boldsymbol{U}^*)\boldsymbol{X}(\boldsymbol{I}_W - \boldsymbol{V}\boldsymbol{V}^*).$$

A sufficient condition for the uniqueness of the minimizer to (4.2.1) is given by the following Proposition [19, 44].

Proposition 5. *The matrix $\boldsymbol{X}$ is the unique minimizer to* (4.2.1) *if* $\exists \boldsymbol{Y} \in$ *Range*$(\mathcal{A}^*)$ *such that*

$$\|\mathcal{P}_{T^\perp}(\boldsymbol{Z})\|_* - \|\boldsymbol{U}\boldsymbol{V}^* - \mathcal{P}_T(\boldsymbol{Y})\|_F \|\mathcal{P}_T(\boldsymbol{Z})\|_F - \|\mathcal{P}_{T^\perp}(\boldsymbol{Y})\| \|\mathcal{P}_{T^\perp}(\boldsymbol{Z})\|_* > 0,$$

for all $\boldsymbol{Z} \in$ *Null*$(\mathcal{A})$.

Proposition 5 implies that the uniqueness of the minimizer is gauranteed, if $\exists \boldsymbol{Y} \in$ Range$(\mathcal{A}^*)$, such that

$$\|\mathcal{P}_T(\boldsymbol{Y}) - \boldsymbol{U}\boldsymbol{V}^*\|_F \leq \sqrt{\frac{\Omega}{9W}}, \quad \|\mathcal{P}_{T^\perp}(\boldsymbol{Y})\| \leq \frac{1}{2}, \tag{4.5.1}$$

holds. Also for $\boldsymbol{Z} \neq \boldsymbol{0}$, and $\forall \boldsymbol{Z} \in$ Null$(\mathcal{A})$ the following

$$\|\mathcal{P}_{T^\perp}(\boldsymbol{Z})\|_F \geq \sqrt{\frac{\Omega}{2W}} \|\mathcal{P}_T(\boldsymbol{Z})\|_F \tag{4.5.2}$$

is true. To show (4.5.2), for $\boldsymbol{Z} \in \text{Null}(\mathcal{A})$

$$\begin{aligned} 0 &= \|\mathcal{A}(\boldsymbol{Z})\|_F \\ 0 &\geq \|\mathcal{A}(\mathcal{P}_T(\boldsymbol{Z}))\|_F - \|\mathcal{A}(\mathcal{P}_{T^\perp}(\boldsymbol{Z}))\|_F, \end{aligned}$$

which after using the fact that $\|\mathcal{A}\| = \sqrt{W/\Omega}$ implies that

$$\|\mathcal{A}(\mathcal{P}_{T^\perp}(\boldsymbol{Z}))\|_F \leq \sqrt{\frac{W}{\Omega}} \|\mathcal{P}_T^\perp(\boldsymbol{Z})\|_F. \tag{4.5.3}$$

In addition, for an arbitrary $\boldsymbol{Z}$, we have

$$\begin{aligned} \|\mathcal{A}(\mathcal{P}_T(\boldsymbol{Z}))\|_F^2 &= \langle \mathcal{A}(\mathcal{P}_T(\boldsymbol{Z})), \mathcal{A}(\mathcal{P}_T(\boldsymbol{Z})) \rangle \\ &= \langle \boldsymbol{Z}, \mathcal{P}_T \mathcal{A}^* \mathcal{A} \mathcal{P}_T(\boldsymbol{Z}) \rangle \\ &\geq (1 - \|\mathcal{P}_T \mathcal{A}\mathcal{A}^* \mathcal{P}_T - \mathcal{P}_T\|) \|\mathcal{P}_T(\boldsymbol{Z})\|_F^2 \\ &\geq \frac{1}{2} \|\mathcal{P}_T(\boldsymbol{Z})\|_F^2, \end{aligned} \tag{4.5.4}$$

where the last inequality is obtained by plugging in $\|\mathcal{P}_T \mathcal{A}\mathcal{A}^* \mathcal{P}_T - \mathcal{P}_T\| \leq \frac{1}{2}$, which is true with probability at least $1 - O(WM)^{-\beta}$ by the application of Corollary 4, using $\Omega \geq C\beta R(\mu_1^2(W/M) + \mu_2^2) \log^2(WM)$. Collecting the facts in (4.5.3), and (4.5.4), the result in (4.5.2) is obtained.

4.5.1 Measurements as a matrix trace inner product

The (i, j)th sample taken by the ADC in the i-th branch in Figure 20 will be expressed using trace inner product as

$$y_{ij} = \langle \boldsymbol{A}_{ij}, \boldsymbol{X}_0 \rangle = \text{tr}(\boldsymbol{A}_{ij}^* \boldsymbol{X}_0) = \sum_{k \in \mathcal{B}_j} d_i[k] X_0[i, k], \quad (i, j) = \{1, \cdots, M\} \times \{1, \cdots, \Omega\}, \tag{4.5.5}$$

where the sampling mask $\boldsymbol{A}_{ij}$ is

$$\boldsymbol{A}_{ij} = \sum_{k \sim \mathcal{B}_j} d_i[k] \boldsymbol{e}_i \bar{\boldsymbol{e}}_k^*. \tag{4.5.6}$$

where $\{\boldsymbol{e}_i\}_{1\le i\le M}$, and $\{\bar{\boldsymbol{e}}_k\}_{1\le k\le W}$ are standard basis vectors of dimension M, and W, respectively. It follows that

$$\mathcal{A}^*\mathcal{A}(\boldsymbol{X}) = \sum_{(i,j)} \langle \boldsymbol{A}_{ij}, \boldsymbol{X}\rangle \boldsymbol{A}_{ij},$$

and

$$\mathcal{A}^*\mathcal{A} = \sum_{(i,j)} \boldsymbol{A}_{ij} \otimes \boldsymbol{A}_{ij}, \tag{4.5.7}$$

where $\otimes$ denotes the tensor product. It is clear that the measurement matrices $\boldsymbol{A}_{ij}$ are rank-1 random matrices. In general, the tensor product of rank-1 matrices $\boldsymbol{u}_1\boldsymbol{v}_1^*$, $\boldsymbol{u}_2\boldsymbol{v}_2^*$ with $\boldsymbol{u}_i \in \mathbb{R}^M$, and $\boldsymbol{v}_i \in \mathbb{R}^W$ is given by the big matrix

$$\boldsymbol{u}_1\boldsymbol{v}_1^* \otimes \boldsymbol{u}_2\boldsymbol{v}_2^* = \begin{bmatrix} u_1[1]^* u_2[1]\boldsymbol{v}_1\boldsymbol{v}_2^* & u_1[1]^* u_2[2]\boldsymbol{v}_1\boldsymbol{v}_2^* & \cdots & u_1[1]^* u_2[N]\boldsymbol{v}_1\boldsymbol{v}_2^* \\ u_1[2]^* u_2[1]\boldsymbol{v}_1\boldsymbol{v}_2^* & u_1[2]^* u_2[2]\boldsymbol{v}_1\boldsymbol{v}_2^* & \cdots & u_1[2]^* u_2[N]\boldsymbol{v}_1\boldsymbol{v}_2^* \\ \vdots & & \ddots & \\ u_1[N]^* u_2[1]\boldsymbol{v}_1\boldsymbol{v}_2^* & \cdots & \cdots & u_1[N]^* u_2[N]\boldsymbol{v}_1\boldsymbol{v}_2^*, \end{bmatrix}$$

and we will denote (α,β)th, $W \times W$ submatrix by

$$\{\boldsymbol{u}_1\boldsymbol{v}_1^* \otimes \boldsymbol{u}_2\boldsymbol{v}_2^*\}_{(\alpha,\beta)} = u_1[\alpha]^* u_2[\beta]\boldsymbol{v}_1\boldsymbol{v}_2^*.$$

Using the above notation, we can write

$$\{\boldsymbol{A}_{ij} \otimes \boldsymbol{A}_{ij}\}_{(\alpha,\beta)} = e_i[\alpha]e_i[\beta] \sum_{k,k'\sim\mathcal{B}_j} d_i[k]d_i[k']\bar{\boldsymbol{e}}_k\bar{\boldsymbol{e}}_{k'}^*. \tag{4.5.8}$$

Taking the expectation, we can see that

$$\{\mathrm{E}(\boldsymbol{A}_{ij} \otimes \boldsymbol{A}_{ij})\}_{(\alpha,\beta)} = e_i[\alpha]e_i[\beta] \sum_{k\sim\mathcal{B}_j} \bar{\boldsymbol{e}}_k\bar{\boldsymbol{e}}_k^*,$$

and using the fact that $e_i[\alpha]e_i[\beta] = 1$ when $\alpha = \beta$ and is zero otherwise, we can see that

$$\sum_{(i,j)} \mathrm{E}(\boldsymbol{A}_{ij} \otimes \boldsymbol{A}_{ij}) = \boldsymbol{I}_{WM},$$

where $\boldsymbol{I}_{WM}$ denotes $WM \times WM$ identity matrix. In operator notation, we have $\mathrm{E}\,\mathcal{A}^*\mathcal{A} = \mathcal{I}$.

Let $\{\boldsymbol{u}_k^*\}_{1\le k\le M}$, and $\{\boldsymbol{v}_k^*\}_{1\le k\le W}$ denote the rows of the matrices $\boldsymbol{U}$, and $\boldsymbol{V}$, respectively. The following quantity will be used repeatedly in the theoretical analysis

$$\begin{aligned}\|\mathcal{P}_T(\boldsymbol{A}_{ij})\|_F^2 &= \langle \mathcal{P}_T(\boldsymbol{A}_{ij}), \boldsymbol{A}_{ij}\rangle \\ &= \langle \boldsymbol{U}^*\boldsymbol{A}_{ij}, \boldsymbol{U}^*\boldsymbol{A}_{ij}\rangle + \langle \boldsymbol{A}_{ij}\boldsymbol{V}, \boldsymbol{A}_{ij}\boldsymbol{V}\rangle - \langle \boldsymbol{U}^*\boldsymbol{A}_{ij}\boldsymbol{V}, \boldsymbol{U}^*\boldsymbol{A}_{ij}\boldsymbol{V}\rangle \\ &= \|\boldsymbol{U}^*\boldsymbol{A}_{ij}\|_F^2 + \|\boldsymbol{A}_{ij}\boldsymbol{V}\|_F^2 - \|\boldsymbol{U}^*\boldsymbol{A}_{ij}\boldsymbol{V}\|_F^2 \le \|\boldsymbol{U}^*\boldsymbol{A}_{ij}\|_F^2 + \|\boldsymbol{A}_{ij}\boldsymbol{V}\|_F^2.\end{aligned}$$

Using the definition (4.5.6), we have

$$\|\boldsymbol{U}^*\boldsymbol{A}_{ij}\|_F^2 = \left\|\sum_{k\sim\mathcal{B}_j} d_i[k]\boldsymbol{u}_i\bar{\boldsymbol{e}}_k^*\right\|_F^2 = \|\boldsymbol{u}_i\|_2^2\left\|\sum_{k\sim\mathcal{B}_j} d_i[k]\bar{\boldsymbol{e}}_k\right\|_2^2 \le \mu_1^2\frac{R}{M}\cdot\frac{W}{\Omega},$$

and

$$\|\boldsymbol{A}_{ij}\boldsymbol{V}\|_F^2 = \left\|\sum_{k\sim\mathcal{B}_j} d_i[k]\boldsymbol{e}_i\boldsymbol{v}_k^*\right\|_F^2 = \|\boldsymbol{e}_i\|_2^2\left\|\sum_{k\sim\mathcal{B}_j} d_i[k]\boldsymbol{v}_k\right\|_2^2.$$

This implies that

$$\|\mathcal{P}_T(\boldsymbol{A}_{ij})\|_F^2 \le \mu_1^2\frac{R(W/M)}{\Omega} + \left\|\sum_{k\sim\mathcal{B}_j} d_i[k]\boldsymbol{v}_k\right\|_2^2. \tag{4.5.9}$$

4.5.2 Golfing scheme for the random modulator

We start with partitioning the measurements indexed by the set

$$\Gamma = \{(i,j)\}_{\substack{1\le i\le M\\ 1\le j\le\Omega}}$$

into κ disjoint partitions $\{\Gamma_k\}_{1\le k\le\kappa}$ of size $|\Gamma_k| = L/\kappa$, such that $\bigcup_k\Gamma_k = \Gamma$, i.e., $\kappa|\Gamma_k| = M\Omega$. We will construct the dual certificate $\boldsymbol{Y}\in\text{Range}(\mathcal{A}^*)$ iteratively using Gross's golfing scheme. Let $\mathcal{A}_k$ denote the operator corresponding to the samples taken in the kth partition, i.e.,

$$\mathcal{A}_k^*\mathcal{A}_k = \sum_{(i,j)\in\Gamma_k}\boldsymbol{A}_{ij}\otimes\boldsymbol{A}_{ij}.$$

As will be clear later in the proof that we want the partitioned linear operator $\kappa\mathcal{A}_k^*\mathcal{A}_k$ to be a close approximation of the $\mathcal{I}$. For this purpose, each of the partition Γ_k is chosen uniformly at random out of the set Γ. Suppose now that we form a new set of partitions $\{\Gamma_k'\}$ defined as

$$\Gamma_k' = \{(i,j) \in \{1,\ldots,M\} \times \{1,\ldots,\Omega\} : \delta_{(i,j)} = 1\}, \tag{4.5.10}$$

where the sequence $\{\delta_{(i,j)}\}_{\substack{1\leq i\leq M\\ 1\leq j\leq \Omega}}$ are independent 0/1 Bernoulli random variables with

$$\mathrm{P}\left\{\delta_{(i,j)} = 1\right\} = \frac{1}{\kappa}.$$

In the the proofs later, we will be interested in bounding events $\eta(\Gamma_k)$ that involve sum of independent random matrices indexed by the partitions $\{\Gamma_k\}_{1\leq k\leq\kappa}$, for instance, define

$$\eta(\Gamma_k) := \left\| \sum_{(i,j)\in\Gamma_k} \kappa \boldsymbol{A}_{ij} \otimes \boldsymbol{A}_{ij} - \mathcal{I} \right\|,$$

and we want to bound the probability $\mathrm{P}\{\eta(\Gamma_k) > \epsilon\}$. Uisng the fact that

$$\mathrm{P}\{\eta(\Gamma_k) > \epsilon\} \leq 2\,\mathrm{P}\{\eta(\Gamma_k') > \epsilon\}, \tag{4.5.11}$$

which implies that probability of an event $\{\eta(\Gamma_k) > \epsilon\}$ over the set Γ_k can be bounded by the probability of a similar event $\{\eta(\Gamma_k') > \epsilon\}$ over the set Γ_k'. As a result, we will now be concerned with only bounding the probability of events of interest over the sets Γ_k'. Thus, we redefine $\mathcal{A}_k^*\mathcal{A}_k$ over Γ_k' as

$$\mathcal{A}_K^*\mathcal{A}_k = \sum_{(i,j)\in\Gamma_k'} \boldsymbol{A}_{ij} \otimes \boldsymbol{A}_{ij} = \sum_{(i,j)} \delta_{(i,j)} \boldsymbol{A}_{ij} \otimes \boldsymbol{A}_{ij}. \tag{4.5.12}$$

The iterative construction of the dual certificate is:

$$\boldsymbol{Y}_k = \boldsymbol{Y}_{k-1} - \kappa\mathcal{A}_k^*\mathcal{A}_k\left(\mathcal{P}_T(\boldsymbol{Y}_{k-1}) - \boldsymbol{U}\boldsymbol{V}^*\right).$$

Projecting on the subspace T on both sides results in

$$\mathcal{P}_T(\boldsymbol{Y}_k) = \mathcal{P}_T(\boldsymbol{Y}_{k-1}) - \kappa\mathcal{P}_T\mathcal{A}_k^*\mathcal{A}_k(\mathcal{P}_T(\boldsymbol{Y}_{k-1}) - \boldsymbol{U}\boldsymbol{V}^*),$$

where it is importatnt to see that $\boldsymbol{Y}_k \in \text{Range}(\mathcal{A}^*)$. Now let

$$\boldsymbol{W}_k := \mathcal{P}_T(\boldsymbol{Y}_k) - \boldsymbol{U}\boldsymbol{V}^*, \tag{4.5.13}$$

which gives

$$\boldsymbol{W}_k = \boldsymbol{W}_{k-1} - \kappa \mathcal{P}_T \mathcal{A}_k^* \mathcal{A}_k \mathcal{P}_T(\boldsymbol{W}_{k-1}).$$

As a result,

$$\|\boldsymbol{W}_k\|_F \le \|\kappa \mathcal{P}_T \mathcal{A}_k^* \mathcal{A}_k \mathcal{P}_T - \mathcal{P}_T\| \|\boldsymbol{W}_{k-1}\|_F,$$

and by Lemma 4.5.1 with $\Omega \ge C\beta\kappa R(\mu_1^2(W/M) + \mu_2^2)\log^2(WM)$, it follows that

$$\begin{aligned} \|\boldsymbol{W}_\kappa\|_F &\le \left(\frac{1}{2}\right)^\kappa \|\boldsymbol{U}\boldsymbol{V}^*\|_F \\ &= 2^{-\kappa}\sqrt{R} \le \sqrt{\frac{\Omega}{9W}}, \quad \text{when} \quad \kappa \ge 0.5 \log_2\left(\frac{9WR}{\Omega}\right), \end{aligned} \tag{4.5.14}$$

which holds with probability $1 - O(\kappa(WM)^{-\beta})$. In view of the coherences of $\boldsymbol{W}_0 = -\boldsymbol{U}\boldsymbol{V}^*$ with $\|\boldsymbol{U}\boldsymbol{V}^*\|_F^2 = R$ defined in (4.2.11), the coherence $\mu_{3,k}^2$ is related to the Frobenius norm of $\boldsymbol{W}_k$ as

$$\max_{\substack{1\le i\le M \\ 1\le j\le \Omega}} \sum_{k\sim\mathcal{B}_j} \langle \boldsymbol{W}_k, \boldsymbol{e}_i \bar{\boldsymbol{e}}_k^* \rangle^2 = \mu_{3,k}^2 \|\boldsymbol{W}_k\|_F^2 \frac{1}{M\Omega}. \tag{4.5.15}$$

Note that we have replaced R in the definition (4.2.5) with $\|\boldsymbol{W}_k\|_F^2$ for proper normalization. Lemma 4.5.3 shows that under appropriate conditions, the conclusion $\mu_{3,k}^2 \le \frac{1}{2}\mu_{3,k-1}^2$ holds with high probability. This implies that

$$\mu_{3,\kappa}^2 \le \mu_3^2 \tag{4.5.16}$$

is true and this fact will be used towards the end of this proof. The iterative dual certificate

$$\boldsymbol{Y} = \boldsymbol{Y}_\kappa = -\sum_{k=1}^{\kappa} \kappa \mathcal{A}_k^* \mathcal{A}_k(\boldsymbol{W}_{k-1})$$

satisfies (4.5.1). To show that $\|\mathcal{P}_{T^\perp}(\boldsymbol{Y}_\kappa)\| \leq \frac{1}{2}$ holds given Lemma 4.5.2, and (4.5.16), we make the following calculation

$$\begin{aligned}\|\mathcal{P}_{T^\perp}(\boldsymbol{Y}_\kappa)\| &\leq \sum_{k=1}^{\kappa} \|\mathcal{P}_{T^\perp}(\kappa \mathcal{A}_k^* \mathcal{A}_k(\boldsymbol{W}_{k-1}))\| = \sum_{k=1}^{\kappa} \|\mathcal{P}_{T^\perp}\left(\kappa \mathcal{A}_k^* \mathcal{A}_k(\boldsymbol{W}_{k-1}) - \boldsymbol{W}_{k-1}\right)\| \\ &\leq \sum_{k=1}^{\kappa} \left(\kappa \mathcal{A}_k^* \mathcal{A}_k(\boldsymbol{W}_{k-1}) - \boldsymbol{W}_{k-1}\right)\| \leq \sum_{k=1}^{\kappa} 2^{-k-1} < 1/2,\end{aligned}$$

which holds given $\Omega \geq C\beta\kappa R(W/M)\mu_3^2 \max(W/M, 1)\log^2(WM)$, the result holds with probabiltiy at least $1 - O(\kappa(WM)^{-\beta})$.

4.5.3 Lemmas for Theorem 4.2.1

We state here the key Lemmas required to prove sampling Theorem 4.2.1.

Lemma 4.5.1. *Suppose Ω measurements are taken through the random demodulator using the setup in* (4.2.8)*. Let $\mathcal{A}_k^*\mathcal{A}_k$, defined in* (4.5.12)*, be the kth partition of $\mathcal{A}^*\mathcal{A}$ indexed by $\Gamma_{k'}$, defined in* (4.5.10)*. Then for all $\beta > 1$,*

$$\max_{1\leq k\leq \kappa} \|\kappa \mathcal{P}_T \mathcal{A}_k^* \mathcal{A}_k \mathcal{P}_T - \mathcal{P}_T\| \leq \frac{1}{2}$$

provided $\Omega \geq C\beta\kappa R(\mu_1^2(W/M)+\mu_2^2)\log^2(WM)$ with probability at least $1-O(\kappa(WM)^{-\beta})$.

Corollary 4. *Suppose Ω measurements are taken through the random demodulator using the setup in* (4.2.8)*. Let $\mathcal{A}^*\mathcal{A}$ be as defined in* (4.5.7)*. Then for all $\beta > 1$,*

$$\|\mathcal{P}_T \mathcal{A}^* \mathcal{A} \mathcal{P}_T - \mathcal{P}_T\| \leq \frac{1}{2}$$

provided $\Omega \geq C\beta R(\mu_1^2(W/M)+\mu_2^2)\log^2(WM)$ with probability at least $1-O((WM)^{-\beta})$.

Proof. Proof of the corollary follows from the proof of Lemma 4.5.1 without partitioning, i.e., $\kappa = 1$. □

Lemma 4.5.2. *Suppose Ω entries are observed using the random demodulator, as in* (4.2.8)*. Let $\boldsymbol{W}_{k-1}$ be a fixed $M \times W$ matrix defined in* (4.5.13)*. Then for all $\beta > 1$,*

$$\max_{1\leq k\leq \kappa} \|\left(\kappa \mathcal{A}_k^* \mathcal{A}_k - \mathcal{I}\right)(\boldsymbol{W}_{k-1})\| \leq 2^{-k-1}$$

with probability at least $1-O(\kappa(WM)^{-\beta})$ provided $\Omega \geq C\beta\kappa\mu_{3,k-1}^2 R \max(W/M, 1)\log^{3/2}(WM)$.

Lemma 4.5.3. *Let $\mu_{3,k}^2$ be the coherence of the iterates as defined in* (4.5.15)*. Then*

$$\mu_{3,k}^2 \leq \frac{1}{2}\mu_{3,k-1}^2$$

holds when $\Omega \geq C\beta\kappa R(\mu_1^2(W/M) + \mu_2^2)\log(WM)$ for $\beta > 2$ with probability at least $1 - O((WM)^{1-\beta})$.

4.6 Proof of Lemmas for Theorem 4.2.1

4.6.1 Proof of Lemma 4.5.1

We want to bound the quantity

$$\eta(\Gamma_k) := \|\kappa\mathcal{P}_T\mathcal{A}_k^*\mathcal{A}_k\mathcal{P}_T - \mathcal{P}_T\| = \left\| \sum_{(i,j)\in\Gamma_k} \kappa\mathcal{P}_T(\boldsymbol{A}_{ij}) \otimes \mathcal{P}_T(\boldsymbol{A}_{ij}) - \mathcal{P}_T \right\|.$$

We are interested in the failure probability of the event $F(\Gamma_k) := \{\eta(\Gamma_k) > \zeta\}$. From (4.5.11), it is clear that

$$\mathrm{P}\left\{F(\Gamma_k)\right\} \leq 2\,\mathrm{P}\left\{F(\Gamma_k')\right\},$$

where the set Γ_k', as defined in (4.5.10), is the partition generated using the Bernoulli model. Hence, it is enough to bound the operator norm

$$\left\| \sum_{(i,j)\in\Gamma_k'} \kappa\mathcal{P}_T(\boldsymbol{A}_{ij}) \otimes \mathcal{P}_T(\boldsymbol{A}_{ij}) - \mathcal{P}_T \right\| = \left\| \sum_{(i,j)} \kappa\delta_{(i,j)}\mathcal{P}_T(\boldsymbol{A}_{ij}) \otimes \mathcal{P}_T(\boldsymbol{A}_{ij}) - \mathcal{P}_T \right\|.$$

Now the fact that the operator $\kappa\mathcal{P}_T\mathcal{A}_k^*\mathcal{A}_k\mathcal{P}_T$ does not deviate from its expected value

$$\begin{aligned}\mathrm{E}(\kappa\mathcal{P}_T\mathcal{A}_k^*\mathcal{A}_k\mathcal{P}_T) &= \kappa\mathcal{P}_T\,\mathrm{E}\sum_{(i,j)\in\Gamma_k'} \boldsymbol{A}_{ij} \otimes \boldsymbol{A}_{ij}\mathcal{P}_T \\ &= \kappa\mathcal{P}_T \sum_{(i,j)} \mathrm{E}\,\delta_{(i,j)}\,\mathrm{E}(\boldsymbol{A}_{ij} \otimes \boldsymbol{A}_{ij})\mathcal{P}_T = \mathcal{P}_T\,\mathrm{E}\,\mathcal{A}^*\mathcal{A}\mathcal{P}_T = \mathcal{P}_T\end{aligned}$$

in the spectral norm can be proven using the matrix Bernstein Inequality. To proceed define the operator $\mathcal{L}_{ij}$ which maps $\boldsymbol{Z}$ to $\langle\mathcal{P}_T(\boldsymbol{A}_{ij}), \boldsymbol{Z}\rangle\,\mathcal{P}_T(\boldsymbol{A}_{ij})$, i.e., $\mathcal{L}_{ij} = \mathcal{P}_T(\boldsymbol{A}_{ij}) \otimes \mathcal{P}_T(\boldsymbol{A}_{ij})$. This operator is rank one, therefore, the operator norm $\|\mathcal{L}_{ij}\| = \|\mathcal{P}_T(\boldsymbol{A}_{ij})\|_F^2$. Let

$$\boldsymbol{Z}_{ij} = \kappa\delta_{(i,j)}\mathcal{L}_{ij} - \kappa\,\mathrm{E}\,\delta_{(i,j)}\,\mathrm{E}\,\mathcal{L}_{ij}$$

We also have

$$\sum_{(i,j)} \kappa^2 \,\mathrm{E}(\mathcal{L}_{ij} - \mathrm{E}\,\mathcal{L}_{ij})^2 = \sum_{(i,j)} \kappa^2 [\mathrm{E}(\delta_{(i,j)}\mathcal{L}_{ij}^2) - (\mathrm{E}\,\delta_{(i,j)}\mathcal{L}_{ij})^2]$$
$$= \sum_{i,j} \kappa^2 \,\mathrm{E}(\delta_{(i,j)} \left\|\mathcal{P}_T(\boldsymbol{A}_{ij})\right\|_F^2 \mathcal{L}_{ij}) - \sum_{i,j} \kappa^2 (\mathrm{E}\,\delta_{(i,j)}\mathcal{L}_{ij})^2.$$

Because $\mathrm{E}\,\mathcal{L}_{ij}^2$, and $(\mathrm{E}\,\mathcal{L}_{ij})^2$ are symmetric, positive-semidefinite matrices, it follows that

$$\left\| \sum_{i=1}^{M} \sum_{j=1}^{\Omega} \mathrm{E}\,\delta_{(i,j)} (\mathcal{L}_{ij} - \mathrm{E}\,\mathcal{L}_{ij})^2 \right\| \leq \left\| \sum_{i,j} \mathrm{E}\,\delta_{(i,j)}\, \mathrm{E} \left\|\mathcal{P}_T(\boldsymbol{A}_{ij})\right\|_F^2 \mathcal{L}_{ij} \right\|$$
$$= \frac{1}{\kappa} \left\| \sum_{i,j} \mathrm{E} \left\|\mathcal{P}_T(\boldsymbol{A}_{ij})\right\|_F^2 \mathcal{L}_{ij} \right\|$$

Using the facts $\mathcal{L}_{ij} = \mathcal{P}_T(\boldsymbol{A}_{ij}) \otimes \mathcal{P}_T(\boldsymbol{A}_{ij})$, $\sum_{ij} \mathrm{E}\,\mathcal{L}_{ij} = \mathcal{P}_T$, and expanding further gives

$$\left\| \mathrm{E} \sum_{i,j} \left\|\mathcal{P}_T(\boldsymbol{A}_{ij})\right\|_F^2 \mathcal{L}_{ij} \right\| \leq \left\| \mathrm{E} \left(\sum_{i,j} \mu_1^2 \frac{R(W/M)}{\Omega} \mathcal{L}_{ij} + \left\| \sum_{k \sim \mathcal{B}_j} d_i[k] \boldsymbol{v}_k \right\|_2^2 \mathcal{L}_{ij} \right) \right\|.$$

Use the notation

$$\rho_{ij}^2 = \left\| \sum_{k \sim \mathcal{B}_j} d_i[k] \boldsymbol{v}_k \right\|_2^2,$$

then

$$\left\| \mathrm{E} \sum_{i,j} \left\|\mathcal{P}_T(\boldsymbol{A}_{ij})\right\|_F^2 \mathcal{L}_{ij} \right\| \leq \mu_1^2 \frac{R(W/M)}{\Omega} \left\| \sum_{i,j} \mathrm{E}\,\mathcal{L}_{ij} \right\| + \left\| \mathrm{E} \sum_{i,j} \rho_{ij}^2 \mathcal{L}_{ij} \right\|$$
$$\leq \mu_1^2 \frac{R(W/M)}{\Omega} + \left\| \mathrm{E} \sum_{i,j} \rho_{ij}^2 \mathcal{L}_{ij} \right\| \tag{4.6.1}$$

The second term in (4.6.1) can be simplified as

$$\left\| \mathrm{E} \sum_{i,j} \rho_{ij}^2 \mathcal{L}_{ij} \right\| = \left\| \mathcal{P}_T\, \mathrm{E} \sum_{i,j} \left(\rho_{ij}^2 (\boldsymbol{A}_{ij} \otimes \boldsymbol{A}_{ij}) \right) \mathcal{P}_T \right\|$$
$$\leq \left\| \mathrm{E} \sum_{i,j} \left(\rho_{ij}^2 (\boldsymbol{A}_{ij} \otimes \boldsymbol{A}_{ij}) \right) \right\|, \tag{4.6.2}$$

where the last line follows form the fact that $\|\mathcal{P}_T\| \leq 1$. Using the definition of ρ_{ij}^2, and (4.5.8), it is easy to see that the $W \times W$ submatrix at (α, β)-th location is given by

$$\{\mathrm{E}\left(\rho_{ij}^2(\boldsymbol{A}_{ij} \otimes \boldsymbol{A}_{ij})\right)\}_{(\alpha,\beta)} = e_i[\alpha]e_i[\beta]\left[\sum_{k\sim\mathcal{B}_j}\|\boldsymbol{v}_k\|_2^2\sum_{\ell\sim\mathcal{B}_j}\bar{\boldsymbol{e}}_\ell\bar{\boldsymbol{e}}_\ell^* + \sum_{k\neq k'\sim\mathcal{B}_j} 2\langle\boldsymbol{v}_k,\boldsymbol{v}_{k'}\rangle\bar{\boldsymbol{e}}_k\bar{\boldsymbol{e}}_{k'}^*\right]. \tag{4.6.3}$$

The following identity is very useful

$$\langle\boldsymbol{A}_{ij},\boldsymbol{A}_{i'j'}\rangle = 0,$$

which holds true when either $i \neq i'$, or/and $j \neq j'$. Given this fact, we have

$$\|\sum_{i,j}\boldsymbol{A}_{ij}\otimes\boldsymbol{A}_{ij}\| = \max_{ij}\|\boldsymbol{A}_{ij}\otimes\boldsymbol{A}_{ij}\|.$$

Using this fact, we can write

$$\left\|\sum_{i,j}\mathrm{E}\left(\rho_{ij}^2(\boldsymbol{A}_{ij}\otimes\boldsymbol{A}_{ij})\right)\right\| = \max_{i,j}\left\|\mathrm{E}\left(\rho_{ij}^2(\boldsymbol{A}_{ij}\otimes\boldsymbol{A}_{ij})\right)\right\|.$$

Using (4.6.3), we obtain

$$\begin{aligned}\left\|\sum_{i,j}\mathrm{E}\left(\rho_{ij}^2(\boldsymbol{A}_{ij}\otimes\boldsymbol{A}_{ij})\right)\right\| &\leq \left\|\sum_{k\sim\mathcal{B}_j}\|\boldsymbol{v}_k\|_2^2\sum_{\ell\sim\mathcal{B}_j}\bar{\boldsymbol{e}}_\ell\bar{\boldsymbol{e}}_\ell^*\right\| + 2\left\|\sum_{k\neq k'\sim\mathcal{B}_j}\langle\boldsymbol{v}_k,\boldsymbol{v}_{k'}\rangle\bar{\boldsymbol{e}}_k\bar{\boldsymbol{e}}_{k'}^*\right\| \\ &\leq \sum_{k\sim\mathcal{B}_j}\|\boldsymbol{v}_k\|_2^2\left\|\sum_{\ell\sim\mathcal{B}_j}\bar{\boldsymbol{e}}_\ell\bar{\boldsymbol{e}}_\ell^*\right\| + 2\|\boldsymbol{v}_k\|_2^2\left\|\sum_{k\neq k'\sim\mathcal{B}_j}\bar{\boldsymbol{e}}_k\bar{\boldsymbol{e}}_{k'}^*\right\| \\ &= \sum_{k\sim\mathcal{B}_j}\|\boldsymbol{v}_k\|_2^2 + 2\frac{W}{\Omega}\|\boldsymbol{v}_k\|_2^2 \leq 3\mu_2^2\frac{R}{\Omega},\end{aligned} \tag{4.6.4}$$

where the second ineqaulity follows from the application of Cauchy-Schwartz inequality in the second term of the R.H.S., the last equality is the result of the facts that

$$\left\|\sum_{\ell\sim\mathcal{B}_j}\bar{\boldsymbol{e}}_\ell\bar{\boldsymbol{e}}_\ell^*\right\| = 1,$$

and

$$\left\|\sum_{k\neq k'\sim\mathcal{B}_j}\bar{\boldsymbol{e}}_k\bar{\boldsymbol{e}}_{k'}^*\right\| \leq \frac{W}{\Omega},$$

and the last inequality follows form the definition of the coherence in (4.2.10). Plugging (4.6.4) in (4.6.1), we have the bound

$$\begin{aligned}\left\|\mathrm{E}\sum_{i,j}\boldsymbol{Z}_{ij}^{*}\boldsymbol{Z}_{ij}\right\| &\leq \kappa\left\|\mathrm{E}\sum_{i,j}\|\mathcal{P}_T(\boldsymbol{A}_{ij})\|_F^2\,\mathcal{L}_{ij}\right\| \\ &\leq C\kappa\frac{R(\mu_1^2(W/M)+\mu_2^2)}{\Omega}. \end{aligned} \tag{4.6.5}$$

Finally, we calculate the orlicz norm, the last ingredient to obtain the Bernstein bound. First, it is important to see that

$$\|\boldsymbol{Z}_{ij}\| = \|\mathcal{L}_{ij} - \mathrm{E}\,\mathcal{L}_{ij}\| \leq 2\|\mathcal{L}_{ij}\| = 2\|\mathcal{L}_{ij}\|_F = 2\|\mathcal{P}_T(\boldsymbol{A}_{ij})\|_F^2,$$

where the second-last equality follows form the fact that $\mathcal{L}_{ij}$ is the rank-1 operator. Using the last equation, and (4.5.9), we have

$$\begin{aligned} U_1 := \|\boldsymbol{Z}_{ij}\|_{\psi_1} &\leq 2\kappa\left\|\mu_1^2 R\frac{(W/M)}{\Omega} + \sum_{r=1}^{R}\left(\sum_{\gamma\sim\mathcal{B}_j} d_i[k]v_{kr}\right)^2\right\|_{\psi_1} \\ &\leq C\mu_1^2\kappa R\frac{(W/M)}{\Omega} + C\kappa\sum_{k\sim\mathcal{B}_j}\|\boldsymbol{v}_k\|_2^2 \\ &\leq C\mu_1^2\kappa R\frac{(W/M)}{\Omega} + C\mu_2^2\kappa\frac{R}{\Omega}. \end{aligned} \tag{4.6.6}$$

Using the notation $\Lambda = \mu_1^2(W/M) + \mu_2^2$, we obtain

$$U_1\log\left(\frac{M\Omega\cdot U_1^2}{\sigma_Z^2}\right) = C\kappa R\frac{\Lambda}{\Omega}\log(\kappa RM\Lambda).$$

Plugging (4.6.5), and (4.6.6), and using $t = \beta\log(WM)$ in the non-commutative Bernstein's Inequality in Proposition 2, we have

$$\left\|\sum_{i=1}^{M}\sum_{j=1}^{\Omega}\boldsymbol{Z}_{ij}\right\| \leq 2\max\{\sqrt{\kappa R\frac{\Lambda}{\Omega}}\sqrt{\beta\log(WM)}, \kappa R\frac{\Lambda}{\Omega}\log(\kappa RM\Lambda)(\beta\log(WM))\}$$

The claim follwis by taking $t = \beta\log(WM)$, and the fact that $RM\Lambda \leq WM$, and $\Omega \geq C(\mu_1^2(W/M)+\mu_2^2)\kappa R\beta\log^2(WM)$ with probabiliy at least $1-(WM)^{-\beta}$.

4.6.2 Proof of Lemma 4.5.2

We will use the Bernstein bound in Proposition 2 to prove this Lemma. We want to bound

$$\|(\kappa \mathcal{A}_k^* \mathcal{A}_k - \mathcal{I})(\boldsymbol{W}_{k-1})\| = \left\| \sum_{(i,j)\in\Gamma_k} \kappa \langle \boldsymbol{A}_{ij}, \boldsymbol{W}_{k-1}\rangle \boldsymbol{A}_{ij} - \mathrm{E} \sum_{(i,j)\in\Gamma_k} \kappa \langle \boldsymbol{A}_{ij}, \boldsymbol{W}_{k-1}\rangle \boldsymbol{A}_{ij} \right\|,$$

which follows from

$$\boldsymbol{W}_{k-1} = \mathrm{E} \sum_{(i,j)\in\Gamma_k} \kappa \langle \boldsymbol{A}_{ij}, \boldsymbol{W}_{k-1}\rangle \boldsymbol{A}_{ij}.$$

Using the reasoning similar to that in Lemma 4.5.1, it is clear that bounding the following sum of random matrices over Γ_k' matrices

$$\left\| \sum_{(i,j)\in\Gamma_k'} \kappa \langle \boldsymbol{A}_{ij}, \boldsymbol{W}_{k-1}\rangle \boldsymbol{A}_{ij} - \mathrm{E} \sum_{(i,j)\in\Gamma_k} \kappa \langle \boldsymbol{A}_{ij}, \boldsymbol{W}_{k-1}\rangle \boldsymbol{A}_{ij} \right\|$$

suffices. Define a zero-mean random variable as follows:

$$\boldsymbol{Z}_{ij} = \kappa \delta_{(i,j)} \langle \boldsymbol{A}_{ij}, \boldsymbol{W}_{k-1}\rangle \boldsymbol{A}_{ij} - \kappa \,\mathrm{E}\, \delta_{(i,j)} \langle \boldsymbol{A}_{ij}, \boldsymbol{W}_{k-1}\rangle \boldsymbol{A}_{ij}.$$

The first variance term in (2.5.3) is

$$\begin{aligned}\sum_{(i,j)} \mathrm{E}\, \boldsymbol{Z}_{ij} \boldsymbol{Z}_{ij}^* = &\sum_{(i,j)} \kappa^2 \,\mathrm{E}\, \delta_{(i,j)} \langle \boldsymbol{A}_{ij}, \boldsymbol{W}_{k-1}\rangle^2 \boldsymbol{A}_{ij} \boldsymbol{A}_{ij}^* \\ &- \sum_{i,j} \kappa^2 (\mathrm{E}\, \delta_{(i,j)})^2 \,\mathrm{E}(\langle \boldsymbol{A}_{ij}, \boldsymbol{W}_{k-1}\rangle \boldsymbol{A}_{ij}) \,\mathrm{E}(\langle \boldsymbol{A}_{ij}, \boldsymbol{W}_{k-1}\rangle \boldsymbol{A}_{ij})^*,\end{aligned}$$

where

$$\langle \boldsymbol{A}_{ij}, \boldsymbol{W}_{k-1}\rangle = \sum_{\gamma\sim\mathcal{B}_j} d_i[\gamma] W_{k-1}[i,\gamma].$$

The following can be easily verified and will be used in the proof of this Lemma

$$\begin{aligned}\left\| \sum_{(i,j)} \mathrm{E}\, \delta_{(i,j)} \boldsymbol{Z}_{ij} \boldsymbol{Z}_{ij}^* \right\| &\le \left\| \sum_{(i,j)} \kappa^2 \,\mathrm{E}\, \delta_{(i,j)} \,\mathrm{E} \langle \boldsymbol{A}_{ij}, \boldsymbol{W}_{k-1}\rangle^2 \boldsymbol{A}_{ij} \boldsymbol{A}_{ij}^* \right\| \\ &= \left\| \sum_{(i,j)} \kappa \,\mathrm{E} \langle \boldsymbol{A}_{ij}, \boldsymbol{W}_{k-1}\rangle^2 \boldsymbol{A}_{ij} \boldsymbol{A}_{ij}^* \right\|.\end{aligned}$$

In the calculations below, we assemble the ingredients to calculate the variance. First by (4.5.6), we have

$$\begin{aligned}\langle \boldsymbol{A}_{ij}, \boldsymbol{W}_{k-1}\rangle^2 \boldsymbol{A}_{ij}\boldsymbol{A}_{ij}^* &= \langle \boldsymbol{A}_{ij}, \boldsymbol{W}_{k-1}\rangle^2 \boldsymbol{e}_i\boldsymbol{e}_i^* \sum_{\gamma,\gamma'\sim\mathcal{B}_j} d_i[k]d_i[k']\bar{\boldsymbol{e}}_k^*\bar{\boldsymbol{e}}_{k'} \\ &= \langle \boldsymbol{A}_{ij}, \boldsymbol{W}_{k-1}\rangle^2 \boldsymbol{e}_i\boldsymbol{e}_i^* \sum_{\gamma\sim\mathcal{B}_j} d_i[k]^2\|\bar{\boldsymbol{e}}_k\|_2^2 \\ &= \frac{W}{\Omega}\langle \boldsymbol{A}_{ij}, \boldsymbol{W}_{k-1}\rangle^2 \boldsymbol{e}_i\boldsymbol{e}_i^*.\end{aligned}$$

Taking summation over i, and j on both sides and using above relation gives us

$$\begin{aligned}\frac{W}{\Omega}\left\|\sum_{(i,j)} \mathrm{E}\langle \boldsymbol{A}_{ij}, \boldsymbol{W}_{k-1}\rangle^2 \boldsymbol{e}_i\boldsymbol{e}_i^*\right\| &\le \left\|\sum_{i=1}^{M} \boldsymbol{e}_i\boldsymbol{e}_i^*\right\| \cdot \max_i \frac{W}{\Omega}\sum_{j=1}^{\Omega} \mathrm{E}\langle \boldsymbol{A}_{ij}, \boldsymbol{W}_{k-1}\rangle^2 \\ &= \frac{W}{\Omega}\max_i \sum_{j=1}^{\Omega}\sum_{\gamma\sim\mathcal{B}_j} W_{k-1}^2[i,\gamma].\end{aligned}$$

This gives the first term in the variance (2.5.3)

$$\left\|\sum_{(i,j)\in\Gamma_k'} \mathrm{E}\, \boldsymbol{Z}_{ij}\boldsymbol{Z}_{ij}^*\right\| \le \kappa\frac{W}{\Omega}\sum_{j=1}^{\Omega}\sum_{\gamma\sim\mathcal{B}_j} W_{k-1}^2[i,\gamma] = \|\boldsymbol{W}_{k-1}\|_F^2\kappa\frac{(W/M)}{\Omega}\mu_{3,k-1}^2, \qquad (4.6.7)$$

where the last inequality follows from (4.2.9). The second variance term in (2.5.3) is

$$\begin{aligned}\sum_{(i,j)\in\Gamma_k'} \mathrm{E}\, \boldsymbol{Z}_{ij}^*\boldsymbol{Z}_{ij} &= \sum_{(i,j)} \kappa^2\, \mathrm{E}\,\delta_{(i,j)}\, \mathrm{E}\langle \boldsymbol{A}_{ij}, \boldsymbol{W}_{k-1}\rangle^2 \boldsymbol{A}_{ij}^*\boldsymbol{A}_{ij} - \\ &\quad - \sum_{i,j} \mathrm{E}\,\delta_{(i,j)}\, \mathrm{E}(\langle \boldsymbol{A}_{ij}, \boldsymbol{W}_{k-1}\rangle \boldsymbol{A}_{ij})^*\, \mathrm{E}(\langle \boldsymbol{A}_{ij}, \boldsymbol{W}_{k-1}\rangle \boldsymbol{A}_{ij}) \\ &= \kappa\sum_{i,j} \mathrm{E}\langle \boldsymbol{A}_{ij}, \boldsymbol{W}_{k-1}\rangle^2 \boldsymbol{A}_{ij}^*\boldsymbol{A}_{ij} - \kappa\sum_{i,j} \mathrm{E}(\langle \boldsymbol{A}_{ij}, \boldsymbol{W}_{k-1}\rangle \boldsymbol{A}_{ij})^*\, \mathrm{E}(\langle \boldsymbol{A}_{ij}, \boldsymbol{W}_{k-1}\rangle \boldsymbol{A}_{ij}),\end{aligned}$$

which implies that

$$\left\|\sum_{(i,j)} \mathrm{E}\, \boldsymbol{Z}_{ij}\boldsymbol{Z}_{ij}^*\right\| \le \kappa\left\|\sum_{(i,j)} \mathrm{E}\langle \boldsymbol{A}_{ij}, \boldsymbol{W}_{k-1}\rangle^2 \boldsymbol{A}_{ij}\boldsymbol{A}_{ij}^*\right\|.$$

We begin with

$$\langle \boldsymbol{A}_{ij}, \boldsymbol{W}_{k-1}\rangle^2 \boldsymbol{A}_{ij}^*\boldsymbol{A}_{ij} = \langle \boldsymbol{A}_{ij}, \boldsymbol{W}_{k-1}\rangle^2 \|\boldsymbol{e}_i\|_2^2 \sum_{\gamma,\gamma'\sim\mathcal{B}_j} d_i[\gamma]d_i[\gamma']\bar{\boldsymbol{e}}_\gamma\bar{\boldsymbol{e}}_{\gamma'}^*.$$

The expectation of the operand on the right hand side gives

$$\begin{aligned}\mathrm{E}\langle \boldsymbol{A}_{ij}, \boldsymbol{W}_{k-1}\rangle^2 \boldsymbol{A}_{ij}^* \boldsymbol{A}_{ij} &= \left(\sum_{\gamma} d_i[\gamma] W_{k-1}[i,\gamma]\right)^2 \left(\sum_{\gamma,\gamma' \sim \mathcal{B}_j} d_i[\gamma] d_i[\gamma'] \bar{\boldsymbol{e}}_{\gamma} \bar{\boldsymbol{e}}_{\gamma'}^*\right) \\ &= \sum_{\gamma \sim \mathcal{B}_j} W_{k-1}^2[i,\gamma] \sum_{\gamma \sim \mathcal{B}_j} \bar{\boldsymbol{e}}_{\gamma} \bar{\boldsymbol{e}}_{\gamma}^* + 2 \sum_{\gamma,\gamma' \sim \mathcal{B}_j} W_{k-1}[i,\gamma] W_{k-1}[i,\gamma'] \bar{\boldsymbol{e}}_{\gamma} \bar{\boldsymbol{e}}_{\gamma'}^*.\end{aligned}$$

Next step is to take the operator norm, and summation over j on both sides. The orthogonality of $\{\bar{\boldsymbol{e}}_{\gamma}\}_{1 \le \gamma \le W}$, and $\mathcal{B}_j \cap \mathcal{B}_{j'} = \phi$ implies that

$$\begin{aligned}&\left\| \sum_{j=1}^{\Omega} \mathrm{E}\langle \boldsymbol{A}_{ij}, \boldsymbol{W}_{k-1}\rangle^2 \boldsymbol{A}_{ij}^* \boldsymbol{A}_{ij} \right\| \le \\ &\quad \le \left\| \sum_{j=1}^{\Omega} \sum_{\gamma \sim \mathcal{B}_j} W_{k-1}^2[i,\gamma] \sum_{\gamma \sim \mathcal{B}_j} \bar{\boldsymbol{e}}_{\gamma} \bar{\boldsymbol{e}}_{\gamma}^* \right\| + 2 \left\| \sum_{j=1}^{\Omega} \sum_{\gamma,\gamma' \sim \mathcal{B}_j} W_{k-1}[i,\gamma] W_{k-1}[i,\gamma'] \bar{\boldsymbol{e}}_{\gamma} \bar{\boldsymbol{e}}_{\gamma'}^* \right\| \\ &\le \max_j \left\| \sum_{\gamma \sim \mathcal{B}_j} W_{k-1}^2[i,\gamma] \sum_{\gamma \sim \mathcal{B}_j} \bar{\boldsymbol{e}}_{\gamma} \bar{\boldsymbol{e}}_{\gamma}^* \right\| + 2 \max_j \left\| \sum_{\gamma,\gamma' \sim \mathcal{B}_j} W_{k-1}[i,\gamma] W_{k-1}[i,\gamma'] \bar{\boldsymbol{e}}_{\gamma} \bar{\boldsymbol{e}}_{\gamma'}^* \right\|\end{aligned}$$

Now using the fact that

$$\left\| \sum_{\gamma,\gamma' \sim \mathcal{B}_j} W_{k-1}[i,\gamma] W_{k-1}[i,\gamma'] \bar{\boldsymbol{e}}_{\gamma} \bar{\boldsymbol{e}}_{\gamma'}^* \right\| = \sum_{\gamma \sim \mathcal{B}_j} W_{k-1}^2[i,\gamma]$$

Summing over i, we obtain the second variance

$$\begin{aligned}\left\| \sum_{(i,j) \in \Gamma_k'} \mathrm{E}\, \boldsymbol{Z}_{ij}^* \boldsymbol{Z}_{ij} \right\| &\le 3\kappa \sum_{i=1}^{M} \max_j \sum_{\gamma \sim \mathcal{B}_j} W_{k-1}^2[i,\gamma] \\ &= 3\kappa \sum_{i=1}^{M} \|\boldsymbol{W}_{k-1}\|_F^2 \mu_{3,k-1}^2 \frac{1}{M\Omega} = 3\kappa \mu_{3,k-1}^2 \frac{1}{\Omega} \|\boldsymbol{W}_{k-1}\|_F^2. \qquad (4.6.8)\end{aligned}$$

Given (4.6.7), and (4.6.8), we can obtain the variance using (2.5.3). We now calculte the ψ_2 norm of matrix $\langle \boldsymbol{A}_{ij}, \boldsymbol{W}_{k-1}\rangle \boldsymbol{A}_{ij} - \mathrm{E}\langle \boldsymbol{A}_{ij}, \boldsymbol{W}_{k-1}\rangle \boldsymbol{A}_{ij}$. Since $\langle \boldsymbol{A}_{ij}, \boldsymbol{W}_{k-1}\rangle \boldsymbol{A}_{ij}$ is a rank one matrix, this gives

$$\begin{aligned}\|\langle \boldsymbol{A}_{ij}, \boldsymbol{W}_{k-1}\rangle \boldsymbol{A}_{ij} - \mathrm{E}\langle \boldsymbol{A}_{ij}, \boldsymbol{W}_{k-1}\rangle \boldsymbol{A}_{ij}\|_{\psi_2} &\le 2 \|\langle \boldsymbol{A}_{ij}, \boldsymbol{W}_{k-1}\rangle \boldsymbol{A}_{ij}\|_{\psi_2} \\ &\le 2\|\boldsymbol{A}_{ij}\| \|\langle \boldsymbol{A}_{ij}, \boldsymbol{W}_{k-1}\rangle\|_{\psi_2} \\ &= 2\frac{W}{\Omega} \|\langle \boldsymbol{A}_{ij}, \boldsymbol{W}_{k-1}\rangle\|_{\psi_2}.\end{aligned}$$

This gives the result

$$U_2^2 = \max_{ij} \|\langle \boldsymbol{A}_{ij}, \boldsymbol{W}_{k-1}\rangle \boldsymbol{A}_{ij} - \mathrm{E}\langle \boldsymbol{A}_{ij}, \boldsymbol{W}_{k-1}\rangle \boldsymbol{A}_{ij}\|_{\psi_2}$$
$$\leq C\kappa \frac{W}{\Omega} \max_{ij} \sum_{\gamma \sim \mathcal{B}_j} W_{k-1}^2[i,\gamma] = C\kappa \frac{(W/M)}{\Omega^2} \mu_{3,k-1}^2 \|\boldsymbol{W}_{k-1}\|_F^2, \tag{4.6.9}$$

and hence

$$U_2 \log^{1/2}\left(\frac{M\Omega \cdot U_2^2}{\sigma_Z^2}\right) \leq \sqrt{C\kappa\mu_{3,k-1}^2 \frac{W/M}{\Omega^2}} \|\boldsymbol{W}_{k-1}\|_F \log^{1/2}(WM).$$

The results in (4.6.7), (4.6.8), and (4.6.9) can be plugged in Proposition 2 to obtain

$$\|\mathcal{A}_k^* \mathcal{A}_k(\boldsymbol{W}_{k-1}) - \boldsymbol{W}_{k-1}\|_F \leq$$
$$C\kappa \|\boldsymbol{W}_{k-1}\|_F \max\left\{ \sqrt{\frac{\kappa\mu_{3,k-1}^2 \max(W/M,1)}{\Omega}} \sqrt{\beta \log(WM)}, \sqrt{\kappa \frac{\mu_{3,k-1}^2 (W/M)}{\Omega^2}} \beta \log^{3/2}(WM) \right\} \tag{4.6.10}$$

with $t = \beta \log(WM)$, which holds with probability at least $1 - (WM)^{-\beta}$. Using (4.5.14), it becomes clear that the right hand side can be controlled with high probability by selecting $\Omega \geq C\beta\kappa\mu_{3,k-1}^2 R \max(W/M, 1) \log(WM)$.

4.6.3 Proof of Lemma 4.5.3

Coherence of iterates $\boldsymbol{W}_k$ was defined earlier in (4.5.15). This Lemma is dedicated to showing that the coherence of the iterates is bounded. We start with matrix $\boldsymbol{W}_k$ and its coherences $\mu_{1,k}^2$ and $\mu_{2,k}^2$. The iterates are related as

$$\boldsymbol{W}_k = (\kappa \mathcal{P}_T \mathcal{A}_k^* \mathcal{A}_k \mathcal{P}_T - \mathcal{P}_T)(\boldsymbol{W}_{k-1}).$$

Since $\boldsymbol{W}_k \in T$, we start with writing out

$$\boldsymbol{W}_k = \kappa \mathcal{P}_T \mathcal{A}_k^* \mathcal{A}_k(\boldsymbol{W}_{k-1}) - \boldsymbol{W}_{k-1}$$
$$= \sum_{(i,j)\in\Gamma_k} \kappa \langle \boldsymbol{A}_{ij}, \boldsymbol{W}_{k-1}\rangle \mathcal{P}_T(\boldsymbol{A}_{ij}) - \boldsymbol{W}_{k-1}$$

The coherence $\mu_{3,k}^2$ of $\boldsymbol{W}_k$ is then

$$\mu_{3,k}^2 = \frac{M\Omega}{R} \max_{\substack{1\le m\le M\\ 1\le \omega\le \Omega}} \sum_{n\sim\mathcal{B}_\omega} \left(\sum_{(i,j)\in\Gamma_k} \kappa \langle \boldsymbol{A}_{ij}, \boldsymbol{W}_{k-1}\rangle [\mathcal{P}_T(\boldsymbol{A}_{ij})]_{(m,n)} - [\boldsymbol{W}_{k-1}]_{(m,n)} \right)^2 \tag{4.6.11}$$

We sart with bounding the following quantity with high probability

$$\eta_{mn}(\Gamma_k) := \left| \sum_{(i,j)\in\Gamma_k} \kappa \langle \boldsymbol{A}_{ij}, \boldsymbol{W}_{k-1}\rangle [\mathcal{P}_T(\boldsymbol{A}_{ij})]_{(m,n)} - [\boldsymbol{W}_{k-1}]_{(m,n)} \right| \tag{4.6.12}$$

using the scalar Bernstein bound. Instead of bounding $\{\eta_{mn}(\Gamma_k) > \epsilon\}$, we will bound the event $\{\eta_{mn}(\Gamma_k') > \epsilon\}$, where the set Γ_k' is selected using Bernoulli model, i.e., we will bound the following quantity

$$\eta_{mn}(\Gamma_k') := \left| \sum_{(i,j)\in\Gamma_k} \kappa \delta_{(i,j)} \langle \boldsymbol{A}_{ij}, \boldsymbol{W}_{k-1}\rangle [\mathcal{P}_T(\boldsymbol{A}_{ij})]_{(m,n)} - [\boldsymbol{W}_{k-1}]_{(m,n)} \right|$$

Let

$$Z_{ij} = \kappa \delta_{(i,j)} \langle \boldsymbol{A}_{ij}, \boldsymbol{W}_{k-1}\rangle [\mathcal{P}_T(\boldsymbol{A}_{ij})]_{(m,n)} - [\boldsymbol{W}_{k-1}]_{(m,n)}. \tag{4.6.13}$$

For this purpose, we need to calculate the variance

$$\sum_{(i,j)\in\Gamma_k'} \mathrm{E}\, Z_{ij} Z_{ij}^* \le \sum_{(i,j)} \kappa^2\, \mathrm{E}\, \delta_{(i,j)} \langle \boldsymbol{A}_{ij}, \boldsymbol{W}_{k-1}\rangle^2 [\mathcal{P}_T(\boldsymbol{A}_{ij})]_{(m,n)}^2$$

$$[\mathcal{P}_T(\boldsymbol{A}_{ij})]_{(m,n)} = [\boldsymbol{U}\boldsymbol{U}^*\boldsymbol{A}_{ij}]_{(m,n)} + [\boldsymbol{A}_{ij}\boldsymbol{V}\boldsymbol{V}^*]_{(m,n)} - [\boldsymbol{U}\boldsymbol{U}^*\boldsymbol{A}_{ij}\boldsymbol{V}\boldsymbol{V}^*]_{(m,n)}.$$

It follows that

$$[\mathcal{P}_T(\boldsymbol{A}_{ij})]_{(m,n)}^2 \le 3\left([\boldsymbol{U}\boldsymbol{U}^*\boldsymbol{A}_{ij}]_{(m,n)}^2 + [\boldsymbol{A}_{ij}\boldsymbol{V}\boldsymbol{V}^*]_{(m,n)}^2 + [\boldsymbol{U}\boldsymbol{U}^*\boldsymbol{A}_{ij}\boldsymbol{V}\boldsymbol{V}^*]_{(m,n)}^2 \right). \tag{4.6.14}$$

Using Lemma 4.7.1, we now calculate the variance term by term. The first term in the variance is

$$\begin{aligned}\sum_{(i,j)} \mathrm{E}[\boldsymbol{U}\boldsymbol{U}^*\boldsymbol{A}_{ij}]_{(m,n)}^2 \langle \boldsymbol{A}_{ij}, \boldsymbol{W}_{k-1}\rangle^2 &\le 3\sum_{i=1}^{M} \langle \boldsymbol{u}_m, \boldsymbol{u}_i\rangle^2 \cdot \sum_{j=1}^{\Omega} \sum_{\gamma\sim\mathcal{B}_j} \langle \bar{\boldsymbol{e}}_\gamma, \bar{\boldsymbol{e}}_n\rangle^2 \cdot \max_{ij} \sum_{\gamma\sim\mathcal{B}_j} W_{k-1}^2[i,\gamma] \\ &\le 3\|\boldsymbol{u}_m\|_2^2 \cdot \mu_{3,k-1}^2 \frac{R}{M\Omega},\end{aligned} \tag{4.6.15}$$

where the first inequality follows by the application of Lemma 4.7.2. For the second inequality, we have used the the definition of coherence in (4.2.11), and the fact that

$$\sum_{j=1}^{\Omega} \sum_{\gamma \sim \mathcal{B}_j} \langle \bar{\boldsymbol{e}}_\gamma, \bar{\boldsymbol{e}}_n \rangle^2 = 1$$

for any given index (m, n). Using Lemma 4.7.1, and 4.7.2 again, we obtain

$$\begin{aligned}
\sum_{(i,j)} \mathrm{E}[\boldsymbol{A}_{ij} \boldsymbol{V}\boldsymbol{V}^*]^2_{(m,n)} \langle \boldsymbol{A}_{ij}, \boldsymbol{W}_{k-1} \rangle^2 &\leq 3 \sum_{(i,j)} \left(\sum_{\gamma \sim \mathcal{B}_j} W^2_{k-1}[i,\gamma] \cdot \sum_{\gamma \sim \mathcal{B}_j} \langle \boldsymbol{v}_\gamma, \boldsymbol{v}_n \rangle^2 \right) \langle \boldsymbol{e}_m, \boldsymbol{e}_i \rangle^2 \\
&= 3 \max_{ij} \sum_{\gamma \sim \mathcal{B}_j} W^2_{k-1}[i,\gamma] \cdot \sum_{j=1}^{\Omega} \sum_{\gamma \sim \mathcal{B}_j} \langle \boldsymbol{v}_\gamma, \boldsymbol{v}_n \rangle^2 \cdot \sum_{i=1}^{M} \langle \boldsymbol{e}_m, \boldsymbol{e}_i \rangle^2 \\
&\leq 3 \max_{ij} \sum_{\gamma \sim \mathcal{B}_j} W^2_{k-1}[i,\gamma] \|\boldsymbol{v}_n\|_2^2 \cdot \|\boldsymbol{e}_m\|_2^2 \leq 3 \mu^2_{3,k-1} \frac{R}{M\Omega} \|\boldsymbol{v}_n\|_2^2. \qquad (4.6.16)
\end{aligned}$$

Similarly, the last variance term is

$$\begin{aligned}
&\sum_{(i,j)} \mathrm{E}[\boldsymbol{U}\boldsymbol{U}^* \boldsymbol{A}_{ij} \boldsymbol{V}\boldsymbol{V}^*]^2_{(m,n)} \langle \boldsymbol{A}_{ij}, \boldsymbol{W}_{k-1} \rangle^2 \leq \\
&\qquad \leq 3 \sum_{i=1}^{M} \langle \boldsymbol{u}_n, \boldsymbol{u}_i \rangle^2 \cdot \sum_{j=1}^{\Omega} \sum_{\gamma \sim \mathcal{B}_j} \langle \boldsymbol{v}_\gamma, \boldsymbol{v}_n \rangle^2 \cdot \max_{ij} \sum_{\gamma \sim \mathcal{B}_j} W^2_{k-1}[i,\gamma] \\
&\qquad \leq 3 \|\boldsymbol{u}_m\|_2^2 \cdot \|\boldsymbol{v}_n\|_2^2 \cdot \mu^2_{3,k-1} \frac{R}{M\Omega}. \qquad (4.6.17)
\end{aligned}$$

Using the fact that $\|\boldsymbol{v}_n\|_2^2 \leq 1$, we see that (4.6.16) dominates (4.6.17). Putting (4.6.15), (4.6.16), and (4.6.17) together, we have

$$\sigma_Z^2 = \sum_{(i,j)} \mathrm{E}\, Z_{ij} Z_{ij}^* \leq C\kappa(\|\boldsymbol{u}_m\|_2^2 + \|\boldsymbol{v}_n\|_2^2) \mu^2_{3,k-1} \frac{R}{M\Omega}. \qquad (4.6.18)$$

Now, we need to calculate the Orlicz-1 norm $\max_{ij} \|Z_{ij}\|_{\psi_1}$. Using standard argumnets in probability theory, see [99], we can show that

$$\|[\boldsymbol{U}\boldsymbol{U}^* \boldsymbol{A}_{ij}]_{(m,n)}\|_{\psi_2} \leq C \langle \boldsymbol{u}_m, \boldsymbol{u}_i \rangle \left(\sum_{\gamma \sim \mathcal{B}_j} \langle \bar{\boldsymbol{e}}_\gamma, \bar{\boldsymbol{e}}_n \rangle^2 \right)^{1/2} \leq C \|\boldsymbol{u}_i\|_2 \|\boldsymbol{u}_m\|_2$$

where the first inequality follows from the fact that for a fixed (m, n)

$$\sum_{\gamma \sim \mathcal{B}_j} \langle \bar{\boldsymbol{e}}_\gamma, \bar{\boldsymbol{e}}_n \rangle^2 \leq 1,$$

and that $\langle \boldsymbol{u}_m, \boldsymbol{u}_i \rangle \leq \|\boldsymbol{u}_i\|_2 \|\boldsymbol{u}_m\|_2 \leq \|\boldsymbol{u}_m\|_2$, as $\|\boldsymbol{u}_i\|_2 \leq 1$. Also,

$$\|[\boldsymbol{A}_{ij}\boldsymbol{V}\boldsymbol{V}^*]_{(m,n)}\|_{\psi_2} \leq C\langle \boldsymbol{e}_m, \boldsymbol{e}_i \rangle \left(\sum_{\gamma \sim \mathcal{B}_j} \langle \boldsymbol{v}_\gamma, \boldsymbol{v}_n \rangle^2 \right)^{1/2} \leq C\|\boldsymbol{v}_n\|_2,$$

the second inequality follows from the identity

$$\sum_{j=1}^{\Omega} \sum_{\gamma \sim \mathcal{B}_j} \langle \boldsymbol{v}_\gamma, \boldsymbol{v}_n \rangle^2 = \|\boldsymbol{v}_n\|_2^2,$$

and that $\langle \boldsymbol{e}_m, \boldsymbol{e}_i \rangle \leq 1$ for a fixed (m, n). Similaraly, we can show that

$$\|[\boldsymbol{U}\boldsymbol{U}^*\boldsymbol{A}_{ij}\boldsymbol{V}\boldsymbol{V}^*]_{(m,n)}\|_{\psi_2} \leq C\|\boldsymbol{u}_m\|_2\|\boldsymbol{v}_n\|_2.$$

In addition, as before, we have

$$\|\langle \boldsymbol{A}_{ij}, \boldsymbol{W}_{k-1} \rangle\|_{\psi_2} \leq C \left(\sum_{\gamma \sim \mathcal{B}_j} W_{k-1}^2[i, \gamma] \right)^{1/2}.$$

Using Lemma 4.7.3, Equation (4.6.13), (4.6.14), and the fact that $\delta_{(i,j)} \leq 1$, we see that $\|Z_{ij}\|_{\psi_1} < \infty$, and

$$\begin{aligned}
\max_{ij} \|Z_{ij}\|_{\psi_1}^2 &\leq C\kappa^2 \max_{ij} \left(\|[\boldsymbol{U}\boldsymbol{U}^*\boldsymbol{A}_{ij}]_{(m,n)}\|_{\psi_2}^2 + \|[\boldsymbol{A}_{ij}\boldsymbol{V}\boldsymbol{V}^*]_{(m,n)}\|_{\psi_2}^2 \right) \|\langle \boldsymbol{A}_{ij}, \boldsymbol{W}_{k-1} \rangle\|_{\psi_2}^2 \\
&\leq C\kappa^2 \max_{ij} \left(\|\boldsymbol{u}_n\|_2^2 + \|\boldsymbol{v}_m\|_2^2 \right) \cdot \sum_{\gamma \sim \mathcal{B}_j} W_{k-1}^2[i, \gamma] \\
&\leq C\kappa^2 \left(\mu_1^2 \frac{R}{M} + \mu_2^2 \frac{R}{W} \right) \mu_{3,k-1}^2 \frac{R}{M\Omega}.
\end{aligned}$$

Then the Orlicz term in the Bernstein bound is

$$U_1 \log \left(\frac{M\Omega \cdot U_1^2}{\sigma_Z^2} \right) \leq C\kappa \frac{R(\mu_1^2(W/M) + \mu_2^2)}{\Omega} \mu_{3,k-1}^2 \frac{R}{M\Omega} \log(WM).$$

Clearly, the Orlicz bound dominates the variance bound. Select $t = \beta \log(WM)$ in the Bernstein bound, which implies that

$$\begin{aligned}
|\eta_{mn}(\Gamma_k')|^2 &\leq C\beta\kappa(\|\boldsymbol{u}_m\|_2^2 + \|\boldsymbol{v}_n\|_2^2)\mu_{3,k-1}^2 \frac{R}{M\Omega} \log^2(WM) \\
&\leq C\beta\kappa \frac{R(\mu_1^2(W/M) + \mu_2^2)}{\Omega} \mu_{3,k-1}^2 \frac{R}{M\Omega} \log^2(WM)
\end{aligned}$$

holds with probability at least $1-(WM)^{-\beta}$. The second ineequality follwos fram the definitions in (4.2.9), and (4.2.10). Using the bound on $|\eta_{mn}(\Gamma'_k)|^2$, we can find a bound on the coherence of the iterates in (4.6.11), which is

$$\mu_{3,k}^2 \leq C\kappa \sum_{n\sim\mathcal{B}_\omega} (\mu_1^2 \frac{R}{M} + \mu_2^2 \frac{R}{W})\mu_{3,k-1}^2 \log^2(WM)$$

Select $\Omega \geq C\beta\kappa R(\mu_1^2(W/M)+\mu_2^2)\log^2(WM)$, we can arrange for a constant C such that

$$\mu_{3,k}^2 \leq \frac{1}{2}\mu_{3,k-1}^2 \tag{4.6.19}$$

holds with probability at least $1-(WM)^{-\beta}$.

4.7 Auxiliary Lemmas for Theorem 4.2.1

Follwing Lemma will be useful in carying out several calculations in the proofs of the above lemmas.

Lemma 4.7.1. *Take $\boldsymbol{A}_{ij}$ as defined in* (4.5.6)*, and suppose $\boldsymbol{U}: M\times R$, and $\boldsymbol{V}: W\times R$ are orthogonal matrices with $\{\boldsymbol{u}_i\}_{1\leq i\leq M}$, $\{\boldsymbol{v}_i\}_{1\leq i\leq W}$ as rows, respectively. Then*

$$[\boldsymbol{U}\boldsymbol{U}^*\boldsymbol{A}_{ij}]_{(m,n)}^2 = \langle \boldsymbol{u}_m, \boldsymbol{u}_i\rangle^2 \left(\sum_{\gamma\sim\mathcal{B}_j} d_i[\gamma]\langle \bar{\boldsymbol{e}}_\gamma, \bar{\boldsymbol{e}}_n\rangle\right)^2, \tag{4.7.1}$$

$$[\boldsymbol{V}\boldsymbol{V}^*\boldsymbol{A}_{ij}^*]_{(m,n)}^2 = \langle \boldsymbol{e}_m, \boldsymbol{e}_i\rangle^2 \left(\sum_{\gamma\sim\mathcal{B}_j} d_i[\gamma]\langle \boldsymbol{v}_\gamma, \boldsymbol{v}_n\rangle\right)^2, \tag{4.7.2}$$

and

$$[\boldsymbol{U}\boldsymbol{U}^*\boldsymbol{A}_{ij}\boldsymbol{V}\boldsymbol{V}^*]_{(m,n)}^2 = \langle \boldsymbol{u}_m, \boldsymbol{u}_i\rangle^2 \left(\sum_{\gamma\sim\mathcal{B}_j} d_i[\gamma]\langle \boldsymbol{v}_\gamma, \boldsymbol{v}_n\rangle\right)^2. \tag{4.7.3}$$

Proof. We will use the definition of $\boldsymbol{A}_{ij}$ in (4.5.6). Begin with

$$\begin{aligned}
[\boldsymbol{U}\boldsymbol{U}^*\boldsymbol{A}_{ij}]_{(m,n)} &= \langle \boldsymbol{U}\boldsymbol{U}^*\boldsymbol{A}_{ij}, \boldsymbol{e}_m\bar{\boldsymbol{e}}_n^*\rangle = \boldsymbol{e}_m^*\boldsymbol{U}\boldsymbol{U}^* \sum_{\gamma\sim\mathcal{B}_j} d_i[\gamma]\boldsymbol{e}_i\bar{\boldsymbol{e}}_\gamma^*\bar{\boldsymbol{e}}_n \\
&= \sum_{\gamma\sim\mathcal{B}_j} d_i[\gamma]\boldsymbol{e}_m^*\boldsymbol{U}\boldsymbol{u}_i\bar{\boldsymbol{e}}_\gamma^*\bar{\boldsymbol{e}}_n = \sum_{\gamma\sim\mathcal{B}_j} d_i[\gamma]\boldsymbol{e}_m^*\boldsymbol{U}\boldsymbol{u}_i\bar{\boldsymbol{e}}_\gamma^*\bar{\boldsymbol{e}}_n \\
&= \langle \boldsymbol{u}_m, \boldsymbol{u}_i\rangle \sum_{\gamma\sim\mathcal{B}_j} d_i[\gamma]\bar{\boldsymbol{e}}_\gamma^*\bar{\boldsymbol{e}}_n,
\end{aligned}$$

Second,

$$[\boldsymbol{A}_{ij}\boldsymbol{V}\boldsymbol{V}^*]_{(m,n)} = \langle \boldsymbol{A}_{ij}\boldsymbol{V}\boldsymbol{V}^*, \boldsymbol{e}_m\bar{\boldsymbol{e}}_n^*\rangle = \sum_{\gamma\sim\mathcal{B}_j} d_i[\gamma]\boldsymbol{e}_m^*\boldsymbol{e}_i\bar{\boldsymbol{e}}_\gamma^*\boldsymbol{V}\boldsymbol{V}^*\bar{\boldsymbol{e}}_n$$
$$= \langle \boldsymbol{e}_m, \boldsymbol{e}_i\rangle \sum_{\gamma\sim\mathcal{B}_j} d_i[\gamma]\langle \boldsymbol{v}_\gamma, \boldsymbol{v}_n\rangle.$$

Finally,

$$\begin{aligned}[\boldsymbol{U}\boldsymbol{U}^*\boldsymbol{A}_{ij}\boldsymbol{V}\boldsymbol{V}^*]_{(m,n)} &= \langle \boldsymbol{U}\boldsymbol{U}^*\boldsymbol{A}_{ij}\boldsymbol{V}\boldsymbol{V}^*, \boldsymbol{e}_m\bar{\boldsymbol{e}}_n^*\rangle \\ &= \boldsymbol{e}_m^*\boldsymbol{U}\boldsymbol{U}^*\left(\sum_{\gamma\sim\mathcal{B}_j} d_i[\gamma]\boldsymbol{e}_i\bar{\boldsymbol{e}}_\gamma^*\right)\boldsymbol{V}\boldsymbol{V}^*\bar{\boldsymbol{e}}_n \\ &= \sum_{\gamma\sim\mathcal{B}_j} d_i[\gamma]\boldsymbol{e}_m^*\boldsymbol{U}\boldsymbol{u}_i\boldsymbol{v}_\gamma^*\boldsymbol{V}^*\bar{\boldsymbol{e}}_n \\ &= \langle \boldsymbol{u}_m, \boldsymbol{u}_i\rangle\left(\sum_{\gamma\sim\mathcal{B}_j} d_i[\gamma]\langle \boldsymbol{v}_\gamma, \boldsymbol{v}_n\rangle\right),\end{aligned}$$

□

Lemma 4.7.2. *Take $\boldsymbol{A}_{ij}$ as defined in* (4.5.6)*, and let $\boldsymbol{x}_k$, and $\boldsymbol{y}_k$ denote scalars or vectors. Then*

$$\mathrm{E}\left(\sum_{\gamma,\gamma'\sim\mathcal{B}_j} d_i[\gamma]d_i[\gamma']\boldsymbol{x}_\gamma\boldsymbol{x}_{\gamma'}^*\right)\left(\sum_{\gamma,\gamma'\sim\mathcal{B}_j} d_i[\gamma]d_i[\gamma']\boldsymbol{y}_\gamma\boldsymbol{y}_{\gamma'}^*\right) =$$
$$= \left(\sum_{\gamma\sim\mathcal{B}_j}\boldsymbol{x}_k\boldsymbol{x}_k^*\right)\left(\sum_{\gamma\sim\mathcal{B}_j}\boldsymbol{y}_\gamma\boldsymbol{y}_\gamma^*\right) + 2\sum_{\gamma,\gamma'}\boldsymbol{x}_\gamma\boldsymbol{x}_{\gamma'}^*\boldsymbol{y}_\gamma\boldsymbol{y}_{\gamma'}^*.$$

Proof. The proof of this Lemma is simple involves expanding and moving the expectation inside. We will use the result of this Lemma in cases when $\boldsymbol{x}_\gamma$, $\boldsymbol{y}_\gamma$ are both scalars and when one of these is a vector and other is a scalar. Furthermore, when both $\boldsymbol{x}_\gamma$, and $\boldsymbol{y}_\gamma$ are scalars then the result can be simplified using Cauchy-Schwartz inequality to yield

$$\mathrm{E}\left(\sum_{\gamma,\gamma'\sim\mathcal{B}_j} d_i[\gamma]d_i[\gamma']\boldsymbol{x}_\gamma\boldsymbol{x}_{\gamma'}^*\right)\left(\sum_{\gamma,\gamma'\sim\mathcal{B}_j} d_i[\gamma]d_i[\gamma']\boldsymbol{y}_\gamma\boldsymbol{y}_{\gamma'}^*\right) \le 3\left(\sum_\gamma \boldsymbol{x}_\gamma^2\right)\left(\sum_\gamma \boldsymbol{y}_\gamma^2\right).$$

□

Lemma 4.7.3. *Let X_1, and X_2 be two subgaussian random variables, i.e., $\|X_1\|_{\psi_2} < \infty$, and $\|X_2\|_{\psi_2} < \infty$. Then the product X_1X_2 is a sub exponential random variable with*

$$\|X_1X_2\|_{\psi_1} \leq c\|X_1\|_{\psi_2}\|X_2\|_{\psi_2}.$$

Proof. For a subgaussian random variable, the tail behaviour is

$$\mathrm{P}\left\{|X| > t\right\} \leq e \exp\left(\frac{-ct^2}{\|X\|_{\psi_2}^2}\right) \quad \forall t > 0;$$

see, for example, [99]. We are interested in

$$\begin{aligned}\mathrm{P}\left\{|X_1X_2| > \lambda\right\} &\leq \mathrm{P}\left\{|X_1| > t\right\} + \mathrm{P}\left\{|X_2| > \lambda/t\right\} \\ &\leq e \cdot \exp\left(-ct^2/\|X_1\|_{\psi_2}^2\right) + e \cdot \exp\left(-c\lambda^2/t^2\|X_2\|_{\psi_2}^2\right).\end{aligned}$$

Select $t^2 = \lambda\|X_1\|_{\psi_2}/\|X_2\|_{\psi_2}$, which gives

$$\mathrm{P}\left\{|X_1X_2| > \lambda\right\} \leq 2e \cdot \exp\left(-c\lambda/\|X_1\|_{\psi_2}\|X_2\|_{\psi_2}\right).$$

Now Lemma 2.2.1 in [37] imples that a random variable Z which obeys $\mathrm{P}\left\{|Z| > u\right\} \leq \alpha e^{-\beta u}$. Then $\|Z\|_{\psi_1} \leq (1+\alpha)/\beta$. Using this result, we obtain

$$\|X_1X_2\|_{\psi_1} \leq c\|X_1\|_{\psi_2}\|X_2\|_{\psi_2},$$

which proves the result. □

4.8 Proof of Theorem 4.2.2

In this section, we show that the nuclear norm penalized estimators give ideal performance for the stable recovery of $\boldsymbol{X}_0$ in the presence of additive measurement noise. We will consider the measurement model in (4.2.2), and the noise characteristics in (4.2.15).

Proof. As will be clear later, the proof involves bounding the spectral norm:

$$\|\boldsymbol{\Theta}\| = \|\mathcal{A}^*(\boldsymbol{y}) - \mathrm{E}\,\mathcal{A}^*(\boldsymbol{y})\| \leq \|(\mathcal{A}^*\mathcal{A} - \mathcal{I})(\boldsymbol{X}_0)\| + \|\mathcal{A}^*(\boldsymbol{\xi})\| \tag{4.8.1}$$

The bound on $\|(\mathcal{A}^*\mathcal{A} - \mathcal{I})(\boldsymbol{X}_0)\|$ can be obtained directly using Corollary 5, and the quantity $\|\mathcal{A}^*(\boldsymbol{\xi})\|$ is controlled using Lemma 4.8.1. Given these two results, the proof of Theorem 4.2.2 follows from the following main result in [53].

Theorem 4.8.1 (Oracle inequlaity in [53]). *Let $\hat{\boldsymbol{X}}$ be the solution of the* (4.2.14)*, and $\boldsymbol{X}_0 \in \mathbb{R}^{M\times W}$ matrix of rank R. If $\lambda \geq 2\|\boldsymbol{\Theta}\|$, then*

$$\|\hat{\boldsymbol{X}} - \boldsymbol{X}_0\|_F^2 \leq \min\left\{2\lambda\|\boldsymbol{X}_0\|_*, 1.46\lambda^2 R\right\}.$$

Corollary 5. *Suppose Ω entries are observed using modulated multiplexing setup and let $\boldsymbol{Z}$ be a fixed $W \times M$ matrix with coherence μ_3^2 as defined* (4.2.11)*. Then for all $\beta > 0$,*

$$\|(\mathcal{A}^*\mathcal{A} - \mathcal{I})(\boldsymbol{Z})\| \leq C\|\boldsymbol{Z}\|_F\sqrt{\frac{\mu_3^2\max(W/M,1)}{\Omega}}\sqrt{\beta\log(WM)}$$

with probability at least $1-(WM)^{-\beta}$ provided $\Omega \geq C\beta\log^2(WM)$.

Proof. The proof of the Corollry follows from Lemma 4.5.2 by selecting the number of partitions $\kappa = 1$. The result in the statement of the corollary is obtained from the bound in (4.6.10). In particular, the first term in the maximum in (4.6.10) dominates, when we select $\Omega \geq C\beta\log^2(WM)$. This proves the above corollary. □

Lemma 4.8.1. *Let $\boldsymbol{A}_{ij}$ be independent as defined* (4.5.6) *and pairs $(\boldsymbol{A}_{ij}, y_{ij})$ be independent. For $\beta > 1$ and $\Omega \geq C\min(W/M,1)\beta\log^2(WM)$, the following*

$$\|\mathcal{A}^*(\boldsymbol{\xi})\| \leq C\|\boldsymbol{\xi}\|_{\psi_2}\sqrt{\frac{\max(W/M,1)}{\Omega}}\sqrt{\beta\log(WM)},$$

holds with probability at least $1-(WM)^{-\beta}$ for a fixed constant C.

Using Lemma 4.5.1, and Lemma 4.8.1, we can bound (4.8.1), and obtain

$$\lambda \geq \sqrt{\frac{C\beta\{\|\boldsymbol{X}_0\|_F^2\mu_3^2\max(W/M,1) + \|\boldsymbol{\xi}\|_{\psi_2}^2\max(W/M,1)\}\log(WM)}{\Omega}}$$

with probability at least $1 - O(WM)^{-\beta}$ for a fixed constant C. Taking $\|\boldsymbol{X}_0\|_F = 1$ without loss of generality, and $\Omega \geq C\beta\mu_3^2\max(W/M,1)\log^2(WM)$, which is in

agreement with the assumptions on Ω in Corollary 5, and Lemma 4.8.1, we can control the right hand side. This proves Theorem 4.2.2. $\square$

4.8.1 Proof of Lemma 4.8.1

The proof of this Lemma requires the use of matrix Bernstein's inequality 2. As it is required to bound the spectral norm of the sum $\mathcal{A}^*(\boldsymbol{\xi}) = \sum_{i,j} \xi_{ij} \boldsymbol{A}_{ij}$, we start with the summands $\boldsymbol{Z}_{ij} = \xi_{ij} \boldsymbol{A}_{ij}$. Because variables ξ_{ij} are zero mean, it follows that $E\boldsymbol{Z}_{ij} = \boldsymbol{0}$. The first quantity required is

$$\left\| \sum_{i,j} \mathrm{E}\, \boldsymbol{Z}_{ij} \boldsymbol{Z}_{ij}^* \right\| = \left\| \sum_{i,j} \mathrm{E}\, \xi_{ij}^2 \cdot \mathrm{E}\, \boldsymbol{A}_{ij} \boldsymbol{A}_{ij}^* \right\| \leq \max_{\substack{1 \leq i \leq M \\ 1 \leq j \leq \Omega}} \mathrm{E}\, \xi_{ij}^2 \left\| \mathrm{E} \sum_{i,j} \boldsymbol{A}_{ij} \boldsymbol{A}_{ij}^* \right\|.$$

Using the definition of $\boldsymbol{A}_{ij}$ in (4.5.6), we have

$$\begin{aligned} \left\| \sum_{i,j} \mathrm{E}\, \boldsymbol{Z}_{ij} \boldsymbol{Z}_{ij}^* \right\| &\leq \max_{\substack{1 \leq i \leq M \\ 1 \leq j \leq \Omega}} \mathrm{E}\, \xi_{ij}^2 \left\| \sum_{i,j} \mathrm{E} \sum_{k,k' \sim \mathcal{B}_j} d_i[k] d_i[k'] \boldsymbol{e}_i \bar{\boldsymbol{e}}_k^* \bar{\boldsymbol{e}}_{k'} \boldsymbol{e}_i^* \right\| \\ &= \max_{\substack{1 \leq i \leq M \\ 1 \leq j \leq \Omega}} \mathrm{E}\, \xi_{ij}^2 \left\| \sum_{j=1}^{\Omega} \sum_{k \sim \mathcal{B}_j} \sum_{i=1}^{M} \boldsymbol{e}_i \boldsymbol{e}_i^* \right\| \\ &\leq W \max_{ij} \mathrm{E}\, \xi_{ij}^2 = \frac{(W/M)}{\Omega} \|\boldsymbol{\xi}\|_{\psi_2}^2, \end{aligned} \tag{4.8.2}$$

where the first equality follows from the independence of ξ_{ij} and $\boldsymbol{A}_{ij}$ and the last equality follows from (4.2.15). The second quantity required to calculate the variance (2.5.3) is

$$\begin{aligned} \left\| \sum_{i,j} \mathrm{E}\, \boldsymbol{Z}_{ij}^* \boldsymbol{Z}_{ij} \right\| &= \left\| \sum_{i,j} \mathrm{E}\, \xi_{ij}^2 \cdot \mathrm{E}\, \boldsymbol{A}_{ij}^* \boldsymbol{A}_{ij} \right\| \\ &\leq \max_{ij} \mathrm{E}\, \xi_{ij}^2 \left\| \sum_{i,j} \mathrm{E}\, \boldsymbol{A}_{ij}^* \boldsymbol{A}_{ij} \right\| \\ &= \frac{\|\boldsymbol{\xi}\|_{\psi_2}^2}{M\Omega} \cdot \left\| \sum_{i,j} \mathrm{E} \sum_{k,k' \sim \mathcal{B}_j} d_i[k] d_i[k'] \bar{\boldsymbol{e}}_k \boldsymbol{e}_i^* \boldsymbol{e}_i \bar{\boldsymbol{e}}_{k'}^* \right\| \\ &= \frac{\|\boldsymbol{\xi}\|_{\psi_2}^2}{M\Omega} \left\| \sum_{i=1}^{M} \sum_{j=1}^{\Omega} \sum_{k \sim \mathcal{B}_j} \bar{\boldsymbol{e}}_k \bar{\boldsymbol{e}}_k^* \right\| \\ &= \frac{\|\boldsymbol{\xi}\|_{\psi_2}^2}{\Omega} \end{aligned} \tag{4.8.3}$$

Combining (4.8.2) and (4.8.3) and using (2.5.3) gives

$$\sigma_Z = \|\boldsymbol{\xi}\|_{\psi_2}\sqrt{\frac{\max(W/M,1)}{\Omega}}.$$

The final quantity required is the Orlicz norm of the summand matrices $\boldsymbol{Z}_{ij}$, i.e.,

$$\begin{aligned}\|\boldsymbol{Z}_{ij}\|_{\psi_2}^2 &= \|\xi_{ij}\|_{\psi_2}^2\|\boldsymbol{A}_{ij}\|^2 \\ &\leq C\frac{\|\boldsymbol{\xi}\|_{\psi_2}^2}{M\Omega}\cdot\frac{W}{\Omega},\end{aligned}$$

then

$$\|\boldsymbol{Z}_{ij}\|_{\psi_2}\log^{1/2}\left(\frac{M\Omega\cdot\|\boldsymbol{Z}_{ij}\|_{\psi_2}^2}{\sigma_Z^2}\right) \leq C\sqrt{\|\boldsymbol{\xi}\|_{\psi_2}^2\frac{W/M}{\Omega^2}}\log^{1/2}(WM).$$

Hence, we obtain using $P = \Omega M$, and $t = \beta\log(WM)$ in the Bernstein's bound (2.5.4)

$$\left\|\sum_{ij}\xi_{ij}\boldsymbol{A}_{ij}\right\| \leq \max\left\{\|\boldsymbol{\xi}\|_{\psi_2}\sqrt{\frac{\max(W/M,1)}{\Omega}}\sqrt{\beta\log(WM)}, \|\boldsymbol{\xi}\|_{\psi_2}\sqrt{\frac{W/M}{\Omega^2}}(\beta\log^{3/2}(WM))\right\}.$$

Select $\Omega \geq C\beta\min(W/M,1)\log^2(WM)$, then the first term dominates and the claim in Lemma 4.8.1 follows.

CHAPTER V

COMPRESSIVE MULTIPLEXERS FOR CORRELATED SIGNALS

5.1 Introduction

In this chapter, we design two multiplexing architectures for the sub-Nyquist acquisition of the ensembles of correlated signals. The problem is illustrated in Figure 15 and 16: M signals, each of which is bandlimited to $W/2$ radians/sec, are outputs from a sensor array. Since the signals are bandlimited, they can be captured completely at MW samples per second. A conventional way of acquisition using a multiplexer is to use M frequency modulators that assign the signals to disjoint frequency bands before combining them. The resultant signal is then sampled at MW samples per second using an analog-to-digital converter (ADC). Alternatively, the signals might be time multiplexed onto a single output leading to an ADC sampling at rate MW.

We will show that if the signals are correlated, meaning that the ensemble can be written as (or closely approximated by) distinct linear combinations of $R \ll M$ latent signals, then this net sampling rate can be reduced considerably by using random modulators. We will precede the ADC in the multiplexers by some simple analog computing devices, meaning that ultimately the ADC does not take samples of the signals in the ensemble but instead takes more general linear measurements. The multiplexed sampling architectures we propose are blind to the *correlation structure* of the signals; i.e., this structure is discovered as the signals are reconstructed.

We recast the problem of recovering the signal ensemble as a low-rank recovery problem [40]. Over the course of one second, we want to acquire an $M \times W$

matrix comprised of samples of the ensemble taken at the Nyquist rate. The proposed sampling architectures produce a series of linear combinations of entries of this matrix. The conditions (on the signals and the acquisition system) under which this type of recovery is effective have undergone intensive study in the recent literature [19, 27, 41, 44, 52, 76]. The main contribution of this chapter are as follows: first, the design of *practical* multiplexers constructed from components that can be implemented in hardware [2]; second, the statement and proof of sampling theorems that characterize the sampling rate sufficient for the successful reconstruction of the signal ensembles. As with most compressive sensing measurement systems, randomness will play a crucial role in the operation of the sampling systems. Theorem 5.2.1, 5.2.2, and 5.2.3 in Section 5.2.1, and Section 5.2.2 below can be interpreted as low-rank recovery results from *structured random measurements*.

The compressive multiplexers presented in this chapter are variations of a simple sampling architecture shown in Figure 27. The architecture follows a simple two step approach. In the first step, the M input signals $\{x_m(t)\}_{1\leq m\leq M}$ are modulated using *near orthogonal* waveforms $\{d_m(t)\}_{1\leq m\leq M}$, alternating at rate Ω. In the second step, the signals are added and then sampled uniformly at a rate Ω. We will refer to this architecture as the modulating multiplexer (M-Mux). One of the main topics considered in this chapter is to show that the M-Mux is an optimal sampling strategy for an ensemble of correlated signals $\boldsymbol{X}_c(t)$:

$$\boldsymbol{X}_c(t) = \{x_m(t) : x_m(t) \approx \sum_{r=1}^{R} A[m,r]s_r(t),\ 1 \leq m \leq M\},$$

where $s_r(t)$ are the latent building blocks in the composition of M signals $x_m(t)$, and $A[m,r]$ are entries of a matrix $\boldsymbol{A}$. In particular, we show that we can reconstruct the signal ensemble $\boldsymbol{X}_c(t)$ when we operate the ADC at rate $\Omega \gtrsim RW\log^3(WM)$, which is roughly the optimal sampling rate and improves upon the Nyquist rate MW; especially, in the case when $R \ll M$.

The chapter is organized as follows. In the remainder of this section, we describe

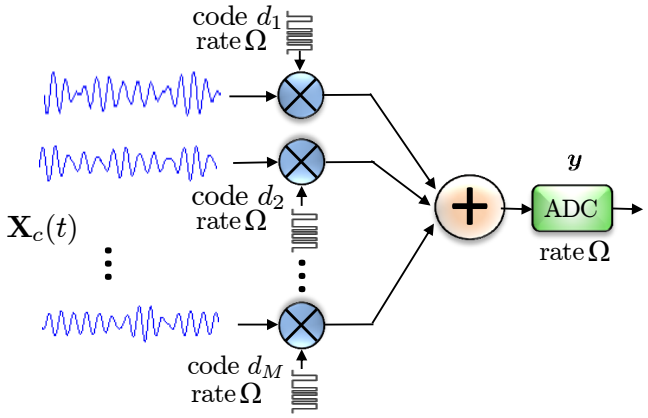

Figure 27: The M-Mux for the efficient acquisition of correlated ensembles. Signals $\{x_m(t),\}_{1\leq m\leq M}$ in the ensemble $\boldsymbol{X}_c(t)$ are multiplied by independently generated random binary waveform $d_1(t), d_2(t), \ldots, d_M(t)$, respectively. The binary waveforms alternate at rate Ω. After the modulation the signals are added and sampled at rate Ω. The reconstruction algorithm uses the nuclear-norm minimization.

the signal model, and our main results followed by applications. Section 5.3 is devoted to numerical simulations, illustrating our results. Finally, Sections 5.4,5.6, and 5.7 contains the proofs of the sampling theorems.

The signals model was introduced in Section 4.1.1. For the reasons that will be clear later, we will be interested here in equally spaced samples of $x_m(t)$ at rate $\Omega > W$, and these samples will be placed as m-th row of an $M \times \Omega$ matrix $\boldsymbol{X}_0$. We can write

$$\boldsymbol{X}_0 = \boldsymbol{C}_0 \tilde{\boldsymbol{F}}, \tag{5.1.1}$$

where $\tilde{\boldsymbol{F}}$ is a $W \times \Omega$ matrix formed by taking first W rows of the normalized discrete Fourier matrix $\boldsymbol{F}$ with entries

$$F[\omega, n] = \frac{1}{\sqrt{W}} \mathrm{e}^{-\mathrm{j}2\pi\omega n/W}, \quad 0 \leq \omega, n \leq \Omega - 1,$$

and $\boldsymbol{C}_0$ is an $M \times W$ matrix whose rows contain Fourier series coefficients for the

signals in $\boldsymbol{X}_c(t)$.

$$C_0[m,\omega] = \begin{cases} \alpha_m[\omega] & \omega = 0, 1, \ldots, (W-1)/2 \\ \alpha_m[\omega - W]^* & \omega = (W+1)/2, \ldots, W-1 \end{cases}.$$

Matrix $\boldsymbol{F}$ is orthonormal, while $\boldsymbol{C}_0$ inherits the correlation structure of the original ensemble. Of course, knowing every entry in matrix $\boldsymbol{C}_0 \in \mathbb{C}^{M \times W}$ is the same as knowing the entire signal ensemble.

We will consider the case in which $\boldsymbol{C}_0$ is exactly rank R and the case in which $\boldsymbol{C}_0$ is technically full rank, but which can be very closely approximated by a low-rank matrix (i.e., the spectrum of singular values decays rapidly). We will also take into account the contamination by the additive measurement noise in our analysis.

5.1.1 Related work

The M-Mux has been proposed previously in the literature [88] for the compressive acquisition of multiple spectrally sparse signals. Using the notation of this chapter, the main results suggest that if the Fourier spectrum of the input signals can be approximated by active frequency components $S \ll MW$, then [80] shows that for the successful reconstruction of the signal ensemble, the ADC is required to operate at rate $\Omega \approx S \log^q MW$, where $q > 1$ is a small constant. A simple implementation of the M-Mux using a passive averager is also discussed in [88]. Similar results have also been shown to hold true for other compressive sampling architectures for the acquisition of sparse signals based on the random modulator in the literature [67, 96] with implementation studied in multiple applications [49, 50, 56, 68, 71]. In contrast to the the acquisition of sparse signals, this chapter considers the efficient acquisition of correlated signals that are not assumed to be sparse rather the structure in the signal ensemble is hidden in the relationship between the signals. As will be shown later, this requires a new set of tools and approach that is completely different from the sparse recovery framework.

As will be shown in the sections below that the signal reconstruction problem from the samples taken by the ADC in Figure 27 can be framed as a low-rank matrix recovery problem from a multi-Toeplitz measurement ensemble. Our results show the recovery of a low-rank matrix with rank $R \geq 1$. In contrast, the results in [4] mainly consider only a rank $R = 1$ recovery problem from a multi-Toeplitz measurement ensemble. These results are studied in context of a very different application; namely, the blind deconvolution. In particular, the results suggest that length-L vectors $\boldsymbol{w}$ and $\boldsymbol{x}$ living in known "generic" subspaces of dimensions K and N, respectively, can be successfully deconvolved when $L \gtrsim \max(K, N) \log^3(KN)$. The other variations of compressive multiplexer for correlated signals presented in this chapter involve preprocessing in analog with random filters [97]. The random filters aim at dispersing the input signal by convolving them with a long and diverse impulse response. A low-rate ADC preceded by a convolution with a random waveform is an effective strategy for the sub-Nyquist acquisition of a sparse signal [97]. Briefly, the results show that a signal with S active components in a fixed basis can be acquired using a random filter plus an ADC operating at a rate that scales linearly in S and logarithmically in ambient dimension W [46, 48, 97].

5.2 Main Results: Compressive Multiplexers and Sampling Theorems

In this section, we present the compressive multiplexers, express the samples taken by the ADC in discrete time as linear measurements of a low-rank matrix, and state theorems dictating the sampling rate required for the reconstruction of the signal ensemble.

5.2.1 M-Mux: A compressive multiplexer for the time-dispersed correlated signals

This section is devoted to model the samples taken by the ADC in the M-Mux, shown in Figure 27, as discrete linear transformations of the discretized input signals. The multiplexer contains M input channels with a modulator in each channel. The modulator multiplies the input analog signal $x_m(t)$ with binary ± 1 waveform $d_m(t)$ alternating at rate $\Omega > W$. In other words, modulator switches the sign of the analog signal after every interval of width $1/\Omega$. Since the sampling operation commutes with the addition, we can equivalently add the rate Ω samples of modulators outputs $\{d_m(t)x_m(t)\}_{1\leq m\leq M}$ to produce the samples taken by the ADC. To this effect, write the Ω samples $\boldsymbol{y}_m$ of $d_m(t)x_m(t)$ on $[0,1)$ as

$$\boldsymbol{y}_m = \boldsymbol{D}_m \tilde{\boldsymbol{F}}^* \boldsymbol{c}_m,$$

where $\boldsymbol{c}_m$ is the W-vector containing the Fourier coefficients of $x_m(t)$, $\tilde{\boldsymbol{F}}$ is the $W \times \Omega$ matrix defined in (5.1.1), and $\boldsymbol{D}_m$ is an $\Omega \times \Omega$ diagonal matrix containing the Ω samples $\boldsymbol{d}^{(m)} = \{d_1[m], \ldots, d_\Omega[m]\}$ of $d_m(t)$ along the diagonal. The partial Fourier matrix $\tilde{\boldsymbol{F}}$ is the interpolation matrix that produces samples of the signals at a rate greater than the Nyquist rate to cater for the fact that the switching is occurring at rate $\Omega > W$. We will choose a binary sequence that randomly generates $d_m(t)$, which amounts to $\boldsymbol{D}_m$ being a random matrix of the following form:

$$\boldsymbol{D}_m = \begin{bmatrix} d_1[m] & & & \\ & d_2[m] & & \\ & & \ddots & \\ & & & d_\Omega[m] \end{bmatrix} \quad \text{where } d_\omega[m] = \pm 1 \text{ with probability } 1/2, \tag{5.2.1}$$

and the $d_\omega[m]$ are independent $\forall(\omega, m) \in \{1, \ldots, \Omega\} \times \{1, \ldots, M\}$. Conceptually, the modulator embeds $x_m(t)$ into a higher dimensional space — this allows us to add several such embedded signals together and then "untangle" them using their

structure. We use the superscript notation $\boldsymbol{d}^{(m)}$ to specify vector $[d_1[m], \ldots, d_\Omega[m]]^{\mathrm{T}}$, whereas the subscript notation $\boldsymbol{d}_\omega$ is reserved to signify vector $[d_\omega[1], \ldots, d_\omega[M]]^{\mathrm{T}}$ later on in this manuscript.

The ADC takes Ω samples of $\sum_{m=1}^{M} x_m(t)d_m(t)$ on $[0, 1)$. We can write the vector of samples $\boldsymbol{y}$ as

$$\begin{aligned}\boldsymbol{y} &= \sum_{m=1}^{M} \boldsymbol{D}_m \tilde{\boldsymbol{F}}^* \boldsymbol{c}_m = [\boldsymbol{D}_1 \tilde{\boldsymbol{F}}^*, \boldsymbol{D}_2 \tilde{\boldsymbol{F}}^*, \cdots, \boldsymbol{D}_M \tilde{\boldsymbol{F}}^*] \cdot \mathrm{vec}(\boldsymbol{C}_0^*) \\ &= \mathcal{A}(\boldsymbol{C}_0), \end{aligned} \tag{5.2.2}$$

where $\boldsymbol{C}_0$ is the $M \times W$ matrix with $\boldsymbol{c}_m^*$ as its rows; in addition, in the first equality, $\mathrm{vec}(\cdot)$ takes a matrix and returns a vector obtained by stacking its columns, and in the second equality, $\mathcal{A} : \mathbb{C}^{M \times W} \to \mathbb{R}^\Omega$ denotes the linear operator that performs equivalent action on $\boldsymbol{C}_0$ to produce $\boldsymbol{y}$.

Intuitively, the M-Mux is not an effective sampling strategy for the signals that are sparse across time. Take an example of sparse-correlated signals in a given finite window of time with a corresponding matrix of samples $\boldsymbol{X}_0$ of rank-1, such that it contains only one non-zero column with degrees of freedom being M. Then the vector of samples, produced by the ADC in the window of time under consideration, will be at most one sparse. However, it is impossible to discover the M unknowns in $\boldsymbol{X}_0$ from this one-sparse measurement vector. This intuition is supported by our theoretical analysis for the M-Mux. As we will see later that the sampling performance of the M-Mux depends on a mild incoherence condition, which quantifies the dispersion of the input signal ensemble across time.

5.2.2 FM-Mux: A uniform compressive multiplexer for correlated signals

As mentioned in the previous section, the M-Mux is more effective for efficiently acquiring correlated signals that are dispersed across time. In this section, we present the filtering, and modulating multiplexer (FM-Mux) that is equally effective for any

ensemble of correlated signals regardless of its initial energy distribution. To achieve this, we add linear time-invariant (LTI) filters in each channel that force the signal energy to be equally distributed. The FM-Mux is depicted in Figure 28.

The analog preprocessing on each of the input signal in the FM-Mux includes: first, modulation with a ± 1-binary waveform switching at rate $\Omega > W$ that disperses the frequency spectrum of the signals over a larger bandwidth Ω; second, convolution with a diverse waveform that diffuses signal across time; and third, addition of pre-processed signals. The resultant signal is sampled by a uniform ADC at rate Ω. As

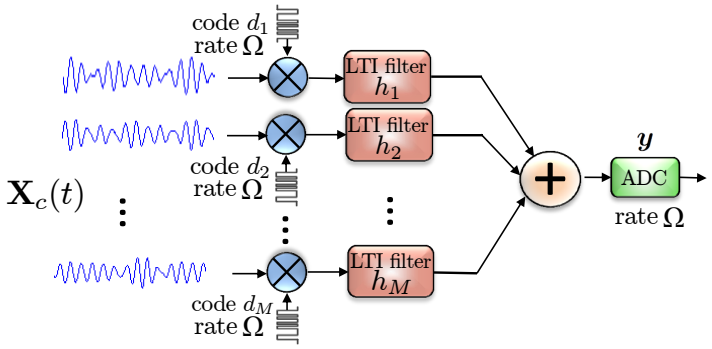

Figure 28: The FM-Mux for the efficient acquisition of correlated signals. Each of the input signal $\{x_m(t)\}$ is modulated separately with ± 1-binary waveform $\{d_m(t)\}$ alternating at rate Ω. Afterwards, the signals are convolved with diverse waveforms using random LTI filters in each channel. The resultant signals are then combined and sampled at a rate Ω using a single ADC.

before, the modulators in the FM-Mux take the input signals $x_1(t), \ldots, x_M(t)$ and multiply them with $d_1(t), \ldots, d_M(t)$, respectively. Each of the $d_m(t)$ is an independent and random binary ± 1 waveform that is constant over a time interval of length $1/\Omega$, where $\Omega > W$ and W is the bandwidth of the signals. The LTI filter in the m-th channel takes the resultant signals $x_m(t)d_m(t)$, which is bandlimited to $\Omega/2$, and convolves it with a fixed and known impulse response $h_m(t)$. We will disregard some implementation issues by assuming for now that we have complete control over $h_m(t)$. We write the action of the LTI filter $h_m(t)$ as an $\Omega \times \Omega$ circular matrix $\boldsymbol{H}_m$ (the first

row of $\boldsymbol{H}$ consists of samples $\boldsymbol{h}_m$ of $h_m(t)$) operating on the Nyquist rate samples $\boldsymbol{D}_m\tilde{\boldsymbol{F}}^*\boldsymbol{c}_m$ in $[0,1)$ of $x_m(t)d_m(t)$. The circulant matrix $\boldsymbol{H}_m$ is diagonalized by the discrete Fourier transform:

$$\boldsymbol{H}_m = \boldsymbol{F}^*\hat{\boldsymbol{H}}_m\boldsymbol{F},$$

where $\hat{\boldsymbol{H}}_m$ is a diagonal matrix whose entries are $\hat{\boldsymbol{h}}_m = \sqrt{\Omega}\boldsymbol{F}\boldsymbol{h}_m$. The vector $\hat{\boldsymbol{h}}_m$ is a scaled version of the non-zero Fourier series coefficients of $h_m(t)$.

To generate the impulse response, we will use a random unit-magnitude sequence in the Fourier domain [79, 97]. In particular, we will take

$$\hat{\boldsymbol{H}}_m = \begin{bmatrix} \hat{h}_m(0) & & & \\ & \hat{h}_m(1) & & \\ & & \ddots & \\ & & & \hat{h}_m(\Omega-1) \end{bmatrix},$$

where

$$\hat{h}_m(\omega) = \begin{cases} \pm 1, \text{with prob. } 1/2, & \omega = 0 \\ \mathrm{e}^{j\theta_\omega}, \text{ where } \theta_\omega \sim \text{Uniform}([0,2\pi]), & 1 \le \omega \le (\Omega-1)/2 \\ \hat{h}_m(\Omega-\omega+1)^*, & (\Omega+1)/2 \le \omega \le \Omega-1 \end{cases}.$$

These symmetry constraints are imposed so that $\boldsymbol{h}_m$ (and hence, $h_m(t)$) is real-valued. Conceptually, convolution with $h_m(t)$ disperses a signal over time while maintaining fixed energy (note that $\boldsymbol{H}_m$ is an orthonormal matrix).

In light of the discussion above, the Nyquist samples of $(x_m(t)d_m(t)) * h_m(t)$ are given by Ω-vector $\boldsymbol{H}_m\boldsymbol{D}_m\tilde{\boldsymbol{F}}^*\boldsymbol{c}_m$. Hence, the samples $\boldsymbol{y}$ in $[0,1)$ of the signal $y(t) = \sum_{m=1}^{M}(x_m(t)d_m(t)) * h_m(t)$ are

$$\begin{aligned} \boldsymbol{y} &= \sum_{m=1}^{M} \boldsymbol{H}_m\boldsymbol{D}_m\tilde{\boldsymbol{F}}^*\boldsymbol{c}_m \\ &= [\boldsymbol{H}_1\boldsymbol{D}_1\tilde{\boldsymbol{F}}^*, \boldsymbol{H}_2\boldsymbol{D}_2\tilde{\boldsymbol{F}}^*, \cdots, \boldsymbol{H}_M\boldsymbol{D}_M\tilde{\boldsymbol{F}}^*] \cdot \mathrm{vec}(\boldsymbol{C}_0^*) \\ &= \mathcal{B}(\boldsymbol{C}_0) \end{aligned} \tag{5.2.3}$$

where $\mathcal{B} : \mathbb{C}^{M\times W} \to \mathbb{R}^{\Omega}$ denotes the equivalent linear transformation. That is, the samples are obtained by linear combinations of the entries of the $M \times W$ low-rank $\boldsymbol{C}_0$. The linear operator $\mathcal{B}$ is a random block-circulant matrix with columns modulated by random signs, i.e., the randomness appears in a structured form. Low-rank matrix recovery results from such structured random linear operators have not been considered before in the literature and require a considerably more involved analysis to show the exact and stable recovery. One of the main contribution of this manuscript is to show that the structured random $\mathcal{B}$ obeys the restricted isometry property for all low-rank matrices.

It is worth mentioning here that we can swap filters and modulators in the compressive multiplexer. In this case, it will be sufficient to use filters of bandwidth W rather than the Ω bandwidth used in Figure 28. The theoretical analysis for the multiplexer in Figure 29 is similar to the FM-Mux in Figure 28 and will not be shown here.

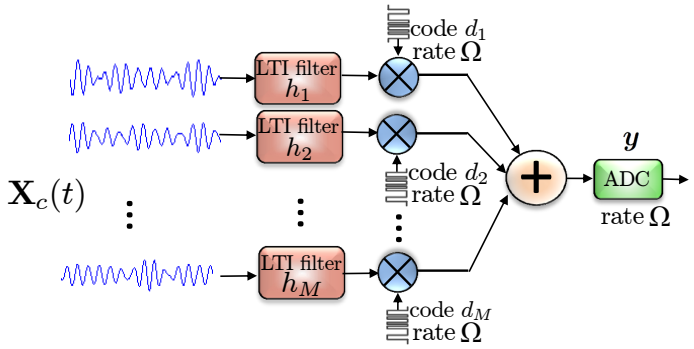

Figure 29: An equivalent FM-Mux obtained by reversing the order of filters and modulators. The modulators operates exactly as before, however, the random filters operate in a bandwidth W instead of operating in a larger bandwidth Ω as in the previous FM-Mux architecture.

In contrast to the M-Mux, the FM-Mux is a equally effective for all correlated signals irrespective of the initial energy distribution of the input signals. Intuitively, this universality of the FM-Mux is the result of the convolution of the input signals

with a diverse waveform, which disperses signal energy equally across time regardless of the initial distribution of signal energy. Thus, the samples observed by the ADC are *mostly* non-zero and hence contribute useful information towards the signal reconstruction.

5.2.3 Methodology for signal reconstruction

The samples $\boldsymbol{y}$ taken by the ADC in the M-Mux (5.2.2) and in the FM-Mux (5.2.3) are different linear transformations $\mathcal{A}$, and $\mathcal{B}$, respectively, of the low-rank matrix $\boldsymbol{C}_0$. The discussion in this subsection applies to both the linear operators $\mathcal{A}$ and $\mathcal{B}$. Therefore, we will use a common symbol $\mathcal{T} : \mathbb{C}^{M\times W} \to \mathbb{R}^{\Omega}$ to signify the linear operators $\mathcal{A}$, and $\mathcal{B}$. In other words, we are working with the measurements $\boldsymbol{y}$

$$\boldsymbol{y} = \mathcal{T}(\boldsymbol{C}_0). \tag{5.2.4}$$

We will first consider the case when the correlation structure $\boldsymbol{A}$ in (4.1.1) is known. The matrix $\boldsymbol{C}_0$ in (5.1.1) inherits its low-rank structure from $\boldsymbol{X}_0$, and can be decomposed as

$$\boldsymbol{C}_0 = \boldsymbol{A}\boldsymbol{C}_s,$$

where $\boldsymbol{C}_s \in \mathbb{C}^{R\times W}$ coefficient matrix that contains the Fourier coefficients of the signals $\{s_r(t)\}_{1\le r\le R}$ as its columns. Define an operator $\mathcal{T}_{\boldsymbol{A}} : \mathbb{C}^{W\times R} \to \mathbb{R}^{\Omega}$ obtained by subsuming the known correlation structure $\boldsymbol{A}$, i.e.,

$$\begin{aligned}\mathcal{T}_{\boldsymbol{A}} &= \mathcal{T} \circ \vec{\boldsymbol{A}} \\ &= \mathbf{T}\begin{bmatrix} A[1,1]\boldsymbol{I} & A[1,2]\boldsymbol{I} & \dots & A[1,R]\boldsymbol{I} \\ A[2,1]\boldsymbol{I} & A[2,2]\boldsymbol{I} & \dots & A[2,R]\boldsymbol{I} \\ \vdots & \vdots & \ddots & \vdots \\ A[M,1]\boldsymbol{I} & A[M,2]\boldsymbol{I} & \dots & A[M,R]\boldsymbol{I} \end{bmatrix},\end{aligned}$$

where $\mathbf{T}$ is the $\Omega \times MW$ matrix representation of linear operator $\mathcal{T}$, $\vec{\boldsymbol{A}}$ is the $WM \times WR$ matrix, and $\boldsymbol{I}$ denotes the $W \times W$ identity matrix.

This means that we can write the measurements $\boldsymbol{y}$ in (5.2.4) as

$$\boldsymbol{y} = \mathcal{T}_{\boldsymbol{A}}(\boldsymbol{C}_s).$$

Since there is no low-dimensional structure on $\boldsymbol{C}_s$, an optimal decoding strategy is using the following least-squares program

$$\min_{\boldsymbol{C}\in\mathbb{C}^{R\times W}} \quad \|\boldsymbol{y} - \mathcal{T}_{\boldsymbol{A}}(\boldsymbol{C})\|_2^2. \tag{5.2.5}$$

The solution $\tilde{\boldsymbol{C}}_s$ to which is given by the following simple analytical form

$$\tilde{\boldsymbol{C}}_s = (\mathcal{T}_{\boldsymbol{A}}^*\mathcal{T}_{\boldsymbol{A}})^{-1}\mathcal{T}_{\boldsymbol{A}}^*(\boldsymbol{y}).$$

A simple argument can show that $(\mathcal{T}_{\boldsymbol{A}}^*\mathcal{T}_{\boldsymbol{A}})^{-1}$ is well-conditioned when the sampling rate Ω obeys

$$\Omega \gtrsim cRW\log^q(W) \tag{5.2.6}$$

for a constant c and a small number $q \geq 1$. The sampling rate Ω in (5.2.6) is optimal to within a constant and log factors. The estimate $\tilde{\boldsymbol{C}}$ of the unknown is given by $\boldsymbol{C}_0$ is then $\tilde{\boldsymbol{C}} = \boldsymbol{A}\tilde{\boldsymbol{C}}_s$.

In practice the correlation structure $\boldsymbol{A}$ is unknown. In this case the unknown $M \times W$ matrix $\boldsymbol{C}_0$ cannot be recovered at an optimal sampling rate using the least-squares approach above. Since rank $(\boldsymbol{C}_0) \leq R$, the low-rank matrix recovery framework can be used to reproduce the Shannon-Nyquist performance for the correlated signals using limited number of samples. To solve for $\boldsymbol{C}_0$, we use the nuclear-norm minimization program subject to affine constraints as below:

$$\begin{aligned} &\min \quad \|\boldsymbol{C}\|_* \\ &\text{subject to} \quad \boldsymbol{y} = \mathcal{T}(\boldsymbol{C}), \end{aligned} \tag{5.2.7}$$

where $\|\boldsymbol{C}\|_*$ is the nuclear norm; the sum of the singular values of $\boldsymbol{C}$. In a realistic scenario, the measurements are contaminated

$$\boldsymbol{y} = \mathcal{T}(\boldsymbol{C}_0) + \boldsymbol{\xi},$$

where $\boldsymbol{\xi}$ is the noise vector such that either $\|\boldsymbol{\xi}\|_2 \leq \delta$, or $\|\boldsymbol{\xi}\|_{\psi_2} \leq \delta$. To recover $\boldsymbol{C}_0$, we solve the nuclear-norm minimization subject to quadratic constraints:

$$\begin{aligned} \min \quad & \|\boldsymbol{C}\|_* \\ \text{subject to} \quad & \|\boldsymbol{y} - \mathcal{T}(\boldsymbol{C})\|_2 \leq \delta. \end{aligned} \tag{5.2.8}$$

Using the available technology, the nuclear norm minimization can be solved efficiently for medium-size matrices $\boldsymbol{C}$. For this purpose, several first order gradient schemes exist, and solvers have been implemented; see, for example, [9, 11].

An *optimal* sampler would recover $\boldsymbol{C}_0$ from $\boldsymbol{y}$ when we sample at a rate of $R(W+M-R)$, which is the degrees of freedom in the unknown-coefficient matrix $\boldsymbol{C}_0$. It is known that if $\mathcal{A}$ is i.i.d. Gaussian, then we can obtain a stable recovery of matrix $\boldsymbol{C}_0$ in noise when the measurements Ω exceed $cR(W+M)$ for a fixed constant c [76]. In addition, it is also known that if we directly observe a randomly selected subset of the entries of low-rank matrix $\boldsymbol{C}_0$ at random, then we can recover $\boldsymbol{C}_0$ exactly when the number of measurements roughly exceed $c\mu_0^2 R(W+M)\log W$, where μ_0^2 is the coherence of matrix $\boldsymbol{C}_0$; for details, see [19,44,75]. In contrast, the measurements in (5.2.2) and in (5.2.3) are obtained as a result of structured-random operations. There are no matrix recovery results from such specialized linear measurements. This chapter develops low-rank matrix recovery results form such structured-random measurement operations.

5.2.4 Sampling theorems for the M-Mux

Each entry $y[\omega]$ of the measurement vector $\boldsymbol{y}$ in (5.2.2) is

$$y[\omega] = \langle \boldsymbol{C}_0, \boldsymbol{A}_\omega \rangle = \mathrm{Tr}\left(\boldsymbol{C}_0 \boldsymbol{A}_\omega^*\right), \quad \omega = 1, \ldots, \Omega,$$

where $\langle \cdot, \cdot \rangle$ is the trace inner product, and

$$\boldsymbol{A}_\omega = \boldsymbol{d}_\omega \boldsymbol{f}_\omega^* \tag{5.2.9}$$

is the $M \times W$ rank-1 matrix formed by the outer product of $\boldsymbol{d}_\omega = [d_\omega[1], \ldots, d_\omega[M]]^{\mathrm{T}}$, and the columns $\boldsymbol{f}_\omega$ of the partial Fourier matrix $\tilde{\boldsymbol{F}}$. The notation $d_\omega[m]$ was introduced in (5.2.1). Let

$$\boldsymbol{C}_0 = \boldsymbol{U}\boldsymbol{\Sigma}\boldsymbol{V}^*$$

be the svd of rank-R coefficient matrix $\boldsymbol{C}_0$, where $\boldsymbol{U} : M \times R$ and $\boldsymbol{V} : W \times R$ are matrices of left and right singular vectors, respectively. The diagonal matrix $\boldsymbol{\Sigma} : R \times R$ contains the singular values of $\boldsymbol{C}_0$. The signal dispersion across time is quantified by the coherence parameter defined as

$$\mu^2(V) := \frac{\Omega}{R} \max_{1 \le \omega \le \Omega} \|\boldsymbol{V}^* \boldsymbol{f}_\omega\|_2^2. \tag{5.2.10}$$

Summing both sides of (5.2.10) over ω, we obtain

$$\sum_{\omega=1}^{\Omega} \mu^2(V) \ge \frac{\Omega}{R} \sum_{\omega=1}^{\Omega} \|\boldsymbol{V}^* \boldsymbol{f}_\omega\|_2^2 = \frac{\Omega}{R} \|\boldsymbol{V}^*\|_F^2,$$

which implies that $\mu^2(V) \ge 1$. The coherence $\mu^2(V)$ achieves the lower bound when

$$\|\boldsymbol{V}^* \boldsymbol{f}_\omega\|_2^2 = \frac{R}{\Omega}$$

for each $\omega \in \{1, \ldots, \Omega\}$. This happen, for instance, when the Ω-point Fourier transform of the columns of $\boldsymbol{V}$ is equally distributed. In other words, the signals are well dispersed across time. In addition, the upper bound is given by

$$\mu^2(V) \le \frac{\Omega}{R} \max_{1 \le \omega \le \Omega} \|\boldsymbol{V}^*\|^2 \|\boldsymbol{f}_\omega\|_2^2 \le \frac{W}{R}.$$

Using an argument similar to above, it can be seen that the coherence achieves the upper bound for signals that are sparse across time. Thus, the coherence quantifies the dispersion of signal energy across time. The following theorem guarantees the exact recovery of the ensemble $\boldsymbol{X}_c(t)$ at a sub-Nyquist sampling rate.

Theorem 5.2.1. *Let $\boldsymbol{C}_0 \in \mathbb{C}^{M \times W}$ be a matrix of rank R defined in* (5.1.1)*. Assume that the coherence $\mu^2(V) \le \mu_0^2$. Suppose Ω measurements $\boldsymbol{y}$ of $\boldsymbol{C}_0$ are taken through*

the M-Mux setup (5.2.4). *If*

$$\Omega \geq C\beta \left(\mu_0^2 M + W\right) R \log^3(WM)$$

for some $\beta > 1$, *then the minimizer* $\tilde{\boldsymbol{C}}$ *to the problem* (5.2.7) *is unique and equal to* $\boldsymbol{C}_0$ *with probability at least* $1 - O(WM)^{1-\beta}$.

The sampling theorem above indicates that the time dispersed correlated signals ($\mu_0^2 \approx O(1)$) can be acquired at a sampling rate close (to within log factors and a constant) to the optimal sampling rate $R(W+M)$. This is a significant improvement over the Nyquist rate WM especially when $R \ll \min(M, W)$. The above result is also important as it is a low-rank matrix recovery result from a linear transformation $\mathcal{A}$, which can be applied more efficiently compared to the dense, *completely* random linear operators such as i.i.d. Gaussian linear operators.

In the real world, the samples are almost always contaminated with noise. We observe

$$\boldsymbol{y} = \mathcal{A}(\boldsymbol{C}_0) + \boldsymbol{\xi} \tag{5.2.11}$$

with $\boldsymbol{\xi}$ being the Ω-vector accounting for the measurement noise. Conventionally, the matrix Lasso in (5.2.8) is solved for the recovery of $\boldsymbol{C}_0$. While the matrix Lasso performs well empirically in the noisy case, it has only been shown to obey weaker theoretical stable recovery results so far. For the recovery of $\boldsymbol{C}_0$, we will consider a simpler optimization program [53]:

$$\tilde{\boldsymbol{C}} = \text{argmin}_{\boldsymbol{C}} \left[\|\boldsymbol{C}\|_F^2 - 2\langle \boldsymbol{y}, \mathcal{A}(\boldsymbol{C}) \rangle + \lambda \|\boldsymbol{C}\|_* \right], \tag{5.2.12}$$

where $\lambda > 0$ is the regularization parameter. Although the above program; namely, the KLT estimator, does not perform empirically as well as the matrix Lasso, but its analysis proves that the nuclear norm penalized estimators obey near-optimal noise recovery results. The KLT estimator can be thought of as a version of matrix Lasso obtained after taking into account the knowledge of the distribution of $\mathcal{A}$,

and using the fact $\mathrm{E}\,\|\mathcal{A}(\boldsymbol{C})\|_2^2 = \|\boldsymbol{C}\|_F^2$ holds in our case. In other words, for non-random operators $\mathcal{A}$, the quadratic part of the KLT estimator reduces to the empirical risk $\|\boldsymbol{y} - \mathcal{A}(\boldsymbol{C})\|_2$. It is worth mentioning that the KLT estimate reduces to a soft thresholding

$$\tilde{\boldsymbol{C}} = \sum_i (\sigma_i(\mathcal{A}^*(\boldsymbol{y})) - \lambda/2)_+ \boldsymbol{u}_i(\mathcal{A}^*(\boldsymbol{y}))\boldsymbol{v}_i(\mathcal{A}^*(\boldsymbol{y})),$$

where $x_+ = \max(x, 0)$, the vectors $\boldsymbol{u}_i(\mathcal{A}^*(\boldsymbol{y}))$, and $\boldsymbol{v}_i(\mathcal{A}^*(\boldsymbol{y}))$ are the left and right singular vectors of $\mathcal{A}^*(\boldsymbol{y})$, respectively, with $\sigma_i(\mathcal{A}^*(\boldsymbol{y}))$ being the corresponding singular values. Our main stable recovery result treats the noise vector as a random vector with statistics

$$\max_{1\le\omega\le\Omega} \mathrm{E}\exp(\frac{|\xi[\omega]|^2}{\sigma^2}) < c, \quad \forall 1 \le \omega \le \Omega, \tag{5.2.13}$$

where the components $\xi[\omega]$ are independent. It then follows that $\|\xi[\omega]\|_{\psi_2}^2 \le c\|\boldsymbol{\xi}\|_{\psi_2}^2/\Omega$. The following theorem states the stable recovery results for the KLT estimate.

Theorem 5.2.2. *Let $\boldsymbol{C}_0 \in \mathbb{C}^{M\times W}$ be an unknown rank-R matrix, and $\boldsymbol{y}$, in* (5.2.11)*, be the measurements of $\boldsymbol{C}_0$ contaminated with the noise $\boldsymbol{\xi}$ with statistics in* (5.2.13)*, such that $\|\boldsymbol{\xi}\|_{\psi_2} \le \delta$. If $\Omega \ge c\beta R(W + \mu_0^2 M)\log^2(WM)$, for some $\beta > 1$, then the solution $\tilde{\boldsymbol{C}}$ to* (5.2.12) *obeys*

$$\|\tilde{\boldsymbol{C}} - \boldsymbol{C}_0\|_F \le 2\delta. \tag{5.2.14}$$

with probability at least $1 - (WM)^{-\beta}$.

As an illustration, we compare the stable recovery result above with the result in [27], which shows that under the conditions of Theorem 5.2.1, the solution $\tilde{\boldsymbol{C}}$ of (5.2.8) obeys

$$\|\tilde{\boldsymbol{C}} - \boldsymbol{C}_0\|_F \le c\sqrt{\min(W, M)}\delta.$$

The above result is derived by only assuming that the noise $\boldsymbol{\xi}$ is bounded (i.e., $\|\boldsymbol{\xi}\|_2 \le \delta$) with no statistical assumptions; see Lemma 1 in [4] for the proof. In comparison, the result in (5.2.14) is smaller by a factor of $1/\sqrt{\min(W, M)}$.

5.2.5 Sampling theorem for the FM-Mux

Again, we can express the measurements in (5.2.3) as a linear operator $\mathcal{B} : \mathbb{C}^{M\times W} \rightarrow \mathbb{R}^{\Omega}$ that maps the matrix of coefficients $\boldsymbol{C}_0$ to the samples $\boldsymbol{y}$ taken by the ADC

$$\boldsymbol{y} = \mathcal{B}(\boldsymbol{C}_0). \tag{5.2.15}$$

We are interested in recovering $\boldsymbol{C}_0$ of $\text{rank}\,(\boldsymbol{C}_0) \leq R$ from under-determined set of measurements $\boldsymbol{y}$ above that may, in addition, be contaminated with noise as follows:

$$\boldsymbol{y} = \mathcal{B}(\boldsymbol{C}_0) + \boldsymbol{\xi}, \tag{5.2.16}$$

where $\boldsymbol{\xi}$ is the noise vector with $\|\boldsymbol{\xi}\|_2 \leq \delta$. Our main theoretical result for the FM-Mux is based on showing that the linear operator $\mathcal{B}$ satisfies the restricted-isometry property (RIP) for low-rank matrices. The matrix RIP [76] is defined below.

Definition 4. *[76] A linear map $\mathcal{B} : \mathbb{C}^{M\times W} \rightarrow \mathbb{R}^{\Omega}$ is said to satisfy the R-restricted isometry property if for every integer $1 \leq R \leq M$, we have a smallest constant $\delta_R(\mathcal{B})$ such that*

$$(1 - \delta_R(\mathcal{B}))\,\|\boldsymbol{C}\|_F \leq \|\mathcal{B}(\boldsymbol{C})\|_2 \leq (1 + \delta_R(\mathcal{B}))\,\|\boldsymbol{C}\|_F$$

for all matrices of rank$(\boldsymbol{C}) \leq R$.

The matrix RIP for the linear operator $\mathcal{B}$, defined in (5.2.15), is sufficient condition to establish that the exact and stable recovery of $\boldsymbol{C}_0$ of $\text{rank}\,(\boldsymbol{C}_0) \leq R$ can be obtained by solving (5.2.7), and (5.2.8), respectively. Following theorem gives the matrix RIP for the measurement operator $\mathcal{B}$ when the sampling rate Ω roughly exceeds the optimal sampling rate of $R(W + M)$.

Theorem 5.2.3. *Fix $\delta \in (0, 1)$ then for every integer $1 \leq R \leq M$ the linear map $\mathcal{B} : \mathbb{C}^{M\times W} \rightarrow \mathbb{R}^{\Omega}$ satisfies the R-restricted isometry property with probability at least $1 - \exp(-c_2(\delta)\Omega/\log^4(\Omega M)) - \exp(-c\Omega)$, whenever $\Omega \geq c_1 R(M + W)\log^4(\Omega M)$.*

In comparison to the sampling theorems for the M-Mux that provide the recovery results for a given ensemble with coherence $\mu^2(V)$, Theorem 5.2.3 provides is a uniform result, which asserts that the FM-Mux is universally efficient sampling strategy for *all* ensembles of correlated signals regardless of the initial energy distribution.

The RIP not only guarantees exact recovery for the noiseless case (5.2.15) but also guarantees the stable recovery in the case when the matrix $\boldsymbol{C}_0$ is not exactly rank R but is a close approximation of a rank R matrix and the measurements are contaminated with noise as in (5.2.16). The stable recovery results [41] assert that given the matrix RIP, the solution $\tilde{\boldsymbol{C}}$ to the optimization program in (5.2.8) satisfies the following error bound

$$\|\tilde{\boldsymbol{C}} - \boldsymbol{C}_0\|_F \leq c_* \frac{\|\boldsymbol{C}_0 - \boldsymbol{C}_{0,R}\|_*}{\sqrt{R}} + c_{**}\delta,$$

where $\boldsymbol{C}_{0,R}$ is the best rank-R approximation of $\boldsymbol{C}_0$. If we set $\delta = 0$, then the exact recovery for $\boldsymbol{C}_0$ of rank R also follows from the above result. In a nutshell, the result illustrates that we can recover an ensemble of correlated signals $\boldsymbol{X}_c(t)$ by analog preprocessing and sampling at a rate that scales linearly with R and is within a constant and logarithmic factors of the optimal sampling rate.

5.2.6 Extension to a more general class of signals

The signal model considered so far establishes the sampling results for the correlated signals that are also periodic across time. The results can be extended to encompass general non-periodic signals. For that matter, we will use smoothing windows $\mathcal{W}(t)$ to divide the time scale into overlapping sections such that $\mathcal{W}(t - n/2) = 1,\ n \in \mathbb{N}$ and $t \in \mathbb{R}$. That is, instead of reconstructing signals $\{x_m(t)\}_m$, we will be reconstructing $\{x_m(t) \cdot \mathcal{W}(t - n/2)\}$. To avoid nefarious high-frequency content due to windowing, the window for a given section of time smoothly vanishes into the consecutive sections. Since this makes the windows of two consecutive sections over lapping, we need to sample consecutive signal sections separately. This technical problem can be handled

with minor modifications in the sampling architectures. For instance, we might add a parallel multiplexer, so that each of the consecutive sections of time are handled independently to avoid the sampling conflict in the over lapping sections. Furthermore, to furnish the multiplexers with windowed ensemble $\{x_m(t) \cdot \mathcal{W}(t - n/2)\}$, we can use a variable gain amplifier, calibrated to produce windowed signals, at the front end of the multiplexers.

5.2.7 Application: Micro-sensor arrays

In many applications in array processing, wavefronts incident on a large number of closely located antenna arrays generate signals that share a lot in common. In other words, these signals may live in a subspace with dimension much smaller than the total number of signals. This is especially true for micro sensor arrays with closely located sensors. Micro-sensor arrays may be used in on-chip radars; in sensors in robotics, for example, large number of closely located sensors in a robotic hand to sense a touch; and in polytrodes, containing many closely located recording sites that are used in some specific applications; for example, to study the brain tissues. We will describe here an application in which the correlated signals arise in the recordings from a polytrode array inserted in the brain tissue to study neurons.

Neuronal recordings in visual neurophysiology

Correlated signals arise in neuronal recordings from brain tissues in response to some visual stimuli. The recorded information is helpful in understanding how visual stimulus is encoded and processed by neurons. The recorded signals are also useful for detecting the exact locations of neurons and the classifications of cell types. To record the information from neurons in the cortical columns of brain, a tiny silicon electrode array; namely, polytrode containing many closely located recording sites is inserted in the brain of a specie (either cat or a monkey). Figure 30 shows the multi neuron evoked responses—signals are highly correlated— recorded by electrode arrays in a

real experiment conducted on a specie's brain to understand the neuronal activity in result of a visual stimuli. Figure 30 also shows the polytrode that contains fifty-four recording sites. An electrode array may contain hundreds of recording sites that

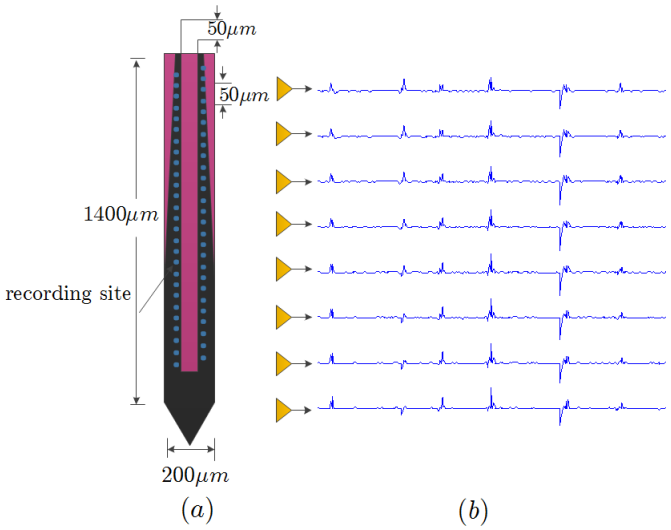

Figure 30: Application in neuronal recordings from brain tissues. (a) A ploytrode with fifty-four recording sites, shown as blue dots, arranged in two columns $50\mu m$ apart. Polytrodes with dense recording sites provide detailed field recordings and span roughly $1mm$ of the brain tissue [14]. (b) The signals recorded by sensors in a real experiment. The data is taken from [1].

are recording as many correlated signals. The signals are multiplexed, continuously sampled by ADCs, and streamed to a hard disk at a high quantization resolution. Because the signals are highly correlated and their may be a large number of such signals in such a batch of recordings, the data generated over the course of typical experiment lasting over twenty four hours may reach Tera bytes. In particular, [63] describes a data acquisition hardware for an electrode array containing 512-recording sites. The 512-signals recorded are bandpass filtered, amplified, and then multiplexed using 64:1 analog multiplexers onto eight channels. Each of the eight multiplexed signals is sampled at 1.28 mega Hertz, which corresponds to a sampling rate of 20 kilo Hertz for each signal recorded at the electrode. All the samples are then digitized at 15 megabytes per second. It is clear that the sampling burden on the ADCs increases

with increasing density of the recording sites, and so does the amount of the data generated; especially, for experiments lasting over many hours. The signals can be acquired more efficiently by taking into account the correlated signal structure that exists in the ensemble. We can deploy the sampling architectures presented in this chapter and hence, compressively acquire the signal ensembles to effectively use sampling resources, and to minimize the amount of data generated over the course of an experiment.

Another design consideration in polytrodes is that the number of electrodes on a polytrode are limited by the number of conductors, carrying the signal from each electrode, that can pass through the shank of the polytrode. If the multiplexing can be performed at micro scale, then the signals can be combined before directing these signals through the shank of the polytrode. Hence, the resultant number of conductors reduce, which enables us to increase the density of recording sites for given thickness of the shank of polytrode. Since the multiplexing architecture uses simple modulators, it may be possible to built such modulators at micro scale. Additionally, the reduction in the sampling rate reduces the power dissipation of the ADC, which is an important factor in some acquisition devices.

5.3 Numerical Experiments

This section illustrates our theoretical results with numerical experiments. The experiments demonstrate the sampling performance of the compressive multiplexers, the effectiveness of the reconstruction algorithm in the presence of additive noise, and the performance of the multiplexers on a data set obtained from an actual neural experiment.

5.3.1 Sampling performance

The unknown-rank-R matrix $\boldsymbol{C}_0$ in all the experiments in subsections 5.3.1 and 5.3.2 is generated at random by the multiplication of a tall $M \times R$ and a fat $R \times W$ matrix,

each with i.i.d. Gaussian entries. A random matrix $\boldsymbol{C}_0$ of coefficients corresponds to a time-dispersed signal ensemble. Since the M-Mux and the FM-Mux perform identically on such ensembles, we will simulate only the M-Mux in all the experiments in this section. The successful reconstruction occurs when

$$\text{Relative error} = \frac{\|\tilde{\boldsymbol{C}} - \boldsymbol{C}_0\|_F}{\|\boldsymbol{C}_0\|_F} \leq 10^{-3}.$$

In this subsection, we will evaluate the sampling performance using the indicators that include the sampling efficiency $\eta := R(W + M - R)/\Omega$, the compression factor $\gamma := \Omega/(WM)$, and the oversampling factor $\Omega/R(W + M - R)$. The success rate in all the subsequent experiments in this subsection is computed over 100 iterations with different random instances of $\boldsymbol{C}_0$ in each iteration. In the first set of experiments, we take $M = 100$ signals, each bandlimited to $W/2 = 512$Hz. The phase transition in Figure 31(a) relates the sampling efficiency with the compression factor. The shade represents the empirical probability of success. It is clear that the efficiency is high and improves further with increasing sampling rate. The phase transition in Figure 31(b) depicts the trend of the sampling rate for the successful recovery against the increasing rank. Interestingly, the sampling efficiency increases with the increasing values of R. Under the same conditions, the plot in Figure 32(a) depicts the relationship between the lowest sampling rate Ω, required for the 99% success rate, and the number R of independent signals. For clarity, the vertical axis shows the values of the compression factor instead of showing the plane sampling rate. It is evident that the sampling rate scales linearly with R and is actually with in a small constant of the optimal sampling rate.

In the final experiment, we take $M = 20\alpha, W = 200\alpha$, and $R = 15$. The blue line in Figure 32(b) illustrates the effect of varying the number of signals, and their bandwidth (by varying α) on the minimum sampling rate required using the M-Mux for the successful reconstruction, while keeping fixed number R of independent signals. For reference, the red line plots the corresponding Nyquist rate for each value of α.

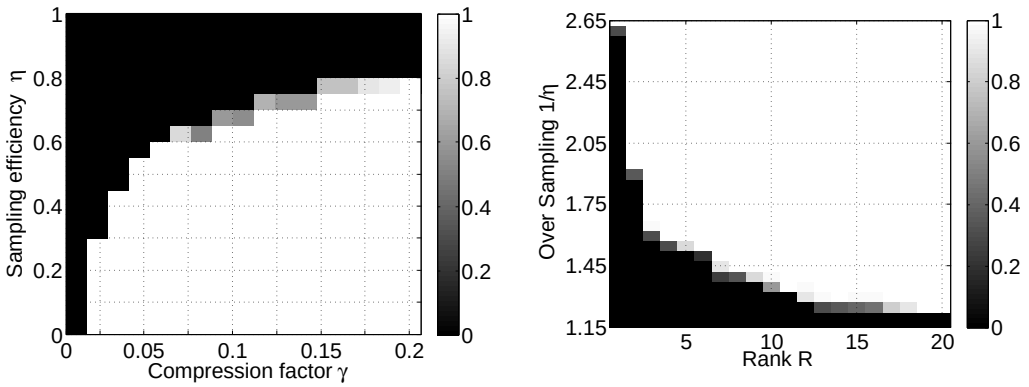

(a) (b)

Figure 31: Empirical probability of success for the compressive signal acquisition using the simulated M-Mux. In these experiments, we take an ensemble with 100 signals, each bandlimited to 512Hz. The shade shows the probability of success. (a) Success rate as a function of the compression factor and the sampling efficiency. (b) Success rate as a function of number of independent signals and the oversampling.

The graph Ω depends linearly on α, while Nyquist rate, of course, scales with α^2. That is, the gap between Ω and the Nyquist rate widens very rapidly with increasing M and W. The graph also shows that the sampling efficiency does not decrease much with the increasing M and W. Hence, the sampling efficiency only depends on R.

5.3.2 Recovery in the presence of noise

This section simulates the setup when the samples taken by the multiplexers are contaminated with additive noise $\boldsymbol{\xi} \sim \mathcal{N}(0, \sigma^2 \boldsymbol{I})$ as in (5.2.11). For the signal reconstruction, we solve the optimization program in (5.2.8) with $\delta = (\Omega + \sqrt{\Omega})^{1/2}\sigma$; a natural choice as $\|\boldsymbol{\xi}\|_2 \leq \delta$ holds with high probability. In all of the experiments in this section, we select $M = 100$, $W = 1024$, and $R = 15$. In the first set of experiments shown in Figure 33, we solve the optimization program in (5.2.8) for the reconstruction of the signals. Figure 33(a) shows the signal-to-noise ratio (SNR) in dBs ($10\log_{10}(\|\boldsymbol{C}_0\|_F^2/\|\boldsymbol{\xi}\|_2^2)$) versus the relative error in dBs ($10\log_{10}((\text{relative error})^2)$). Each data point is generated by averaging over ten iterations, each time with independently generated matrices $\boldsymbol{C}_0$, and the noise vector $\boldsymbol{\xi}$. The graph shows that

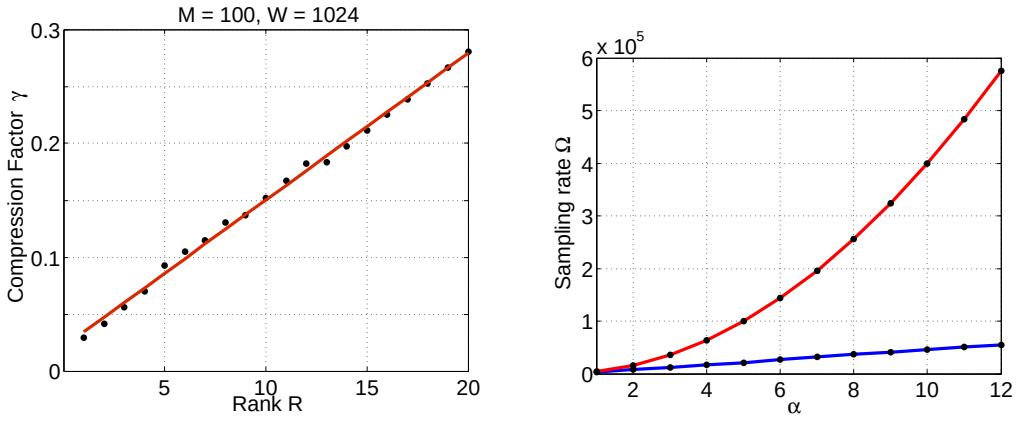

(a) (b)

Figure 32: (a) Sampling as a function of number of independent signals. The simulated M-Mux takes an ensemble of 100 signals, each bandlimited to 512Hz. The discs mark the lowest sampling rate for the signal reconstruction with empirical success rate of 99%. For clarity, the vertical axis lists the values of the scaled sampling rate $\Omega/(WM)$. The The red line is the linear least squares fit of the data points. (b) Sampling rate as a function of M, and W. The simulated M-Mux takes an ensemble of $M = 20\alpha$ signals, each bandlimited to $W/2 = 100\alpha$Hz with number of underlying independent signals fixed at $R = 15$. The discs mark the lowest sampling rate for the signal reconstruction with empirical success rate of 99%. The red line shows the corresponding Nyquist rate.

the error increases gracefully with decreasing SNR. Figure 33(b) depicts the decay of relative error with increasing sampling rate. The second set of experiments in this section, shown in Figure 34, depict the comparison between the performance of the matrix Lasso in (5.2.8), and the one step thresholding estimator in (5.2.12). The first plot compares the two techniques for at an SNR = 40dB; it is clear that the matrix Lasso outperforms the KLT estimator by big margin. The second plot shows that the reconstruction results are at least comparable in the presence of large (SNR = 6dB, 10dB) noise. The results suggest that although the KLT estimator gives optimal recovery results in theory, but it does not perform well in practice.

5.3.3 Neuronal experiment

In this subsection, we evaluate the performance of the M-Mux on the data set obtained from an actual neural experiment [1] described in Section 5.2.7. We take neural signals

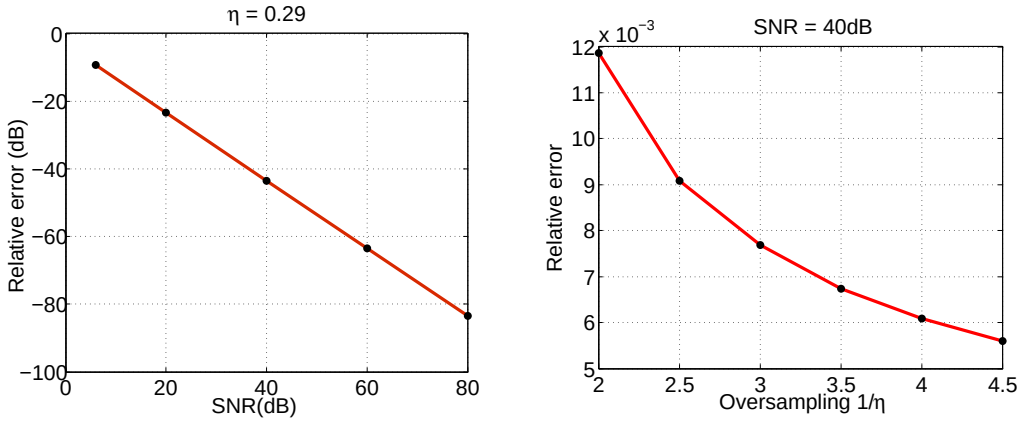

Figure 33: Recovery using matix Lasso in the presence of noise. The input ensemble to the simulated M-Mux consists of 100 signals, each bandlimited to 512Hz with number $R = 15$ of latent independent signals.(a) The SNR in dB versus the relative error in dB. The sampling rate is fixed and is given by the parameter $\eta = 0.29$. (b) Relative error as a function of the sampling rate. The SNR is fixed at 40dB.

recorded by two polytrodes containing a total of 108 recording sites. The signals recorded at each site are required to be sampled at 100,000 samples per second. That is, the Nyquist sampling rate for the acquisition of entire ensemble is 10.8 million samples per second. As mentioned earlier, the signals recorded from such micro senor arrays are correlated, in particular, the 108×1000 matrix of samples over a window of 10ms can be approximated by a rank $R = 22$ matrix (to within a relative error of 0.018). The result in Figure 5.3.3 shows that we can reliably acquire the recorded ensemble for this application using the M-Mux at a smaller rate compared to the Nyquist rate. The compression factor is expected to drop further as the number of recording sites continue to increase.

5.4 Proof of Theorem 5.2.1

Let

$$\boldsymbol{C}_0 = \boldsymbol{U}\boldsymbol{\Sigma}\boldsymbol{V}^* \tag{5.4.1}$$

be the SVD of $\boldsymbol{C}_0$ and let T be the linear space spanned by rank-one matrices of the form $\boldsymbol{u}_r\boldsymbol{y}^*$ and $\boldsymbol{x}\boldsymbol{v}_r^*$, $1 \leq r \leq R$, where $\boldsymbol{x}$ and $\boldsymbol{y}$ are arbitrary. The orthogonal

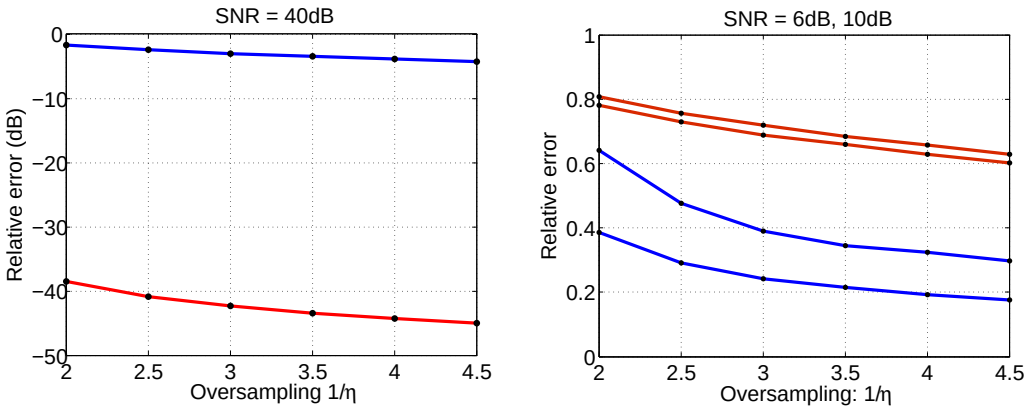

(a) (b)

Figure 34: Comparison of the effectiveness of the matrix Lasso in (5.2.8) with KLT estimator in (5.2.12) for the signal reconstruction in the presence of noise. The input ensemble to the simulated M-Mux consists of 100 signals, each bandlimited to 512Hz with number $R = 15$ of latent independent signals.(a) Relative error in dB versus Oversampling; the red, and blue lines depict the performance of matrix Lasso, and the KLT estimator, respectively. The SNR is fixed at 40dB. (b) Relative error versus the Oversampling; the red, and blue lines depict the performance of matrix Lasso, and the KLT estimator, respectively. The plots are for the SNR of 6dB, and 10dB.

projection of $\mathcal{P}_T$ onto T is defined as

$$\mathcal{P}_T(\boldsymbol{Z}) = \boldsymbol{U}\boldsymbol{U}^*\boldsymbol{Z} + \boldsymbol{Z}\boldsymbol{V}\boldsymbol{V}^* - \boldsymbol{U}\boldsymbol{U}^*\boldsymbol{Z}\boldsymbol{V}\boldsymbol{V}^*, \tag{5.4.2}$$

and orthogonal projection $\mathcal{P}_{T^\perp}$ onto the orthogonal complement $T^\perp$ of T is then

$$\mathcal{P}_{T^\perp}(\boldsymbol{Z}) = (\mathcal{I} - \mathcal{P}_T)(\boldsymbol{Z}) = (\boldsymbol{I}_M - \boldsymbol{U}\boldsymbol{U}^*)(\boldsymbol{Z})(\boldsymbol{I}_W - \boldsymbol{V}\boldsymbol{V}^*),$$

where $\boldsymbol{I}_d$ denotes the $d \times d$ identity matrix. It follows form the definition of $\mathcal{P}_T$ that

$$\mathcal{P}_T(\boldsymbol{A}_\omega) = (\boldsymbol{U}\boldsymbol{U}^*\boldsymbol{d}_\omega)\boldsymbol{f}_\omega^* + \boldsymbol{d}_\omega(\boldsymbol{V}\boldsymbol{V}^*\boldsymbol{f}_\omega)^* - (\boldsymbol{U}\boldsymbol{U}^*\boldsymbol{d}_\omega)(\boldsymbol{V}\boldsymbol{V}^*\boldsymbol{f}_\omega)^*.$$

Using (5.2.9), we have

$$\begin{aligned}
\|\mathcal{P}_T(\boldsymbol{A}_\omega)\|_F^2 &= \langle \mathcal{P}_T(\boldsymbol{A}_\omega), \boldsymbol{A}_\omega \rangle \\
&= \langle \boldsymbol{U}\boldsymbol{U}^*\boldsymbol{d}_\omega\boldsymbol{f}_\omega^*, \boldsymbol{d}_\omega\boldsymbol{f}_\omega^* \rangle + \langle \boldsymbol{d}_\omega\boldsymbol{f}_\omega^*\boldsymbol{V}\boldsymbol{V}^*, \boldsymbol{d}_\omega\boldsymbol{f}_\omega^* \rangle - \langle \boldsymbol{U}\boldsymbol{U}^*\boldsymbol{d}_\omega\boldsymbol{f}_\omega^*\boldsymbol{V}\boldsymbol{V}^*, \boldsymbol{d}_\omega\boldsymbol{f}_\omega^* \rangle \\
&= \|\boldsymbol{f}_\omega\|_2^2\|\boldsymbol{U}^*\boldsymbol{d}_\omega\|_2^2 + \|\boldsymbol{V}^*\boldsymbol{f}_\omega\|_2^2\|\boldsymbol{d}_\omega\|_2^2 - \|\boldsymbol{U}^*\boldsymbol{d}_\omega\|_2^2\|\boldsymbol{V}^*\boldsymbol{f}_\omega\|_2^2 \\
&\leq \frac{W}{\Omega}\|\boldsymbol{U}^*\boldsymbol{d}_\omega\|_2^2 + M\|\boldsymbol{V}^*\boldsymbol{f}_\omega\|_2^2,
\end{aligned} \tag{5.4.3}$$

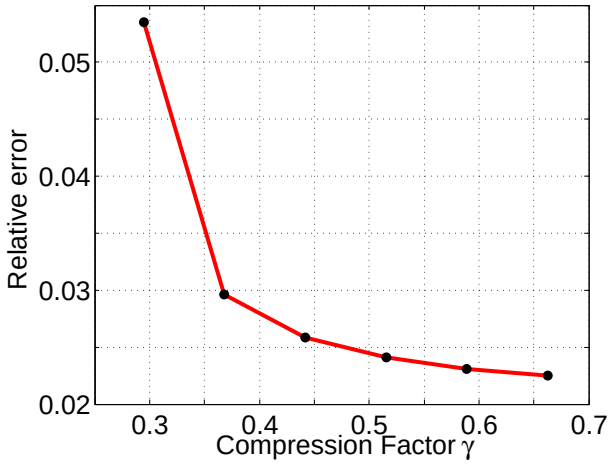

Figure 35: The performance of the M-Mux in an actual neural experiment. Compression factor as a function of the relative error. An ensemble of 108 signals, recorded using polytrodes, and each required to be sampled at 100KHz, is acquired using the M-Mux. Even by cutting the sampling rate in half the ensemble can be acquired with 97% accuracy.

where the last inequality follows from the fact that $\|\boldsymbol{U}^*\boldsymbol{d}_\omega\|_2^2\|\boldsymbol{V}^*\boldsymbol{f}_\omega\|_2^2 \geq 0$, and that $\|\boldsymbol{d}_\omega\|_2^2 = M$, $\|\boldsymbol{f}_\omega\|_2^2 = \frac{W}{\Omega}$. Standard results in duality theory for semidefinite programming assert that the sufficient conditions for the uniqueness of the minimizer of (5.2.7) are as follows:

- The linear operator $\mathcal{A}$ is injective on the subspace T
- $\exists \boldsymbol{Y} \in \text{Range}(\mathcal{A}^*)$, such that

$$\|\mathcal{P}_T(\boldsymbol{Y}) - \boldsymbol{U}\boldsymbol{V}^*\|_F \leq \frac{1}{2\sqrt{2}\gamma}, \quad \|\mathcal{P}_{T^\perp}(\boldsymbol{Y})\| \leq \frac{1}{2}, \tag{5.4.4}$$

where $\gamma := \|\mathcal{A}\|$. The above conditions are also referred to as inexact duality [19,27]. The operator norm $\|\mathcal{A}\|$ can be bounded with high probability using the matrix Chernoff bound [93]. In particular, it can be shown– using an argument similar to Lemma 1 of [4]– that for some $\beta > 1$

$$\gamma \leq \sqrt{M \log(M^2 \Omega W)} \tag{5.4.5}$$

with probability at least $1 - O((WM)^{-\beta})$.

5.4.1 Golfing scheme for the modulated multiplexing

To prove the bounds in (5.4.4), we will use the standard golfing scheme [44]. We start with portioning Ω into κ disjoint partitions $\{\Gamma_k\}_{1\leq k\leq \kappa}$, each of size $|\Gamma_k| = \Delta$, such that $\Omega = \Delta\kappa$. We take $\Gamma_k = \{k + (j-1)\kappa : j \in \{1, \ldots, \Delta\}\}$. As will be shown later, we will be interested in knowing how closely the quantity $\mathrm{E}\,\mathcal{A}_k^*\mathcal{A}_k(\boldsymbol{W})$ approximates $\boldsymbol{W}$. Suppose the measurements indexed by the set Γ_k are provided by linear operator $\mathcal{A}_k$, that is,

$$\mathcal{A}_k(\boldsymbol{W}) = \{\mathrm{Tr}\,(\boldsymbol{f}_\omega \boldsymbol{d}_\omega^* \boldsymbol{W})\}_{\omega\in\Gamma_k}. \tag{5.4.6}$$

This means

$$\mathcal{A}_k^*\mathcal{A}_k(\boldsymbol{W}) = \sum_{\omega\in\Gamma_k} \boldsymbol{d}_\omega \boldsymbol{d}_\omega^* \boldsymbol{W} \boldsymbol{f}_\omega \boldsymbol{f}_\omega^*,$$

which implies that

$$\mathrm{E}\,\mathcal{A}_k^*\mathcal{A}_k(\boldsymbol{W}) = \sum_{\omega\in\Gamma_k} \boldsymbol{W} \boldsymbol{f}_\omega \boldsymbol{f}_\omega^* = \frac{1}{\kappa}\boldsymbol{W}.$$

The last equality follows from the fact

$$\mathrm{E}\,\boldsymbol{d}_\omega \boldsymbol{d}_\omega^* = \boldsymbol{I}_M, \qquad \sum_{\omega\in\Gamma_k} \boldsymbol{f}_\omega \boldsymbol{f}_\omega^* = \frac{1}{\kappa}\boldsymbol{I},$$

as $\boldsymbol{f}_\omega$ are the columns of partial Fourier matrix $\tilde{\boldsymbol{F}}$ obtained by selecting the first W rows of the DFT matrix, as defined in (5.1.1). In contrast to the signals with first W active frequency components, we can extend the golfing argument to signals with W active frequency components located anywhere in the set $\{1, \ldots, \Omega\}$; for details, see the golfing scheme in [4]. In other words, the MMux works equally well for the bandlimited signals regardless of the location of the active band in the total bandwidth Ω.

We begin by iteratively constructing the dual certificate $\boldsymbol{Y} \in \mathrm{Range}(\mathcal{A}^*)$ as follows. Let $\boldsymbol{Y}_0 = 0$, and setup the iteration

$$\boldsymbol{Y}_k = \boldsymbol{Y}_{k-1} + \kappa\mathcal{A}_k^*\mathcal{A}_k\left(\boldsymbol{U}\boldsymbol{V}^* - \mathcal{P}_T(\boldsymbol{Y}_{k-1})\right) \quad \text{Note that} \quad \boldsymbol{Y}_k \in \mathrm{Range}(\mathcal{A}^*), \tag{5.4.7}$$

from which it follows that

$$\mathcal{P}_T(\boldsymbol{Y}_k) = \mathcal{P}_T(\boldsymbol{Y}_{k-1}) + \kappa \mathcal{P}_T(\mathcal{A}_k^*\mathcal{A}_k)\mathcal{P}_T\left(\boldsymbol{U}\boldsymbol{V}^* - \mathcal{P}_T(\boldsymbol{Y}_{k-1})\right);$$

furthermore, define

$$\boldsymbol{W}_k := \mathcal{P}_T(\boldsymbol{Y}_k) - \boldsymbol{U}\boldsymbol{V}^*, \tag{5.4.8}$$

which gives an equivalent iteration

$$\begin{aligned}\boldsymbol{W}_k &= \boldsymbol{W}_{k-1} - \kappa \mathcal{P}_T\mathcal{A}_k^*\mathcal{A}_k\mathcal{P}_T(\boldsymbol{W}_{k-1}) \\ &= \left(\mathcal{P}_T - \kappa \mathcal{P}_T\mathcal{A}_k^*\mathcal{A}_k\mathcal{P}_T\right)(\boldsymbol{W}_{k-1}).\end{aligned} \tag{5.4.9}$$

Now the Frobenius norm of the iterates $\boldsymbol{W}_k$ is

$$\|\boldsymbol{W}_k\|_F \leq \max_{1\leq k\leq \kappa} \|\mathcal{P}_T - \kappa \mathcal{P}_T\mathcal{A}_k^*\mathcal{A}_k\mathcal{P}_T\| \|\boldsymbol{W}_{k-1}\|_F,$$

which by the repeated application of Lemma 5.4.1 gives the Frobenius norm of the final iterate

$$\|\boldsymbol{W}_k\|_F \leq \left(\frac{1}{2}\right)^k \|\boldsymbol{U}\boldsymbol{V}^*\|_F = 2^{-k}\sqrt{R}, \tag{5.4.10}$$

which, by Lemma 5.4.1, holds when $\Omega \geq c\beta\kappa R(\mu_0^2 M + W)\log^2(WM)$ with probability at least $1 - O(\kappa(WM)^{-\beta})$. Hence, the final iterate obeys

$$\|\boldsymbol{W}_\kappa\|_F \leq \frac{1}{2\sqrt{2}\gamma}, \quad \text{when} \quad \kappa \geq 0.5\log_2(8\gamma^2 R)$$

with probability at least $1 - O(\kappa(WM)^{-\beta})$. This proves the first bound in (5.4.4). In light of (5.2.10), the coherence of kth iterate $\boldsymbol{W}_k$ denoted by μ_k^2 is

$$\mu_k^2 = \frac{\Omega}{R} \max_{\omega\in\Gamma_k} \|\boldsymbol{W}_k \boldsymbol{f}_\omega\|_2^2. \tag{5.4.11}$$

It will be shown in Lemma 5.4.3 that $\mu_k^2 \leq 0.5\mu_{k-1}^2$, which implies that

$$\mu_k^2 \leq \mu_0^2, \quad \forall k \in \{1, \ldots, \kappa\} \tag{5.4.12}$$

holds with probability at least $1-O(\Omega(WM)^{-\beta})$. The final iterate $\boldsymbol{Y}_\kappa = -\sum_{k=1}^{\kappa} \kappa \mathcal{A}_k^* \mathcal{A}_k \boldsymbol{W}_{k-1}$ of the iteration (5.4.7) will be our choice of the dual certificate. We will now show that $\boldsymbol{Y}_\kappa$ obeys the conditions (5.4.4).

$$\begin{aligned}
\|\mathcal{P}_{T^\perp}(\boldsymbol{Y}_\kappa)\| &\leq \sum_{k=1}^{\kappa} \|\mathcal{P}_{T^\perp}(\kappa \mathcal{A}_k^* \mathcal{A}_k \boldsymbol{W}_{k-1})\| = \sum_{k=1}^{\kappa} \|\mathcal{P}_{T^\perp}(\kappa \mathcal{A}_k^* \mathcal{A}_k \boldsymbol{W}_{k-1} - \boldsymbol{W}_{k-1})\| \\
&\leq \sum_{k=1}^{\kappa} \|(\kappa \mathcal{A}_k^* \mathcal{A}_k - \mathcal{I})\boldsymbol{W}_{k-1}\|_F \leq \sum_{k=1}^{\kappa} \max_{1\leq k\leq \kappa} \|(\kappa \mathcal{A}_k^* \mathcal{A}_k - \mathcal{I})\boldsymbol{W}_{k-1}\|_F \\
&\leq \sum_{k=1}^{\kappa} 2^{-k-1} < \frac{1}{2},
\end{aligned}$$

where the third inequality holds with probability at least $1 - O(\kappa(WM)^{-\beta})$ when

$$\Omega \geq c\beta\kappa R \max(\mu_0^2 M, W) \log^2(WM),$$

which is implied by Lemma 5.4.2, and Equation (5.4.12). Combining all these results and the probabilities gives us the conclusion of Theorem 5.2.1 with probaility at least $1 - O(\Omega(WM)^{-\beta})$. Since the sampling architectures are only interesting when the sampling rate is sub-Nyquist, i.e., $\Omega \leq WM$, we can simplify the success probability to $1 - O((WM)^{1-\beta})$

5.4.2 Main lemmas

Lemma 5.4.1. *Let $\mathcal{A}_k$ be as defined in* (5.4.6)*, and κ be the number of partitions used in the golfing scheme; see Section 5.4.1. Then for all $\beta > 1$,*

$$\max_{1\leq k\leq \kappa} \|\kappa \mathcal{P}_T \mathcal{A}_k^* \mathcal{A}_k \mathcal{P}_T - \mathcal{P}_T\| \leq \frac{1}{2}$$

provided $\Omega \geq c\beta\kappa R(\mu_0^2 M + W)\log^2(WM)$ with probability at least $1 - O(\kappa(WM)^{-\beta})$.

Lemma 5.4.2. *Let μ_{k-1}^2, as in* (5.4.11) *be the coherence of the iterate $\boldsymbol{W}_{k-1}$, defined in* (5.4.8)*. Then for all $\beta > 1$*

$$\max_{1\leq k\leq \kappa} \|\kappa \mathcal{A}_k^* \mathcal{A}_k(\boldsymbol{W}_{k-1}) - \boldsymbol{W}_{k-1}\| \leq 2^{-k-1}$$

with probability at least $1-O(\kappa(WM)^{-\beta})$ provided $\Omega \geq c\beta\kappa \max(W, \mu_{k-1}^2 M)\log^2(WM)$, where κ is the total partitions used in the golfing scheme.

Lemma 5.4.3. *Let $\boldsymbol{W}_k$, and μ_k^2 be as in* (5.4.8)*, and* (5.4.11)*. If $\Omega \geq c\kappa\beta R(\mu_0^2 M + W)\log^2(WM)$, then*

$$\mu_k^2 \leq \frac{1}{2}\mu_{k-1}^2$$

holds for all $k \in \{1, \ldots, \kappa\}$ with probability at least $1 - O(\Omega(WM)^{-\beta})$. The number κ is the total partitions used in golfing in Section 5.4.1.

5.5 Proof of Main Lemmas Required to Prove Theorem 5.2.1

5.5.1 Proof of Lemma 5.4.1

In this section, we are concerned with bounding the centered random process

$$\begin{aligned}\kappa\mathcal{P}_T\mathcal{A}_k^*\mathcal{A}_k\mathcal{P}_T - \mathcal{P}_T &= \kappa\mathcal{P}_T\mathcal{A}_k^*\mathcal{A}_k\mathcal{P}_T - \mathrm{E}\,\kappa\mathcal{P}_T(\mathcal{A}_k^*\mathcal{A}_k)\mathcal{P}_T \\ &= \kappa\sum_{\omega\in\Gamma_k}(\mathcal{P}_T(\boldsymbol{A}_\omega)\otimes\mathcal{P}_T(\boldsymbol{A}_\omega) - \mathrm{E}\,\mathcal{P}_T(\boldsymbol{A}_\omega)\otimes\mathcal{P}_T(\boldsymbol{A}_\omega)),\end{aligned}$$

where we have used the fact

$$\kappa\,\mathrm{E}\,\mathcal{P}_T\mathcal{A}_k^*\mathcal{A}_k\mathcal{P}_T = \kappa\mathcal{P}_T\,\mathrm{E}(\mathcal{A}_k^*\mathcal{A}_k)\mathcal{P}_T = \mathcal{P}_T$$

The last equality follows from the fact that

$$\mathrm{E}(\mathcal{A}_k^*\mathcal{A}_k) = \frac{1}{\kappa}\mathcal{I}.$$

Now define $\mathcal{L}_\omega$, which maps $\boldsymbol{C}$ to $\langle\mathcal{P}_T(\boldsymbol{A}_\omega), \boldsymbol{C}\rangle\mathcal{P}_T(\boldsymbol{A}_\omega)$. This operator is rank-1 with operator norm $\|\mathcal{L}_\omega\| = \|\mathcal{P}_T(\boldsymbol{A}_\omega)\|_F^2$, and we are interested in bounding the operator norm

$$\|\kappa\mathcal{P}_T\mathcal{A}_k^*\mathcal{A}_k\mathcal{P}_T - \mathcal{P}_T\| = \kappa\sum_{\omega\in\Gamma_k}(\mathcal{L}_\omega - \mathrm{E}\,\mathcal{L}_\omega)$$

For this purpose, we will use matrix Bernstein's bound in Proposition 2. Since $\mathcal{L}_\omega$ is symmetric, we only need to calculate the following for variance

$$\kappa^2\|\sum_{\omega\in\Gamma_k}\mathrm{E}\,\mathcal{L}_\omega^2 - (\mathrm{E}\,\mathcal{L}_\omega)^2\| \leq \kappa^2\|\sum_{\omega\in\Gamma_k}\mathrm{E}\,\mathcal{L}_\omega^2\| = \kappa^2\|\,\mathrm{E}\sum_{\omega\in\Gamma_k}\|\mathcal{P}_T(\boldsymbol{A}_\omega)\|_F^2\mathcal{L}_\omega\|, \quad (5.5.1)$$

where the inequality follows from the fact that $\mathrm{E}\,\mathcal{L}_\omega^2$, and $(\mathrm{E}\,\mathcal{L}_\omega)^2$ are symmetric positive-semidefinite (PSD) matrices, and for PSD matrices $\boldsymbol{A}$, and $\boldsymbol{B}$, we have $\|\boldsymbol{A}-\boldsymbol{B}\| \leq \max\{\|\boldsymbol{A}\|, \|\boldsymbol{B}\|\}$. Plugging in the definition of $\mathcal{L}_\omega$ and using (5.4.3), we have

$$\begin{aligned}\left\|\mathrm{E}\sum_{\omega\in\Gamma_k}\|\mathcal{P}_T(\boldsymbol{A}_\omega)\|_F^2\mathcal{L}_\omega\right\| &\leq \left\|\sum_{\omega\in\Gamma_k}\mathrm{E}\left\{\left(\frac{W}{\Omega}\|\boldsymbol{U}^*\boldsymbol{d}_\omega\|_2^2 + M\|\boldsymbol{V}^*\boldsymbol{f}_\omega\|_2^2\right)\mathcal{L}_\omega\right\}\right\| \\ &\leq \frac{W}{\Omega}\left\|\mathrm{E}\sum_{\omega\in\Gamma_k}\|\boldsymbol{U}^*\boldsymbol{d}_\omega\|_2^2\mathcal{L}_\omega\right\| + M\|\boldsymbol{V}^*\boldsymbol{f}_\omega\|_2^2\left\|\sum_{\omega\in\Gamma_k}\mathrm{E}\,\mathcal{L}_\omega\right\| \\ &\leq \frac{W}{\Omega}\left\|\mathrm{E}\sum_{\omega\in\Gamma_k}\|\boldsymbol{U}^*\boldsymbol{d}_\omega\|_2^2\mathcal{L}_\omega\right\| + \mu_0^2R\frac{M}{\Omega}\left\|\sum_{\omega\in\Gamma_k}\mathrm{E}\,\mathcal{L}_\omega\right\|. \quad (5.5.2)\end{aligned}$$

The last inequality follows form the definition of the coherence (5.2.10). Before proceeding further, we write out the tensor $\boldsymbol{A}_\omega \otimes \boldsymbol{A}_\omega$ in the matrix form:

$$\begin{aligned}\boldsymbol{d}_\omega\boldsymbol{f}_\omega^* \otimes \boldsymbol{d}_\omega\boldsymbol{f}_\omega^* &= \begin{bmatrix} d_\omega[1]d_\omega[1]\boldsymbol{f}_\omega\boldsymbol{f}_\omega^* & d_\omega[1]d_\omega[2]\boldsymbol{f}_\omega\boldsymbol{f}_\omega^* & \cdots & d_\omega[1]d_\omega[M]\boldsymbol{f}_\omega\boldsymbol{f}_\omega^* \\ d_\omega[2]d_\omega[1]\boldsymbol{f}_\omega\boldsymbol{f}_\omega^* & d_\omega[2]d_\omega[2]\boldsymbol{f}_\omega\boldsymbol{f}_\omega^* & \cdots & d_\omega[2]d_\omega[M]\boldsymbol{f}_\omega\boldsymbol{f}_\omega^* \\ \vdots & \vdots & \ddots & \vdots \\ d_\omega[M]d_\omega[1]\boldsymbol{f}_\omega\boldsymbol{f}_\omega^* & d_\omega[M]d_\omega[2]\boldsymbol{f}_\omega\boldsymbol{f}_\omega^* & \cdots & d_\omega[M]d_\omega[M]\boldsymbol{f}_\omega\boldsymbol{f}_\omega^* \end{bmatrix} \\ &= \{d_\omega[\alpha]d_\omega[\beta]\boldsymbol{f}_\omega\boldsymbol{f}_\omega^*\}_{(\alpha,\beta)}.\end{aligned}$$

We will use $\bar{\boldsymbol{u}}_\alpha$ to denote the αth row of the matrix $\boldsymbol{U}$, and δ_x is the indicator function when the condition x is true. Using these notations, we can simplify the following quantity of interest

$$\begin{aligned}\|\,\mathrm{E}\,\|\boldsymbol{U}^*\boldsymbol{d}_\omega\|_2^2(\mathcal{P}_T(\boldsymbol{A}_\omega)\otimes\mathcal{P}_T(\boldsymbol{A}_\omega))\| &\leq \|\mathcal{P}_T\|\|\,\mathrm{E}\,\|\boldsymbol{U}^*\boldsymbol{d}_\omega\|_2^2(\boldsymbol{A}_\omega\otimes\boldsymbol{A}_\omega)\|\|\mathcal{P}_T\| \\ &\leq \|\,\mathrm{E}\,\|\boldsymbol{U}^*\boldsymbol{d}_\omega\|_2^2\{d_\omega[\alpha]d_\omega[\beta]\boldsymbol{f}_\omega\boldsymbol{f}_\omega^*\}_{\alpha,\beta}\| \\ &= \left\|\{\|\boldsymbol{U}\|_F^2\boldsymbol{f}_\omega\boldsymbol{f}_\omega^*\delta_{(\alpha=\beta)} + 2\langle\bar{\boldsymbol{u}}_\alpha,\bar{\boldsymbol{u}}_\beta\rangle\boldsymbol{f}_\omega\boldsymbol{f}_\omega^*\delta_{(\alpha\neq\beta)}\}_{(\alpha,\beta)}\right\|,\end{aligned}$$

where second inequality follows form the fact that $\|\mathcal{P}_T\| \leq 1$ and the third equality follows by expanding and taking expectation on each entry of the matrix. Summing

over $\omega \in \Gamma_k$ gives

$$\begin{aligned}\left\| \mathrm{E} \sum_{\omega \in \Gamma_k} \|\boldsymbol{U}^* \boldsymbol{d}_\omega\|_2^2 \mathcal{P}_T(\boldsymbol{A}_\omega) \otimes \mathcal{P}_T(\boldsymbol{A}_\omega) \right\| &\leq \left\| \sum_{\omega \in \Gamma_k} \{\|\boldsymbol{U}\|_F^2 \boldsymbol{f}_\omega \boldsymbol{f}_\omega^* \delta_{(\alpha=\beta)} + 2\langle \bar{\boldsymbol{u}}_\alpha, \bar{\boldsymbol{u}}_\beta \rangle \boldsymbol{f}_\omega \boldsymbol{f}_\omega^* \delta_{(\alpha \neq \beta)}\}_{(\alpha,\beta)} \right\| \\ &= \left\| \{\|\boldsymbol{U}\|_F^2 \sum_{\omega \in \Gamma_k} \boldsymbol{f}_\omega \boldsymbol{f}_\omega^* \delta_{(\alpha=\beta)} + 2\langle \bar{\boldsymbol{u}}_\alpha, \bar{\boldsymbol{u}}_\beta \rangle \sum_{\omega \in \Gamma_k} \boldsymbol{f}_\omega \boldsymbol{f}_\omega^* \delta_{(\alpha \neq \beta)}\}_{(\alpha,\beta)} \right\| \\ &= \left\| \{\|\boldsymbol{U}\|_F^2 \frac{1}{\kappa} \boldsymbol{I}_W \delta_{(\alpha=\beta)}\}_{(\alpha,\beta)} + \{2\langle \bar{\boldsymbol{u}}_\alpha, \bar{\boldsymbol{u}}_\beta \rangle \frac{1}{\kappa} \boldsymbol{I}_W \delta_{(\alpha \neq \beta)}\}_{(\alpha,\beta)} \right\|.\end{aligned}$$

Now, it follows by simple linear algebra

$$\left\| \mathrm{E} \sum_{\omega \in \Gamma_k} \|\boldsymbol{U}^* \boldsymbol{d}_\omega\|_F^2 \mathcal{P}_T(\boldsymbol{A}_\omega) \otimes \mathcal{P}_T(\boldsymbol{A}_\omega) \right\| \leq \frac{1}{\kappa}(\|\boldsymbol{U}\|_F^2 + 2\|\boldsymbol{U}\boldsymbol{U}^*\|) \leq \frac{R+2}{\kappa}.$$

Plugging the above result, together with (5.5.2) in (5.5.1), we obtain

$$\sigma_Z^2 = \kappa^2 \left\| \sum_{\omega \in \Gamma_k} \mathrm{E}[(\mathcal{L}_\omega - \mathrm{E}\,\mathcal{L}_\omega)^2] \right\| \leq c\kappa R \frac{\mu_0^2 M + W}{\Omega}. \tag{5.5.3}$$

Using the Definition 3, and the fact that $\mathcal{L}_\omega$, and $\mathrm{E}\,\mathcal{L}_\omega$ are positive semidefinite matrices, it follows

$$\kappa \|\mathcal{L}_\omega - \mathrm{E}[\mathcal{L}_\omega]\|_{\psi_1} \leq \kappa \max\{\|\mathcal{L}_\omega\|_{\psi_1}, \|\mathrm{E}\,\mathcal{L}_\omega\|_{\psi_1}\} \tag{5.5.4}$$

As shown earlier, we have $\|\mathcal{L}_\omega\| = \|\mathcal{P}_T(\boldsymbol{A}_\omega)\|_F^2$, and also it is easy to show that $\|\mathrm{E}\,\mathcal{L}_\omega\| = W/\Omega$. Using it together with Definition 3, and (5.4.3), we obtain the Orlicz-1 norm

$$\begin{aligned}\kappa \|\mathcal{L}_\omega\|_{\psi_1} &\leq \mu_0^2 \kappa R \frac{M}{\Omega} + \kappa \frac{W}{\Omega} \left\| \sum_{r=1}^{R} \left(\sum_{m=1}^{M} d_\omega[m] U[m,r] \right)^2 \right\|_{\psi_1} \\ &\leq \mu_0^2 \kappa R \frac{M}{\Omega} + \kappa \frac{W}{\Omega} \sum_{r=1}^{R} \left\| \left(\sum_{m=1}^{M} d_\omega[m] U[m,r] \right)^2 \right\|_{\psi_1}\end{aligned}$$

It can easily be shown that random variable:

$$Y = \sum_{m=1}^{M} d_\omega[m] U[m,r]$$

is subgaussian, which implies that Y^2 is a sub-exponential random variable; see Lemma 2.5.3. In addition, by the independence of $\{d_\omega[m]\}_{1\le m\le M}$ and using Lemma 2.5.2, we have

$$\sum_{r=1}^{R}\left\|\left(\sum_{m=1}^{M} d_\omega[m]U[m,r]\right)\right\|_{\psi_2}^2 \le c\sum_{r=1}^{R}\sum_{m=1}^{M}\|d_\omega[m]U[m,r]\|_{\psi_2}^2 \le cR.$$

Hence,

$$\kappa\|\mathcal{L}_\omega\|_{\psi_1} \le \mu_0^2\kappa R\frac{M}{\Omega} + cR\kappa\frac{W}{\Omega},$$

which dominates the maximum in (5.5.4), and thus $\kappa\|\mathcal{L}_\omega - \mathrm{E}[\mathcal{L}_\omega]\|$ is sub-exponential; hence, $\alpha = 1$ in (2.5.4). Let $\Lambda = \mu_0^2 M + W$, and as defined earlier that $|\Gamma_k| = \Delta$, and $\kappa = \Omega/\Delta$. Then

$$U_1\log\left(\frac{|\Gamma_k|U_1^2}{\sigma_Z^2}\right) \le c\kappa R\frac{\Lambda}{\Omega}\log(R\Lambda) \tag{5.5.5}$$

Plugging (5.5.3), and (5.5.5) in (2.5.4), we have

$$\|\kappa\mathcal{P}_T\mathcal{A}_k^*\mathcal{A}_k\mathcal{P}_T - \mathcal{P}_T\| \le c\max\left\{\sqrt{\frac{\kappa R\Lambda\beta\log(WM)}{\Omega}}, \frac{\kappa R\Lambda}{\Omega}\log(R\Lambda)\beta\log(WM)\right\}.$$

The result of the Lemma 5.4.1 follows by taking $\Omega \ge c\beta\kappa R\Lambda\log(WM)\log(R\Lambda)$, $t = \beta\log(WM)$, and using the union bound over κ indpendent partitions.

5.5.2 Proof of Lemma 5.4.2

We are interested in controlling the operator norm of

$$\kappa\mathcal{A}_k^*\mathcal{A}_k(\boldsymbol{W}_{k-1}) - \boldsymbol{W}_{k-1} = \sum_{\omega\in\Gamma_k}\kappa(\langle\boldsymbol{W}_{k-1},\boldsymbol{A}_\omega\rangle\boldsymbol{A}_\omega - \mathrm{E}\langle\boldsymbol{W}_{k-1},\boldsymbol{A}_\omega\rangle\boldsymbol{A}_\omega). \tag{5.5.6}$$

To control the operator norm of the sum of random matrices

$$\boldsymbol{Z}_\omega = \kappa(\langle\boldsymbol{W}_{k-1},\boldsymbol{A}_\omega\rangle\boldsymbol{A}_\omega - \mathrm{E}\langle\boldsymbol{W}_{k-1},\boldsymbol{A}_\omega\rangle\boldsymbol{A}_\omega)$$

on the r.h.s. of (5.5.6), we will again refer to Proposition 2. We begin by evaluating the first variance term

$$\left\|\sum_{\omega\in\Gamma_k}\mathrm{E}\,\boldsymbol{Z}_\omega\boldsymbol{Z}_\omega^*\right\| \le \kappa^2\left\|\sum_{\omega\in\Gamma_k}\mathrm{E}\,|\langle\boldsymbol{W}_{k-1},\boldsymbol{A}_\omega\rangle|^2\boldsymbol{A}_\omega\boldsymbol{A}_\omega^*\right\| = \kappa^2\|\boldsymbol{f}_\omega\|^2\left\|\sum_{\omega\in\Gamma_k}\mathrm{E}\,|\langle\boldsymbol{W}_{k-1},\boldsymbol{A}_\omega\rangle|^2\boldsymbol{d}_\omega\boldsymbol{d}_\omega^*\right\|,$$

where last equality follows form (5.2.9). Lemma 5.5.1 shows that

$$\mathrm{E}\,|\langle \boldsymbol{W}_{k-1}, \boldsymbol{A}_\omega\rangle|^2 \boldsymbol{d}_\omega \boldsymbol{d}_\omega^* \preccurlyeq 3\|\boldsymbol{W}_{k-1}\boldsymbol{f}_\omega\|_2^2 \boldsymbol{I}_M.$$

Summation over $\omega \in \Gamma_k$ gives

$$\sum_{\omega\in\Gamma_k} \mathrm{E}\,|\langle \boldsymbol{W}_{k-1}, \boldsymbol{A}_\omega\rangle|^2 \boldsymbol{d}_\omega \boldsymbol{d}_\omega^* \preccurlyeq \frac{3}{\kappa}\|\boldsymbol{W}_{k-1}\|_F^2 \boldsymbol{I}_M,$$

which implies that

$$\left\|\sum_{\omega\in\Gamma_k} \mathrm{E}\,\boldsymbol{Z}_\omega^*\boldsymbol{Z}_\omega\right\| \le 3\kappa\frac{W}{\Omega}\|\boldsymbol{W}_{k-1}\|_F^2. \tag{5.5.7}$$

The second variance term needs

$$\left\|\sum_{\omega\in\Gamma_k} \mathrm{E}\,\boldsymbol{Z}_\omega\boldsymbol{Z}_\omega^*\right\| \le \kappa^2 \left\|\sum_{\omega\in\Gamma_k} \mathrm{E}\,|\langle \boldsymbol{W}_{k-1}, \boldsymbol{A}_\omega\rangle|^2 \boldsymbol{A}_\omega\boldsymbol{A}_\omega^*\right\| \le M\kappa^2\|\sum_{\omega\in\Gamma_k} \boldsymbol{f}_\omega\boldsymbol{f}_\omega^*\| \max_\omega \mathrm{E}\,|\langle \boldsymbol{W}_{k-1}, \boldsymbol{A}_\omega\rangle|^2.$$

It is easy to see

$$\mathrm{E}\,|\langle \boldsymbol{W}_{k-1}, \boldsymbol{A}_\omega\rangle|^2 = \|\boldsymbol{W}_{k-1}\boldsymbol{f}_\omega\|_2^2,$$

and $\sum_{\omega\in\Gamma_k} \boldsymbol{f}_\omega\boldsymbol{f}_\omega^* = (1/\kappa)\boldsymbol{I}_W$, which gives

$$\left\|\sum_{\omega\in\Gamma_p} \mathrm{E}\,\boldsymbol{Z}_\omega\boldsymbol{Z}_\omega^*\right\| \le \mu_{k-1}^2\kappa\frac{M}{\Omega}\|\boldsymbol{W}_{k-1}\|_F^2, \tag{5.5.8}$$

which follows by (5.2.10). Plugging (5.5.7), and (5.5.8) in (2.5.3), we obtain

$$\sigma_Z = \max\left\{\sqrt{\mu_{k-1}^2\kappa\frac{M}{\Omega}}\,\|\boldsymbol{W}_{k-1}\|_F\,, \sqrt{3\kappa\frac{W}{\Omega}}\,\|\boldsymbol{W}_{k-1}\|_F\right\}, \tag{5.5.9}$$

The fact that $\boldsymbol{Z}_\omega$ are subgaussian can be proven by showing that $\|\boldsymbol{Z}_\omega\|_{\psi_2} < \infty$. First, note that

$$\|\boldsymbol{Z}_\omega\|_{\psi_2} \le 2\|\kappa\langle \boldsymbol{W}_{k-1}, \boldsymbol{A}_\omega\rangle\boldsymbol{A}_\omega\|_{\psi_2}.$$

Second, the operator norm of the matrix under consideration is

$$\|\langle \boldsymbol{W}_{k-1}, \boldsymbol{A}_\omega\rangle\boldsymbol{A}_\omega\| \le \sqrt{\frac{WM}{\Omega}}|\langle \boldsymbol{W}_{k-1}, \boldsymbol{A}_\omega\rangle|.$$

Using the Definition 3, we obtain

$$\|\boldsymbol{Z}_\omega\|_{\psi_2} \leq 2\kappa\sqrt{\frac{WM}{\Omega}}\|\langle \boldsymbol{W}_{k-1}, \boldsymbol{A}_\omega\rangle\|_{\psi_2}.$$

Let $\boldsymbol{w}_m^*$ denote the rows of the $M \times W$ matrix $\boldsymbol{W}_{k-1}$. We can write

$$\langle \boldsymbol{W}_{k-1}, \boldsymbol{A}_\omega\rangle = \sum_{m=1}^{M} d_\omega[m]\boldsymbol{w}_m^*\boldsymbol{f}_\omega,$$

and using the independence of $d_\omega[m]$ with Lemma 2.5.2, we see that

$$\|\langle \boldsymbol{W}_{k-1}, \boldsymbol{A}_\omega\rangle\|_{\psi_2}^2 \leq c\sum_{m=1}^{M}\|\boldsymbol{w}_m^*\boldsymbol{f}_\omega\|_{\psi_2}^2 \leq \frac{\mu_{k-1}^2}{\Omega}\|\boldsymbol{W}_{k-1}\|_F^2.$$

Hence, U_2 in Proposition 2.5.4 is

$$U_2 = \|\boldsymbol{Z}_\omega\|_{\psi_2} \leq c\left(\kappa^2\mu_{k-1}^2\|\boldsymbol{W}_{k-1}\|_F^2\frac{WM}{\Omega^2}\right)^{1/2},$$

and using $\kappa = \Omega/\Delta$, and $\Lambda_{\min} = \min(\mu_{k-1}^2 M, W)$, we have

$$U_2\log^{1/2}\left(\frac{|\Gamma_k|U_2^2}{\sigma_Z^2}\right) \leq c\frac{\sqrt{\kappa^2\mu_{k-1}^2 WM}}{\Omega}\|\boldsymbol{W}_{k-1}\|_F\log^{1/2}(\Lambda_{\min}). \tag{5.5.10}$$

Suppose $\Lambda_{\max} = \max(\mu_{k-1}^2 M, W)$, using (5.5.9), and (5.5.10) in (2.5.4) with $t = \beta\log(WM)$, we have

$$\|\kappa\mathcal{A}_k^*\mathcal{A}_k(\boldsymbol{W}_{k-1}) - \boldsymbol{W}_{k-1}\| \leq$$
$$c\|\boldsymbol{W}_{k-1}\|_F\sqrt{\frac{\beta\kappa\log(WM)}{\Omega}}\max\left\{\sqrt{\Lambda_{\max}}, \sqrt{\frac{\beta\kappa\mu_{k-1}^2 WM\log(\Lambda_{\min})\log(WM)}{\Omega}}\right\}. \tag{5.5.11}$$

Using (5.4.10), we can select $\Omega \geq c\beta\kappa R\max(W, \mu_{k-1}^2 M)\log^2(WM)$ with appropriate constant c to ensure the desired bound. The result holds with probability $1 - O(\kappa(WM)^{-\beta})$, which follows by using the value of t specified above and then by the union bound over κ independent partitions.

5.5.3 Proof of Lemma 5.4.3

Let $\boldsymbol{W}_k$ be as defined in (5.4.9), and $\boldsymbol{e}_m$ be the length-M standard basis vector with 1 in the mth location. The coherence in (5.4.11) can equivalently be written using trace inner product as

$$\mu_k^2 = \frac{\Omega}{R} \max_{\omega \in \Gamma_k} \sum_{m=1}^{M} \langle \boldsymbol{W}_k, \boldsymbol{e}_m \boldsymbol{f}_\omega^* \rangle^2, \tag{5.5.12}$$

which using iterate relation in (5.4.9) gives

$$\mu_k^2 = \frac{\Omega}{R} \max_{1 \le \omega \le \Omega} \sum_{m=1}^{M} \langle (\kappa \mathcal{P}_T \mathcal{A}_k^* \mathcal{A}_k \mathcal{P}_T - \mathcal{P}_T) \boldsymbol{W}_{k-1}, \boldsymbol{e}_m \boldsymbol{f}_\omega^* \rangle^2.$$

In the rest of the proof, we will be concerned with bounding the summands

$$\langle (\kappa \mathcal{P}_T \mathcal{A}_k^* \mathcal{A}_k \mathcal{P}_T - \mathcal{P}_T) \boldsymbol{W}_{k-1}, \boldsymbol{e}_m \boldsymbol{f}_\omega^* \rangle,$$

which can be expanded as

$$\begin{aligned}
\langle (\kappa \mathcal{P}_T \mathcal{A}_k^* \mathcal{A}_k \mathcal{P}_T - \mathcal{P}_T) \boldsymbol{W}_{k-1}, \boldsymbol{e}_m \boldsymbol{f}_\omega^* \rangle &= \sum_{\nu \in \Gamma_k} \kappa \langle \mathcal{P}_T(\boldsymbol{A}_\nu), \boldsymbol{e}_m \boldsymbol{f}_\omega^* \rangle \langle \boldsymbol{W}_{k-1}, \boldsymbol{A}_\nu \rangle - \langle \boldsymbol{W}_{k-1}, \boldsymbol{e}_m \boldsymbol{f}_\omega^* \rangle \\
&= \sum_{\nu \in \Gamma_k} \kappa \langle \mathcal{P}_T(\boldsymbol{A}_\nu), \boldsymbol{e}_m \boldsymbol{f}_\omega^* \rangle \langle \boldsymbol{W}_{k-1}, \boldsymbol{A}_\nu \rangle - \mathrm{E}\, \kappa \langle \mathcal{P}_T(\boldsymbol{A}_\nu), \boldsymbol{e}_m \boldsymbol{f}_\omega^* \rangle \langle \boldsymbol{W}_{k-1}, \boldsymbol{A}_\nu \rangle.
\end{aligned}$$

To control the deviation of the above sum, we will use the scalar Bernstein inequality. Let

$$Z_\nu = \kappa (\langle \mathcal{P}_T(\boldsymbol{A}_\nu), \boldsymbol{e}_m \boldsymbol{f}_\omega^* \rangle \langle \boldsymbol{W}_{k-1}, \boldsymbol{A}_\nu \rangle - \mathrm{E} \langle \mathcal{P}_T(\boldsymbol{A}_\nu), \boldsymbol{e}_m \boldsymbol{f}_\omega^* \rangle \langle \boldsymbol{W}_{k-1}, \boldsymbol{A}_\nu \rangle).$$

The variance $\sum_{\nu \in \Gamma_k} \mathrm{E}\, Z_\nu Z_\nu^*$ is upper bounded by

$$\begin{aligned}
\sum_{\nu \in \Gamma_k} \mathrm{E}\, Z_\nu Z_\nu^* &\le \kappa^2 \sum_{\nu \in \Gamma_k} \mathrm{E} \langle \mathcal{P}_T(\boldsymbol{A}_\nu), \boldsymbol{e}_m \boldsymbol{f}_\omega^* \rangle \langle \mathcal{P}_T(\boldsymbol{A}_\nu), \boldsymbol{e}_m \boldsymbol{f}_\omega^* \rangle^* \langle \boldsymbol{W}_{k-1}, \boldsymbol{A}_\nu \rangle \langle \boldsymbol{W}_{k-1}, \boldsymbol{A}_\nu \rangle^* \\
&= \kappa^2 \sum_{\nu \in \Gamma_k} \mathrm{E}\, |\langle \mathcal{P}_T(\boldsymbol{A}_\nu), \boldsymbol{e}_m \boldsymbol{f}_\omega^* \rangle|^2 |\langle \boldsymbol{W}_{k-1}, \boldsymbol{A}_\nu \rangle|^2
\end{aligned} \tag{5.5.13}$$

Let $\bar{\boldsymbol{u}}_m^*$ denote the mth row of the matrix $\boldsymbol{U}$. The term $\langle \mathcal{P}_T \boldsymbol{A}_\nu, \boldsymbol{e}_m \boldsymbol{f}_\omega^* \rangle$ can be expanded using (5.4.2) as follows:

$$\begin{aligned}\langle \mathcal{P}_T(\boldsymbol{A}_\nu), \boldsymbol{e}_m \boldsymbol{f}_\omega^* \rangle &= \operatorname{Tr}\left(\mathcal{P}_T(\boldsymbol{A}_\nu) \boldsymbol{f}_\omega \boldsymbol{e}_m^*\right) \\ &= \langle \boldsymbol{U}\boldsymbol{U}^* \boldsymbol{d}_\nu \boldsymbol{f}_\nu^*, \boldsymbol{e}_m \boldsymbol{f}_\omega^* \rangle + \langle \boldsymbol{d}_\nu \boldsymbol{f}_\nu^* \boldsymbol{V}\boldsymbol{V}^*, \boldsymbol{e}_m \boldsymbol{f}_\omega^* \rangle - \langle \boldsymbol{U}\boldsymbol{U}^* \boldsymbol{d}_\nu \boldsymbol{f}_\nu^* \boldsymbol{V}\boldsymbol{V}^*, \boldsymbol{e}_m \boldsymbol{f}_\omega^* \rangle \\ &= \langle \bar{\boldsymbol{u}}_m, \boldsymbol{U}^* \boldsymbol{d}_\nu \rangle (\boldsymbol{f}_\nu^* \boldsymbol{f}_\omega) + \langle \boldsymbol{V}^* \boldsymbol{f}_\nu, \boldsymbol{V}^* \boldsymbol{f}_\omega \rangle d_\nu[m] - \langle \bar{\boldsymbol{u}}_m, \boldsymbol{U}^* \boldsymbol{d}_\nu \rangle \langle \boldsymbol{V}^* \boldsymbol{f}_\nu, \boldsymbol{V}^* \boldsymbol{f}_\omega \rangle \end{aligned} \tag{5.5.14}$$

Let $Y_1 = \langle \bar{\boldsymbol{u}}_m, \boldsymbol{U}^* \boldsymbol{d}_\nu \rangle (\boldsymbol{f}_\nu^* \boldsymbol{f}_\omega)$, $Y_2 = \langle \boldsymbol{V}^* \boldsymbol{f}_\nu, \boldsymbol{V}^* \boldsymbol{f}_\omega \rangle d_\nu[m]$, and $Y_3 = \langle \bar{\boldsymbol{u}}_m, \boldsymbol{U}^* \boldsymbol{d}_\nu \rangle \langle \boldsymbol{V}^* \boldsymbol{f}_\nu, \boldsymbol{V}^* \boldsymbol{f}_\omega \rangle$. Using this notation and combining (5.5.13), (5.5.14), and expanding the square, it is clear that

$$\sum_{\nu \in \Gamma_k} \mathrm{E}\, Z_\nu Z_\nu^* \leq \kappa^2 \,\mathrm{E} \sum_{\nu \in \Gamma_k} 3(|Y_1|^2 + |Y_2|^2 + |Y_3|^2) |\langle \boldsymbol{W}_{k-1}, \boldsymbol{A}_\nu \rangle|^2. \tag{5.5.15}$$

Therefore, the term required to calculate the variance are the following: first,

$$\sum_{\nu \in \Gamma_k} \mathrm{E}\,|Y_1|^2 |\langle \boldsymbol{W}_{k-1}, \boldsymbol{A}_\nu \rangle|^2 \leq \bar{\boldsymbol{u}}_m^* \boldsymbol{U}^* \max_\nu \mathrm{E}(\langle \boldsymbol{W}_{k-1}, \boldsymbol{A}_\nu \rangle^2 \boldsymbol{d}_\nu \boldsymbol{d}_\nu^*) \boldsymbol{U} \bar{\boldsymbol{u}}_m \cdot \boldsymbol{f}_\omega^* \sum_{\nu \in \Gamma_p} (\boldsymbol{f}_\nu \boldsymbol{f}_\nu^*) \boldsymbol{f}_\omega,$$

and the result of Lemma 5.5.1 shows that

$$\mathrm{E}(|\langle \boldsymbol{W}_{k-1}, \boldsymbol{A}_\nu \rangle|^2 \boldsymbol{d}_\nu \boldsymbol{d}_\nu^*) \preccurlyeq 3 \|\boldsymbol{W}_{k-1} \boldsymbol{f}_\nu\|_2^2 \boldsymbol{I}_M.$$

Thus,

$$\sum_{\nu \in \Gamma_k} \mathrm{E}\,|Y_1|^2 |\langle \boldsymbol{W}_{k-1}, \boldsymbol{A}_\nu \rangle|^2 \leq 3 \bar{\boldsymbol{u}}_m^* \boldsymbol{U}^* \boldsymbol{U} \bar{\boldsymbol{u}}_m \, \|\boldsymbol{W}_{k-1} \boldsymbol{f}_\nu\|_2^2 \cdot \frac{1}{\kappa} \|\boldsymbol{f}_\omega\|_2^2 \leq 3 \|\bar{\boldsymbol{u}}_m\|_2^2 \mu_{k-1}^2 \frac{WR}{\kappa \Omega^2}; \tag{5.5.16}$$

second,

$$\sum_{\nu \in \Gamma_k} |Y_2|^2 = \boldsymbol{f}_\omega^* \boldsymbol{V}\boldsymbol{V}^* \sum_{\nu \in \Gamma_k} (\boldsymbol{f}_\nu \boldsymbol{f}_\nu^*) \boldsymbol{V}\boldsymbol{V}^* \boldsymbol{f}_\omega = \frac{1}{\kappa} \|\boldsymbol{V}^* \boldsymbol{f}_\omega\|_2^2 \leq \mu_0^2 \frac{R}{\kappa \Omega};$$

and hence

$$\mathrm{E} \sum_{\nu \in \Gamma_k} |Y_2|^2 |\langle \boldsymbol{W}_{k-1}, \boldsymbol{A}_\nu \rangle|^2 \leq \max_\nu \mathrm{E}\,|\langle \boldsymbol{W}_{k-1}, \boldsymbol{A}_\nu \rangle|^2 \cdot \sum_{\nu \in \Gamma_k} |Y_2|^2 \leq \mu_0^2 \mu_{k-1}^2 \frac{R^2}{\kappa \Omega^2}; \tag{5.5.17}$$

third, since $|Y_3|^2 = |Y_1|^2|Y_2|^2/|\boldsymbol{f}_\nu^*\boldsymbol{f}_\omega|^2$, we can combine the first two terms to obtain

$$\mathrm{E}\sum_{\nu\in\Gamma_k}|Y_3|^2|\langle \boldsymbol{W}_{k-1},\boldsymbol{A}_\nu\rangle|^2 \le 3\|\bar{\boldsymbol{u}}_m\|_2^2\mu_0^2\mu_{k-1}^2\frac{R^2}{\kappa\Omega^2}. \tag{5.5.18}$$

Plugging (5.5.16),(5.5.17), and (5.5.18) in (5.5.15),

$$\begin{aligned}\sigma_Z^2 = \sum_{\nu\in\Gamma_k}\mathrm{E}\,Z_\nu Z_\nu^* &\le 3\kappa\left(\mu_0^2\mu_{k-1}^2\frac{R^2}{\Omega^2} + 3\,\|\bar{\boldsymbol{u}}_m\|_2^2\,\mu_{k-1}^2\frac{WR}{\Omega^2} + 3\,\|\bar{\boldsymbol{u}}_m\|_2^2\,\mu_0^2\mu_{k-1}^2\frac{R^2}{\Omega^2}\right)\\ &= 3\kappa\left(4\mu_0^2\mu_{k-1}^2\frac{R^2}{\Omega^2} + 3\,\|\bar{\boldsymbol{u}}_m\|_2^2\,\mu_{k-1}^2\frac{WR}{\Omega^2}\right),\end{aligned}$$

where the last inequality follws by using the fact that $\|\bar{\boldsymbol{u}}_m\|_2 \le 1$. Using $t = \beta\log(WM)$, we obtain the first quantity in the maximum in (2.5.4)

$$\sigma_Z^2\beta\log(WM) \le 3\kappa\left(4\mu_0^2\mu_{k-1}^2\frac{R^2}{\Omega^2} + 3\,\|\bar{\boldsymbol{u}}_m\|_2^2\,\mu_{k-1}^2\frac{WR}{\Omega^2}\right)\beta\log(WM). \tag{5.5.19}$$

Now, we will show that the variable

$$Z_\nu = (Y_1 + Y_2 - Y_3)\langle \boldsymbol{W}_{k-1},\boldsymbol{A}_\nu\rangle$$

is a subexponential random variable. It is easy to show that

$$\|Y_1\|_{\psi_2}^2 \le c\|\bar{\boldsymbol{u}}_m\|_2^2(\boldsymbol{f}_\nu^*\boldsymbol{f}_\omega)^2 \le c\|\bar{\boldsymbol{u}}_m\|_2^2\frac{W^2}{\Omega^2},$$

$$\|Y_2\|_{\psi_2}^2 \le c\langle \boldsymbol{V}^*\boldsymbol{f}_\nu,\boldsymbol{V}^*\boldsymbol{f}_\omega\rangle^2 \le c\mu_0^4\frac{R^2}{\Omega^2},$$

and

$$\|Y_3\|_{\psi_2}^2 \le c\|\bar{\boldsymbol{u}}_m\|_2^2\langle \boldsymbol{V}^*\boldsymbol{f}_\nu,\boldsymbol{V}^*\boldsymbol{f}_\omega\rangle^2 \le c\|\bar{\boldsymbol{u}}_m\|_2^2\mu_0^4\frac{R^2}{\Omega^2}.$$

Then the fact $\|Y_1 + Y_2 - Y_3\|_{\psi_2} \le \|Y_1\|_{\psi_2} + \|Y_2\|_{\psi_2} + \|Y_3\|_{\psi_2}$ implies that the sum $Y_1 + Y_2 - Y_3$ is also a subgaussian. Using another standard calculation, it can be shown that

$$\|\langle \boldsymbol{W}_{k-1},\boldsymbol{A}_\nu\rangle\|_{\psi_2}^2 \le c\|W_{k-1}\boldsymbol{f}_\nu\|_2^2 \le c\mu_{k-1}^2\frac{R}{\Omega}.$$

It is shown in Lemma 2.5.4 that product X of two subgaussian random variables X_1, and X_2 is subexponential and $\|X\|_{\psi_1} \le c\|X_1\|_{\psi_2}\|X_2\|_{\psi_2}$. This fact now implies that

Z_ν is a subexponential random variable with Orlicz-1 norm

$$\begin{aligned}\|Z_\nu\|_{\psi_1}^2 &\leq \kappa^2\mu_0^4\mu_{k-1}^2\frac{R^3}{\Omega^3} + 3\kappa^2\mu_{k-1}^2\frac{W^2R}{\Omega^3}\|\bar{\boldsymbol{u}}_m\|_2^2 + 3\|\bar{\boldsymbol{u}}_m\|_2^2\kappa^2\mu_0^4\mu_{k-1}^2\frac{R^3}{\Omega^3}\\ &\leq 4\kappa^2\mu_0^4\mu_{k-1}^2\frac{R^3}{\Omega^3} + 3\kappa^2\mu_{k-1}^2\frac{W^2R}{\Omega^3}\|\bar{\boldsymbol{u}}_m\|_2^2,\end{aligned}$$

where the last inequality follows from $\|\bar{\boldsymbol{u}}_m\|_2^2 \leq 1$. Choosing $t = \beta\log(WM)$, as before, gives the second quantity in the maximum in (2.5.4)

$$U_1^2\log^2\left(|\Gamma_k|\frac{U_1^2}{\sigma_Z^2}\right)\beta^2\log^2(WM) \leq \kappa^2\mu_{k-1}^2\frac{4\mu_0^4R^3 + 3\|\bar{\boldsymbol{u}}_m\|_2^2W^2R}{\Omega^3}\beta^2\log^4(WM). \tag{5.5.20}$$

Using Bernstein bound, it follows that $|\langle \boldsymbol{W}_k, \boldsymbol{e}_m\boldsymbol{f}_\omega^*\rangle|$ is dominated by the maximum of (5.5.19), and (5.5.20) with probability at least $1-(WM)^{-\beta}$. Using this bound in (5.5.12), and using the fact that $\sum_{m=1}^M\|\bar{\boldsymbol{u}}_m\|_2^2 = R$, we obtain the following bound on μ_k^2 with probability (using the union bound) at least $1-O(|\Gamma_k|(WM)^{-\beta})$

$$\mu_k^2 \leq c\mu_{k-1}^2\max\left\{3\kappa\frac{4\mu_0^2MR + 3\mu_{k-1}^2WR}{\Omega}\beta\log(WM), \kappa^2\frac{4\mu_0^4MR^2 + 3W^2R}{\Omega^2}\beta^2\log^4(WM)\right\}.$$

Now taking $\Omega \geq c\beta\kappa R(\mu_0^2M+W)\log^2(WM)$ gives us the desired bound on the coherence μ_k^2 for a fixed value of k with probability $1-O(|\Gamma_k|(WM)^{-\beta})$. Using union bound over κ independent partitions, the failure probability becomes $1-O(\Omega(WM)^{-\beta})$.

Lemma 5.5.1. *Let $\boldsymbol{d}_\omega \in \{-1,1\}^M$ denote the binary length-M random vectors as defined in* (5.2.9)*. Then*

$$\mathrm{E}\,|\langle \boldsymbol{C}, \boldsymbol{A}_\omega\rangle|^2\boldsymbol{d}_\omega\boldsymbol{d}_\omega^* \preccurlyeq 3\|\boldsymbol{C}\boldsymbol{f}_\omega\|_2^2\boldsymbol{I}_M$$

Proof. Let $\{\boldsymbol{c}_m^*\}_{1\leq m\leq M}$ denote the rows of the matrix $\boldsymbol{C}\in\mathbb{C}^{M\times W}$, $\{\boldsymbol{X}\}_{(\alpha,\beta)}$ denote the (α,β)th entry of $\boldsymbol{X}$, and $\boldsymbol{A}_\omega$ as defined in (5.2.9). Then we can write

$$\begin{aligned}\{\mathrm{E}(|\langle \boldsymbol{C}, \boldsymbol{A}_\omega\rangle|^2\boldsymbol{d}_\omega\boldsymbol{d}_\omega^*)\}_{(\alpha,\beta)} &= \mathrm{E}\left|\sum_{m=1}^M d_\omega[m]\boldsymbol{c}_m^*\boldsymbol{f}_\omega\right|^2\{\boldsymbol{d}_\omega\boldsymbol{d}_\omega^*\}_{(\alpha,\beta)}\\ &= \sum_{m=1}^M|\boldsymbol{c}_\alpha^*\boldsymbol{f}_\omega|^2\delta_{(\alpha=\beta)} + 2\langle \boldsymbol{c}_\alpha^*\boldsymbol{f}_\omega, \boldsymbol{c}_\beta^*\boldsymbol{f}_\omega\rangle\delta_{\alpha\neq\beta},\end{aligned}$$

where $\delta_{(\alpha=\beta)}$ is 1 when $\alpha = \beta$ and is 0 otherwise. Similarly $\delta_{\alpha\neq\beta}$ is 1 when $\alpha \neq \beta$ and is 0 otherwise. This implies that

$$\begin{aligned}\mathrm{E}(|\langle \boldsymbol{C}, \boldsymbol{A}_\omega\rangle|^2 \boldsymbol{d}_\omega \boldsymbol{d}_\omega^*) &= \|\boldsymbol{C}\boldsymbol{f}_\omega\|_2^2 \boldsymbol{I}_M + 2\boldsymbol{C}\boldsymbol{f}_\omega\boldsymbol{f}_\omega^*\boldsymbol{C}^* - 2\mathrm{diag}(\boldsymbol{C}\boldsymbol{f}_\omega\boldsymbol{f}_\omega^*\boldsymbol{C}^*) \\ &\prec \|\boldsymbol{C}\boldsymbol{f}_\omega\|_2^2 \boldsymbol{I}_M + 2\boldsymbol{C}\boldsymbol{f}_\omega\boldsymbol{f}_\omega^*\boldsymbol{C}^* \preccurlyeq 3\|\boldsymbol{C}\boldsymbol{f}_\omega\|_2^2 \boldsymbol{I}_M\end{aligned}$$

where the first inequality follows from the fact that $\mathrm{diag}(\boldsymbol{C}\boldsymbol{f}_\omega\boldsymbol{f}_\omega^*\boldsymbol{C}^*)$ is a positive-semidefinite matrix, and the last inequality is valid because for a vector $\boldsymbol{x}$, we have $\|\boldsymbol{x}\|_2^2 \boldsymbol{I} \succcurlyeq \boldsymbol{x}\boldsymbol{x}^*$. □

5.6 Proof of Theorem 5.2.2

Given the contaminated measurements, as in (5.2.11), and the linear operator $\mathcal{A}^*$, which is the adjoint $\mathcal{A}$, defined in (5.2.2), we have

$$\begin{aligned}\|\mathcal{A}^*(\boldsymbol{y}) - \mathrm{E}\,\mathcal{A}^*(\boldsymbol{y})\| &\leq \|(\mathcal{A}^*\mathcal{A} - \mathcal{I})(\boldsymbol{C}_0)\| + \|\mathcal{A}^*(\boldsymbol{\xi})\| \\ &= \theta_1 + \theta_2 \qquad (5.6.1)\end{aligned}$$

The result of Theorem 5.2.2 can be considered as the corollary of the following result in [53].

Theorem 5.6.1. *[53] Let $\tilde{\boldsymbol{C}} \in \mathbb{C}^{M\times W}$ be the estimate of rank-R matrix $\boldsymbol{C}_0$, defind in* (5.1.1)*, from the measurements $\boldsymbol{y}$ in* (5.2.11) *using the estimator in* (5.2.12)*. If $\lambda \geq 2\|\mathcal{A}^*\boldsymbol{y}\|$, then*

$$\|\tilde{\boldsymbol{C}} - \boldsymbol{C}_0\|_F^2 \leq \min\{2\lambda\|\boldsymbol{C}_0\|_*, 1.5\lambda^2 R\} \qquad (5.6.2)$$

To prove Theorem 5.2.2, we only need to compute a bound on the operator norm in (5.6.1). The bound on θ_1 in (5.6.1) is provided by the following corollary of Lemma 5.4.2. With out loss of generality, we will assume that $\|\boldsymbol{C}_0\|_F = 1$.

Corollary 6. *Let μ_0^2, defined in* (5.2.10)*, be the coherence of rank-R matrix $\boldsymbol{C}_0$ in* (5.1.1)*. Then for all $\beta \geq 1$*

$$\|\mathcal{A}^*\mathcal{A}(\boldsymbol{C}_0) - \boldsymbol{C}_0\|^2 \leq c\sqrt{\frac{\beta\max(\mu_0^2 M, W)\log(WM)}{\Omega}}\,\|\boldsymbol{C}_0\|_F$$

with probability at least $1-(WM)^{-\beta}$ *provided* $\Omega \geq c\beta \min(\mu_0^2 M, W)\log^2(WM)$.

The proof of the corollary follows from Lemma 5.4.2. In particular, the corollary is a direct result of the bound (5.5.11) by taking $k=1$. The first term in (5.5.11) dominates when $\Omega \geq c\beta \min(\mu_0^2 M, W)\log^2(WM)$.

The upper bound on θ_2 follows from the following Lemma.

Lemma 5.6.1. *Let* $\mathcal{A}^* : \mathbb{R}^{\Omega} \to \mathbb{C}^{M\times W}$ *be the adjoint of the linear operator* $\mathcal{A}$ *defined in* (5.2.2)*, and* $\boldsymbol{\xi}$ *be the noise random variable with statistics given in* (5.2.13)*, and* $\|\boldsymbol{\xi}\|_{\psi_2} \leq \delta$*. Then for* $\beta \geq 1$*, the conclusion:*

$$\|\mathcal{A}^*(\boldsymbol{\xi})\|^2 \leq c\|\boldsymbol{\xi}\|_{\psi_2}\sqrt{\frac{\beta \max(W,M)\log(WM)}{\Omega}}$$

holds with probability at least $1-(WM)^{-\beta}$*, when* $\Omega \geq c\beta \min(W,M)\log^2(WM)$.

Combining the above bounds with (5.6.1) gives

$$\|\mathcal{A}^*(\boldsymbol{y}) - \mathrm{E}\,\mathcal{A}^*(\boldsymbol{y})\| \leq c\sqrt{\frac{\beta\{\max(W,\mu_0^2 M) + \|\boldsymbol{\xi}\|_{\psi_2}^2 \max(W,M)\}\log(WM)}{\Omega}} \quad (5.6.3)$$

with high probability. The second term is meaningful in the minimum in (5.6.2) in Theorem 5.6.1 when we select the sampling rate Ω large enough that makes $\lambda^2 \ll 1$. Theorem 5.6.1, and (5.6.3) assert that

$$\|\tilde{\boldsymbol{C}} - \boldsymbol{C}_0\|_F^2 \leq c\|\boldsymbol{\xi}\|_{\psi_2} \leq c\delta,$$

when $\Omega \geq c\beta R \max(W,\mu_0^2 M)\log^2(WM)$, which does not violate the upper bounds on Ω in Corollary 6, and Lemma 5.6.1. This proves Theorem 5.2.2.

5.6.1 Proof of Lemma 5.6.1

We will use the orlicz version of the matrix Bernstein's inequality 2.

Proof. We are interested in bounding $\mathcal{A}^*(\boldsymbol{\xi}) = \sum_{\omega=1}^{\Omega} \xi[\omega]\boldsymbol{A}_\omega$. Let $\boldsymbol{Z}_\omega = \xi[\omega]\boldsymbol{A}_\omega$. It is clear that $\mathrm{E}\,\boldsymbol{Z}_\omega = \boldsymbol{0}$, which follows by the independence of $\xi[\omega]$, and $\boldsymbol{A}_\omega$, and by the

fact that $\mathrm{E}\,\xi[\omega] = 0$. To use the Bernstein bound, we need to calculate the variance (2.5.3). We begin with

$$\|\sum_{\omega=1}^{\Omega} \mathrm{E}\,\boldsymbol{Z}_\omega \boldsymbol{Z}_\omega^*\| = \left\|\mathrm{E}\sum_{\omega=1}^{\Omega} \xi[\omega]^2 \boldsymbol{f}_\omega \boldsymbol{d}_\omega^* \boldsymbol{d}_\omega \boldsymbol{f}_\omega^*\right\| = \left\|\mathrm{E}\sum_{\omega=1}^{\Omega} \xi[\omega]^2 \|\boldsymbol{d}_\omega\|_2^2 \boldsymbol{f}_\omega \boldsymbol{f}_\omega^*\right\|$$
$$= M \max_\omega \mathrm{E}\,\xi[\omega]^2 \left\|\sum_{\omega=1}^{\Omega} \boldsymbol{f}_\omega \boldsymbol{f}_\omega^*\right\| \leq M \max_\omega \|\xi[\omega]\|_{\psi_2}^2 = c\frac{M}{\Omega}\|\boldsymbol{\xi}\|_{\psi_2}^2$$

Similarly,

$$\left\|\sum_{\omega=1}^{\Omega} \mathrm{E}\,\boldsymbol{Z}_\omega^* \boldsymbol{Z}_\omega\right\| = \left\|\sum_{\omega=1}^{\Omega} \mathrm{E}\,\xi[\omega]^2 \boldsymbol{f}_\omega^* \,\mathrm{E}(\boldsymbol{d}_\omega \boldsymbol{d}_\omega^*) \boldsymbol{f}_\omega\right\| \leq \max_\omega \|\xi\|_{\psi_2}^2 \sum_{\omega=1}^{\Omega} \|\boldsymbol{f}_\omega\|_2^2 = c\frac{W}{\Omega}\|\boldsymbol{\xi}\|_{\psi_2}^2$$

Then, we obtain

$$\sigma_Z^2 = c\|\boldsymbol{\xi}\|_{\psi_2}^2 \frac{\max(W, M)}{\Omega}.$$

Since $\|\boldsymbol{Z}_\omega\| = |\xi[\omega]|\|\boldsymbol{A}_\omega\| \leq |\xi[\omega]|(WM)/\Omega$, we have

$$\|\boldsymbol{Z}_\omega\|_{\psi_2} \leq c\|\boldsymbol{\xi}\|_{\psi_2}\sqrt{\frac{WM}{\Omega^2}}.$$

Thus,

$$U_2 \log^{1/2}\left(\frac{\Omega U_2^2}{\sigma_Z^2}\right) \leq c\|\boldsymbol{\xi}\|_{\psi_2}\sqrt{\frac{WM}{\Omega^2}}\log^{1/2}(WM).$$

Now using $t = \beta\log(WM)$, we obtain

$$\|\mathcal{A}^*(\boldsymbol{\xi})\| \leq c\|\boldsymbol{\xi}\|_{\psi_2} \max\left\{\sqrt{\frac{\beta\max(W,M)\log(WM)}{\Omega}}, \sqrt{\beta^2\frac{WM\log^3(WM)}{\Omega^2}}\right\}$$

with probability at least $1 - (WM)^{-\beta}$. The first term in the minimum dominates when $\Omega \geq c\beta\min(W, M)\log^2(WM)$. This proves the Lemma. □

5.7 Proof of Theorem 5.2.3

In this section, we will establish the matrix RIP for the operator $\mathcal{B}$ defined in (5.2.3). The first step in this direction is given by the following lemma that gives the concentration result of operator $\mathcal{B}$ for a fixed matrix $\boldsymbol{C}$.

Lemma 5.7.1. *Let $\mathcal{B} : \mathbb{C}^{M\times W} \to \mathbb{R}^{\Omega}$ be as in* (5.2.3). *Then for any $\boldsymbol{C} \in \mathbb{C}^{M\times W}$ the random variable $\|\mathcal{B}(\boldsymbol{C})\|_2^2$ is strongly concentrated about its expected value, i.e.,*

$$\mathrm{P}\left\{|\|\mathcal{B}(\boldsymbol{C})\|_2^2 - \|\boldsymbol{C}\|_F^2| \le \epsilon\|\boldsymbol{C}\|_F^2\right\} \ge 1 - 2\mathrm{e}^{-c_0\epsilon^2\Omega/\log^4(\Omega M)}.$$

Proof of this Lemma is given in Section 5.7.1. Using now standard covering number argument, we can convert the above concentration result for a fixed matrix to a matrix-RIP result for all rank-R matrices $\boldsymbol{C}$. We will briefly give here the covering argument for completeness; see, for details, [18].

We start by defining the set $\mathcal{C}$ of all low-rank matrices of dimensions $M \times W$

$$\mathcal{C} = \{\boldsymbol{C} \in \mathbb{C}^{M\times W} : \mathrm{rank}\,(\boldsymbol{C}) \le R, \|\boldsymbol{C}\|_F = 1\}.$$

Choose a δ-net; namely, $\mathcal{Q}_R \subset \mathcal{C}$ such that for every $\boldsymbol{C} \in \mathcal{C}$, there exists $\boldsymbol{Q} \in \mathcal{Q}_R$, which satisfies

$$\|\boldsymbol{C} - \boldsymbol{Q}\|_F \le \delta.$$

The cardinality of set $\mathcal{Q}_R$ [18, 76] is

$$|\mathcal{Q}_R| \le \left(\frac{c_6}{\delta}\right)^{(W+M)R}.$$

Using Lemma 5.7.1 for any $\boldsymbol{Q} \in \mathcal{Q}_R$ with $\epsilon = \delta/2$, we obtain

$$\mathrm{P}\left\{|\|\mathcal{B}(\boldsymbol{Q})\|_2^2 - \|\boldsymbol{Q}\|_F^2| > \delta/2\right\} \le 2\mathrm{e}^{-c_0(\delta/2)^2\Omega/\log^4(W\Omega)}.$$

Now union bound over the finite set of points in $\mathcal{Q}_R$ gives

$$\begin{aligned}\mathrm{P}\left\{\max_{\boldsymbol{Q}\in\mathcal{Q}_R} |\|\mathcal{B}(\boldsymbol{Q})\|_2^2 - \|\boldsymbol{Q}\|_F^2| > \delta/2\right\} &\le 2|\mathcal{Q}_R|\mathrm{e}^{-c_0(\delta/2)^2\Omega/\log^4(M\Omega)} \\ &\le 2\left(\frac{c_6}{\delta}\right)^{(W+M)R}\mathrm{e}^{-c_0(\delta/2)^2\Omega/\log^4(M\Omega)} \\ &= 2\mathrm{e}^{(W+M)R\log(c_6/\delta)-c_0(\delta/2)^2\Omega/\log^4(M\Omega)}.\end{aligned}$$

Choose $(W + M)R \le c_1\Omega/\log^4(M\Omega)$ for a constant $c_1 > 0$, and let

$$c_2 = c_0(\delta/2)^2 - c_1\log(c_6/\delta).$$

We can make $c_2 > 0$ by taking small enough c_1, which implies

$$\mathrm{P}\left\{\left|\|\mathcal{B}(\boldsymbol{Q})\|_2^2 - \|\boldsymbol{Q}\|_F^2\right| > \delta/2\right\} \leq \mathrm{e}^{-c_2(\delta)\Omega/\log^4(M\Omega)},$$

i.e., $\forall \boldsymbol{Q} \in \mathcal{Q}_R$

$$(1-\delta/2)\,\|\boldsymbol{Q}\|_F^2 \leq \|\mathcal{B}(\boldsymbol{Q})\|_2^2 \leq (1+\delta/2)\|\boldsymbol{Q}\|_F^2$$

holds with probability $\geq 1 - 2e^{-c_2(\delta)\Omega/\log^4(M\Omega)}$. Now using exactly the same approach as in Section 3.2 of [18], we can extend this statement from $\forall \boldsymbol{Q} \in \mathcal{Q}_R$ to all $\boldsymbol{C} \in \mathcal{C}$, and obtain the conclusion:

$$(1-\delta)\|\boldsymbol{C}\|_F \leq \|\mathcal{B}(\boldsymbol{C})\|_2 \leq (1+\delta)\|\boldsymbol{C}\|_F.$$

This proves Theorem 5.2.3.

5.7.1 Proof of Lemma 5.7.1

The measurements in (5.2.3) can be expressed as

$$\boldsymbol{y} = \mathcal{B}(\boldsymbol{C}_0) = \boldsymbol{\Phi}\boldsymbol{D} \cdot \mathrm{vec}(\boldsymbol{C}_0\tilde{\boldsymbol{F}}), \tag{5.7.1}$$

where $\boldsymbol{\Phi} = [\boldsymbol{H}_1, \cdots, \boldsymbol{H}_M]$ is a block-toeplitz matrix, and $\boldsymbol{D} : \Omega M \times \Omega M$ is the diagonal matrix formed by cascading smaller diagonal matrices $\{\boldsymbol{D}_m\}_{1\leq m\leq M}$ along the diagonal. To prove Lemma 5.7.1, we invoke two results: first, matrix $\boldsymbol{\Phi}$ satisfies restricted isometry property for k-sparse vectors, see [80]; second, $\boldsymbol{\Phi}\boldsymbol{D}$ satisfies concentration inequality, see [54]. The restricted-isometry property for sparse vectors is defined as below.

Definition 5. *A matrix $\boldsymbol{\Phi} : \mathbb{R}^{\Omega M} \to \mathbb{R}^{\Omega}$ is said to satisfy the restricted k-isometry property if for an integer $1 \leq k \leq \Omega M$ there is a smallest constant $\epsilon_k(\boldsymbol{\Phi})$ such that*

$$(1-\epsilon_k(\boldsymbol{\Phi}))\,\|\boldsymbol{x}\|_2 \leq \|\boldsymbol{\Phi}\boldsymbol{x}\|_2 \leq (1+\epsilon_k(\boldsymbol{\Phi}))\,\|\boldsymbol{x}\|_2$$

for all k-sparse vectors $\boldsymbol{x} \in \mathbb{R}^{\Omega M}$.

The block-toeplitz matrix

$$\boldsymbol{\Phi} = \left[\boldsymbol{F}^* \hat{\boldsymbol{H}}_1 \boldsymbol{F}, \boldsymbol{F}^* \hat{\boldsymbol{H}}_2 \boldsymbol{F}, \cdots, \boldsymbol{F}^* \hat{\boldsymbol{H}}_M \boldsymbol{F}\right] \tag{5.7.2}$$

obeys the RIP for k-sparse vectors, which is given by following theorem.

Theorem 5.7.1 (k-sparse RIP for $\boldsymbol{\Phi}$; see [80]). *Fix a $\epsilon \in (0,1)$ then the matrix $\boldsymbol{\Phi} : \mathbb{R}^{M\Omega} \to \mathbb{R}^{\Omega}$ satisfies the k-restricted isometry property given above for $\epsilon_k(\mathcal{A}) \leq \epsilon$ with probability at least $1 - \exp(-c\Omega)$ when $k \leq c_4\epsilon^2\Omega/\log^4 M\Omega$. The constant c above depends mildly upon length of the vector $\boldsymbol{x}$.*

Given the RIP of $\boldsymbol{\Phi}$, we can apply the following result [54] to show that the matrix $\boldsymbol{\Phi D}$ satisfies concentration for any fixed $\boldsymbol{x} \in \mathbb{R}^{M\Omega}$.

Lemma 5.7.2 (Concetration inequality for $\mathcal{B}$; see [54]). *Fix $\epsilon > 0$ and suppose that there is a constant c_4 such that for all k-sparse vectors and Ω measurements with $k \leq c_4\epsilon^2\Omega/\log^4(M\Omega)$, the matrix $\boldsymbol{\Phi} \in \mathbb{R}^{\Omega \times M\Omega}$ has restricted isometry property of order k and isometry constant ϵ. Fix $\boldsymbol{x} \in \mathbb{R}^{M\Omega}$ and let $\boldsymbol{D} \in \mathbb{R}^{M\Omega \times M\Omega}$ contain along its diagonal a Rademacher sequence, i.e., uniformly distributed $\{-1,1\}^{M\Omega}$. Then for a constant c_5 such that for all Ω, $\boldsymbol{\Phi D}$ satisfies the concentration inequality, which can be written here as*

$$\begin{aligned} \mathrm{P}\left\{ |\|\boldsymbol{\Phi D}\,\mathrm{vec}(\boldsymbol{C}\tilde{\boldsymbol{F}})\|_2^2 - \|\,\mathrm{vec}(\boldsymbol{C}\tilde{\boldsymbol{F}})\|_2^2| \geq \epsilon \|\,\mathrm{vec}(\boldsymbol{C}\tilde{\boldsymbol{F}})\|_2^2 \right\} &\leq 2\exp(-c_5 k) \\ &\leq 2\exp(-c_0\epsilon^2\Omega\log^{-4}(M\Omega)), \end{aligned}$$

where $0 < \epsilon < 1$ and $c_0 = c_4 c_5$.

Using the fact that $\|\,\mathrm{vec}(\boldsymbol{C}\tilde{\boldsymbol{F}})\|_2^2 = \|\boldsymbol{C}\tilde{\boldsymbol{F}}\|_F^2 = \|\boldsymbol{C}\|_F^2$, and by the definition of $\mathcal{B}$, we have the result

$$\Pr\left(|\|\mathcal{B}(\boldsymbol{C})\|_2^2 - \|\boldsymbol{C}\|_F^2| \geq \epsilon \|\boldsymbol{C}\|_F^2 \right) \leq 2\exp(-c_0\epsilon^2\Omega\log^{-4}(M\Omega)).$$

CHAPTER VI

SAMPLING ARCHITECTURES WITH LEAST-SQUARES DECODING

In comparison to the nuclear-norm minimization, we can also solve a simpler least-squares program for the recovery of an unknown low-rank matrix. However, to use least squares as a decoding strategy, the measurements are required to be the samples of the row and the column space of the unknown low-rank matrix $\boldsymbol{X}_0$. The row, and column measurements; namely, $\boldsymbol{Y}_1$, and $\boldsymbol{Y}_2$ are matrices whose rows, and columns can be thought of as samples drawn at random from the row, and column space of $\boldsymbol{X}_0$, respectively. That is, each row of $\boldsymbol{Y}_1$ (each column of $\boldsymbol{Y}_2$) can be expressed as a linear combination of the rows (columns) of $\boldsymbol{X}_0$. Hence, the matrices $\boldsymbol{Y}_1$ and $\boldsymbol{Y}_2$ can be expressed as

$$\text{Row measurements:} \quad \boldsymbol{Y}_1 = \boldsymbol{\Phi}_1 \boldsymbol{X}_0 \tag{6.0.3}$$

$$\text{Column measurements:} \quad \boldsymbol{Y}_2 = \boldsymbol{X}_0 \boldsymbol{\Phi}_2^*, \tag{6.0.4}$$

where $\boldsymbol{\Phi}_1 : \Delta \times M$, and $\boldsymbol{\Phi}_2 : \Omega \times W$ will be referred to as the measurement matrices. The measurement matrices will be random with various distributions. The measurements $\boldsymbol{Y}_1$, and $\boldsymbol{Y}_2$ produce an orthonormal basis for the row and the column space of $\boldsymbol{X}_0$. As we will see later, the knowledge of the row and the column space of the unknown $\boldsymbol{X}_0$ allows us to use a convenient least-squares program for LRMR.

The randomness in the measurement matrices $\boldsymbol{\Phi}_1$, and $\boldsymbol{\Phi}_2$ plays a central role in the successful reconstruction [47]. To see this, consider a simple example: Suppose, we seek a basis for the column space of a matrix $\boldsymbol{X}_0$ of *exact* rank R. Form a vector

$$\boldsymbol{y}_i = \boldsymbol{X}_0 \boldsymbol{\phi}_i, \quad i = 1, \ldots, R,$$

where ϕ_i is a random vector. Intuitively, the vector $\boldsymbol{y}_i$ is a random sample of the column space of $\boldsymbol{X}_0$. Repeat this process R times, each time with a new choice of a random vector $\boldsymbol{\phi}_i$ to obtain a set of samples $\{\boldsymbol{y}_i : i = 1, \ldots, R\}$ of the column space of $\boldsymbol{X}_0$. Since the vectors $\{\boldsymbol{\phi}_i : i = 1, \ldots, R\}$ are independent, it is improbable that these vectors will fall into the null space of $\boldsymbol{X}_0$. This implies that the vectors $\{\boldsymbol{y}_i : i = 1, \ldots, R\}$ are also independent and span the column space of $\boldsymbol{X}_0$, and hence the basis of column space can be obtained from these samples. Exact same reasoning applies to the construction of the basis of the row space of $\boldsymbol{X}_0$.

In general, if the matrix $\boldsymbol{X}_0$ is not *exactly* rank R but is rather compressible, that is, the spectrum of the singular values of $\boldsymbol{X}_0$ decays rapidly after first R significant singular values, then we can write such a matrix $\boldsymbol{X}_0 = \boldsymbol{Z} + \boldsymbol{\xi}$, where $\boldsymbol{Z}$ is a rank-R matrix under consideration and $\boldsymbol{\xi}$ accounts for the perturbation. Now we take the samples of the range space of $\boldsymbol{X}_0$, and we observe

$$\boldsymbol{y}_i = \boldsymbol{X}_0\boldsymbol{\phi}_i = \boldsymbol{Z}\boldsymbol{\phi}_i + \boldsymbol{\xi}\boldsymbol{\phi}_i, \quad i = 1, \ldots, R + \kappa,$$

where κ is the amount of oversampling. We are interested in the column space of $\boldsymbol{Z}$; instead, the samples $\{\boldsymbol{y}_i\}$ observed are deviated outside of the column space of $\boldsymbol{Z}$ because of the perturbation $\boldsymbol{\xi}$. Intuitively, we oversample to make sure that we cover as much of the column space of $\boldsymbol{X}_0$ as possible. As will be clear from theoretical results presented later that a small amount of oversampling, $\kappa = 5, 10$, suffices for many practical situations; for details, see [47].

We estimate the column and row spaces of $\boldsymbol{X}_0$ by computing the svd of $\boldsymbol{Y}_1$ and $\boldsymbol{Y}_2$, then truncating them to R terms. We factor

$$\begin{aligned} \boldsymbol{Y}_1 &\approx \boldsymbol{U}_1\boldsymbol{\Sigma}_1\boldsymbol{V}_1^* \\ \boldsymbol{Y}_2 &\approx \boldsymbol{U}_2\boldsymbol{\Sigma}_2\boldsymbol{V}_2^*, \end{aligned} \tag{6.0.5}$$

where $\boldsymbol{U}_1 : \Delta \times R$, $\boldsymbol{\Sigma}_1 : R \times R$, $\boldsymbol{V}_1 : W \times R$, $\boldsymbol{U}_2 : M \times R$, $\boldsymbol{\Sigma}_2 : R \times R$, $\boldsymbol{V}_2 : \Omega \times R$. We will use $\boldsymbol{U}_2$ as an orthobasis for the column space of our estimate and $\boldsymbol{V}_1$ as an

orthobasis for the row space of our estimate; we will take the estimate $\tilde{\boldsymbol{X}}$ of unknown matrix $\boldsymbol{X}_0$ as

$$\tilde{\boldsymbol{X}} = \boldsymbol{U}_2 \boldsymbol{A} \boldsymbol{V}_1^*, \tag{6.0.6}$$

for some $R \times R$ matrix $\boldsymbol{A}$. We will choose $\boldsymbol{A}$ so that $\boldsymbol{\Phi}_1 \tilde{\boldsymbol{X}}$ and $\tilde{\boldsymbol{X}} \boldsymbol{\Phi}_2^*$ are as close to $\boldsymbol{Y}_1$ and $\boldsymbol{Y}_2$, respectively, as possible. That is, we take

$$\begin{aligned} \tilde{\boldsymbol{A}} &= \operatorname{argmin}_{\boldsymbol{A}} \|\boldsymbol{U}_2 \boldsymbol{A} \boldsymbol{V}_1^* \boldsymbol{\Phi}_2^* - \boldsymbol{Y}_2\|_F^2 + \|\boldsymbol{\Phi}_1 \boldsymbol{U}_2 \boldsymbol{A} \boldsymbol{V}_1^* - \boldsymbol{Y}_1\|_F^2 \\ &= \operatorname{argmin}_{\boldsymbol{A}} \|\boldsymbol{A} \boldsymbol{V}_1^* \boldsymbol{\Phi}_2^* - \boldsymbol{U}_2^* \boldsymbol{Y}_2\|_F^2 + \|\boldsymbol{\Phi}_1 \boldsymbol{U}_2 \boldsymbol{A} - \boldsymbol{Y}_1 \boldsymbol{V}_1\|_F^2. \end{aligned} \tag{6.0.7}$$

Using Lemma 6.0.3, we know that $\tilde{\boldsymbol{A}}$ must obey the normal equations

$$\boldsymbol{U}_2^* \boldsymbol{\Phi}_1^* \boldsymbol{\Phi}_1 \boldsymbol{U}_2 \tilde{\boldsymbol{A}} + \tilde{\boldsymbol{A}} \boldsymbol{V}_1^* \boldsymbol{\Phi}_2^* \boldsymbol{\Phi}_2 \boldsymbol{V}_1 = \boldsymbol{U}_2^* \boldsymbol{\Phi}_1^* \boldsymbol{Y}_1 \boldsymbol{V}_1 + \boldsymbol{U}_2^* \boldsymbol{Y}_2 \boldsymbol{\Phi}_2 \boldsymbol{V}_1$$

or

$$\boldsymbol{H} \tilde{\boldsymbol{A}} + \tilde{\boldsymbol{A}} \boldsymbol{G} = \boldsymbol{F},$$

where $\boldsymbol{H} = \boldsymbol{U}_2^* \boldsymbol{\Phi}_1^* \boldsymbol{\Phi}_1 \boldsymbol{U}_2$, $\boldsymbol{G} = \boldsymbol{V}_1^* \boldsymbol{\Phi}_2^* \boldsymbol{\Phi}_2 \boldsymbol{V}_1$, and $\boldsymbol{F} = \boldsymbol{U}_2^* \boldsymbol{\Phi}_1^* \boldsymbol{Y}_1 \boldsymbol{V}_1 + \boldsymbol{U}_2^* \boldsymbol{Y}_2 \boldsymbol{\Phi}_2 \boldsymbol{V}_1$. We can write this $R^2 \times R^2$ system of equations in vectorized form (columns stacked on one another) as

$$\boldsymbol{K} \tilde{\boldsymbol{a}} = \boldsymbol{f},$$

where $\tilde{\boldsymbol{a}} = \operatorname{vec}(\tilde{\boldsymbol{A}})$, $\boldsymbol{f} = \operatorname{vec}(\boldsymbol{F})$, and

$$\boldsymbol{K} = \begin{bmatrix} \boldsymbol{H} & & & \\ & \boldsymbol{H} & & \\ & & \ddots & \\ & & & \boldsymbol{H} \end{bmatrix} + \begin{bmatrix} \boldsymbol{G}_{1,1}\boldsymbol{I} & \boldsymbol{G}_{2,1}\boldsymbol{I} & \dots & \boldsymbol{G}_{R,1}\boldsymbol{I} \\ \boldsymbol{G}_{1,2}\boldsymbol{I} & \boldsymbol{G}_{2,2}\boldsymbol{I} & \dots & \boldsymbol{G}_{R,2}\boldsymbol{I} \\ \vdots & \vdots & \ddots & \vdots \\ \boldsymbol{G}_{1,R}\boldsymbol{I} & \boldsymbol{G}_{2,R}\boldsymbol{I} & \dots & \boldsymbol{G}_{R,R}\boldsymbol{I} \end{bmatrix}.$$

So we take $\tilde{\boldsymbol{a}} = \boldsymbol{K}^{-1} \boldsymbol{f}$, and unstack the columns to get $\tilde{\boldsymbol{A}}$.

Instead of using the least-squares program in (6.0.7), we can solve a simpler version [101]:

$$\tilde{\boldsymbol{A}} = \operatorname{argmin}_{\boldsymbol{A}} \|\boldsymbol{U}_2 \boldsymbol{A} \boldsymbol{V}_1^* \boldsymbol{\Phi}_2^* - \boldsymbol{Y}_2\|_F^2, \tag{6.0.8}$$

which gives almost the same performance as the least-squares program in (6.0.7); for details, see [101]. The corresponding normal equations for the least-squares program (6.0.8) are

$$\boldsymbol{U}_2^*\boldsymbol{\Phi}_1^*\boldsymbol{\Phi}_1\boldsymbol{U}_2\tilde{\boldsymbol{A}} = \boldsymbol{U}_2^*\boldsymbol{\Phi}_1^*\boldsymbol{Y}_1\boldsymbol{V}_1.$$

This gives a simple analytical form of the estimate $\tilde{\boldsymbol{A}}$

$$\tilde{\boldsymbol{A}} = (\boldsymbol{U}_2^*\boldsymbol{\Phi}_1^*\boldsymbol{\Phi}_1\boldsymbol{U}_2)^{-1}\boldsymbol{U}_2^*\boldsymbol{\Phi}_1^*\boldsymbol{Y}_1\boldsymbol{V}_1.$$

The theoretical results presented later will show that the inverse $(\boldsymbol{U}_2^*\boldsymbol{\Phi}_1^*\boldsymbol{\Phi}_1\boldsymbol{U}_2)^{-1}$ is well defined. The lemma below derives the normal equations for the least-squares program in (6.0.7).

Lemma 6.0.3. *Consider the following optimization program*

$$\min_{\boldsymbol{A}} \|\boldsymbol{P}\boldsymbol{A} - \boldsymbol{Y}\|_F^2 + \|\boldsymbol{A}\boldsymbol{Q}^* - \boldsymbol{Z}\|_F^2,$$

where $\boldsymbol{A} : R \times R$, $\boldsymbol{P} : \Delta \times R$, $\boldsymbol{Y} : \Delta \times R$, $\boldsymbol{Q} : \Omega \times R$, $\boldsymbol{Z} : R \times \Omega$. *The solution to the above optimization program satisfies the normal equations:*

$$\boldsymbol{P}^*\boldsymbol{P}\boldsymbol{A} + \boldsymbol{A}\boldsymbol{Q}^*\boldsymbol{Q} = \boldsymbol{P}^*\boldsymbol{Y} + \boldsymbol{Z}\boldsymbol{Q}.$$

Proof. The minimizer $\boldsymbol{A}$ to the least-squares program above satisfies

$$\nabla_{\boldsymbol{A}}\|\boldsymbol{P}\boldsymbol{A} - \boldsymbol{Y}\|_F^2 + \nabla_{\boldsymbol{A}}\|\boldsymbol{A}\boldsymbol{Q}^* - \boldsymbol{Z}\|_F^2 = \boldsymbol{0}.$$

We know that

$$\begin{aligned}\nabla_{\boldsymbol{A}}\|\boldsymbol{P}\boldsymbol{A} - \boldsymbol{Y}\|_F^2 &= \nabla_{\boldsymbol{A}}\|\boldsymbol{P}\boldsymbol{A}\|_F^2 - 2\nabla_{\boldsymbol{A}}\operatorname{Tr}(\boldsymbol{Y}^*\boldsymbol{P}\boldsymbol{A}) \\ &= 2\boldsymbol{P}^*\boldsymbol{P}\boldsymbol{A} - 2\boldsymbol{P}^*\boldsymbol{Y},\end{aligned}$$

and

$$\begin{aligned}\nabla_{\boldsymbol{A}}\|\boldsymbol{A}\boldsymbol{Q}^* - \boldsymbol{Z}\|_F^2 &= \nabla_{\boldsymbol{A}}\|\boldsymbol{A}\boldsymbol{Q}^*\|_F^2 - 2\nabla_{\boldsymbol{A}}\operatorname{Tr}(\boldsymbol{Z}^*\boldsymbol{A}\boldsymbol{Q}^*) \\ &= 2\boldsymbol{A}\boldsymbol{Q}^*\boldsymbol{Q} - 2\boldsymbol{Z}\boldsymbol{Q},\end{aligned}$$

and so the corresponding normal equations are

$$\boldsymbol{P}^*\boldsymbol{P}\boldsymbol{A} + \boldsymbol{A}\boldsymbol{Q}^*\boldsymbol{Q} = \boldsymbol{P}^*\boldsymbol{Y} + \boldsymbol{Z}\boldsymbol{Q}.$$

□

6.1 Compressive Acquisition with Least-squares Decoding

We will present here two compressive sampling architectures for the acquisition of multiple signals lying in a subspace. These architectures process the signals in analog in a way that allows us to use the least-squares program for the reconstruction of the signal ensemble. In this section, we will introduce each of the sampling architecture and model the samples taken by the ADCs as a linear transformation of a low-rank matrix.

6.1.1 Architecture 1

The sampling architecture shown on the left in Figure 36 takes input signal ensemble $\boldsymbol{X}_c(t) = \{x_m(t)\}_{1\leq m\leq M}$ containing M signals. The signals in the ensemble are assumed to be lying in a subspace, i.e.,

$$\boldsymbol{X}_c(t) := \{x_m(t) : x_m(t) \approx \sum_{r=1}^{R} A[m,r]s_r(t), 1 \leq m \leq M\},$$

where $A[m,r]$ are the entries of an unknown $M \times R$ matrix $\boldsymbol{A}$, and $s_r(t)$ are the underlying independent signals. In addition, each signal in the ensemble is bandlimited to $W/2$. The signal model is explained in detail in Chapter 4. We will use the same analog components to build the architectures that were introduced in Chapter 4.

Let $\boldsymbol{X}_0$ be the matrix that contains as its rows the Nyquist rate samples of the signals $x_m(t)$ in $t \in [0,1)$. We can write

$$\boldsymbol{X}_0 = \boldsymbol{C}_0\boldsymbol{F}, \tag{6.1.1}$$

where $\boldsymbol{F}$ is a $W \times W$ normalized discrete Fourier matrix with entries

$$F[\omega,n] = \frac{1}{\sqrt{W}}e^{-j2\pi\omega n/W}, \quad 0 \leq \omega, n \leq W-1,$$

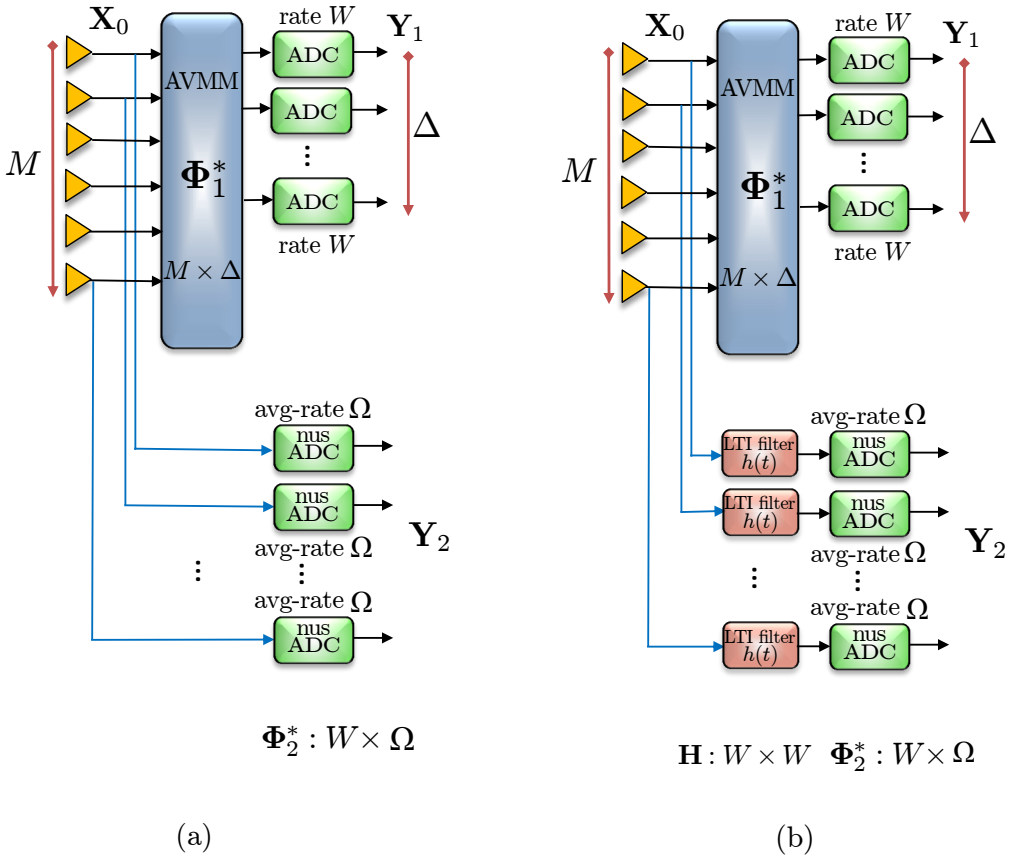

Figure 36: Sampling architectures for multiple signals lying in a subspace: M signals, bandlimited to $W/2$ are preprocessed in analog using an analog vector-matrix multiplier (AVMM) to produce Δ signals, each of which is then sampled at W samples per second. In addition, each of the M input signals is sampled randomly using a non-uniform sampling (nus) ADC at an average rate Ω samples per second. The analog preprocessing is designed to perform row and column operations on matrix of samples $\boldsymbol{X}_0$ so that we can use the least-squares program for decoding. The net sampling rate is $\Omega M + \Delta W$ samples per second.

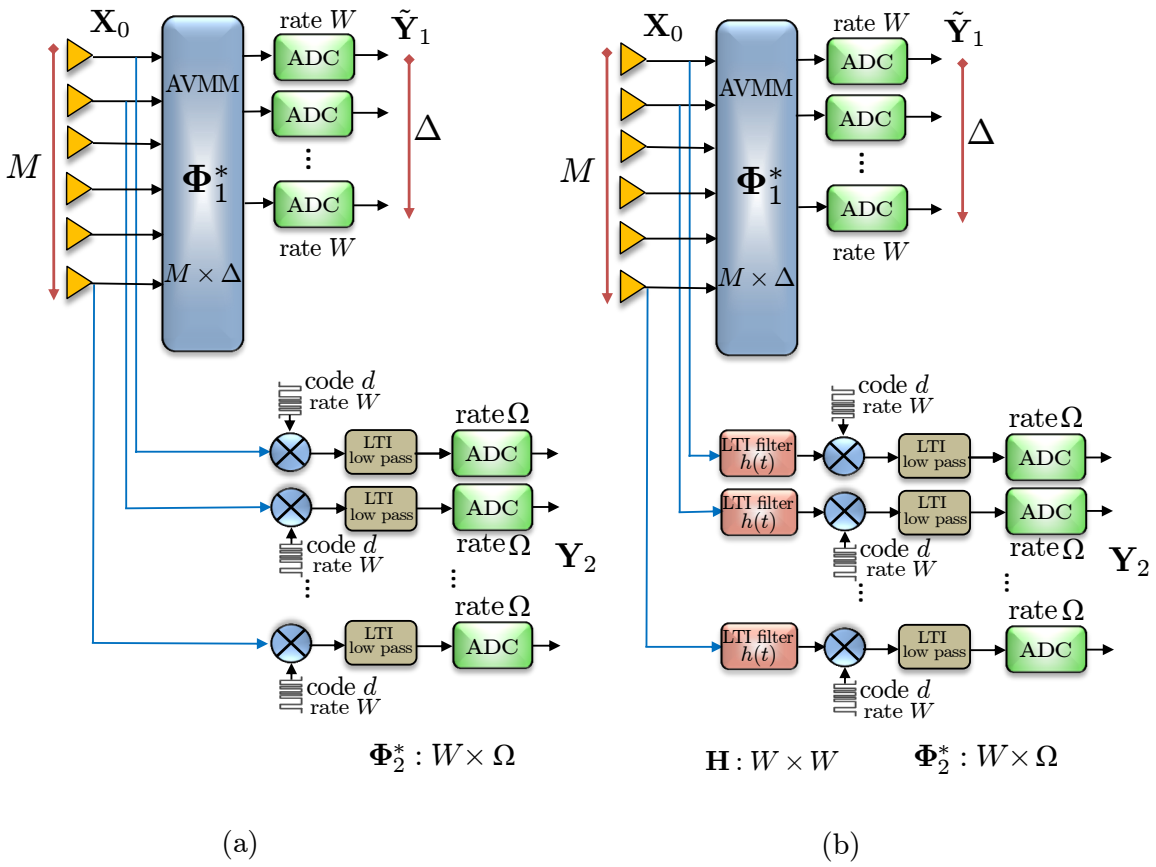

Figure 37: Sampling architecture for multiple signals lying in a subspace: M signals, bandlimited to $W/2$ are preprocessed in analog using an analog vector-matrix multiplier (AVMM) to produce Δ signals, each of which is then sampled at W samples per second. In addition, each of the M input signal is processed by a modulator, and a low-pass filter. The resultant signal is then sampled uniformly at a rate Ω samples per second. The analog preprocessing is designed to perform the row and the column operation on $\boldsymbol{X}_0$ so that a simple least-squares program can be used for decoding. The net sampling rate is $\Omega M + \Delta W$ samples per second.

and $\boldsymbol{C}_0$ is a $M \times W$ matrix whose rows contain Fourier series coefficients for the signals in $\boldsymbol{X}_c(t)$;for details, see Section 4.1.1. The unknown matrix $\boldsymbol{X}_0$ is of rank-R by construction. The analog preprocessing basically aims at obtaining the row and the column space of $\boldsymbol{X}_0$. Firstly, the signals are processed by an AVMM that takes random linear combinations of M input signals to produce Δ output signals. The resultant Δ signals are then sampled uniformly at rate W. In discrete time, the action of the AVMM, and the uniform ADCs can be represented as the left multiplication of a Gaussian matrix $\boldsymbol{\Phi}_1 : \Delta \times M$ with the matrix of samples $\boldsymbol{X}_0$. Hence, the measurements

$$\boldsymbol{Y}_1 = \boldsymbol{\Phi}_1 \boldsymbol{X}_0, \tag{6.1.2}$$

can be viewed as the row measurements of the matrix of samples $\boldsymbol{X}_0$. These measurements will later be utilized in the least-squares program for matrix recovery. Secondly, the M input signals in the ensemble $\boldsymbol{X}_c(t)$ are sampled individually using non-uniformly sampling (nus) ADCs. The nus ADCs operate randomly at an average rate Ω. In a time window $t \in [0, 1)$, all of the nus ADCs take the input signals $\{x_m(t)\}_{1 \leq m \leq M}$ and return the samples

$$\{x_m(t_k), \forall m | t_k \in \Gamma \subset \{0, 1/W, \ldots, 1 - 1/W\}\},$$

where the set Γ is chosen uniformly at random such that $|\Gamma| = \Omega$. It is important to see that all of the nus-ADCs go on-and-off together. Hence, if we place the samples of each of the nus ADCs as the columns of the matrix $\boldsymbol{Y}_2$, then the measurements $\boldsymbol{Y}_2$ can be expressed as

$$\boldsymbol{Y}_2 = \boldsymbol{X}_0 \boldsymbol{\Phi}_2^*, \tag{6.1.3}$$

where

$$\boldsymbol{\Phi}_2 := \sqrt{\frac{W}{\Omega}} \mathcal{R}_\Gamma : \Omega \times W$$

is a matrix that restricts a length-W vector of samples $\boldsymbol{x}_m$ in each channel to the Ω

coordinates, which correspond to the samples selected. Since the nus ADCs go on-and-off together, therefore, in the above formulation, the matrix $\boldsymbol{\Phi}_2^*$ selects an entire row of the matrix of samples $\boldsymbol{X}_0$ at random. Thus, the measurements $\boldsymbol{Y}_2 : M \times \Omega$ can be viewed as the column-space measurements of the unknown low-rank matrix $\boldsymbol{X}_0$. Putting it all together, the ADCs are sampling at a rate $\Delta W + M\Omega$ to obtain the column and the row measurements $\boldsymbol{Y}_1$ and $\boldsymbol{Y}_2$.

Since the nus ADCs are operating at a sub-Nyquist rate, the successful reconstruction hinges on the fact that partial information gathered by the nus ADCs gives us a global information about the signal ensemble. This is not true when the signal ensemble is sparse across time. As in such a situation, many samples of the row space of $\boldsymbol{X}_0$ end up being zero vectors, which do not tell us anything about the row space of the matrix $\boldsymbol{X}_0$. To avoid this scenario, we will then have to sample at a higher rate till we observe enough samples to achieve a reliable estimate of the row space. Hence, the sampling architecture is more effective for the signals that are dispersed across time. This intuition is supported by our theoretical results, and the sufficient sampling rate for the successful reconstruction of the ensemble is dependent on the dispersion of the signal energy across time. The dispersion is quantified by a signal parameter called coherence. Let

$$\boldsymbol{X}_0 = \boldsymbol{U}\boldsymbol{\Sigma}\boldsymbol{V}^*$$

be the singular value decomposition of the matrix $\boldsymbol{X}_0$. Then the coherence μ_0^2 is defined as

$$\mu_0^2 = \frac{W}{R} \max_{1 \leq k \leq W} \|\boldsymbol{V}^* \boldsymbol{e}_k\|_2^2,$$

where it can easily be shown that $1 \leq \mu_0^2 \leq \frac{W}{R}$. In particular, the parameter μ_0^2 achieves the upper bound, when the right singular vectors contain the standard basis vectors. In contrast, the coherence μ_0^2 achieves the lower bound when the entries in the right singular vectors are of the same magnitude. Since the signals are bandlimited,

this means that μ_0^2 is small when the signal are dispersed across time.

Given the measurement set $\boldsymbol{Y}_1$, and $\boldsymbol{Y}_2$, the following theorem provides sufficient sampling rate for the successful reconstruction of the signal ensmbel $\boldsymbol{X}_c(t)$.

Theorem 6.1.1. *Let $\boldsymbol{Y}_1 : \Delta \times M$, and $\boldsymbol{Y}_2 : W \times \Omega$ be as in* (6.1.2)*, and* (6.1.3)*, respectively. Then the unknown matrix $\boldsymbol{X}_0$ can be recovered exactly using the least-squares program in* (6.0.7) *with probability at least $1 - O(W^{-\beta})$, when*

$$\Delta \geq R + C\beta \log W, \quad \Omega \geq C\beta\mu_0^2 R \log W,$$

and hence the number of samples per second $\Delta W + M\Omega$ obey the bound

$$\Delta W + M\Omega \gtrsim C_\beta R(W + \mu_0^2 M) \log W,$$

where C_β is a constant that depends on β.

Thus, we can reconstruct the ensemble $\boldsymbol{X}_c(t)$ by sampling at a rate that is within a constant and log factors of the optimal sampling rate $R(W + M)$.

We will now consider a more realistic case, when the $\boldsymbol{X}_0$ is not exactly of rank-R but is rather compressible, i.e., the spectrum of the singular values consists of R most significant singular values and rest of the singular values decay rapidly. Given the measurements $\boldsymbol{Y}_1$, and $\boldsymbol{Y}_2$ of such an $\boldsymbol{X}_0$, the following theorem gives the signal reconstruction result using the least-squares program as a decoding strategy.

Theorem 6.1.2. *Let $\boldsymbol{Y}_1 : \Delta \times M$, and $\boldsymbol{Y}_2 : W \times \Omega$ be as in* (6.1.2)*, and* (6.1.3)*, respectively. Then the solution $\tilde{\boldsymbol{X}}$ of the least-squares program in* (6.0.7) *obeys*

$$\|\tilde{\boldsymbol{X}} - \boldsymbol{X}_0\|_F \leq C \left(1 + C\sqrt{\frac{R}{\beta \log W}} + \sqrt{\frac{W}{\Omega}}\right) \left(\sum_{j>R} \sigma_j^2\right)^{1/2}$$

with probability at least $1 - O(W^{-\beta})$ when

$$\Delta \geq R + C\beta \log W, \quad \Omega \geq C\beta\mu_0^2 R \log W$$

and hence the sampling rate is

$$\Delta W + M\Omega \gtrsim C_\beta R(W + \mu_0^2 M) \log W,$$

where C_β is a constant that depends on β.

We can also force the coherence μ_0^2 to be small by adding some analog preprocessing in the form of random LTI filters in each channel. The LTI filters are represented using $W \times W$ circulant matrix $\boldsymbol{H}$ as defined in (4.1.5), (4.1.6), and (4.1.7). We will use filters with the same impulse response $h_c(t)$ in each channel. Now we are concerned with a new matrix

$$\boldsymbol{X}_\mathfrak{p} = \boldsymbol{X}_0 \boldsymbol{H},$$

where $\boldsymbol{H}$ is a random orthogonal matrix, and $\boldsymbol{X}_\mathfrak{p}$ stands for matrix of samples of the analog preprocessed ensemble. Since $\boldsymbol{X}_0 = \boldsymbol{U}\boldsymbol{\Sigma}\boldsymbol{V}^*$, the svd of $\boldsymbol{X}_\mathfrak{p}$ is then

$$\boldsymbol{X}_\mathfrak{p} = \boldsymbol{U}\boldsymbol{\Sigma}\boldsymbol{V}_\mathfrak{p}^*,$$

where the matrix of right singular vectors $\boldsymbol{V}_\mathfrak{p} = \boldsymbol{H}\boldsymbol{V}$ is in some sense a random orthogonal matrix, and the following lemma shows that $\boldsymbol{V}_\mathfrak{p}$ is incoherent with high probability.

Lemma 6.1.1. *Fix a matrix $\boldsymbol{V} \in \mathbb{C}^{W \times R}$ of the right singular vectors. Create a random orthonormal matrix $\boldsymbol{H} \in \mathbb{R}^{W \times W}$. Then*

$$\max_{1 \le j \le W} \|\boldsymbol{V}_\mathfrak{p}^* \boldsymbol{e}_j\|_2^2 \le C\beta \max(R, \log W)/W$$

with a probability exceeding $1 - O(W^{-\beta})$.

The column measurements are now

$$\boldsymbol{Y}_2 = \boldsymbol{X}_\mathfrak{p} \boldsymbol{\Phi}_2^*,$$

where $\boldsymbol{\Phi}_2$ is the same column-sensing matrix as before. The sampling theorems for this new sampling architecture can easily be derived from Theorem 6.1.1, and 6.1.2

for the case when $\boldsymbol{X}_{\mathfrak{p}}$ is exactly rank-R, and when it is compressible, respectively. In this case, the sufficient sampling rate for the successful reconstruction of the signal ensemble scales with an additional log factor $\log W$, when $R > \log W$, otherwise, we pay two additional log factors in the sampling rate.

6.1.2 Architecture 2

The second proposed architecture for the efficient sampling of multiple signals lying in a subspace is shown in Figure 37. For the column measurements, we use a block of modulator, low-pass filter, and a uniform ADC in each channel. Each of the M input signals $x_m(t), 1 \leq m \leq M$ is multiplied by a random binary waveform $d(t), \forall m$ alternating at rate W. That is, the output after the modulation in the m-th channel is

$$y_m(t) = x_m(t) \cdot d(t), \quad m = 1, \cdots, M, \text{ and } t \in [0, 1).$$

The $y_m(t)$ are then low-pass filtered using an integrator, which integrates $y_m(t)$ over an interval of width $1/\Omega$ and the result is then sampled at rate Ω using an ADC. The samples taken by the ADC in the m-th channel are

$$y_m[n] = \int_{(n-1)/\Omega}^{n/\Omega} y_m(t)dt, \quad n = 1, \cdots, \Omega.$$

The integration operation commutes with the modulation process; hence, we can equivalently integrate the signals $x_m(t), 1 \leq m \leq M$ over the interval of width $1/W$, and treat them as samples $\boldsymbol{X}_1 \in \mathbb{R}^{M \times W}$ of the ensemble $\boldsymbol{X}_c(t)$. The entries $X_1[m, n]$ of the matrix $\boldsymbol{X}_1$ are

$$\begin{aligned} X_1[m, n] &= \int_{(n-1)/W}^{n/W} x_m(t)dt, \\ &= \sum_{|\omega| \leq W/2} C[m, \omega] \left[\frac{e^{\iota 2\pi\omega/W} - 1}{\iota 2\pi\omega} \right] e^{-\iota 2\pi\omega n/W}, \end{aligned}$$

where the bracketed term representing the low-pass filter

$$\tilde{L}[\omega] = \left[\frac{e^{\iota 2\pi\omega/W} - 1}{\iota 2\pi\omega} \right]$$

is evaluated in the window $\omega = 0, \pm 1, \ldots, \pm(W/2-1), W/2$. We will use an equivalent evaluation $L[\omega]$ of $\tilde{L}[\omega]$ in the window $\omega = 1, \ldots, W$. The Fourier coefficients of $C_0[m, \omega]$ of $\boldsymbol{X}_0$ defined in (4.1.2) are related to the Fourier coefficients $C_0[m, \omega]$ of $\boldsymbol{X}_0$

$$C_1[m, \omega] = C_0[m, \omega] L[\omega] \quad \omega = 1, \cdots, W, \tag{6.1.4}$$

and in time domain

$$\boldsymbol{X}_1 = \boldsymbol{C}_0 \boldsymbol{L} \boldsymbol{F}, \tag{6.1.5}$$

where $\boldsymbol{L}$ is a $W \times W$ diagonal matrix containing $L[\omega]$ as its diagonal entries, $\boldsymbol{F}$ is the $W \times W$ DFT matrix, and $\boldsymbol{C}_1$ is the coefficients matrix with entries defined in (6.1.4). Since $\boldsymbol{C}_1$ inherits its low-rank structure from $\boldsymbol{C}_0$; therefore, $\boldsymbol{X}_1$ is also a low-rank matrix of rank R. As a result, in the rest of this write up, we will be concerned with recovering the rank R matrix $\boldsymbol{X}_1$. Since $\boldsymbol{L}$ is well-conditioned, the recovery of $\boldsymbol{X}_1$ implies the recovery of $\boldsymbol{X}_0$.

In light of (4.1.3), the W equally-spaced samples of $d(t)x_m(t)$ are $\boldsymbol{D}\boldsymbol{x}_m$, where $\boldsymbol{x}_m$ contains the W uniformly-spaced samples of $x_m(t)$, and $\boldsymbol{D}$, as in (4.1.4), is a random diagonal matrix containing random binary signs $d[n]$ along the diagonal. The samples $\boldsymbol{y}_m \in \mathbb{R}^{\Omega}$ in $t \in [0, 1)$ taken by the ADC in the m-th branch are

$$\boldsymbol{y}_m = \boldsymbol{P}\boldsymbol{D}\boldsymbol{x}_m, \quad 1 \leq m \leq M,$$

where $\boldsymbol{x}_m \in \mathbb{R}^W$ are the rows of $\boldsymbol{X}_0$ defined in (6.1.5); $\boldsymbol{D}$ is $W \times W$ random diagonal matrix defined in (4.1.4), and corresponds to the modulator in the m-th branch; and $\boldsymbol{P} : \Omega \times W$ is the matrix that represents the action of the integrator (used as a low-pass filter; for more details, see [96]) that contains ones in locations $(\alpha, \beta) \in (j, \mathcal{B}_j)$, for $j = 1, \cdots, \Omega$, where

$$\mathcal{B}_j = \{(j-1)W/\Omega + 1 : jW/\Omega\} \quad 1 \leq j \leq \Omega,$$

where we are assuming for simplicity that Ω is a factor of W. Since the action of the integrator commutes with the action of the modulator, the operation of the

integrator can be simply represented as a block-diagonal matrix $\boldsymbol{P}$ operating on the modulated entries of the rows of $\boldsymbol{X}_1$, which contains the samples of the integrated signals. Putting it all together, the samples acquired by the ADCs can be written as

$$\boldsymbol{Y}_2 = \boldsymbol{C}_0 \boldsymbol{L} \boldsymbol{F} \boldsymbol{\Phi}_2^* = \boldsymbol{X}_1 \boldsymbol{\Phi}_2^*, \tag{6.1.6}$$

where the column-measurement matrix is $\boldsymbol{\Phi}_2 = \boldsymbol{P}\boldsymbol{D}$.

As before, the AVMM takes the random linear combinations of the M input signals to produce Δ output signals. Each of the Δ resultant signals is then sampled uniformly at rate W. The row measurements are

$$\tilde{\boldsymbol{Y}}_1 = \boldsymbol{\Phi}_1 \boldsymbol{X}_0 = \boldsymbol{\Phi}_1 \boldsymbol{C}_0 \boldsymbol{F},$$

where $\boldsymbol{\Phi}_1 : \Delta \times M$ is a Gaussian matrix. From $\tilde{\boldsymbol{Y}}_1$, we can obtain the row measurements of $\boldsymbol{X}_1$ as

$$\boldsymbol{Y}_1 = \tilde{\boldsymbol{Y}}_1 \boldsymbol{F}^* \boldsymbol{L} \boldsymbol{F} = \boldsymbol{\Phi}_1 \boldsymbol{X}_1. \tag{6.1.7}$$

The ADC in each branch samples the signal energy integrated over intervals of length $1/\Omega$. If the input signals are sparse across time, then most samples of the column space of $\boldsymbol{X}_1$ in $\boldsymbol{Y}_2$ might be zero vectors, which donot contribute any useful information towards the reconstruction of the signal ensemble from the limited measurements observed. Intuitively, the sampling architecture is more effective for signals distributed across time. This observation is supported by our theoretical analysis. Our results again depend on the coherence parameter μ_0^2

$$\mu_0^2 = \frac{W}{R} \max_{1 \le k \le W} \|\boldsymbol{V}^* \boldsymbol{e}_k\|_2^2$$

that quantifies the dispersion of signal energy across time, where $\boldsymbol{V}$ is the matrix of right singular vectors of $\boldsymbol{X}_1 = \boldsymbol{U}\boldsymbol{\Sigma}\boldsymbol{V}^*$.

Theorem 6.1.3. *Let $\boldsymbol{Y}_1 : \Delta \times M$, and $\boldsymbol{Y}_2 : W \times \Omega$ be as in* (6.1.7)*, and* (6.1.6)*. Then the unknown matrix $\boldsymbol{X}_1$ can be recovered exactly using the least-squares program in*

(6.0.7) *with probability at at least* $1 - O(W^{-\beta})$*, when*

$$\Delta \geq R + C\beta \log W, \quad \Omega \geq C\beta\mu_0^2 \log^2 W,$$

and hence the number of samples obey

$$\Delta W + M\Omega \gtrsim C_\beta R(W + \mu_0^2 M) \log^2 W$$

for a fixed constant C_β *that depends on* β*.*

In the case, when $\boldsymbol{X}_1$ is not exactly rank-R, but is a compressible matrix, well approximated by a rank-R matrix, we have the following signal reconstruction result.

Theorem 6.1.4. *Let* $\boldsymbol{Y}_1 : \Delta \times M$*, and* $\boldsymbol{Y}_2 : W \times \Omega$ *be as in* (6.1.7)*, and* (6.1.6)*. Then the solution* $\tilde{\boldsymbol{X}}$ *of the least-squares program in* (6.0.7) *obeys*

$$\|\tilde{\boldsymbol{X}} - \boldsymbol{X}_1\|_F \leq C \left(1 + C\sqrt{\frac{R}{\beta \log W}} + \sqrt{\frac{W}{\Omega}}\right) \left(\sum_{j>R} \sigma_j^2\right)^{1/2},$$

with probability at least $1 - O(W^{-\beta})$ *when*

$$\Delta \geq R + C\beta \log W, \quad \Omega \geq C\beta\mu_0^2 R \log^2 W,$$

and hence the sampling rate obeys

$$\Delta W + M\Omega \gtrsim C_\beta R(W + \mu_0^2 M) \log^2 W,$$

where C_β *is a constant that depends on* β*.*

Using the same strategy as before, we can add random LTI filters in each branch and force the signal energy to be equally distributed across time regardless of the initial energy distribution. Using Lemma 6.1.1, together with Theorem 6.1.3, and 6.1.4, it is clear that for the architecture shown in Figure 37(b), we just need to pay just an additional log factor in the sufficient sampling to obtain same reconstruction results.

6.2 Theory

6.2.1 Proof of Theorem 6.1.1, and 6.1.2

Since for an $\boldsymbol{X}_0$ with rank *exactly* R, only first R singular values $\sigma_1, \ldots, \sigma_R$ are non-zero. Using this fact, the exact recovery result in Theorem 6.1.1 follows from Theorem 6.1.2. Therefore, we will only be concerned with the proof of Theorem 6.1.2. Suppose $\mathcal{P}_{Y_1} = \boldsymbol{V}_1\boldsymbol{V}_1^*$, $\mathcal{P}_{Y_2} = \boldsymbol{U}_2\boldsymbol{U}_2^*$, where $\boldsymbol{V}_1$, and $\boldsymbol{U}_2$ are matrices of the right and left singular vectors (see (6.0.5))of $\boldsymbol{Y}_1$, and $\boldsymbol{Y}_2$, defined in (6.1.2), and (6.1.3), respectively. Then the proof follows from the following two Theorems in [47].

Theorem 6.2.1 (Theorem 10.7 in [47])**.** *Suppose that $\boldsymbol{X}_0$ is a real $M \times W$ matrix with singular values $\sigma_1 \geq \sigma_2 \geq \sigma_3 \geq \cdots$. Choose a target rank $R \geq 2$, and $\Delta \geq R + C\beta \log W$, with $\beta \geq 1$, and $\Delta \leq \min(M, W)$. Draw a $\Delta \times M$ standard Gaussian matrix $\boldsymbol{\Phi}_2$, and construct the sample matrix $\boldsymbol{Y}_1 = \boldsymbol{\Phi}_1\boldsymbol{X}_0$. Then*

$$\|\boldsymbol{X}_0(\mathcal{I} - \mathcal{P}_{Y_1})\|_F \leq \left(1 + C\sqrt{\frac{R}{\beta \log W}}\right)\left(\sum_{j>R}\sigma_j^2\right)^{1/2}$$

with probability at least $1 - O(W^{-\beta})$.

Theorem 6.2.2 (Theorem 11.2 in [47])**.** *Fix an $M \times W$ matrix $\boldsymbol{X}_0$ with singular values $\sigma_1 \geq \sigma_2 \geq \sigma_3 \geq \ldots$. Draw an $\Omega \times W$ matrix $\mathcal{R}_\Gamma$ such that*

$$\boldsymbol{\Phi}_2 = \sqrt{\frac{W}{\Omega}}\mathcal{R}_\Gamma,$$

where

$$C\beta\mu_0^2 R \log W \leq \Omega \leq W.$$

Construct the sample matrix $\boldsymbol{Y}_2 = \boldsymbol{X}_0\boldsymbol{\Phi}_2^*$. Then

$$\|(\mathcal{I} - \mathcal{P}_{Y_2})\boldsymbol{X}_0\|_F \leq \sqrt{1 + 7W/\Omega} \cdot \left(\sum_{j\geq R}\sigma_j^2\right)^{1/2}$$

with failure probability at least $1 - O(W^{-\beta})$.

Proof follows by combining above two theorems with the result in Theorem 6.2.4.

6.2.2 Proof of Theorem 6.1.3, and 6.1.4

Theorem 6.1.4 implies the exact recovery result in Theorem 6.1.3, when we choose $\boldsymbol{X}_0$ to be *exactly* rank-R. Therefore, we only consider proving Theorem 6.1.4 in this section. We will use Theorem 6.2.4 to bound the recovery error of the solution $\tilde{\boldsymbol{X}}$ obtained as a result of the samples taken by the Architecture 2. In Architecture 2, the row-sensing matrix $\boldsymbol{\Phi}_1$ is i.i.d. Gaussian, as for Architecture 1, but the column-sensing matrix $\Phi_2 : \Omega \times W$:

$$\boldsymbol{\Phi}_2 = \boldsymbol{P}\boldsymbol{D},$$

is different form the Architecture 1. Suppose, the svd of the row and the column measurements $\boldsymbol{Y}_1$ and $\boldsymbol{Y}_2$, respectively, truncated to R singular values is given by (6.0.5). Then, following theorem is in order for the column measurements. Let us now define several quantities useful to state the next result in [47]. We define the svd of matrix $\boldsymbol{X}_1$

$$\boldsymbol{X}_1 = \boldsymbol{U} \begin{bmatrix} \boldsymbol{\Sigma}^a & \\ & \boldsymbol{\Sigma}^b \end{bmatrix} \begin{bmatrix} (\boldsymbol{V}^a)^* & (\boldsymbol{V}^b)^* \end{bmatrix},$$

where $\boldsymbol{V}^a : R \times \min(M, W)$, and $\boldsymbol{V}^b : (W - R) \times \min(M, W)$ are the matrices of right singular vectors corresponding to singular values in $\boldsymbol{\Sigma}^a$, and $\boldsymbol{\Sigma}^b$. Thus, the matrix of right singular vectors $\boldsymbol{V}$ is the concatenation of $\boldsymbol{V}^a$, and $\boldsymbol{V}^b$, i.e., $\boldsymbol{V} = [\boldsymbol{V}^a \ \boldsymbol{V}^b]$. Using this notation, we have

$$\boldsymbol{\Phi}_2 \boldsymbol{V} = \boldsymbol{\Phi}_2 [\boldsymbol{V}^a \quad \boldsymbol{V}^b]. \tag{6.2.1}$$

The error bound depends on the properties of $\boldsymbol{\Phi}_2 \boldsymbol{V}^a$ and $\boldsymbol{\Phi}_2 \boldsymbol{V}^b$. Suppose $\mathcal{P}_{Y_2} = \boldsymbol{U}_2 \boldsymbol{U}_2^*$, where $\boldsymbol{U}_2$ is a matrix of the left singular vectors (see (6.0.5))of $\boldsymbol{Y}_2$, defined in (6.1.6). Now we state here the result in [47].

Theorem 6.2.3 (Theorem 9.1 in [47])**.** *Let $\boldsymbol{X}_1$ be a $M \times W$ matrix with singular value decomposition $\boldsymbol{X}_1 = \boldsymbol{U}\boldsymbol{\Sigma}\boldsymbol{V}^*$. Choose a target rank $R \geq 2$. Draw a random*

matrix

$$\boldsymbol{\Phi}_2 = \boldsymbol{P}\boldsymbol{D},$$

and construct the sample matrix $\boldsymbol{Y}_2 = \boldsymbol{X}_1\boldsymbol{\Phi}_2^*$. *Partition* $\boldsymbol{\Phi}_2\boldsymbol{V}$ *as specified above, and define* $\boldsymbol{\Phi}_2\boldsymbol{V}^a$ *and* $\boldsymbol{\Phi}_2\boldsymbol{V}^b$. *Assuming* $\boldsymbol{\Phi}_2\boldsymbol{V}^a$ *has full-column rank, the approximation error satisfies*

$$\|(\mathcal{I} - \mathcal{P}_{Y_2})\boldsymbol{X}_1\|_F^2 \leq \|\boldsymbol{\Sigma}^b\|_F^2 + \|\boldsymbol{\Sigma}^b(\boldsymbol{\Phi}_2\boldsymbol{V}^b)(\boldsymbol{\Phi}_2\boldsymbol{V}^a)^\dagger\|_F^2.$$

The above theorem gives us the following result

$$\|(\mathcal{I} - \mathcal{P}_{Y_2})\boldsymbol{X}_1\|_F \leq \|\boldsymbol{\Sigma}^b\|_F[1 + \|(\boldsymbol{\Phi}_2\boldsymbol{V}^a)^\dagger\|^2.\|\boldsymbol{\Phi}_2\boldsymbol{V}^b\|^2]^{1/2}.$$

Using Lemma 6.2.3, we have

$$\|(\boldsymbol{\Phi}_2\boldsymbol{V}^a)^\dagger\|^2 \leq \frac{1}{\left(1/\sqrt{2}\right)^2} = 2.$$

Also,

$$\|\boldsymbol{\Phi}_2\boldsymbol{V}^b\| = \|\boldsymbol{\Phi}_2\boldsymbol{V}^b\| \leq \|\boldsymbol{V}^b\|\|\boldsymbol{P}\boldsymbol{D}\| = \sqrt{\frac{W}{\Omega}},$$

which means that

$$\|(\mathcal{I} - \mathcal{P}_{Y_2})\boldsymbol{X}_1\|_F \leq \sqrt{1 + 2\frac{W}{\Omega}}\left(\sum_{j>R}\sigma_j^2\right)^{1/2}.$$

Combining the above bound with Theorem 6.2.1, and Theorem 6.2.4, we obtain the result in Theorem 6.1.4.

6.2.3 The row- and column-sensing matrices preserve geometry

Our first set of lemmas suggest that the all of the row, and column sensing matrices that arise in the discrete formulation of the proposed sampling schemes preserve the geometry of the subspace under consideration.

Lemma 6.2.1 (Gaussian matrix $\boldsymbol{\Phi}_1$ preserves geometry; Proposition 10.4 in [47])**.** *Fix a* $M \times R$ *orthonormal matrix* $\boldsymbol{U}$, *and draw a* $\Delta \times M$ *Gaussian matrix* $\boldsymbol{\Phi}_1$. *For*

a positive parameter β, select the sample size

$$\Delta \geq R + C\beta \log W$$

with $\beta \geq 1$. Then,

$$\sigma_R(\boldsymbol{\Phi}_1 \boldsymbol{U}) \geq C\frac{\sqrt{R + \beta \log W}}{\beta \log W}$$

with probability at least $1 - O(W^{-\beta})$.

Lemma 6.2.2 (The *random sampling* matrix $\boldsymbol{\Phi}_2 = \sqrt{\frac{W}{\Omega}}\mathcal{R}_\Gamma$ preserves geometry;Theorem 3.1 in [94])**.** *Fix a $W \times R$ orthonormal matrix $\boldsymbol{V}$, and draw an $W \times \Omega$ SRFT matrix $\boldsymbol{\Phi}_2$. For a positive parameter β, select the sample size*

$$C\beta\mu_0^2 R \log W \leq \Omega \leq W.$$

Then,

$$0.707 \leq \sigma_R(\boldsymbol{\Phi}_2 \boldsymbol{V}) \quad \textit{and} \quad \sigma_1(\boldsymbol{\Phi}_2 \boldsymbol{V}) \leq 1.25$$

with probability at least $1 - O(W^{-\beta})$ for $\beta > 1$.

We will extend the results above, and will show that the matrix $\boldsymbol{\Phi}_2 = \boldsymbol{PD}$ that arises in the column sensing of $\boldsymbol{X}_1$ in Architecture 2 also preserves the geometry.

Lemma 6.2.3 (The *modulate, filter, and integrate* matrix $\boldsymbol{\Phi}_2 = \boldsymbol{PD}$ preserves geometry)**.** *Let $\boldsymbol{V}$ be a $W \times R$ matrix with orthonormal columns. Let μ_0^2 be the coherence of matrix $\boldsymbol{V}$. For a positive parameter β, select the sample size*

$$\Omega \geq C\beta\mu_0^2 R \log^2 W.$$

Create a matrix $\boldsymbol{\Phi}_2$ of size $\Omega \times W$ as defined before. Then

$$0.707 \leq \sigma_R(\boldsymbol{\Phi}_2 \boldsymbol{V}), \quad \sigma_1(\boldsymbol{\Phi}_2 \boldsymbol{V}) \leq 1.25,$$

with probability at least $1 - O(W^{-\beta})$ for $\beta > 1$.

Proof. The column sensing matrix $\boldsymbol{\Phi}_2$ is

$$\boldsymbol{\Phi}_2 = \boldsymbol{P}\boldsymbol{D} = \sum_{\omega=1}^{\Omega} \sum_{k \sim \mathcal{B}_\omega} d[k] \boldsymbol{e}_\omega \bar{\boldsymbol{e}}_k^*,$$

where $\{\boldsymbol{e}_\omega\}_{1 \le \omega \le \Omega}$, and $\{\bar{\boldsymbol{e}}_k\}_{1 \le k \le W}$ are the standard basis vectors of length Ω, and W, respectively. Also $\{d[k]\}_{1 \le k \le W}$ are independent binary random variables. Let $\{\bar{\boldsymbol{v}}_\omega\}_{1 \le \omega \le W}$ denote the rows of $\boldsymbol{V}$. Then, we can write

$$\boldsymbol{\Phi}_2 \boldsymbol{V} = \sum_{\omega=1}^{\Omega} \sum_{k \sim \mathcal{B}_\omega} d[k] \boldsymbol{e}_\omega \bar{\boldsymbol{v}}_k^*,$$

which means

$$\begin{aligned}(\boldsymbol{\Phi}_2 \boldsymbol{V})^* (\boldsymbol{\Phi}_2 \boldsymbol{V}) &= \sum_{\omega, \omega'=1}^{\Omega} \sum_{k, k' \sim \mathcal{B}_\omega} d[k] d[k'] \langle \boldsymbol{e}_\omega, \boldsymbol{e}_{\omega'} \rangle \bar{\boldsymbol{v}}_{k'} \bar{\boldsymbol{v}}_k^* \\ &= \sum_{\omega=1}^{\Omega} \sum_{k, k' \sim \mathcal{B}_\omega} d[k] d[k'] \bar{\boldsymbol{v}}_{k'} \bar{\boldsymbol{v}}_k^*,\end{aligned}$$

where the last equality follows from the fact that $\langle \boldsymbol{e}_\omega, \boldsymbol{e}_{\omega'} \rangle = 1$ only when $\omega = \omega'$. Let

$$\boldsymbol{Z}_\omega = \sum_{k, k' \sim \mathcal{B}_\omega} d[k] d[k'] \bar{\boldsymbol{v}}_{k'} \bar{\boldsymbol{v}}_k^*; \tag{6.2.2}$$

note that $\mathrm{E}\, \boldsymbol{Z}_\omega = \sum_{k \sim \mathcal{B}_\omega} \bar{\boldsymbol{v}}_{k'} \bar{\boldsymbol{v}}_k^*$. To bound the eigenvalues of the following sum of independent random matrices:

$$\sum_{\omega=1}^{\Omega} \boldsymbol{Z}_\omega = \sum_{\omega=1}^{\Omega} \sum_{k, k' \sim \mathcal{B}_\omega} d[k] d[k'] \bar{\boldsymbol{v}}_{k'} \bar{\boldsymbol{v}}_k^*,$$

we will use the matrix Bernstein's Inequality. The variance is

$$\begin{aligned}\left\| \sum_{\omega=1}^{\Omega} \mathrm{E}\, \boldsymbol{Z}_\omega \boldsymbol{Z}_\omega^* \right\| &\le \left\| \sum_{k \sim \mathcal{B}_\omega} \bar{\boldsymbol{v}}_k \bar{\boldsymbol{v}}_k^* \right\| \left\| \sum_{\omega=1}^{\Omega} \sum_{j \sim \mathcal{B}_\omega} \bar{\boldsymbol{v}}_j \bar{\boldsymbol{v}}_j^* \right\| + 2 \sum_{k \sim \mathcal{B}_\omega} \|\bar{\boldsymbol{v}}_k^*\|_2^2 \left\| \sum_{\omega=1}^{\Omega} \sum_{k' \sim \mathcal{B}_\omega} \bar{\boldsymbol{v}}_{k'} \bar{\boldsymbol{v}}_{k'}^* \right\| \\ &\le 3 \sum_{k \sim \mathcal{B}_\omega} \|\bar{\boldsymbol{v}}_k^*\|_2^2 \\ &\le 3 \mu_0^2 \frac{R}{\Omega}\end{aligned}$$

where the first inequality follows from Lemma 6.2.4, and the second inequality is the result of the fact that

$$\sum_{\omega=1}^{\Omega} \sum_{k \sim \mathcal{B}_\omega} \bar{\boldsymbol{v}}_k \bar{\boldsymbol{v}}_k^* = \boldsymbol{V}^* \boldsymbol{V} = \boldsymbol{I},$$

and

$$\left\| \sum_{k\sim\mathcal{B}_\omega} \bar{\boldsymbol{v}}_k \bar{\boldsymbol{v}}_k^* \right\| \leq \sum_{k\sim\mathcal{B}_\omega} \|\bar{\boldsymbol{v}}_k\|_2^2,$$

which results from triangle inequality and that the summands are rank-1 matrices. To calculate the Orlicz-1 norm of $\boldsymbol{Z}_\omega$, we begin with writing

$$\boldsymbol{Z}_\omega = \boldsymbol{z}_\omega \boldsymbol{z}_\omega^*.$$

First, we show that $\boldsymbol{z}_\omega$ is a subgaussian vector, i.e., $\|\boldsymbol{z}_\omega\|_{\psi_2} < \infty$. The Orlicz-2 norm of the vector $\boldsymbol{z}_\omega$ is

$$\begin{aligned} \left\| \sum_{k\sim\mathcal{B}_\omega} d[k]\bar{\boldsymbol{v}}_k \right\|_{\psi_2}^2 &\leq C \sum_{k\sim\mathcal{B}_\omega} \|d[k]\bar{\boldsymbol{v}}_k\|_{\psi_2}^2 \\ &= C \sum_{k\sim\mathcal{B}_\omega} \|\bar{\boldsymbol{v}}_k\|_2^2 \leq C\mu_0^2 \frac{R}{\Omega}, \end{aligned}$$

where the inequality follows from the independence of $\{d[k]\}_{k\sim\mathcal{B}_\omega}$. Since $\boldsymbol{z}_\omega$ is subgaussian, it follows from $\|\boldsymbol{Z}_\omega\| = \|\boldsymbol{z}_\omega\|_2^2$ that $\boldsymbol{Z}_\omega = \boldsymbol{z}_\omega \boldsymbol{z}_\omega^*$ is subexponential, and $\|\boldsymbol{Z}_\omega\|_{\psi_1} \leq \|\boldsymbol{z}_\omega\|_{\psi_2}^2$. Hence,

$$\|\boldsymbol{Z}_\omega\|_{\psi_1} \leq \|\boldsymbol{z}_\omega\|_{\psi_2}^2 \leq C\mu_0^2 \frac{R}{\Omega}.$$

Now use the Bernstein bound, and select $t = \beta \log R$, we obtain

$$\|(\boldsymbol{\Phi}_2\boldsymbol{V})^*(\boldsymbol{\Phi}_2\boldsymbol{V}) - \boldsymbol{I}\| \leq \max\left\{ \sqrt{3\mu_0^2 \frac{R}{\Omega}} \sqrt{\beta \log W}, \mu_0^2 \frac{R}{\Omega} \beta \log(\mu_0^2 R) \log W \right\}.$$

Select $\Omega \geq C\beta\mu_0^2 R \log^2 W$, which gives

$$\|(\boldsymbol{\Phi}_2\boldsymbol{V})^*(\boldsymbol{\Phi}_2\boldsymbol{V}) - \boldsymbol{I}\| \leq 0.5,$$

which further means

$$0.5 \leq \lambda_{\min}((\boldsymbol{\Phi}_2\boldsymbol{V})^*(\boldsymbol{\Phi}_2\boldsymbol{V})) \leq \lambda_{\max}((\boldsymbol{\Phi}_2\boldsymbol{V})^*(\boldsymbol{\Phi}_2\boldsymbol{V})) \leq 1.5$$

holds with probability at least $1 - O(W^{-\beta})$. □

We used the following lemma in the proof of Lemma 6.2.3.

Lemma 6.2.4. *Let $\boldsymbol{Z}_\omega$ be the matrix as defined in* (6.2.2)*. Then*

$$\mathrm{E}\,\boldsymbol{Z}_\omega \boldsymbol{Z}_\omega^* = \left(\sum_{k\sim\mathcal{B}_\omega} \bar{\boldsymbol{v}}_k \bar{\boldsymbol{v}}_k^*\right)\left(\sum_{j\sim\mathcal{B}_\omega} \bar{\boldsymbol{v}}_j \bar{\boldsymbol{v}}_j^*\right)^* + 2\sum_{k\sim\mathcal{B}_\omega} \|\bar{\boldsymbol{v}}_k^*\|_2^2 \cdot \sum_{k'\sim\mathcal{B}_\omega} \bar{\boldsymbol{v}}_{k'} \bar{\boldsymbol{v}}_{k'}^*.$$

Proof.

$$\mathrm{E}\,\boldsymbol{Z}_\omega \boldsymbol{Z}_\omega^* = \mathrm{E}\left(\sum_{k,k'\sim\mathcal{B}_\omega} d[k]d[k']\bar{\boldsymbol{v}}_{k'}\bar{\boldsymbol{v}}_k^*\right)\left(\sum_{j,j'\sim\mathcal{B}_\omega} d[j]d[j']\bar{\boldsymbol{v}}_{j'}\bar{\boldsymbol{v}}_j^*\right)^*.$$

The expectation is non-zero when $k = k', j = j'$, or $k = j, k' = j'$, or $k = j', k' = j$. In each of these cases the expectation is bounded by the same upper bound. First, consider the case $k = k', j = j'$

$$\mathrm{E}\,\boldsymbol{Z}_\omega \boldsymbol{Z}_\omega^* = \left(\sum_{k\sim\mathcal{B}_\omega} \bar{\boldsymbol{v}}_k \bar{\boldsymbol{v}}_k^*\right)\left(\sum_{j\sim\mathcal{B}_\omega} \bar{\boldsymbol{v}}_j \bar{\boldsymbol{v}}_j^*\right)^*;$$

second, the case $k = j, k' = j'$

$$\begin{aligned}\mathrm{E}\,\boldsymbol{Z}_\omega \boldsymbol{Z}_\omega^* &= \sum_{k,k'\sim\mathcal{B}_\omega} (\bar{\boldsymbol{v}}_{k'}\bar{\boldsymbol{v}}_k^*)(\bar{\boldsymbol{v}}_{k'}\bar{\boldsymbol{v}}_k^*)^* \\ &= \sum_{k\sim\mathcal{B}_\omega} \|\bar{\boldsymbol{v}}_k^*\|_2^2 \cdot \sum_{k'\sim\mathcal{B}_\omega} \bar{\boldsymbol{v}}_{k'}\bar{\boldsymbol{v}}_{k'}^*;\end{aligned}$$

third, the case $k = j, k' = j'$ is exactly the same as the second case. Adding all three cases, the result in the lemma follows. □

6.2.4 Analysis of the matrix least squares

In this section, we establish that the solution $\tilde{\boldsymbol{X}}$ to the least-squares program (6.0.7) obeys

Theorem 6.2.4. *Let $\boldsymbol{Y}_1$, and $\boldsymbol{Y}_2$ be the row- and column-space measurements, as in* (6.0.3), (6.0.4)*, respectively, of an unknown matrix $\boldsymbol{X} = \boldsymbol{U}\boldsymbol{\Sigma}\boldsymbol{V}^*$. Suppose, the pseudo inverses $(\boldsymbol{\Phi}_1\boldsymbol{U})^\dagger$, and $(\boldsymbol{\Phi}_2\boldsymbol{V})^\dagger$ are well defined. Then the solution $\tilde{\boldsymbol{X}} = \boldsymbol{U}_2\boldsymbol{A}\boldsymbol{V}_1^*$, as in* (6.0.6) *of the least-squares program* (6.0.7) *obeys the following main result.*

$$\|\tilde{\boldsymbol{X}} - \boldsymbol{X}\|_F \leq 3\|(\mathcal{I} - \mathcal{P}_{Y_2})\boldsymbol{X}\|_F + \|\boldsymbol{X}(\mathcal{I} - \mathcal{P}_{Y_1})\|_F.$$

Proof of this theorem follows the template of the proof in [101], which establishes a similar result for a least-squares program (6.0.8). The combination of following three lemmas establishes the above theorem.

Lemma 6.2.5. *Suppose* $\boldsymbol{Q}_1, \boldsymbol{P}_1 : M \times R$, *and* $\boldsymbol{Q}_2, \boldsymbol{P}_2 : W \times R$. *Then under the conditions of Lemma 6.2.1, 6.2.2, 6.2.3, there exist* $\boldsymbol{\Theta}_1 : M \times \Delta$, *and* $\boldsymbol{\Theta}_2 : W \times \Omega$ *such that*

$$\boldsymbol{\Theta}_1 \boldsymbol{\Phi}_1 \boldsymbol{Q}_1 = \boldsymbol{Q}_1, \quad \boldsymbol{\Theta}_2 \boldsymbol{\Phi}_2 \boldsymbol{Q}_2 = \boldsymbol{Q}_2$$
$$\boldsymbol{\Theta}_1 \boldsymbol{\Phi}_1 \boldsymbol{P}_1 = \boldsymbol{P}_1, \quad \boldsymbol{\Theta}_2 \boldsymbol{\Phi}_2 \boldsymbol{P}_2 = \boldsymbol{P}_2,$$

and

$$\|\boldsymbol{\Theta}_1\| \leq 0.5, \quad \|\boldsymbol{\Theta}_2\| \leq 0.5.$$

Proof. Let $\boldsymbol{U} : M \times J_1, \boldsymbol{V} : W \times J_2$ be the matrices whose columns form the orthonormal basis of the subspaces spanned by the columns of $[\boldsymbol{Q}_1; \boldsymbol{P}_1]$, and $[\boldsymbol{Q}_2; \boldsymbol{P}_2]$, respectively, where $[\boldsymbol{A}; \boldsymbol{B}]$ is the matrix formed by concatenating the matrices $\boldsymbol{A}$, and $\boldsymbol{B}$. This implies that $J_1, J_2 \leq 2R$. Using the results of lemmas, we have

$$\sigma_{\min}(\boldsymbol{\Phi}_1 \boldsymbol{V}) \geq \frac{1}{\sqrt{2}}, \quad \sigma_{\min}(\boldsymbol{\Phi}_2 \boldsymbol{U}) \geq \frac{1}{\sqrt{2}}$$

holds with high probability. This means

$$\boldsymbol{\Theta}_1 := \boldsymbol{U} \left((\boldsymbol{\Phi}_1 \boldsymbol{U})^* (\boldsymbol{\Phi}_1 \boldsymbol{U}) \right)^{-1} (\boldsymbol{\Phi}_1 \boldsymbol{U})^*, \quad \boldsymbol{\Theta}_2 := \boldsymbol{V} \left((\boldsymbol{\Phi}_2 \boldsymbol{V})^* (\boldsymbol{\Phi}_2 \boldsymbol{V}) \right)^{-1} (\boldsymbol{\Phi}_2 \boldsymbol{V})^*$$

are well defined. It follows from above that

$$\boldsymbol{\Theta}_1 \boldsymbol{\Phi}_1 \boldsymbol{U} = \boldsymbol{U}, \quad \boldsymbol{\Theta}_2 \boldsymbol{\Phi}_2 \boldsymbol{V} = \boldsymbol{V},$$

which directly gives the first part of the lemma. The second part follows from the definition of $\boldsymbol{\Theta}_1$, and $\boldsymbol{\Theta}_2$. □

Lemma 6.2.6. *Given the set of matrices defined earlier in Lemma 6.2.5; suppose now, a matrix* $\boldsymbol{A} : R \times R$ *minimizes the quantity*

$$\|\boldsymbol{\Phi}_1 \boldsymbol{Q}_1 \boldsymbol{A} - \boldsymbol{\Phi}_1 \boldsymbol{P}_1\| + \|\boldsymbol{A}\boldsymbol{Q}_2^* \boldsymbol{\Phi}_2^* - \boldsymbol{P}_2^* \boldsymbol{\Phi}_2^*\|,$$

and $\boldsymbol{Y} : R \times R$ *minimizes the quantity*

$$\|\boldsymbol{Q}_1 \boldsymbol{Y} - \boldsymbol{P}_1\| + \|\boldsymbol{Y}\boldsymbol{Q}_2^* - \boldsymbol{P}_2^*\|.$$

Then,

$$\|\boldsymbol{\Phi}_1 \boldsymbol{Q}_1 \boldsymbol{A} - \boldsymbol{\Phi}_1 \boldsymbol{P}_1\| + \|\boldsymbol{A}\boldsymbol{Q}_2^* \boldsymbol{\Phi}_2^* - \boldsymbol{P}_2^* \boldsymbol{\Phi}_2^*\| \leq \|\boldsymbol{Q}_1 \boldsymbol{Y} - \boldsymbol{P}_1\| + \|\boldsymbol{Y}\boldsymbol{Q}_2^* - \boldsymbol{P}_2^*\|$$

holds with high probability.

Proof. Using Lemma 6.2.5, we have that

$$\begin{aligned}
\|\boldsymbol{Q}_1 \boldsymbol{A} - \boldsymbol{P}_1\| + \|\boldsymbol{A}\boldsymbol{Q}_2^* - \boldsymbol{P}_2^*\| &= \|\boldsymbol{\Theta}_1 \boldsymbol{\Phi}_1 \boldsymbol{Q}_1 \boldsymbol{A} - \boldsymbol{\Theta}_1 \boldsymbol{\Phi}_1 \boldsymbol{P}_1\| + \|\boldsymbol{A}\boldsymbol{Q}_2^* \boldsymbol{\Phi}_2^* \boldsymbol{\Theta}_2^* - \boldsymbol{P}_2^* \boldsymbol{\Phi}_2^* \boldsymbol{\Theta}_2^*\| \\
&\leq 0.5\|\boldsymbol{\Phi}_1 \boldsymbol{Q}_1 \boldsymbol{A} - \boldsymbol{\Phi}_1 \boldsymbol{P}_1\| + 0.5\|\boldsymbol{A}\boldsymbol{Q}_2^* \boldsymbol{\Phi}_2^* - \boldsymbol{P}_2^* \boldsymbol{\Phi}_2^*\| \\
&\leq 0.5\|\boldsymbol{\Phi}_1 \boldsymbol{Q}_1 \boldsymbol{Y} - \boldsymbol{\Phi}_1 \boldsymbol{P}_1\| + 0.5\|\boldsymbol{Y}\boldsymbol{Q}_2^* \boldsymbol{\Phi}_2^* - \boldsymbol{P}_2^* \boldsymbol{\Phi}_2^*\|,
\end{aligned}$$

where the second inequality follows because $\boldsymbol{A}$ minimizes the right hand side. It follows form the fact that $\boldsymbol{A}$ minimizes the first inequality. We can find matrices $\boldsymbol{G}_1 : J_1 \times R$, and $\boldsymbol{G}_2 : R \times J_2$ such that

$$\boldsymbol{Q}_1 \boldsymbol{Y} = \boldsymbol{U}\boldsymbol{G}_1, \quad \boldsymbol{Y}\boldsymbol{Q}_2^* = \boldsymbol{G}_2 \boldsymbol{V}^*,$$

and matrices $\boldsymbol{C}_1 : J_1 \times R$, and $\boldsymbol{C}_2 : R \times J_2$ such that

$$\boldsymbol{P}_1 = \boldsymbol{U}\boldsymbol{C}_1, \quad \boldsymbol{P}_2^* = \boldsymbol{C}_2 \boldsymbol{V}^*$$

hold. This gives

$$\begin{aligned}
\|\boldsymbol{\Phi}_1 \boldsymbol{Q}_1 \boldsymbol{Y} - \boldsymbol{\Phi}_1 \boldsymbol{P}_1\| + \|\boldsymbol{Y}\boldsymbol{Q}_2^* \boldsymbol{\Phi}_2^* - \boldsymbol{P}_2^* \boldsymbol{\Phi}_2^*\| &= \|\boldsymbol{\Phi}_1 \boldsymbol{U}\boldsymbol{G}_1 - \boldsymbol{\Phi}_1 \boldsymbol{U}\boldsymbol{C}_1\| + \|\boldsymbol{G}_2 \boldsymbol{V}^* \boldsymbol{\Phi}_2^* - \boldsymbol{C}_2 \boldsymbol{V}^* \boldsymbol{\Phi}_2^*\| \\
&\leq 2\|\boldsymbol{G}_1 - \boldsymbol{C}_1\| + 2\|\boldsymbol{G}_2 - \boldsymbol{C}_2\| \\
&= 2\|\boldsymbol{Q}_1 \boldsymbol{Y} - \boldsymbol{P}_1\| + 2\|\boldsymbol{Y}\boldsymbol{Q}_2^* - \boldsymbol{P}_2^*\|.
\end{aligned}$$

□

Lemma 6.2.7. *Using the same notation for matrices as introduced in Lemma 6.2.5. If matrix $\boldsymbol{A} : R \times R$ minimizes the quantity*

$$\|\boldsymbol{\Phi}_1 \boldsymbol{Q}_1 \boldsymbol{A} - \boldsymbol{\Phi}_1 \boldsymbol{P}_1\| + \|\boldsymbol{A}\boldsymbol{Q}_2^* \boldsymbol{\Phi}_2^* - \boldsymbol{P}_2^* \boldsymbol{\Phi}_2^*\|,$$

then

$$\|\tilde{\boldsymbol{X}} - \boldsymbol{X}\| \leq 3\|(\boldsymbol{I} - \boldsymbol{U}_2\boldsymbol{U}_2^*)\boldsymbol{X}\| + \|\boldsymbol{X}(\boldsymbol{I} - \boldsymbol{V}_1\boldsymbol{V}_1^*)\|.$$

Proof. It follows from the triangle inequality that

$$\begin{aligned}
\|\boldsymbol{U}_2\boldsymbol{A}\boldsymbol{V}_1^* - \boldsymbol{X}\| &\leq \|\boldsymbol{U}_2\boldsymbol{A}\boldsymbol{V}_1^* - \boldsymbol{X}\boldsymbol{V}_1\boldsymbol{V}_1^*\| + \|\boldsymbol{U}_2\boldsymbol{A}\boldsymbol{V}_1^* - \boldsymbol{U}_2\boldsymbol{U}_2^*\boldsymbol{X}\| + \\
&\quad + \|\boldsymbol{U}_2\boldsymbol{A}\boldsymbol{V}_1^* - \boldsymbol{X}\boldsymbol{V}_1\boldsymbol{V}_1^*\| + \|\boldsymbol{U}_2\boldsymbol{U}_2^*\boldsymbol{X} - \boldsymbol{X}\| \\
&\leq 2\|\boldsymbol{U}_2\boldsymbol{A}\boldsymbol{V}_1^* - \boldsymbol{X}\boldsymbol{V}_1\boldsymbol{V}_1^*\| + \|\boldsymbol{U}_2\boldsymbol{A}\boldsymbol{V}_1^* - \boldsymbol{U}_2\boldsymbol{U}_2^*\boldsymbol{X}\| + \|\boldsymbol{U}_2\boldsymbol{U}_2^*\boldsymbol{X} - \boldsymbol{X}\| \\
&= 2\|\boldsymbol{U}_2\boldsymbol{A} - \boldsymbol{X}\boldsymbol{V}_1\| + \|\boldsymbol{A}\boldsymbol{V}_1^* - \boldsymbol{U}_2^*\boldsymbol{X}\| + \|\boldsymbol{U}_2\boldsymbol{U}_2^*\boldsymbol{X} - \boldsymbol{X}\|.
\end{aligned}$$

Since $\boldsymbol{A} = \boldsymbol{U}_2^*\boldsymbol{X}\boldsymbol{V}_1$ minimizes the above expression, the result of Lemma 6.2.6 implies

$$\begin{aligned}
\|\boldsymbol{U}_2\boldsymbol{A}\boldsymbol{V}_1^* - \boldsymbol{X}\|_F &\leq 2\|\boldsymbol{U}_2\boldsymbol{U}_2^*\boldsymbol{X}\boldsymbol{V}_1 - \boldsymbol{X}\boldsymbol{V}_1\| + \|\boldsymbol{U}_2^*\boldsymbol{X}\boldsymbol{V}_1\boldsymbol{V}_1^* - \boldsymbol{U}_2^*\boldsymbol{X}\| + \|\boldsymbol{U}_2\boldsymbol{U}_2^*\boldsymbol{X} - \boldsymbol{X}\| \\
&\leq 2\|\boldsymbol{U}_2\boldsymbol{U}_2^*\boldsymbol{X} - \boldsymbol{X}\| + \|\boldsymbol{X}\boldsymbol{V}_1\boldsymbol{V}_1^* - \boldsymbol{X}\| + \|\boldsymbol{U}_2\boldsymbol{U}_2^*\boldsymbol{X} - \boldsymbol{X}\| \\
&\leq 3\|\boldsymbol{U}_2\boldsymbol{U}_2^*\boldsymbol{X} - \boldsymbol{X}\| + \|\boldsymbol{X}\boldsymbol{V}_1\boldsymbol{V}_1^* - \boldsymbol{X}\|.
\end{aligned}$$

Since $\boldsymbol{V}_1$, and $\boldsymbol{U}_2$ are orthobases for the row and the column space of $\boldsymbol{Y}_1$, and $\boldsymbol{Y}_2$, as in (6.0.5), then the orthogonal projection $\mathcal{P}_{Y_1}$ on the row space of $\boldsymbol{Y}_1$ is $\mathcal{P}_{Y_1} = \boldsymbol{V}_1\boldsymbol{V}_1^*$, and the orthogonal projection $\mathcal{P}_{Y_2}$ on the column space of $\boldsymbol{Y}_2$ is $\mathcal{P}_{Y_2} = \boldsymbol{U}_2\boldsymbol{U}_2^*$. Hence, we have

$$\|\tilde{\boldsymbol{X}} - \boldsymbol{X}\|_F \leq 3\|(\mathcal{I} - \mathcal{P}_{Y_2})(\boldsymbol{X})\|_F + \|(\boldsymbol{X})(\mathcal{I} - \mathcal{P}_{Y_1})\|_F,$$

which proves the claim. □

CHAPTER VII

FUTURE WORK

The research results in this thesis open interesting future research directions that are outlined very briefly in the paragraphs below.

7.1 Multi-channel blind deconvolution

Our novel approach to address the blind deconvolution problem in Chapter 3 may provide an new perspective to tackle the related problems such as the blind source separation, dictionary learning and the multiple channel estimation. An important research direction with a lot of room for new results is the multi-channel blind deconvolution methods. We are currently working on the extension of our blind deconvolution method to the case when instead of observing a single convolution $\boldsymbol{y}(t) = \boldsymbol{w}(t) * \boldsymbol{x}(t)$, we are observing a sum of many convolutions $\boldsymbol{y}(t) = \boldsymbol{w}_1(t) * \boldsymbol{x}_1(t) + \cdots + \boldsymbol{w}_K(t) * \boldsymbol{x}_K(t)$—this sort of observation model arises in the important MIMO communications as shown in Figure 2(b). In this case, the deconvolution task is even more challenging as we not only want to deconvolve the unknown signals but also want to separate the convolved signals by observing only their sum.

7.2 Multiple channel estimation

Another interesting version of multi-channel blind deconvolution problem and a subject of ongoing research is that suppose we observe $y_1(t) = s(t) * h_1(t), y_2(t) = s(t) * h_2(t), \cdots, y_K(t) = s(t) * h_K(t)$; convolutions of K linear time-invariant channels $h_1(t), h_2(t), \cdots, h_K(t)$ with a common noise source $s(t)$, and our goal is to recover the impulse responses of the channels without the knowledge of the source signal $s(t)$. The problem is depicted in Figure 2(a). The problem can be framed as a low-rank

matrix recovery problem from a limited number of measurements. One application of this problem arises in under water communications.

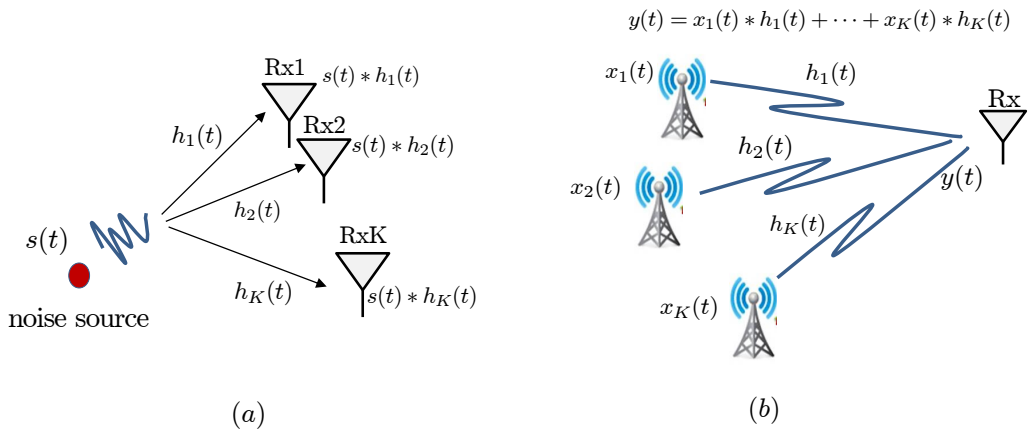

Figure 38: Multi-channel blind deconvolution. (a) Multiple channels driven by a single noise source. We observe the convolution of the unknown noise with each of the unknown channel and want to recover all the unknown channel responses $h_1(t), \cdots, h_K(t)$. (b) MISO and MIMO communications in unknown channels. We observe at the receiver the sum of the convolutions of different transmitted messages $x_1(t), \cdots, x_K(t)$ with channels $h_1(t), \cdots, h_K(t)$.

7.3 Parallel MRI

Blind deconvolution arises naturally in image deblurring applications. An important scope of research in this direction exists in parallel magnetic resonance imaging (MRI), where we observe a series of convolutions of an unknown image of an organ with several unknown blur kernels of magnetic coils. The recovery problem of original image from multiple convolutions can be framed as a rank-1 matrix recovery problem. Hence, this problem is actually an extension of our blind deconvolution method.

7.4 Solving systems of bilinear equations

The methodology adopted to convert the non-linear problem of blind deconvolution into a rank-1 matrix recovery problem is referred to as 'lifting'. In general, the exact same strategy can be employed to solve the systems of bilinear, and quadratic equations, i.e., we can convert the problem of solving bilinear equations into a linear

rank-1 matrix recovery problem. The reason is simple: taking the outer product of $\boldsymbol{w}$ and $\boldsymbol{x}$ produces a rank-1 matrix that contains all the different combinations of the entries of $\boldsymbol{w}$ multiplied with the entries in $\boldsymbol{x}$:

$$\boldsymbol{w}\boldsymbol{x}^* = \begin{bmatrix} w[1]x[1] & w[1]x[2] & \cdots & w[1]x[L] \\ w[2]x[1] & w[2]x[2] & \cdots & w[2]x[L] \\ \vdots & \vdots & & \vdots \\ w[L]x[1] & w[L]x[2] & \cdots & w[L]x[L] \end{bmatrix}.$$

Then any bilinear equation can be written as a linear combination of the entries in this matrix, and any system of equations can be written as a linear operator acting on this matrix. Our work on blind deconvolution provides one set of conditions under which the recovery is successful using lifting. The problem may also be solvable under other more general set of conditions on the subspaces and the unknown signals being convolved, which will result in a general framework under which we can solve systems of bilinear equations using lifting.

7.5 Sampling architectures for sparse and correlated signals

A rigorous stable recovery analysis in the presence of noise, for the sampling architectures presented in Chapter 6, is an open problem and requires further investigation. Our discussion and results relating to the sampling architectures focus on signals that are correlated. Another interesting signal structure is sparse and correlated signals that arise in some other interesting applications. Designing implementable sampling architectures for the efficient acquisition of sparse and correlated signals, and the derivation of corresponding sampling theorems for each sampling architecture are other open research problems in this direction.

REFERENCES

[1] "Multi-neuron recordings in primary visual cortex." `http://crcns.org/data-sets/vc/pvc-3`. Accessed: 3/21/2013.

[2] Ahmed, A. and Romberg, J., "Compressive multiplexers for correlated signals," in *Proc. IEEE Asilomar Conf. on Sig. Sys. and Comp.*, (Pacific Grove, CA), November 2012.

[3] Ahmed, A. and Romberg, J., "Compressive sampling of correlated signals," in *Proc. IEEE Asilomar Conf. on Sig. Sys. and Comp.*, (Pacific Grove, CA), November.

[4] Ahmed, A. and Recht, B. and Romberg, J., "Blind deconvolution using convex programing," *Submitted to IEEE Transactions on Information Theory*, 2012.

[5] Ames, B.P.W., *Convex relaxation for the planted clique, biclique, and clustering problems*. PhD thesis, University of Waterloo, 2011.

[6] Applebaum, L., Bajwa, W., Duarte, M. F., and Calderbank, R., "Asynchronous code-division random access using convex optimization," *Physical Communication*, vol. 5, pp. 129–147, June 2011.

[7] Asif, M. S., Mantzel, W., and Romberg, J., "Random channel coding and blind deconvolution," in *Proc. IEEE Allerton Conf. on Comm., Control, and Comp.*, (Monticello, IL), pp. 1021–1025, September 2009.

[8] Asif, M.S. and Mantzel, W. and Romberg, J., "Channel protection: Random coding meets sparse channels," in *IEEE Information Theory Workshop. ITW.*, pp. 348–352, IEEE, 2009.

[9] Becker, S. and Candes, E.J. and Grant, M., "Tfocs v1. 1 user guide," 2012.

[10] Becker, S.R., *Practical Compressed Sensing: Modern Data Acquisition and Signal Processing*. PhD thesis, California Institute of Technology, 2011.

[11] Becker, S.R. and Candès, E.J. and Grant, M.C., "Templates for convex cone problems with applications to sparse signal recovery," *Mathematical Programming Computation*, pp. 1–54, 2010.

[12] Bennett, J. and Elkan, C. and Liu, B. and Smyth, P. and Tikk, D., "Kdd cup and workshop 2007," *ACM SIGKDD Explorations Newsletter*, vol. 9, no. 2, pp. 51–52, 2007.

[13] Bertsekas, D.P. and Nedi, A. and Ozdaglar, A.E. and others, *Convex analysis and optimization*. Athena Scientific, 2003.

[14] Blanche, T.J. and Spacek, M.A. and Hetke, J.F. and Swindale, N.V., "Polytrodes: high-density silicon electrode arrays for large-scale multiunit recording," *Journal of neurophysiology*, vol. 93, no. 5, pp. 2987–3000, 2005.

[15] Burer, S. and Monteiro, R. D. C., "A nonlinear programming algorithm for solving semidefinite programs via low-rank factorization," *Mathematical Programming (Series B)*, vol. 95, pp. 329–357, 2003.

[16] Burer, S. and Monteiro, R. D. C., "Local minima and convergence in low-rank semidefinite programming," *Mathematical Programming*, vol. 103, no. 3, pp. 427–444, 2005.

[17] Cai, J., Candès, E., and Shen, Z., "A singular value thresholding algorithm for matrix completion," *SIAM Journal on Optimization*, vol. 20, no. 4, pp. 1956–1982, 2010.

[18] Candès, E. and Plan, Y., "Tight oracle bounds for low-rank matrix recovery from a minimal number of random measurements," *IEEE Trans. Inform. Theory*, vol. 57, no. 4, pp. 2342—2359, 2011.

[19] Candès, E. and Recht, B., "Exact matrix completion via convex optimization," *Found. of Comput. Math.*, vol. 9, no. 6, pp. 717–772, 2009.

[20] Candès, E. and Romberg, J., "Sparsity and incoherence in compressive sampling," *Inverse Problems*, vol. 23, pp. 969–986, June 2007.

[21] Candès, E., Strohmer, T., and Voroninski, V., "Phaselift: Exact and stable signal recovery from magnitude measurements via convex programming," *To appear in Comm. Pure Appl. Math.*, 2012.

[22] Candès, E. and Tao, T., "The power of convex relaxation: Near-optimal matrix completion," *IEEE Trans. Inform. Theory*, vol. 56, no. 5, pp. 2053–2080, 2010.

[23] Candès, E. J. and Tao, T., "Decoding by linear programming," *IEEE Trans. Inform. Theory*, vol. 51, pp. 4203–4215, December 2005.

[24] Candes, E., Li, X., Ma, Y., and Wright, J., "Robust principal component analysis?," *Arxiv preprint ArXiv:0912.3599*, 2009.

[25] Candès, E.J., "Compressive sampling," in *Proceedings oh the International Congress of Mathematicians: Madrid, August 22-30, 2006: invited lectures*, pp. 1433–1452, 2006.

[26] Candès, E.J. and Li, X., "Solving quadratic equations via phaselift when there are about as many equations as unknowns," *arXiv preprint arXiv:1208.6247*, 2012.

[27] Candès, E.J. and Plan, Y., "Matrix completion with noise," *Proceedings of the IEEE*, vol. 98, no. 6, pp. 925–936, 2010.

[28] Candès, E.J. and Romberg, J. and Tao, T., "Robust uncertainty principles: Exact signal reconstruction from highly incomplete frequency information," *IEEE Transactions on Information Theory*, vol. 52, no. 2, pp. 489–509, 2006.

[29] Candes, E.J. and Romberg, J.K. and Tao, T., "Stable signal recovery from incomplete and inaccurate measurements," *Communications on pure and applied mathematics*, vol. 59, no. 8, pp. 1207–1223, 2006.

[30] Candès, E.J. and Wakin, M.B., "An introduction to compressive sampling," *IEEE Signal Processing Magazine*, vol. 25, no. 2, pp. 21–30, 2008.

[31] Chan, T. and Wong, C. K., "Total variation blind deconvolution," *IEEE Trans. Image Proc.*, vol. 7, no. 3, pp. 370–375, 1998.

[32] Chan, W. L., Moravec, M. L., Baraniuk, R. G., and Mittleman, D. M., "Terahertz imaging with compressed sensing and phase retrieval," *Opt. Letters*, vol. 33, no. 9, pp. 974–976, 2008.

[33] Chawla, R. and Bandyopadhyay, A. and Srinivasan, V. and Hasler, P., "A 531 nw/mhz, 128× 32 current-mode programmable analog vector-matrix multiplier with over two decades of linearity," in *IEEE Proceedings of the Custom Integrated Circuits Conference.*, pp. 651–654, 2004.

[34] Coifman, R., Geshwind, F., and Meyer, Y., "Noiselets," *Appl. Comp. Harmonic Analysis*, vol. 10, no. 1, pp. 27–44, 2001.

[35] Dasgupta, S. and Gupta, A., "An elementary proof of a theorem of johnson and lindenstrauss," *Random Struct. and Alg.*, vol. 22, no. 1, pp. 60–65, 2003.

[36] Davenport, M.A. and Wakin, M.B., "Compressive sensing of analog signals using discrete prolate spheroidal sequences," *Applied and Computational Harmonic Analysis*, 2012.

[37] der Vaart, A. W. V. and Wellner, J. A., *Weak Convergence and Empirical Processes*. Springer, 1996.

[38] Ding, Z. and Kennedy, RA and Anderson, BDO and Johnson Jr, CR, "Ill-convergence of godard blind equalizers in data communication systems," *IEEE Transactions on Communications*, vol. 39, no. 9, pp. 1313–1327, 1991.

[39] Donoho, D.L., "Compressed sensing," *IEEE Transactions on Information Theory*, vol. 52, no. 4, pp. 1289–1306, 2006.

[40] Fazel, M., *Matrix rank minimization with applications*. PhD thesis, Stanford University, March 2002.

[41] Fazel, M. and Candes, E. and Recht, B. and Parrilo, P., "Compressed sensing and robust recovery of low rank matrices," in *42nd Asilomar Conference on Signals, Systems and Computers, 2008*, pp. 1043–1047, IEEE, 2008.

[42] Fazel, M. and Hindi, H. and Boyd, S.P., "A rank minimization heuristic with application to minimum order system approximation," in *Proceedings of the American Control Conference, 2001*, vol. 6, pp. 4734–4739, IEEE, 2001.

[43] Giannakis, G. B. and Tepedelenlioglu, C., "Basis expansion models and diversity techniques for blind indentification and equalization of time-varying channels," *Proc. IEEE*, vol. 86, pp. 1969–1986, October 1998.

[44] Gross, D., "Recovering low-rank matrices from few coefficients in any basis," *IEEE Trans. Inform. Theory*, vol. 57, no. 3, pp. 1548–1566, 2011.

[45] Gross, D., Liu, Y.-K., Flammia, S., Becker, S., and Eisert, J., "Quantum state tomography via compressed sensing," *Phys. Rev. Letters*, vol. 105, no. 15, 2010.

[46] H. Rauhut and J. Romberg and J. Tropp, "Restricted isometries for partial random circulant matrices," *Appl. and Comp. Harm. Analysis*, vol. 32, no. 2, pp. 242–254, 2012.

[47] Halko, N. and Martinsson, P.G. and Tropp, J.A., "Finding structure with randomness: Probabilistic algorithms for constructing approximate matrix decompositions," *SIAM review*, vol. 53, no. 2, pp. 217–288, 2011.

[48] Haupt, J. and Bajwa, W.U. and Raz, G. and Nowak, R., "Toeplitz compressed sensing matrices with applications to sparse channel estimation," *IEEE Transactions on Information Theory*, vol. 56, no. 11, pp. 5862–5875, 2010.

[49] J. Yoo and C. Turnes and E. Nakamura and C. Le and S. Becker and E. Sovero and M. Wakin and M. Grant and J. Romberg and A. Emami- Neyestanak and E. Candès, "A compressed sensing parameter extraction platform for radar pulse signal acquisition," *Submitted to IEEE J. Emerging Topics Cir. and Sys.*, February 2012.

[50] J. Yoo and S. Becker and M. Loh and M. Monge and E. Candès, "A 100mhz-2ghz 12.5x sub-Nyquist rate receiver in 90nm CMOS," in *Submitted to Proc. IEEE Radio Freq. Integrated Cir. Conf.*, 2012.

[51] Johnson, C. R., Schniter, P., Endres, T. J., Behm, J. D., Brown, D. R., and Casas, R. A., "Blind equalization using the constant modulus criterion: A review," *Proc. IEEE*, vol. 86, pp. 1927–1950, October 1998.

[52] Keshavan, R. H., Montanari, A., and Oh, S., "Matrix completion from a few entries," *IEEE Trans. Inform. Theory*, vol. 56, no. 6, pp. 2980–2998, 2010.

[53] Koltchinkskii, V., Lounici, K., and Tsybakov, A., "Nuclear norm penalization and optimal rates for noisy low rank matrix completion." `arXiv:1011.6256`, December 2010.

[54] Krahmer, F. and Ward, R., "New and improved johnson-lindenstrauss embeddings via the restricted isometry property," *SIAM Journal on Mathematical Analysis*, vol. 43, no. 3, pp. 1269–1281, 2011.

[55] Kundur, D. and Hatzinakos, D., "Blind image deconvolution," *IEEE Signal Proc. Mag.*, vol. 13, pp. 43–64, May 1996.

[56] Laska, J. and Kirilos, S. and Duarte, M. and Ragheb, T. and Baraniuk, R. and Massoud, Y., "Theory and implementation of an analog-to-information converter using random demodulation," in *Proc. IEEE Int. Symp. Circuits and Systems*, pp. 1959–1962, 2007.

[57] Laurent, B. and Massart, P., "Adaptive estimation of a quadratic functional by model selection," *Annals of Statistics*, pp. 1302–1338, 2000.

[58] Ledoux, M., *The concentration of measure phenomenon*, vol. 89. Amer Mathematical Society, 2001.

[59] Lee, J., Recht, B., Srebro, N., Salakhutdinov, R. R., and Tropp, J. A., "Practical large-scale optimization for max-norm regularization," in *Advances in Neural Information Processing Systems*, 2010.

[60] Lee, K. and Bresler, Y., "ADMiRA: Atomic decomposition for minimum rank approximation," *IEEE Trans. Inform. Theory*, vol. 56, pp. 4402–4416, September 2010.

[61] Levin, A., Weiss, Y., Durand, F., and Freeman, W. T., "Understanding blind deconvolution algorithms," *Pattern Analysis and Machine Intelligence, IEEE Transactions on*, vol. 33, no. 12, pp. 2354–2367, 2011.

[62] Lewis, A.S., "The mathematics of eigenvalue optimization," *Mathematical Programming*, vol. 97, no. 1, pp. 155–176, 2003.

[63] Litke, AM and Bezayiff, N. and Chichilnisky, EJ and Cunningham, W. and Dabrowski, W. and Grillo, AA and Grivich, M. and Grybos, P. and Hottowy, P. and Kachiguine, S. and others, "What does the eye tell the brain?: Development of a system for the large-scale recording of retinal output activity," *IEEE Transactions on Nuclear Science*, vol. 51, no. 4, pp. 1434–1440, 2004.

[64] Liu, H., Xu, G., Tong, L., and Kailath, T., "Recent developments in blind channel equalization : From cyclostationnarity to subspaces," *Signal Process.*, vol. 50, pp. 83–99, April 1996.

[65] Liu, Z. and Vandenberghe, L., "Interior-point method for nuclear norm approximation with application to system identification," *SIAM Journal on Matrix Analysis and Applications*, vol. 31, no. 3, pp. 1235–1256, 2009.

[66] Ma, S. and Goldfarb, D. and Chen, L., "Fixed point and bregman iterative methods for matrix rank minimization," *Mathematical Programming*, vol. 128, no. 1, pp. 321–353, 2011.

[67] Mishali, M. and Eldar, Y.C., "Blind multiband signal reconstruction: Compressed sensing for analog signals," *IEEE Transactions on Signal Processing*, vol. 57, no. 3, pp. 993–1009, 2009.

[68] Mishali, M. and Eldar, Y.C. and Dounaevsky, O. and Shoshan, E., "Xampling: Analog to digital at sub-nyquist rates," *Circuits, Devices & Systems, IET*, vol. 5, no. 1, pp. 8–20, 2011.

[69] Mishali, M. and Eldar, Y.C. and Tropp, J.A., "Efficient sampling of sparse wideband analog signals," in *IEEE 25th Convention of Electrical and Electronics Engineers in Israel, 2008.*, pp. 290–294, IEEE, 2008.

[70] Moravec, M., Romberg, J., and Baraniuk, R., "Compressed sensing phase retrieval," *SPIE, Wavelets XII*, vol. 6701, p. 91, 2007.

[71] Murray, T. and Pouliquen, P. and Andreou, A.G. and Lauritzen, K., "Design of a cmos a2i data converter: Theory, architecture and implementation," in *45th Annual Conference on Information Sciences and Systems (CISS),*, pp. 1–6, IEEE, 2011.

[72] Needell, D. and Tropp, J.A., "Cosamp: Iterative signal recovery from incomplete and inaccurate samples," *Applied and Computational Harmonic Analysis*, vol. 26, no. 3, pp. 301–321, 2009.

[73] Nesterov, Y., Wolkowicz, H., and Ye, Y., "Nonconvex quadratic optimization," in *Handbook of Semidefinite Programming* (Wolkowicz, H., Saigal, R., and Vandenberghe, L., eds.), International series in operations research and management science, (Boston, MA), pp. 361–420, Kluwer Academic Publishers, 2000.

[74] Peng, Y. and Ganesh, A. and Wright, J. and Xu, W. and Ma, Y., "RASL: Robust alignment by sparse and low-rank decomposition for linearly correlated images," in *IEEE Conference on Computer Vision and Pattern Recognition (CVPR)*, pp. 763–770, IEEE, 2010.

[75] Recht, B., "A simpler approach to matrix completion," *J. Machine Learning Research*, vol. 12, pp. 3413–3430, 2011.

[76] Recht, B., Fazel, M., and Parrilo, P. A., "Guaranteed minimum-rank solutions of linear matrix equations via nuclear norm minimization," *SIAM Review*, vol. 52, no. 3, pp. 471–501, 2010.

[77] Recht, B. and Ré, C., "Parallel stochastic gradient algorithms for large-scale matrix completion." Submitted to *Mathematical Programming Computation*. Preprint available at `http://www.optimization-online.org/DB_HTML/2011/04/3012.html`, 2011.

[78] Romberg, J. and Neelamani, R., "Sparse channel separation using random probes," *Inverse Problems*, vol. 26, November 2010.

[79] Romberg, J., "Compressive sensing by random convolution," *SIAM Journal on Imaging Sciences*, vol. 2, no. 4, pp. 1098–1128, 2009.

[80] Romberg, J. and Neelamani, R., "Sparse channel separation using random probes," *Inverse Problems*, vol. 26, no. 11, p. 115015, 2010.

[81] Roy, R. and Kailath, T., "Esprit-estimation of signal parameters via rotational invariance techniques," *Acoustics, Speech and Signal Processing, IEEE Transactions on*, vol. 37, no. 7, pp. 984–995, 1989.

[82] Rudelson, M. and Vershynin, R., "Geometric approach to error correcting codes and reconstruction of signals," *Int. Math. Res. Not.*, no. 64, pp. 4019–4041, 2005.

[83] Sato, Y., "A method of self-recovering equalization for multilevel amplitude-modulation," *IEEE Trans. Commun.*, vol. COM-23, pp. 679–682, June 1975.

[84] Schlottmann, C.R. and Hasler, P.E., "A highly dense, low power, programmable analog vector-matrix multiplier: The fpaa implementation," *IEEE Journal on Emerging and Selected Topics in Circuits and Systems*, vol. 1, no. 3, pp. 403–411, 2011.

[85] Schmidt, M., "minFunc: unconstrained differentiable multivariate optimization in Matlab." `http://www.di.ens.fr/~mschmidt/Software/minFunc.html`, 2012.

[86] Schmidt, R., "Multiple emitter location and signal parameter estimation," *Antennas and Propagation, IEEE Transactions on*, vol. 34, no. 3, pp. 276–280, 1986.

[87] Singer, A., "A remark on global positioning from local distances," *Proceedings of the National Academy of Sciences*, vol. 105, no. 28, pp. 9507–9511, 2008.

[88] Slavinsky, J. P., Laska, J., Davenport, M. A., and Baraniuk, R. G., "The compressive multiplexer for multi-channel compressive sensing," in *Proc. IEEE Int. Conf. Acoust. Speech Sig. Proc.*, (Prague, Czech Republic), pp. 3980–3983, May 2011.

[89] So, A.M.C. and Ye, Y., "Theory of semidefinite programming for sensor network localization," *Mathematical Programming*, vol. 109, no. 2, pp. 367–384, 2007.

[90] Toh, K.C. and Yun, S., "An accelerated proximal gradient algorithm for nuclear norm regularized linear least squares problems," *Pacific Journal of Optimization*, vol. 6, no. 615-640, p. 15, 2010.

[91] Tong, L. and Perreau, S., "Multichannel blind identification: From subspace to maximum likelihood methods," *Proc. IEEE*, vol. 86, pp. 1951–1968, October 1998.

[92] Tong, L., Xu, G., and Kailath, T., "Blind identification and equalization based on second-order statistics: A time domain approach," *IEEE Trans. Inform. Theory*, vol. 40, no. 2, pp. 340–349, 1994.

[93] Tropp, J. A., "User-friendly tail bounds for sums of random matrices," *Found. of Comput. Math.*, vol. 12, no. 4, pp. 389–434, 2012.

[94] Tropp, J.A., "Improved analysis of the subsampled randomized hadamard transform," *Advances in Adaptive Data Analysis*, vol. 3, no. 01n02, pp. 115–126, 2011.

[95] Tropp, J.A. and Gilbert, A.C., "Signal recovery from random measurements via orthogonal matching pursuit," *IEEE Transactions on Information Theory*, vol. 53, no. 12, pp. 4655–4666, 2007.

[96] Tropp, J.A. and Laska, J.N. and Duarte, M.F. and Romberg, J.K. and Baraniuk, R.G., "Beyond nyquist: Efficient sampling of sparse bandlimited signals," *IEEE Transactions on Information Theory*, vol. 56, no. 1, pp. 520–544, 2010.

[97] Tropp, J.A. and Wakin, M.B. and Duarte, M.F. and Baron, D. and Baraniuk, R.G., "Random filters for compressive sampling and reconstruction," in *IEEE International Conference on Acoustics, Speech and Signal Processing, 2006. ICASSP 2006 Proceedings.*, vol. 3, pp. III–III, IEEE, 2006.

[98] Tugnait, J., "Identification of linear stochastic systems via second-and fourth-order cumulant matching," *IEEE Transactions on Information Theory*, vol. 33, no. 3, pp. 393–407, 1987.

[99] Vershynin, R., "Introduction to the non-asymptotic theory of random matrices." `arXiv:1011.3027`, November 2010.

[100] Watson, GA, "Characterization of the subdifferential of some matrix norms," *Linear Algebra and its Applications*, vol. 170, pp. 33–45, 1992.

[101] Woolfe, F. and Liberty, E. and Rokhlin, V. and Tygert, M., "A fast randomized algorithm for the approximation of matrices," *Applied and Computational Harmonic Analysis*, vol. 25, no. 3, pp. 335–366, 2008.

[102] Xu, G., Liu, H., Tong, L., and Kailath, T., "A least-sqaures approach to blind channel identification," *IEEE Trans. Sig. Proc.*, vol. 43, pp. 2982–2993, December 1995.